Imperial College of Science, Technology and Medicine
Department of Electrical and Electronic Engineering

# Enhancing Selectivity of Minimally Invasive Peripheral Nerve Interfaces using Combined Stimulation and High Frequency Block: from Design to Application

Adrien Rapeaux

Submitted in part fulfilment of the requirements for the degree of
Doctor of Philosophy in Electrical and Electronic Engineering of Imperial College London,
April 2020

## Declaration of Originality

This thesis represents my own work unless otherwise stated. Any text, figures, tables or other material that is not my own has been appropriately referenced. Any material that I have adapted for this work has been identified as such and where applicable the original source cited.

## Copyright Declaration

# Abstract

The discovery of the excitable property of nerves was a fundamental step forward in our knowledge of the nervous system and our ability to interact with it. As the injection of charge into tissue can drive its artificial activation, devices have been conceived that can serve healthcare by substituting the input or output of the peripheral nervous system when damage or disease has rendered it inaccessible or its action pathological. Applications are far-ranging and transformational as can be attested by the success of neuroprosthetics such as the cochlear implant. However, the body's immune response to invasive implants have prevented the use of more selective interfaces, leading to therapy side-effects and off-target activation. The inherent tradeoff between the selectivity and invasiveness of neural interfaces, and the consequences thereof, is still a defining problem for the field. More recently, continued research into how nervous tissue responds to stimulation has led to the discovery of High Frequency Alternating Current (HFAC) block as a stimulation method with inhibitory effects for nerve conduction. While leveraging the structure of the peripheral nervous system, this neuromodulation technique could be a key component in efforts to improve the selectivity-invasiveness tradeoff and provide more effective neuroprosthetic therapy while retaining the safety and reliability of minimally invasive neural interfaces. This thesis describes work investigating the use of HFAC block to improve the selectivity of peripheral nerve interfaces, towards applications such as bladder control or vagus nerve stimulation where selective peripheral nerve interfaces cannot be used, and yet there is an unmet need for more selectivity from stimulation-based therapy. An overview of the underlying neuroanatomy and electrophysiology of the peripheral nervous system combined with a review of existing electrode interfaces and electrochemistry will serve to inform the problem space. Original contributions are the design of a custom multi-channel stimulator able to combine conventional and high frequency stimulation, establishing a suitable experimental platform for ex-vivo electrophysiology of the rat sciatic nerve model for HFAC block, and exploratory experiments to determine the feasibility of using HFAC block in combination with conventional stimulation to enhance the selectivity of minimally-invasive peripheral nerve interfaces.

# Acknowledgements

I would like to express my most heartfelt thanks to:

- My supervisor Dr. Timothy G. Constandinou, who gave me the freedom to pursue this somewhat unusual line of inquiry within an electronic engineering research group. His expertise in technical matters, pragmatic approach to research focusing on impact and follow-through, his enthusiasm for neuroscience and relentlessly positive outlook have enabled me to cross gaps and scale walls in my pursuit. I have been, am and continue to be honoured to work with him, and I look forward to future endeavours in the group.

- Dr. Ian Williams of Imperial College, who was a first contact when meeting my current research group and has remained a close friend and knowledgeable expert throughout. Discussions with him over coffee have sparked many ideas, to solve existing problems or identify unexplored paths.

- Dr. Lieuwe Leene, previously of Imperial College, now at Novelda AS. His intuitive understanding of complex circuits and vast engineering knowledge completely changed my understanding of the field and pushed me to look 'outside of the box'. His good cheer and no-nonsense approach are sorely missed.

- Dr. Jerry Hunsberger of Galvani Bioelectronics for his expertise on maintaining viability of tissues *ex-vivo* and knowledge of neurophysiology which was instrumental in the design of an adapted experimental platform in the laboratory at Imperial College.

- The Biomaterials Research Group, Imperial College, comprising Dr. Rylie Green, Dr. Omaer Syed and Mz. Estelle Cuttaz for contributions to the *ex-vivo* experiments, especially for giving me access to animal tissue using their license. Our partnership has yielded concrete and useful results and I hope for it to continue.

- The NGNI research group: my colleagues, and dare I say my friends. They are part of what makes this such a good work environment: strong ethic, commitment to high quality output, and kindness. Their expertise and support is invaluable.

- The CBIT or Center for Bioinspired Technology of Imperial College, a collection of amazing individuals of varied background showing how diversity coupled with a sense of community can be such a strong combination for science.

- Last but not least, my family and friends, who've heard me complain more times than I can count and always encouraged me to keep going. I can't thank them enough.

# Dedication

I dedicate this thesis to my wife, who has been incredibly patient with me during the entire PhD period (5 years compared to the usual 3), and especially towards the end of the write-up period as we were both working from home due to the extraordinary circumstances in the UK and around the world. I cannot thank her enough for her support, and keeping me sane.

# Contents

# List of Figures

# List of Tables

# List of Abbreviations

| | |
|---|---|
| ADC | Analog to Digital Converter |
| AWERB | Animal Welfare and Ethical Review Board |
| AWG | Arbitrary Waveform Generator |
| BiCMOS | Bipolar Complementary Metal On Semiconductor |
| CAP | Compound Action Potential |
| CMOS | Complementary Metal On Semiconductor |
| CMRR | Common-Mode Rejection Ratio |
| CNS | Central Nervous System |
| COTS | Commercial Off-the-Shelf |
| CRRSS | Chiu-Richie-Rogart-Stagg-Sweeney (model) |
| DAC | Digital to Analog Converter |
| DALY | Disability Adjusted Life Year |
| DARPA | Defense Advanced Research Projects Administration |
| DC | Direct Current |
| DMA | Direct Memory Access |
| DNL | Differential Non-Linearity |
| DSD | Detrusor Sphincter Dyssynergia |
| ElectRx | Electrical Prescriptions |
| EMG | Electromyogram |
| ENG | Electroneurogram |
| ESD | Electro-Static Discharge |
| FES | Functional Electrical Stimulation |
| FH | Frankenhaeuser-Huxley (model) |
| FINE | Flat Interface Nerve Electrode |
| GM | Gastrocnemius Medialis (muscle) |
| HAPTIX | Hand Proprioception and Touch Interfaces |
| HFAC | High Frequency Alternating Current |
| I2C | Inter Integrated Circuit (Communication Interface) |
| INL | Integral Non-Linearity |
| LIFE | Longitudinal Inter-Fascicular Electrode |
| LUT | Lower Urinary Track |
| LSB | Least Significant Bit |
| MKHB | Modified Krebs-Henseleit Buffer |
| MRG | McIntyre-Richardson-Grill (model) |
| MSB | Most Significant Bit |

| | |
|---|---|
| NI | Neural Interface |
| NLEO | Non-linear Energy Operator |
| NMOS | Negative channel Metal On Semiconductor |
| PCB | Printed Circuit Board |
| PIT | Periodic Interrupt Timer |
| PMOS | Positive channel Metal On Semiconductor |
| PNS | Peripheral Nervous System |
| RS | Ringer's Solution |
| SCI | Spinal Cord Injury |
| SD | Sprague Dawley (rat) |
| SE | Schwarz-Eikhof (model) |
| SNR | Signal to Noise Ratio |
| SPARC | Stimulating Peripheral Activity to Relieve Symptoms |
| SPDT | Single Pole Double Throw |
| SPI | Serial Peripheral Interface |
| SPST | Single Pole Single Throw |
| SRB | Schwarz-Reid-Bostock (model) |
| SSRI | Selective Serotonin Reuptake Inhibitor |
| TA | Tibialis Anterior (muscle) |
| TIME | Transverse Intrafascicular Mutichannel Electrode |
| UART | Universal Asynchronous Receiver Transmitter |
| USEA | Utah Slanted Electrode Array |
| VNS | Vagus Nerve Stimulation |

# Foreword

The design and use of Neural Stimulators is a complex topic. These devices are at the interface between biology and engineering, and present a unique challenge for study due to the interdependence of so many aspects of their design from the point of view of both fields. From all angles, there is an inevitable amount of interdependency between the electrical and electronic engineering in stimulator design, the materials science and electrochemistry of electrodes and electrolytes as found in living tissue, and the underlying neuroanatomy and neurophysiology of the peripheral nervous system. To add to the complexity, living systems are often chaotic and their study requires careful control of experimental variables combined with stochastic analysis of results to mitigate the inherent variability of measurement results. This thesis attempts to compartmentalise background knowledge where possible, however an amount of cross-referencing is to be expected.

Appreciation for the multi-disciplinary nature of this field has been one of the most important lessons I learned during this thesis.

# Chapter 1

# Introduction

As of today the cost of diseases of neurological origin is very high to society; for spinal cord injuries alone it has been reported to be between $270,000 and $420,000 for initial treatment and then $31,000 to $75,000 annually in 1992 US dollars [1], a cost that is likely to have increased. A different study measuring Disability-Adjusted-Life-Years (DALYs) identified neurological disorders as the leading cause of DALYs and second leading cause of deaths [2], with the biggest contributors being stroke, migraine, Alzheimer's disease and other dementias as well as meningitis. It is evident that many neurological diseases are debilitating and that patients often require 24-hour care, which has driven significant research and development effort to find solutions: several research programs have been dedicated to this task, such as the NIH SPARC [3], DARPA HAPTIX [4] and ElectRx [5] and the GSK Electroceutical [6] initiatives.

Already a significant body of work exists describing interventions on the nervous system to alleviate disease symptoms, repair neural damage and restore healthy normal function. Current approaches to change nerve function can involve drugs such as Selective Serotonin Re-uptake Inhibitors (SSRIs) in the case of depression, to more invasive surgical interventions such as vagotomy for peptic ulcer [7] or resection for epilepsy [8]. A more recent approach is to directly stimulate nerves to modulate the activity of connected organs [9]–[11], providing a theoretically more selective alternative to the traditional use of drugs in this role, which often behave systemically [12]. Functional Electrical Stimulation (FES) has enabled a completely different type

of therapy not previously possible [13]–[15], addressing conditions such as spinal cord injury and stroke by directly stimulating nerves connected to muscles no longer under voluntary control. Whether targeting somatic or autonomic function, stimulation is carried out by a range of devices implanted within the body, generally close to the target stimulation location in a suitable cavity, with leads branching out from the battery and electronics casing to specially manufactured electrodes which then excite neural tissue [9], [16]–[18] to obtain a therapeutic effect. A number of existing commercial devices and their target locations for stimulation within the body are shown in figure 1.1.

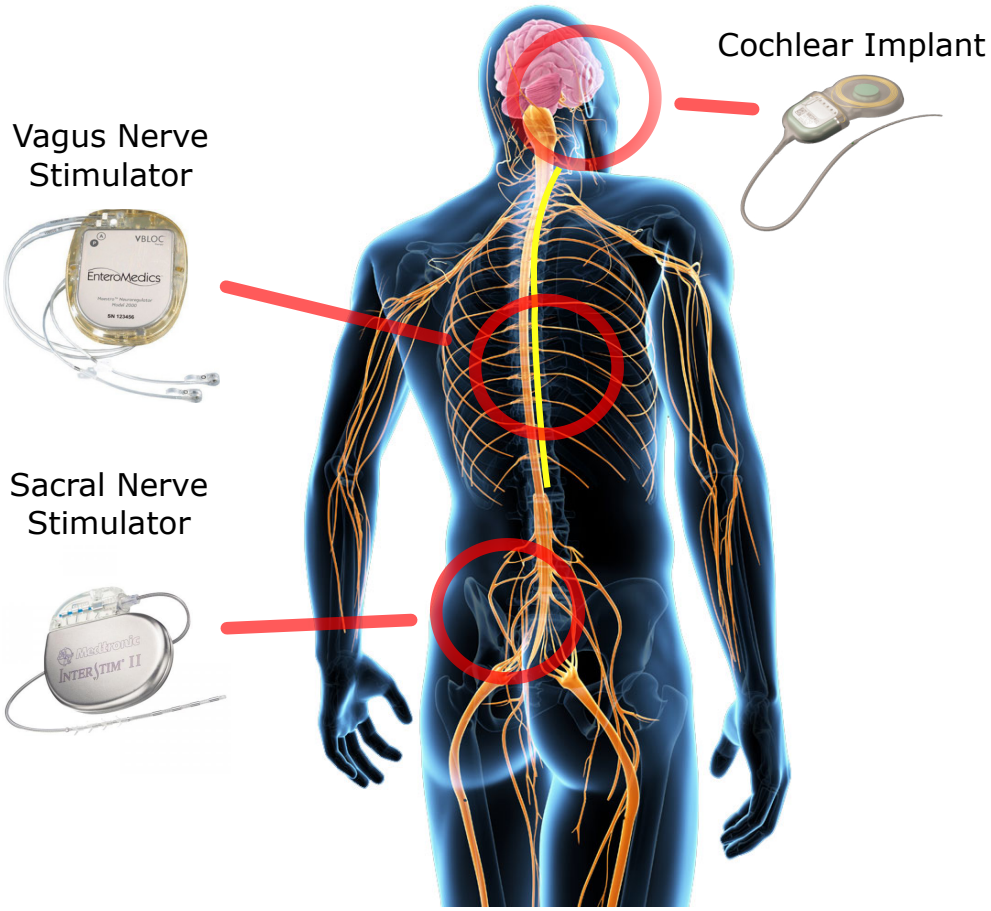


Figure 1.1: Examples of stimulators used to treat neurological diseases and their approximate locations in the body. The vagus nerve stimulator is the EnteroMedics vBloc®. The sacral nerve stimulator is the Medtronic Interstim®. The cochlear implant is the Med-El Synchrony 2®.[1]

Conventional peripheral nerve stimulation has always been excitatory as it aims to generate action potentials in a system which can be simplified as a relay to and from the central nervous

[1]Images taken from multiple sources. Nervous system picture from [19]. Vagus nerve stimulator from [20]. Sacral nerve stimulator from [21]. Cochlear implant from [22].

system. Precise control of what is stimulated is crucial to enable high therapy effectiveness with a minimum of side-effects [6]. Selectivity is the capability for a neural stimulation device to precisely activate certain fibers within whole nerve and prevent activation of nerve fibers innervating unrelated or antagonistic targets [23]. In each application of neural stimulation, the lack of selectivity of current approaches has led to side-effects, driving research and development effort to improve this metric [24], focusing on modifying electrodes [25], stimulation waveforms[23], or leveraging neuroanatomy and neurophysiology [26], [27]. However, these approaches have been limited by the body's immune response to invasive implants [28], [29], or the sparsity of locations where neuroanatomy allows the use of simple and robust interfaces while retaining selectivity [27].

Selectivity remains a challenge for the application of stimulation for therapy. More recently, devices have targeted the autonomous nervous system for therapeutic stimulation [11]. In this case the goal of stimulation is to modulate the activity of the implanted nerve with powerful results for anxiety, obesity or depression [30]. A key difference for this type of stimulation is that therapy can require both excitatory or inhibitory action through nerve block [31]. A relatively new stimulation method allows nerves to be reversibly blocked by a stimulator [32]. Stimulating using specific High-Frequency Alternating Current (HFAC) waveforms can prevent conduction of neural information, reproducing the effect of surgical resection of nerve with the potential to tune stimulation to avoid side-effects, and the option to reverse the block completely. This new type of stimulation can be a game-changer when considering selectivity as a long-standing challenge in conventional neural stimulation [33], and its use to enhance the selectivity of existing interfaces is the focus of this thesis. In the face of the mixed results resulting from modifying stimulation electrodes to be more selective for example, a natural next step is to look at how the stimulation protocol can be changed to improve stimulation selectivity for already approved cuff electrodes. This idea together with the emergence of HFAC block as a powerful tool for neuromodulation provides a unique opportunity to attempt a combinatorial stimulation approach.

The work in this thesis stems initially from a simulation study of timed block and stimulation in the frog sciatic nerve carried out during the author's MEng degree [34]. The purpose of the

work was to investigate whether timing HFAC block and conventional stimulation would result in selective stimulation in a similar manner to the work of Kuffler [35]. Kuffler's approach involves blocking fast-conducting fibres in a compound nerve while allowing action potentials in slower conducting fibres to carry through to the end organ, as shown figure 1.2 here.

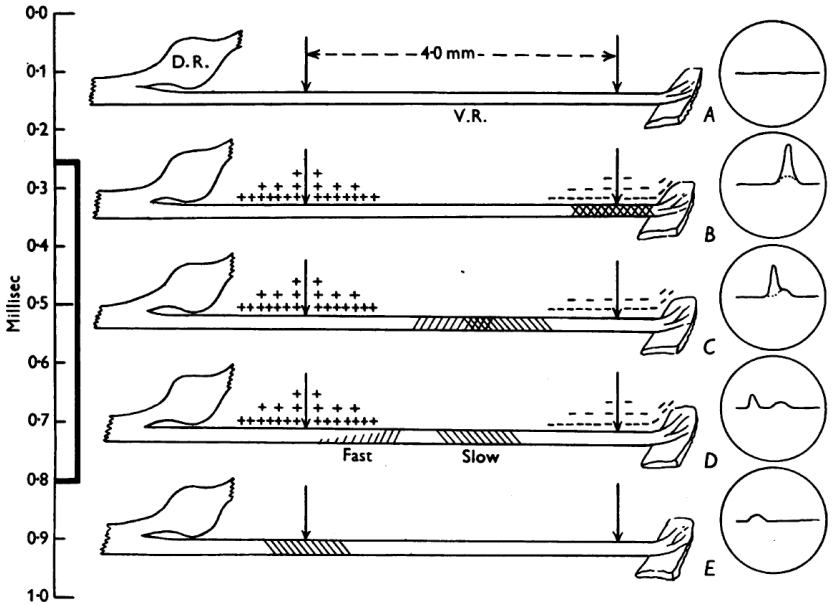


Figure 1.2: Drawing showing the stimulation technique used by Kuffler on frog motor nerves to selectively activate small nerve fibres for study. Cathodic stimulation of the nerve at the proximal (right side) end generates action potentials travelling towards the left at different speeds in compound nerve. Precise positioning of the anode allows selective block of fast action potentials by anodal block. This figure appears in [35].

It isn't possible to use Kuffler's technique directly because it uses a form of DC block, which has been shown to cause nerve damage even with limited use [36]. Therefore the simulation study investigated whether DC block could be substituted with HFAC block, and concluded that it was *a priori* possible. This prompted the work in this thesis, starting with the following hypothesis:

A combination of high-frequency block and timed conventional stimulation will effectively enhance the selectivity of existing cuff electrodes compared to conventional stimulation alone.

This has the potential for direct impact on existing stimulation-based therapies to reduce their side-effects, and possibly pave the way for therapies that could previously not be used due to off-target neural activation. The following chapters attempt to answer parts of this question from the point of view of hardware, the experimental approach, and finally data collection and

analysis to determine whether this technique is feasible and translatable to clinical applications. This can be described in terms of the following objectives:

- **Design and implement a stimulator for carrying out selective stimulation.** Many commercial stimulators exist but key limitations prevent them from being used. Concurrent block and stimulation will require a block-capable, flexible multi-channel device for exploratory experiments.
- **Develop an experimental platform to carry out experiments in a controlled environment** which is not only representative of real world, clinical scenarios so that data and conclusions retain translatability to the clinic, but reduces complexity as much as possible to avoid confounding effects, all the while reducing animal use as much as possible in line with the '3 Rs'. This will enable robust experiments and yield repeatable results with a good tradeoff in resource commitment.
- **Investigate which stimulation parameters would enable selective stimulation and block** based on initial results from computational simulation, and adjusting as results are collected from animal tissue studies.

To answer all research questions and fulfill objectives, the structure of this thesis is as follows:

1. Chapter 2 provides essential background in macro and micro neuroanatomy that set the context for neural stimulation-based therapies, and theory related to how electrodes stimulate nerves and the electrochemical reactions that occur at the interface between electrodes and tissue. This chapter also details results from the simulation project and corresponding conclusions that inform the design of the stimulator and experiments to confirm original predictions, as well as specific opportunities for application of the technique in existing neural stimulation therapies.
2. Chapter 3 details the design, implementation and evaluation of a novel multi-channel stimulator that is block-capable, enabling investigation of stimulation and block in live tissue without the limitations of existing commercial neural stimulation hardware.

3. Chapter 4 describes initial experiments in the *in-vivo* rat model to verify some of the predictions made by modelling in the original simulation project.

4. Chapter 5 presents the results obtained from investigation of stimulation and block *ex-vivo* to enhance the selectivity of cuff electrodes in a tightly controlled environment and draws conclusions on the feasibility of using this technique clinically.

5. Chapter 6 concludes the thesis and provides a summary of contributions while detailing future directions and final thoughts.

6. Chapter 7 provides supplemental materials such as laboratory protocols or information about equipment and electrodes used during experiments, as well as pilot data from experiments showing interesting and potentially useful phenomena observed during *in-vivo* and *ex-vivo* experiments.

# References


[1] G. H. Creasey, K. L. Kilgore, D. L. Brown-Triolo, J. E. Dahlberg, P. H. Peckham, and M. W. Keith, "Reduction of Costs of Disability Using Neuroprostheses," *Assistive Technology*, vol. 12, no. 1, pp. 67–75, Jun. 2000, ISSN: 1040-0435. DOI: 10.1080/10400435.2000.10132010. [Online]. Available: https://doi.org/10.1080/10400435.2000.10132010 (visited on 01/27/2020).

[2] "Global, regional, and national burden of neurological disorders, 1990–2016: A systematic analysis for the Global Burden of Disease Study 2016," *The Lancet. Neurology*, vol. 18, no. 5, pp. 459–480, May 2019, ISSN: 1474-4422. DOI: 10.1016/S1474-4422(18)30499-X. [Online]. Available: https://www.ncbi.nlm.nih.gov/pmc/articles/PMC6459001/ (visited on 02/06/2020).

[3] *Stimulating Peripheral Activity to Relieve Conditions*, en, Library Catalog: ncats.nih.gov, Oct. 2016. [Online]. Available: https://ncats.nih.gov/sparc (visited on 03/26/2020).

[4] *HAPTIX Starts Work to Provide Prosthetic Hands with Sense of Touch.* [Online]. Available: https://www.darpa.mil/news-events/2015-02-08 (visited on 03/26/2020).

[5] E. V. Gieson, *Electrical Prescriptions.* [Online]. Available: https://www.darpa.mil/program/electrical-prescriptions (visited on 03/26/2020).

[6] K. Famm, "A jump-start for electroceuticals," en, p. 3,

[7] J. Hoffmann, H. E. Jensen, J. Christiansen, A. Olesen, F. B. Loud, and O. Hauch, "Prospective controlled vagotomy trial for duodenal ulcer. Results after 11-15 years.," *Annals of Surgery*, vol. 209, no. 1, pp. 40–45, Jan. 1989, ISSN: 0003-4932. [Online]. Available: https://www.ncbi.nlm.nih.gov/pmc/articles/PMC1493889/ (visited on 03/19/2020).

[8] M. Mohan, S. Keller, A. Nicolson, S. Biswas, D. Smith, J. O. Farah, P. Eldridge, and U. Wieshmann, "The long-term outcomes of epilepsy surgery," en, *PLOS ONE*, vol. 13, no. 5, e0196274, May 2018, Publisher: Public Library of Science, ISSN: 1932-6203. DOI: 10.1371/journal.pone.0196274. [Online]. Available: https://journals.plos.org/plosone/article?id=10.1371/journal.pone.0196274 (visited on 03/26/2020).

[9] R. L. Johnson and C. G. Wilson, "A review of vagus nerve stimulation as a therapeutic intervention," *Journal of Inflammation Research*, vol. 11, pp. 203–213, May 2018, ISSN: 1178-7031. DOI: 10.2147/JIR.S163248. [Online]. Available: https://www.ncbi.nlm.nih.gov/pmc/articles/PMC5961632/ (visited on 03/19/2020).

[10] A. L. Benabid, "Deep brain stimulation for Parkinson's disease," en, *Current Opinion in Neurobiology*, vol. 13, no. 6, pp. 696–706, Dec. 2003, ISSN: 0959-4388. DOI: 10.1016/j.conb.2003.11.001. [Online]. Available: http://www.sciencedirect.com/science/article/pii/S0959438803001739 (visited on 03/18/2020).

[11] C. C. Horn, J. L. Ardell, and L. E. Fisher, "Electroceutical Targeting of the Autonomic Nervous System," *Physiology*, vol. 34, no. 2, pp. 150–162, Mar. 2019, ISSN: 1548-9213. DOI: 10.1152/physiol.00030.2018. [Online]. Available: https://www.ncbi.nlm.nih.gov/pmc/articles/PMC6586833/ (visited on 03/19/2020).

[12] T. R. Van Vleet, M. J. Liguori, J. J. Lynch, M. Rao, and S. Warder, "Screening Strategies and Methods for Better Off-Target Liability Prediction and Identification of Small-Molecule Pharmaceuticals," en, *SLAS DISCOVERY: Advancing the Science of Drug Discovery*, vol. 24, no. 1, pp. 1–24, Jan. 2019, ISSN: 2472-5552, 2472-5560. DOI: 10.1177/2472555218799713. [Online]. Available: http://journals.sagepub.com/doi/10.1177/2472555218799713 (visited on 03/26/2020).

[13] W. D. Memberg, K. H. Polasek, R. L. Hart, A. M. Bryden, K. L. Kilgore, G. A. Nemunaitis, H. A. Hoyen, M. W. Keith, and R. F. Kirsch, "An Implanted Neuroprosthesis for Restoring Arm and Hand Function in People with High Level Tetraplegia," *Archives of physical medicine and rehabilitation*, vol. 95, no. 6, 1201–1211.e1, Jun. 2014, ISSN: 0003-9993. DOI: 10.1016/j.apmr.2014.01.028. [Online]. Available: https://www.ncbi.nlm.nih.gov/pmc/articles/PMC4470503/ (visited on 03/05/2020).

[14] K. Dunning, M. W. O'Dell, P. Kluding, and K. McBride, "Peroneal Stimulation for Foot Drop After Stroke: A Systematic Review," en-US, *American Journal of Physical Medicine & Rehabilitation*, vol. 94, no. 8, pp. 649–664, Aug. 2015, ISSN: 0894-9115. DOI: 10.1097/PHM.0000000000000308. [Online]. Available: https://journals.lww.com/ajpmr/Abstract/2015/08000/Peroneal_Stimulation_for_Foot_Drop_After_Stroke__A.9.aspx (visited on 03/19/2020).

[15] K. T. Ragnarsson, "Functional electrical stimulation after spinal cord injury: Current use, therapeutic effects and future directions," *Spinal Cord*, vol. 46, no. 4, pp. 255–274, 2008. [Online]. Available: http://www.nature.com/sc/journal/v46/n4/abs/3102091a.html (visited on 09/21/2015).

[16] C. Shendkar, P. K. Lenka, A. Biswas, R. Kumar, and M. Mahadevappa, "Design and development of a low-cost biphasic charge-balanced functional electric stimulator and its clinical validation," *Healthcare Technology Letters*, vol. 2, no. 5, pp. 129–134, Oct. 2015, ISSN: 2053-3713. DOI: 10.1049/htl.2015.0001. [Online]. Available: https://www.ncbi.nlm.nih.gov/pmc/articles/PMC4625831/ (visited on 03/05/2020).

[17] M. Ortmanns, A. Rocke, M. Gehrke, and H.-J. Tiedtke, "A 232-Channel Epiretinal Stimulator ASIC," *IEEE Journal of Solid-State Circuits*, vol. 42, no. 12, pp. 2946–2959, Dec. 2007, ISSN: 1558-173X. DOI: 10.1109/JSSC.2007.908693.

[18] T. G. Constandinou, J. Georgiou, and C. Toumazou, "A Partial-Current-Steering Biphasic Stimulation Driver for Vestibular Prostheses," *IEEE Transactions on Biomedical Circuits and Systems*, vol. 2, no. 2, pp. 106–113, Jun. 2008, ISSN: 1932-4545, 1940-9990. DOI: 10.1109/TBCAS.2008.927238. [Online]. Available: http://ieeexplore.ieee.org/lpdocs/epic03/wrapper.htm?arnumber=4579124 (visited on 09/21/2015).

[19] *Nerve Stimulation Technology Supplier UK — Polar Medical*. [Online]. Available: https://www.polarmedical.co.uk/nerve-stimulation-technology-supplier-uk/ (visited on 04/02/2020).

[20] *VBLOC pushes ahead with FDA approval despite trial failure — Bariatric News*. [Online]. Available: https://bariatricnews.net/?q=node/830 (visited on 04/02/2020).

[21] *Sacral neuromodulation and InterStim® for overactive bladder (OAB)*. [Online]. Available: https://www.urineincontinence.com.au/overactive-bladder/sacral-neuromodulation-and-interstim-overactive-bladder-oab (visited on 04/02/2020).

[22] *SYNCHRONY 2 Cochlear Implant*. [Online]. Available: https://www.medel.com/en-gb/hearing-solutions/cochlear-implants/synchrony2 (visited on 04/02/2020).

[23] W. Grill and J. Mortimer, "Stimulus waveforms for selective neural stimulation," en, *IEEE Engineering in Medicine and Biology Magazine*, vol. 14, no. 4, pp. 375–385, Aug. 1995, ISSN: 07395175. DOI: 10.1109/51.395310. [Online]. Available: http://ieeexplore.ieee.org/document/395310/ (visited on 03/02/2020).

[24] U. Ghafoor, S. Kim, and K.-S. Hong, "Selectivity and Longevity of Peripheral-Nerve and Machine Interfaces: A Review," English, *Frontiers in Neurorobotics*, vol. 11, 2017, ISSN: 1662-5218. DOI: 10.3389/fnbot.2017.00059. [Online]. Available: https://www.frontiersin.org/articles/10.3389/fnbot.2017.00059/full (visited on 12/12/2019).

[25] J. Badia, T. Boretius, D. Andreu, C. Azevedo-Coste, T. Stieglitz, and X. Navarro, "Comparative analysis of transverse intrafascicular multichannel, longitudinal intrafascicular and multipolar cuff electrodes for the selective stimulation of nerve fascicles," en, *Journal of Neural Engineering*, vol. 8, no. 3, p. 036 023, 2011, ISSN: 1741-2552. DOI: 10.1088/1741-2560/8/3/036023. [Online]. Available: http://stacks.iop.org/1741-2552/8/i=3/a=036023 (visited on 06/08/2016).

[26] N. J. M. Rijkhoff, H. Wijkstra, P. E. V. V. Kerrebroeck, and F. M. J. Debruyne, "Urinary bladder control by electrical stimulation: Review of electrical stimulation techniques in spinal cord injury," en, *Neurourology and Urodynamics*, vol. 16, no. 1, pp. 39–53, 1997, ISSN: 1520-6777. DOI: 10.1002/(SICI)1520-6777(1997)16:1<39::AID-NAU6>3.0.CO;2-F. (visited on 03/05/2020).

[27] B. S. Wilson and M. F. Dorman, "Cochlear implants: A remarkable past and a brilliant future," *Hearing research*, vol. 242, no. 0, pp. 3–21, Aug. 2008, ISSN: 0378-5955. DOI: 10.1016/j.heares.2008.06.005. [Online]. Available: https://www.ncbi.nlm.nih.gov/pmc/articles/PMC3707130/ (visited on 03/19/2020).

[28] W. F. Agnew, D. B. McCreery, T. G. H. Yuen, and L. A. Bullara, "Histologic and physiologic evaluation of electrically stimulated peripheral nerve: Considerations for the selection of parameters," en, *Annals of Biomedical Engineering*, vol. 17, no. 1, pp. 39–60, Jan. 1989, ISSN: 1573-9686. DOI: 10.1007/BF02364272. [Online]. Available: https://doi.org/10.1007/BF02364272 (visited on 02/07/2020).

[29] C. Günter, J. Delbeke, and M. Ortiz-Catalan, "Safety of long-term electrical peripheral nerve stimulation: Review of the state of the art," *Journal of NeuroEngineering and Rehabilitation*, vol. 16, no. 1, p. 13, Jan. 2019, ISSN: 1743-0003. DOI: 10.1186/s12984-018-0474-8. [Online]. Available: https://doi.org/10.1186/s12984-018-0474-8 (visited on 01/27/2020).

[30] D. Guiraud, D. Andreu, S. Bonnet, G. Carrault, P. Couderc, A. Hagège, C. Henry, A. Hernandez, N. Karam, V. L. Rolle, P. Mabo, P. Maciejasz, C.-H. Malbert, E. Marijon, S. Maubert, C. Picq, O. Rossel, and J.-L. Bonnet, "Vagus nerve stimulation: State of the art

of stimulation and recording strategies to address autonomic function neuromodulation," en, *Journal of Neural Engineering*, vol. 13, no. 4, p. 041 002, Jun. 2016, ISSN: 1741-2552. DOI: 10.1088/1741-2560/13/4/041002. [Online]. Available: https://doi.org/10.1088%2F1741-2560%2F13%2F4%2F041002 (visited on 12/12/2019).

[31] C. M. Apovian, S. N. Shah, B. M. Wolfe, S. Ikramuddin, C. J. Miller, K. S. Tweden, C. J. Billington, and S. A. Shikora, "Two-Year Outcomes of Vagal Nerve Blocking (vBloc) for the Treatment of Obesity in the ReCharge Trial," *Obesity Surgery*, vol. 27, no. 1, pp. 169–176, 2017, ISSN: 0960-8923. DOI: 10.1007/s11695-016-2325-7. [Online]. Available: https://www.ncbi.nlm.nih.gov/pmc/articles/PMC5187356/ (visited on 10/17/2017).

[32] N. Bhadra, T. L. Vrabec, N. Bhadra, and K. L. Kilgore, "Reversible conduction block in peripheral nerve using electrical waveforms," *Bioelectronics in Medicine*, vol. 1, no. 1, pp. 39–54, Jan. 2018, ISSN: 2059-1500. DOI: 10.2217/bem-2017-0004. [Online]. Available: https://www.ncbi.nlm.nih.gov/pmc/articles/PMC5811084/ (visited on 09/03/2019).

[33] W. Y. X. Peh, R. Mogan, X. Y. Thow, S. M. Chua, A. Rusly, N. V. Thakor, and S.-C. Yen, "Novel Neurostimulation of Autonomic Pelvic Nerves Overcomes Bladder-Sphincter Dyssynergia," English, *Frontiers in Neuroscience*, vol. 12, 2018, Publisher: Frontiers, ISSN: 1662-453X. DOI: 10.3389/fnins.2018.00186. [Online]. Available: https://www.frontiersin.org/articles/10.3389/fnins.2018.00186/full (visited on 06/12/2020).

[34] A. Rapeaux, K. Nikolic, I. Williams, A. Eftekhar, and T. G. Constandinou, "Fiber size-selective stimulation using action potential filtering for a peripheral nerve interface: A simulation study," in *2015 37th Annual International Conference of the IEEE Engineering in Medicine and Biology Society (EMBC)*, Aug. 2015, pp. 3411–3414. DOI: 10.1109/EMBC.2015.7319125.

[35] S. W. Kuffler and E. M. V. Williams, "Small-nerve junctional potentials. The distribution of small motor nerves to frog skeletal muscle, and the membrane characteristics of

the fibres they innervate*," en, *The Journal of Physiology*, vol. 121, no. 2, pp. 289–317, 1953, ISSN: 1469-7793. DOI: 10.1113/jphysiol.1953.sp004948. [Online]. Available: https://physoc.onlinelibrary.wiley.com/doi/abs/10.1113/jphysiol.1953.sp004948 (visited on 02/11/2020).

[36] N. Bhadra and K. Kilgore, "Direct current electrical conduction block of peripheral nerve," *IEEE Transactions on Neural Systems and Rehabilitation Engineering*, vol. 12, no. 3, pp. 313–324, Sep. 2004, ISSN: 1558-0210. DOI: 10.1109/TNSRE.2004.834205.

# Chapter 2

# Background

## 2.1 Foreword

While significant work has been done to design and use stimulators acting on the Central Nervous System (CNS) such as for Deep Brain [1] or Spinal Cord [2] stimulation, this thesis focuses on the Peripheral Nervous System (PNS) and stimulators designed specifically for interaction with it [3]–[6]. While the PNS and CNS are interconnected, it is the specifics of the macro and micro-anatomy of the PNS that will influence both approaches for therapy and the designs of the devices used to deliver those therapies. Therapies that apply to the peripheral nervous system include Vagus Nerve Stimulation (VNS), Functional electrical Stimulation (FES) such as for foot drop and bladder control, and cochlear stimulation for hearing.

## 2.2 Peripheral Nervous System Compartments

The PNS is further divided into three compartments; the somatic, autonomic, and enteric nervous systems.

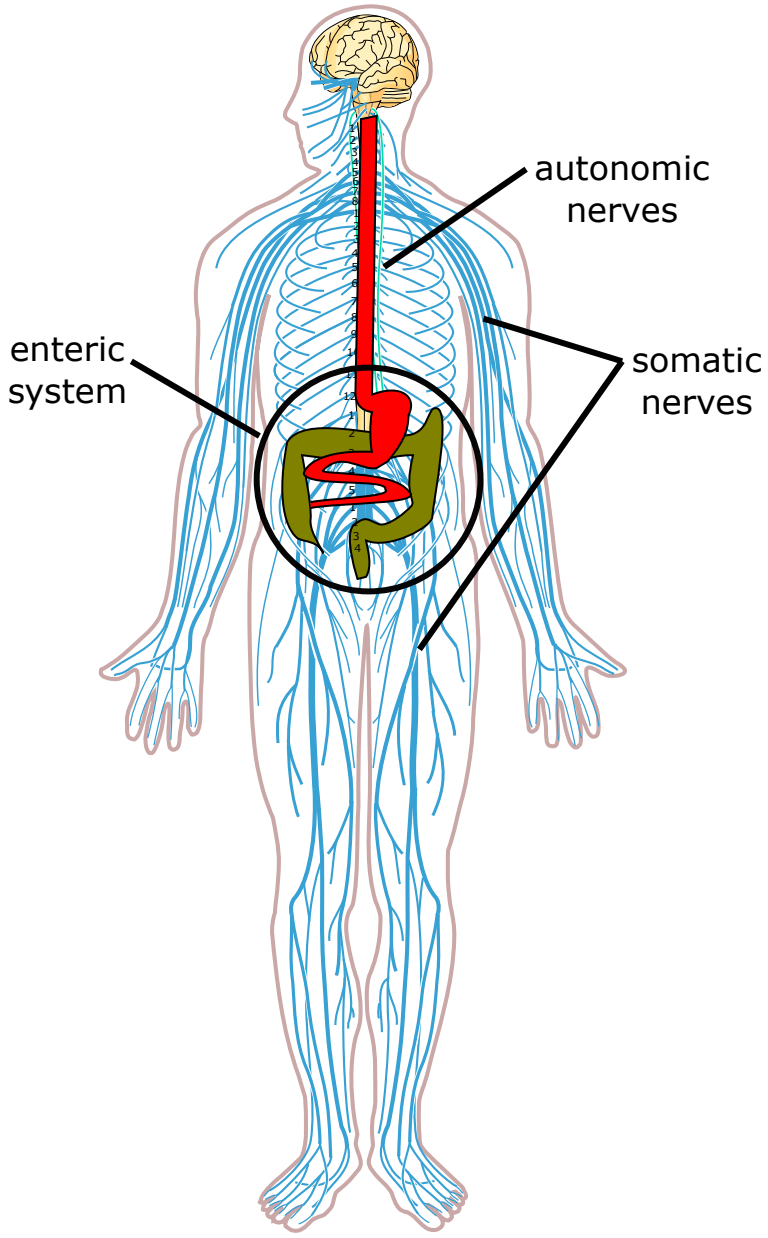


Figure 2.1: Drawing of the primary compartments of the peripheral nervous system: the somatic nerves enabling voluntary control of muscles, and the autonomic nervous system composed of the sympathetic, parasympathetic and enteric nervous systems. Adapted from an SVG drawing on `https://commons.wikimedia.org`. Original drawing by users Jmarchn and Medium69 as unlabelled drawing of the nervous system. License CC-A-SA 4.0.

### 2.2.1 Somatic nervous System

The somatic nervous system's function is to relay signals to and from the central nervous system from muscles and sensory organs and therefore carries out no processing of information, with the notable exception of the reflex pathways. When information travels in the efferent direction, commands from the brain are sent down into the spinal cord where additional processing occurs that results in the activation of lower motor neurons in its ventral horn [7]. These neurons then relay this information directly to their target muscle by way of their axon. Stimulators that focus on this system use interfaces to excite these axons using electrical currents. In this way injuries to the CNS such as spinal cord injuries can be circumvented by providing a means to stimulate muscles which are no longer connected to the central nervous system. For information travelling in the afferent direction, sensory receptors located in the skin such as the different pressure-sensing corpuscles, or in the muscle such as the muscle spindles, relay information back to the CNS via the dorsal root ganglions of the spinal cord. This provides the means to emulate output from disconnected or missing sensory organs by directly stimulating nerves in the afferent direction, provided that the stimulation complies with the encoding of information understood by the brain [8]. Related therapies generally fall under the purview of FES, with experimental work being carried out to improve the precision of motor control derived from stimulation [9], or to develop stimulation protocols to provide sensory input from artificial limbs [10]. A notable success in peripheral sensory stimulators has been the development of cochlear prostheses that enable deafened patients with a functional cochlea to hear again, or for the first time in cases of congenital deafness [11].

This success is notable for several reasons important in understanding the context of the selectivity problem as mentioned in section 1. The cochlea's structure is utilized by cochlear implants as shown in figure 2.2: when sound is transferred by vibration from the tympanum to the cochlea by the bones of the inner ear, the frequency components of input sounds are separated in space by the cochlea [13], and sensitive hairs placed along it are stimulated by vibrations received by the tympanum. By emulating the action of the cochlea and separating recorded sounds into frequency bands, a neural interface featuring electrodes spread along its

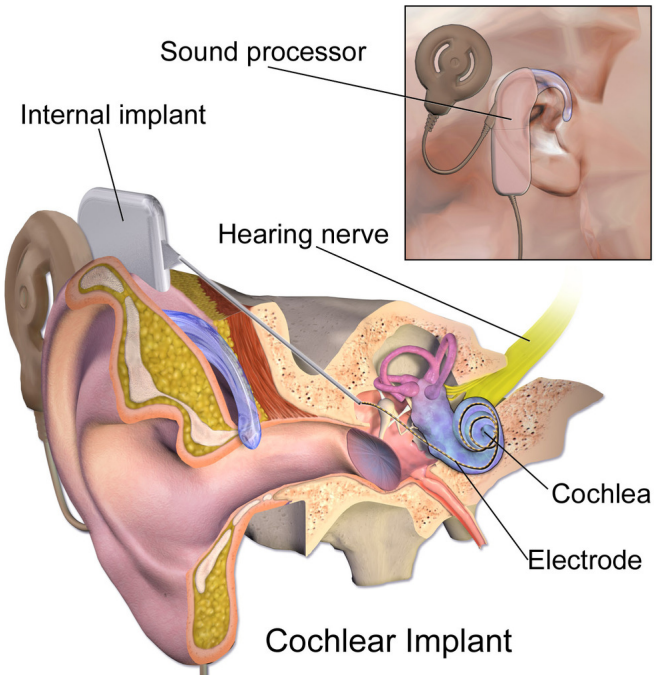


Figure 2.2: Drawing of a cochlear implant showing the structure of the ear and the cochlea into which the stimulating electrode is implanted. This figure appears in [12][1].

length and inserted into the cochlea can then directly utilize this structure by electrically stimulating at the location corresponding to the expected frequency band in the cochlea. While cochlear implants cannot yet restore hearing to natural levels due to limitations in how spatially selective stimulation can be, the brain's flexibility can in this case cover for the nonidealities and allow patients to follow spoken conversation, amongst other tasks they would have otherwise been incapable of doing. The situation isn't as favorable in other neural targets for a number of reasons ranging from the scales involved, for example in the retina [14], to the inherent variability in the distribution of neural pathways from individual to individual, as can be observed in somatic nerves targeted for FES, such as the common peroneal nerve for foot drop stimulators [15]. In these cases, a lack in stimulation selectivity hampers these devices' ability to restore corresponding function. To give an example, the state of the art in commercially available retinal implants today is only able to replace vision with a grid of 10 by 6 points [16]. This is sufficient for slow reading of letters, but not for driving for example.

[1]Image published on Wikipedia "Cochlear Implant" page. License CC-BY 3.0.

### 2.2.2 Autonomic Nervous System

The autonomic nervous system encompasses the sympathetic, parasympathetic and enteric nervous systems, and relays information to and from the central nervous system to the body's organs as shown in figure 2.3. The precise nature of this nervous system's control over the body's organs is still under active research [17]. A key difference between this system and the somatic nervous system is the presence of nerve ganglions distributed throughout the body. These ganglions participate in the transmission and processing of neural information by use of different neurotransmitters, making the autonomic nervous system far more than a collection of relays. Seeing the evidence for autonomic control of the heart, lungs, liver, stomach, kidneys, spleen and gut it is natural to think that modulating the activity of either or both of these systems at specific locations could have potentially therapeutic effects when the corresponding organs are not functioning in a healthy way.

This is precisely the approach of more recent commercially available stimulators such as the vagus nerve stimulator shown in figure 2.4. Vagus nerve stimulation is currently used for epilepsy and depression [19] and is being explored for heart disease amongst other treatments [20]. Note that despite the range of conditions for which VNS has been approved, as well as the variety in terms of the potential end targets such as the brain, the stomach and the heart targeted by therapy, the implantation location for the stimulator's electrodes are all on the same nerve trunk, with some applications using the exact same electrode positioning [20]. This is proof that the information travelling along the vagus nerve has a profound effect both in the afferent and efferent directions. Strikingly, vagotomies that specifically involve the interruption of such an information highway are already well-known procedures with proven therapeutic effects [21], underlining the fact that both stimulation and inhibition of information transfer can have therapeutic effects. It should be noted however, that the irreversible nature of vagotomies will likely make them obsolete once reversible and reliable means to interrupt conduction through the vagus nerve are shown to be effective [2].

[2] As of this writing on the 12th of November 2020, it is also interesting to note that VNS is also being investigated for ventilator-induced lung injury [22], a number of which are likely to result from the wide-ranging use of ventilators to treat SARS-CoV-2 infections. In this case vagotomies and by extension any form of vagus block can make the injury worse, possibly due to off-target effects.

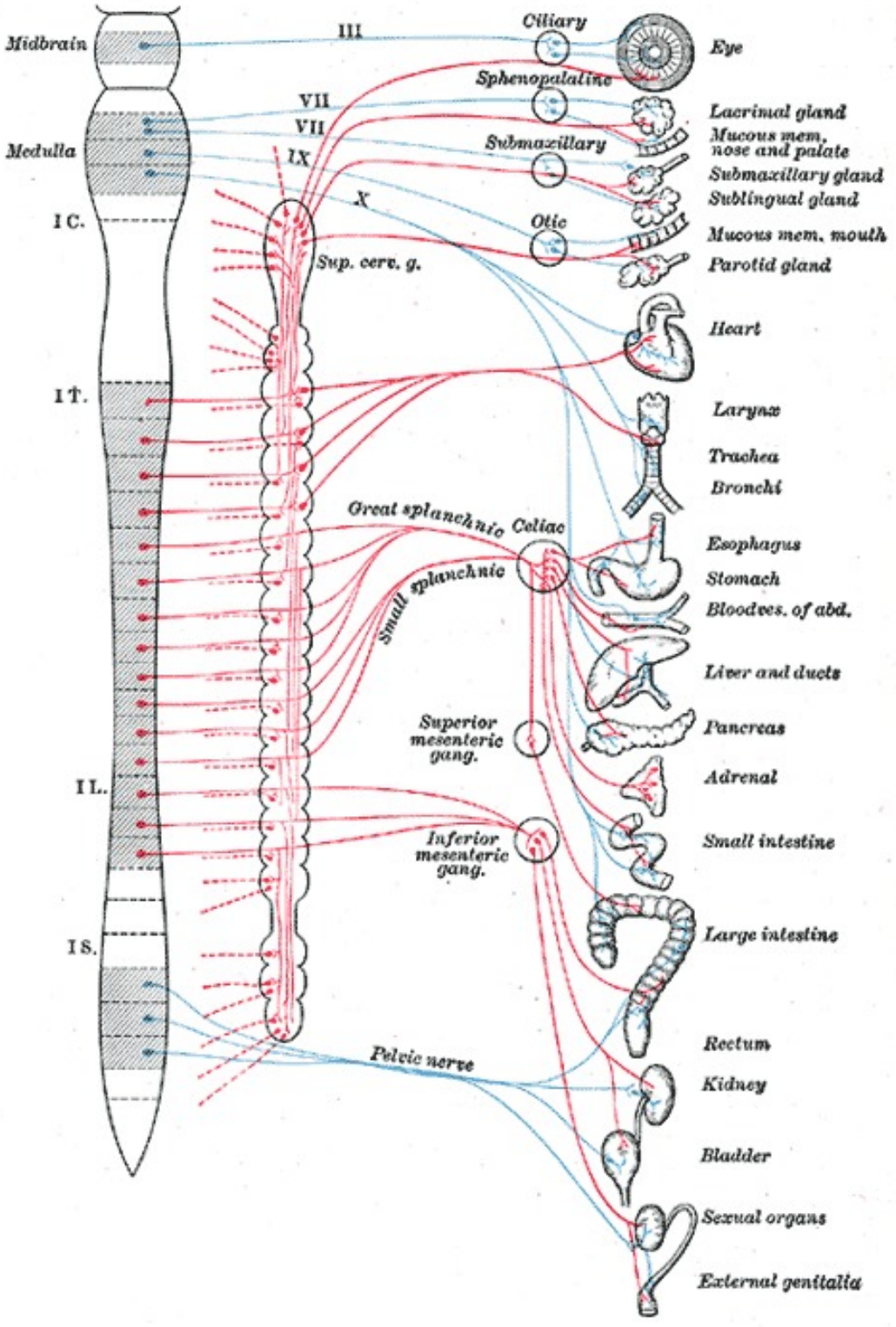


Figure 2.3: A drawing of the structure and connections of the autonomous nervous system showing nerve connections from different segments of the spinal cord through ganglions to the body's internal organs. Original by Henry Gray (1918). This figure appears in [18].

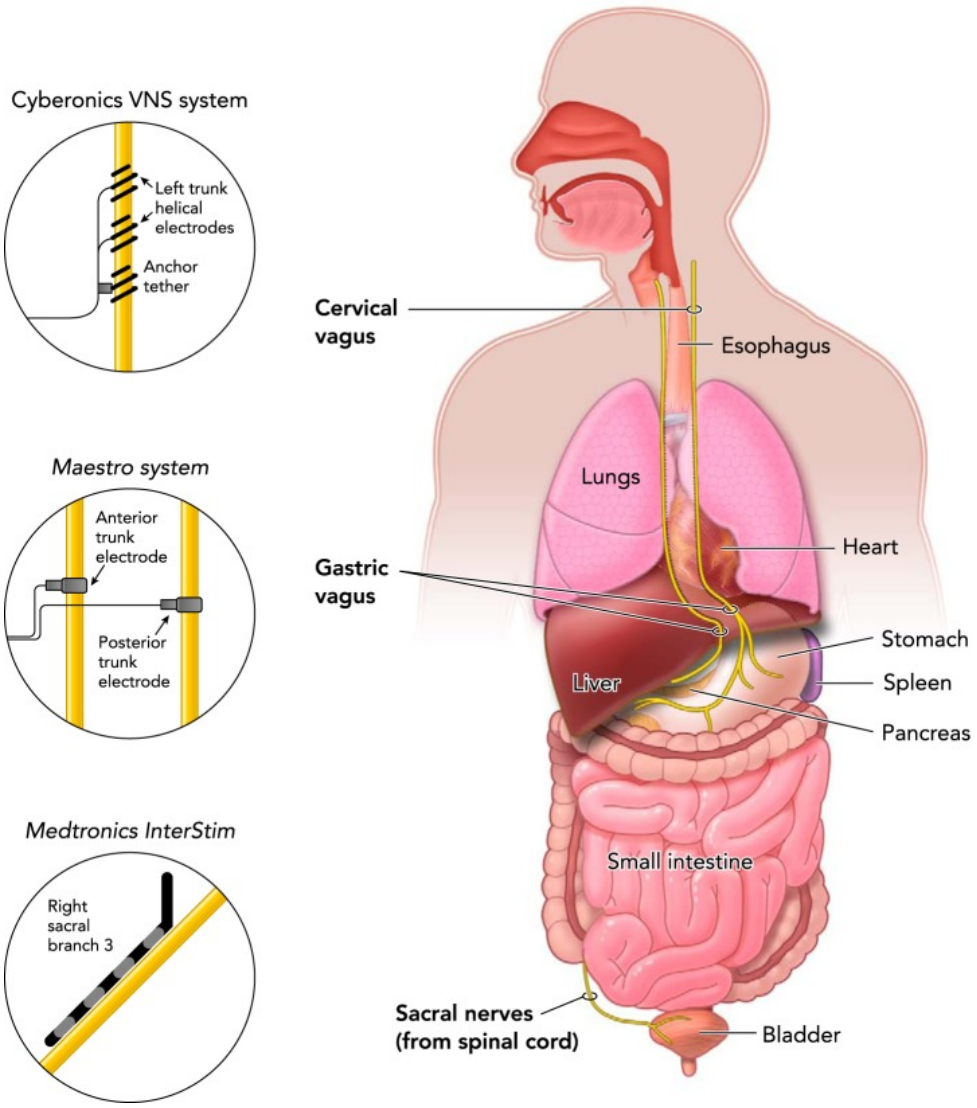


Figure 2.4: Drawing showing implant locations for vagus nerve-related therapies with three different commercially available systems. Applications include treatment for epilepsy and depression, obesity and urinary incontinence. This figure appears in [20].

### 2.2.3 Enteric Nervous System

The enteric nervous system is a subdivision of the autonomous nervous system, however it carries out enough processing on its own and is sufficiently independent from the other systems to be considered a system in itself. The enteric nervous system regulates the activity of the gastro-intestinal tract, for example synchronising the muscular contractions needed for intestinal transit [23]. There has been mounting evidence of the relationship between the enteric nervous system and the immune system [24], leading to potential stimulation-based therapies targeting the enteric nervous system not only for gut motility disorders [25], [26], but also

immune disorders [27]. Some stimulators have been approved to treat certain conditions such as gastroparesis, obesity and diabetes [28]. Overall the system is the subject of much active research as we learn more about its functions, pathophysiology, and potential therapeutic stimulation targets.

## 2.3 Nerve Microstructure and Excitability

The reason why nerves are excitable can be found in their microstructure, which has fundamental impact on how the selectivity problem can be addressed.

### 2.3.1 The voltage-gated ion channel

At the heart of nerve excitability is the voltage-gated ion channel. These transmembrane proteins serve as voltage-controlled valves that allow select ions to traverse the neuron membrane when open [29], and were made known most famously by Hodgkin and Huxley's work on the squid giant axon [30]. The voltage-sensing component of these transmembrane proteins can be activated by changes in the transmembrane potential, in this case by depolarisation of the membrane of neural cells from a negative resting state potential to a more positive potential. The resting state potential is determined by the tightly regulated concentrations of ions inside and outside of the cell [31], in a way that ensures consistent current flow whenever the channels are opened. It is this voltage-gated current flow that makes nerve cell membranes, and by extension nerves themselves, "excitable".

The action potential is the result of the dynamic gating of ion channels in nerve cell membranes. After an initial depolarisation started by neurotransmitter capture at a dendrite [32] or more importantly in the context of this work, an electric field affecting the cell membrane, sodium channels open. As sodium is found in higher concentrations as $Na^+$ outside of the cell, sodium enters the cell. It is a cation, therefore the potential inside of the cell is raised relative to the outside. In the resting state, the inside of the cell is kept at -70 mV relative to the

outside [33]. This means that sodium influx depolarises the membrane nearer to 0 mV. This is turns opens more sodium channels, increasing the flow. A second component of the sodium channel, called the inactivation gate, then closes it after some time [34], allowing the membrane to be repolarized by a second channel which opens when it is significantly depolarized, the potassium channel. As potassium is a cation but its concentration inside the cell is greater than outside, its flow out of the cell repolarizes the membrane to a negative potential and restores it to the resting state. The inactivation gate of the sodium ion channel prevents it from reopening too quickly, thereby leading to the absolute and relative refractory period for nerves, during which it is not possible or harder, respectively, to get a nerve to generate an action potential immediately after the last [35]. A typical shape for an action potential waveform as recorded when measuring the potential difference between the inside and outside of the nerve cell is shown in figure 2.5.

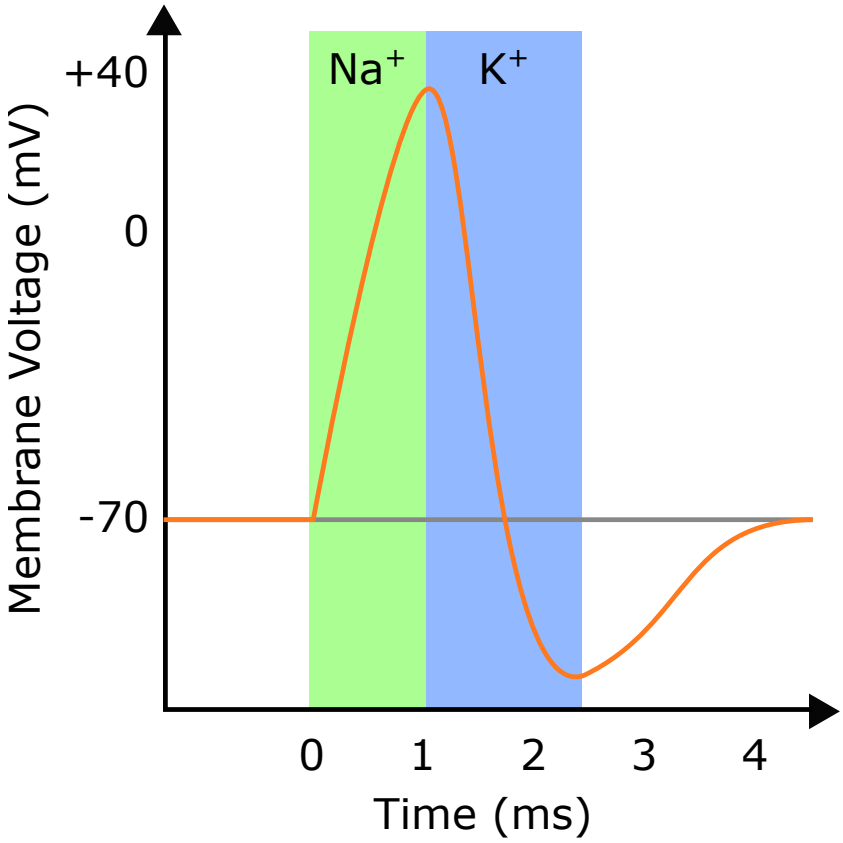


Figure 2.5: Drawing of an action potential, with block regions showing approximate activation times for sodium and potassium channels. Action potential shapes vary greatly depending on species and cell type. Adapted from [36].[3].

[3]Original author of the picture was user Chris 73, license CC-BY-SA 3.0.

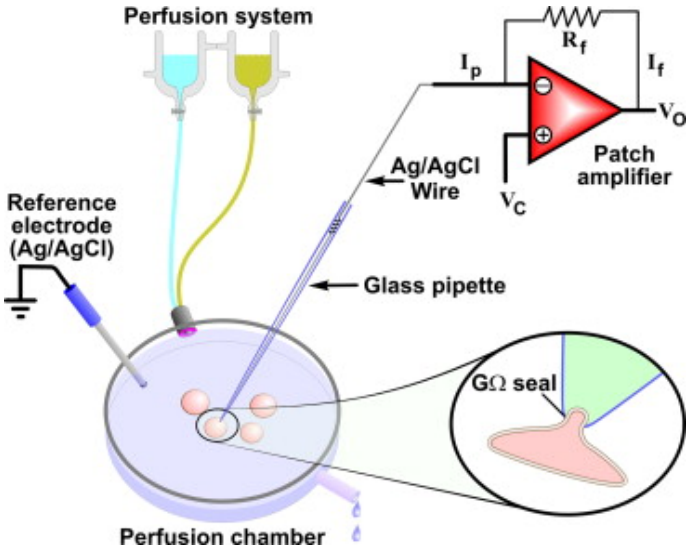


Figure 2.6: Schematic of a patch clamp setup similar to the one used in Hodgkin and Huxley's work [30]. This figure appears in [37].

Hodgkin and Huxley's work explains in a straightforward manner how action potentials can be generated in patch clamp recording and stimulation where the setup gives direct access to the potential inside a neuron as shown in figure 2.6. In this way the transmembrane potential can be directly manipulated, and complete control over when the nerve is made to fire can be achieved. However, this is not translatable to clinical application and does not explain how clinical electrodes, which do not have access to the inside of nerve cells, are able to excite them. A formalism for explaining the action of extracellular potentials on nerve was created by Rattay [38], taking into account the contributions of the different tissues encasing the neurons themselves.

### 2.3.2 Formalism for the peripheral nerve cable model

The representation of neuron membranes as distributed resistance-capacitance compartments within a homogeneous volume conductor as shown in figure 2.7 was a key step for the understanding of extracellular stimulation. Voltage-gated ion channels are represented by variable conductances in series with ion-specific electromotive forces. At equilibrium these forces are determined by the Goldman-Hodgkin-Katz equation 2.1, where R, T and F are the ideal gas constant, temperature in Kelvin and Faraday's constant, $M_i$ is each cation, $A_j$ is each anion,

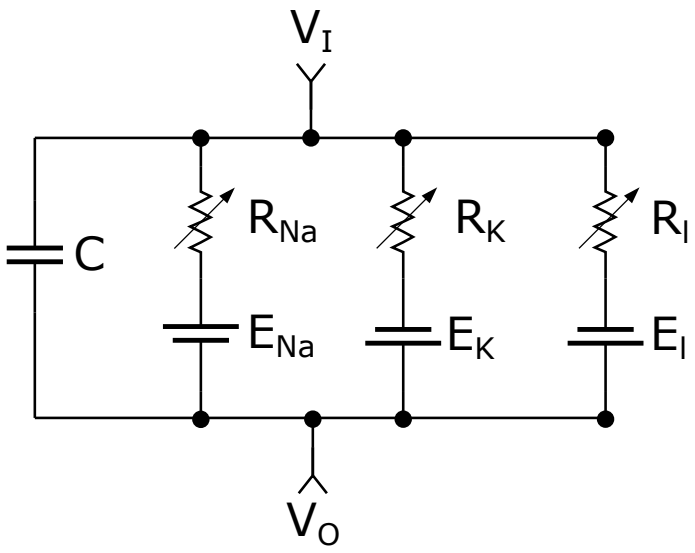


Figure 2.7: Unit element used for the electrical simulation of nerve membranes. Variable conductances due to voltage-gated ion channels are shown using variable resistors for sodium and potassium, and a leak resistance representing the leak conductance of the membrane [30]. Each ionic conductance is associated to a corresponding electromotive force determined by the Nernst equation.

and $P_{ion}$ is the selectivity for each specific ion across the membrane, determined by how well each ion channel type filters out the ions they are not designed to let through. This equation allows the calculation of the potential difference between two aqueous compartments with different ionic concentrations [39] and is derived from the Nernst equation for transmembrane potential when taking into account non-zero ionic flows across the membrane due to active ion pumps. The flow of current between the inside and outside of the cell is thus determined by the resistance of the ion channels and the potential difference for the ion in question. Finally, the thin membrane itself acts as a parallel capacitance due to its thin walls and its insulating nature, being made out of fats.

$$E_m = \frac{RT}{F} \ln \frac{\sum_i^n P_{M_i^+}[M_i^+]_{out} + \sum_i^m P_{A_j^-}[A_j^-]_{in}}{\sum_i^n P_{M_i^+}[M_i^+]_{in} + \sum_i^m P_{A_j^-}[A_j^-]_{out}} \tag{2.1}$$

In patch clamp recordings, a positive current into the nerve will depolarize the membrane and cause the nerve to fire if sufficiently strong. When stimulating with extracellular electrodes, negative currents can be used to depolarize the membrane and cause the nerve to fire, however positive currents can also be used, despite being less effective, and strong negative currents

can have an inhibitory effect. These apparently contradictory observations can be explained by using the activation function developed by Rattay [38], which serves to predict the effect of extracellular potentials on the transmembrane voltage at a specific location of the affected neuron. The activation function described in equation 2.2 takes into account the contribution of currents both external and internal to the cell. These can pass through transmembrane resistances used to model voltage gated ion channels or leakage channels, or charge the membrane capacitance thereby changing the transmembrane potential. It should be noted that the activation function can be calculated without any prior knowledge of ion channel dynamics, as it calculates the derivative of the membrane potential from the resting state when a stimulus is applied externally, before any voltage-gated channels have changed state, where the integer n points to the index of the element we are considering as part of a lumped-sum model of the membrane, $V_e$ is the extracellular potential and $R$ is the intra-axonal resistance. The dots in equation 2.2 represent the terms that must be added when the compartment of index $n$ being considered has more than two neighbours, such as when an axon branches or where the soma of a neuron connects to multiple dendrites.

$$f_n = [\frac{V_{e,n-1} - V_{e,n}}{R_{n-1}/2 + R_n/2} + \frac{V_{e,n+1} - V_{e,n}}{R_{n+1}/2 + R_n/2} + ...]/C_{m,n} \tag{2.2}$$

The activation function conveys the important concept in extracellular stimulation of nerves that stimulation depends on a gradient of potential along the axis of the axon itself. This is why the intra-axonal resistance is determinant for the activation of the nerve. In the simplifying case of a long homogeneous axon such as with an unmyelinated fiber, the activation function is proportional to the second derivative of the extracellular potential relative to the axon axis [38]. The function can be used together with detailed models of both neuroanatomy and electrode geometry to predict the effect of extracellular potentials on the resting state of the neuron. In turn this information can be used to develop more selective stimulation electrodes [40], [41].

Different parts of the neural cell are more or less excitable [38]. In the somatic peripheral nervous system the cell body of neurons containing their nucleus is called the soma and is located in the spinal cord for primary motor neurons and in the dorsal root ganglions for primary sensory

neurons [7]. The axon is more excitable than the soma due to the concentration of voltage-gated ion channels in the membrane, and stretches from the cell body all the way to the end organ, for example a muscle in the leg. This makes the axon far more accessible than the soma, and a more effective stimulation target, which explains why clinical stimulation electrodes all act on axons in some way by interfacing with the nerve somewhere along its path to its destination. For this reason the analysis of nerve tissue structures that surround axons is important to understand stimulation selectivity.

### 2.3.3 Nerve microstructure

The nerves of the peripheral nervous system are highly heterogeneous structures, and also highly organized. Axons are bundled in discrete, functional units called fascicles which can divide or merge along the length of a nerve [42], [43]. Fascicles organize nerves in a functional manner - a fascicle in the somatic nervous system will contain sensory fibers leading to receptors on a contiguous area of skin, or motor units innervating a single muscle target [44]. This functional organization is underpinned by structural compartmentalisation of the nerve, shown in figure 2.8. Axons are bundled together in endoneurium, which is itself encased in a membrane of connective tissue, the perineurium. The fascicles, vasculature and additional connective tissue are encased in epineurium [45].

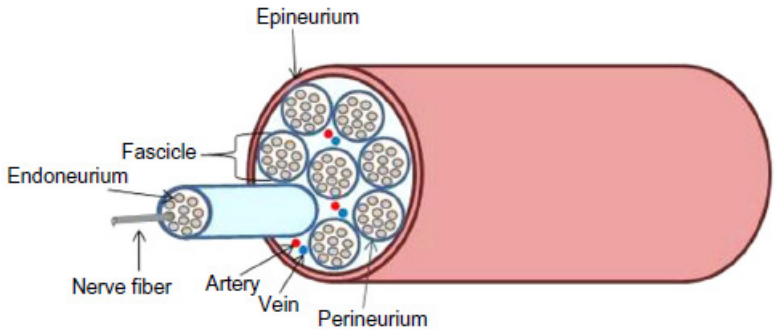


Figure 2.8: Drawing of nerve microstructure detailing the different connective tissue layers, vascularization and fascicular organization. This figure appears in [45].

Each of these tissues has specific electrical properties [46] which influence the way fundamentally *extracellular* electrodes can be used to excite the axons contained within. In addition, depending

on their diameter and function, nerve fibres have different degrees of myelination. Myelin is a structure borne out of Schwann cells surrounding portions of axons with an electrically isolating membrane. Electrically speaking this significantly reduces the membrane capacitance where myelin is located [47]. Gaps between sections of myelin are called nodes of Ranvier [48] and concentrate ion channels normally found spread out along the membrane of unmyelinated nerves. The reduction in membrane capacitance and concentration of ion exchange mechanisms at the nodes of Ranvier results in the saltatory conduction process where the action potential jumps from node to node, as shown in figure 2.9, as opposed to conduction along unmyelinated fibers. Conversely for myelinated fibers extraneural electrodes can only significantly influence the transmembrane potential at nodes of Ranvier, therefore activation of these fibers is done preferentially at these locations by extraneural electrodes. As the length of sections of myelin is proportional to nerve fiber diameter, the distance between each Node of Ranvier increases with fiber diameter. This causes conduction speed to increase with fiber diameter for myelinated axons [49]. Fiber diameter also influences conduction speed in unmyelinated axons but to a lesser degree; a general rule is that for unmyelinated axons conduction speed will be proportional to the square root of the fiber diameter [50], such that conduction of action potentials is only advantageous in terms of speed for small fibers, as shown in figure 2.10. Interestingly enough, it is at the crossover point of the two curves that the transition is seen for unmyelinated fibers to myelinated fibers in nature.

### 2.3.4 Reversal of physiological recruitment order when using electrodes

Naturally, when carrying out a task requiring muscular action, the brain recruits fatigue-resistant motor units first if not much strength is required. This is done by recruiting 'slow twitch' motor units that contract slowly but have high fatigue resistance. When high strength is required the brain will recruit both 'slow-twitch' and 'fast-twitch' motor units. 'Fast-twitch' motor units contract much faster and with much higher strength, at the cost of fatiguing much faster [51]. This physiological order of recruitment is reversed when using electrodes to elec-

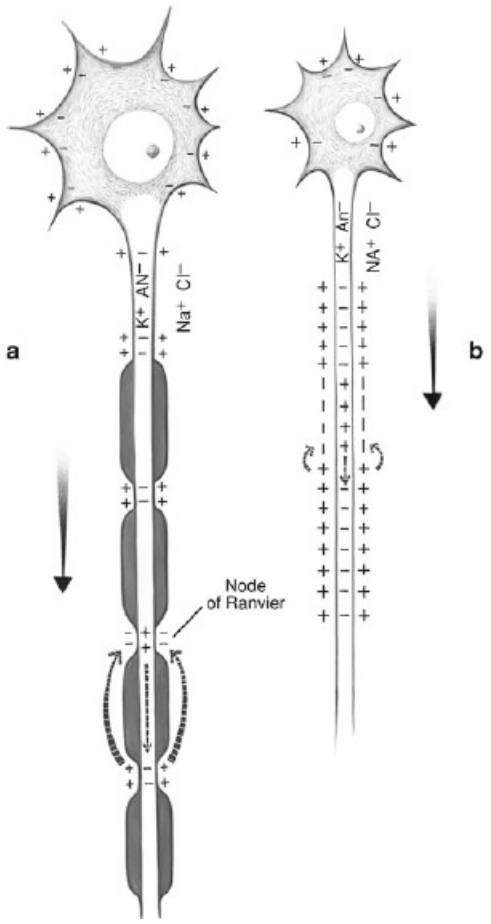


Figure 2.9: (a) Action potential conduction along a myelinated axon. Ion exchange is only carried out at the Nodes of Ranvier between sections of myelin. (b) Action potential conduction along an unmyelinated axon. Ion exchange is carried out along the entire length of the axon. This figure appears in [7].

trically stimulate motor neurons, causing premature fatigue in patients using FES implants to recover function after a neurological injury such as a spinal cord injury (SCI) [52]. The underlying reason for this reversal is that fast-twitch motor units are controlled by nerve fibers with large axonal diameters compared to other fibers. This makes them more sensitive to applied extracellular electric fields [38], and therefore they can be made to fire at lower stimulation intensities than 'slow-twitch' motor neurons. Finding means to restore physiological recruitment order when using FES stimulators is an active topic in research.

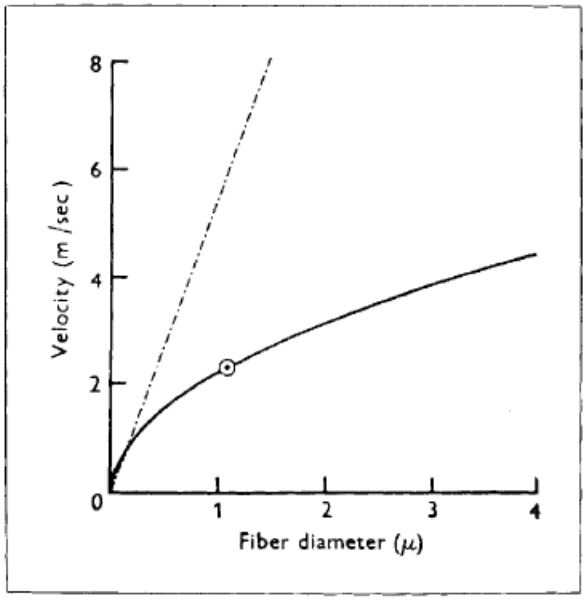


Figure 2.10: Graph showing theoretical action potential propagation speeds for unmyelinated (solid line) and myelinated (dashed line) fibers. Propagation speed in unmyelinated fibers is proportional to the square root of the fiber diameter, while it is directly proportional to the fiber diameter for myelinated axons. This figure appears in [49].

## 2.4 Peripheral nerve electrode types

Many electrodes have been designed for stimulation of the peripheral nervous system, and reviews have regularly been published about this topic - see [53], [54] for good and up to date reviews. Briefly, PNS stimulation electrodes can be placed on a scale of invasiveness and selectivity, where higher invasiveness generally leads to higher selectivity and therefore better control over which part of the implanted nerve is stimulated when electrical current is injected into the tissue through one or more of the stimulation electrode's contacts. Such a scale is shown in figure 2.11.

Higher selectivity is desirable because it enables a reduction of off-target activation of nerve fibers that often leads to side-effects, such as in the case of vagus stimulation [6]. However, it also leads to worse long-term outcomes for the nerve tissue as the foreign body response is often stronger, leading to chronic inflammation and tissue damage [53], [58], [59]. Electrodes types are described in the following list:

- Cuff electrodes are generally considered to be the least selective due to having their

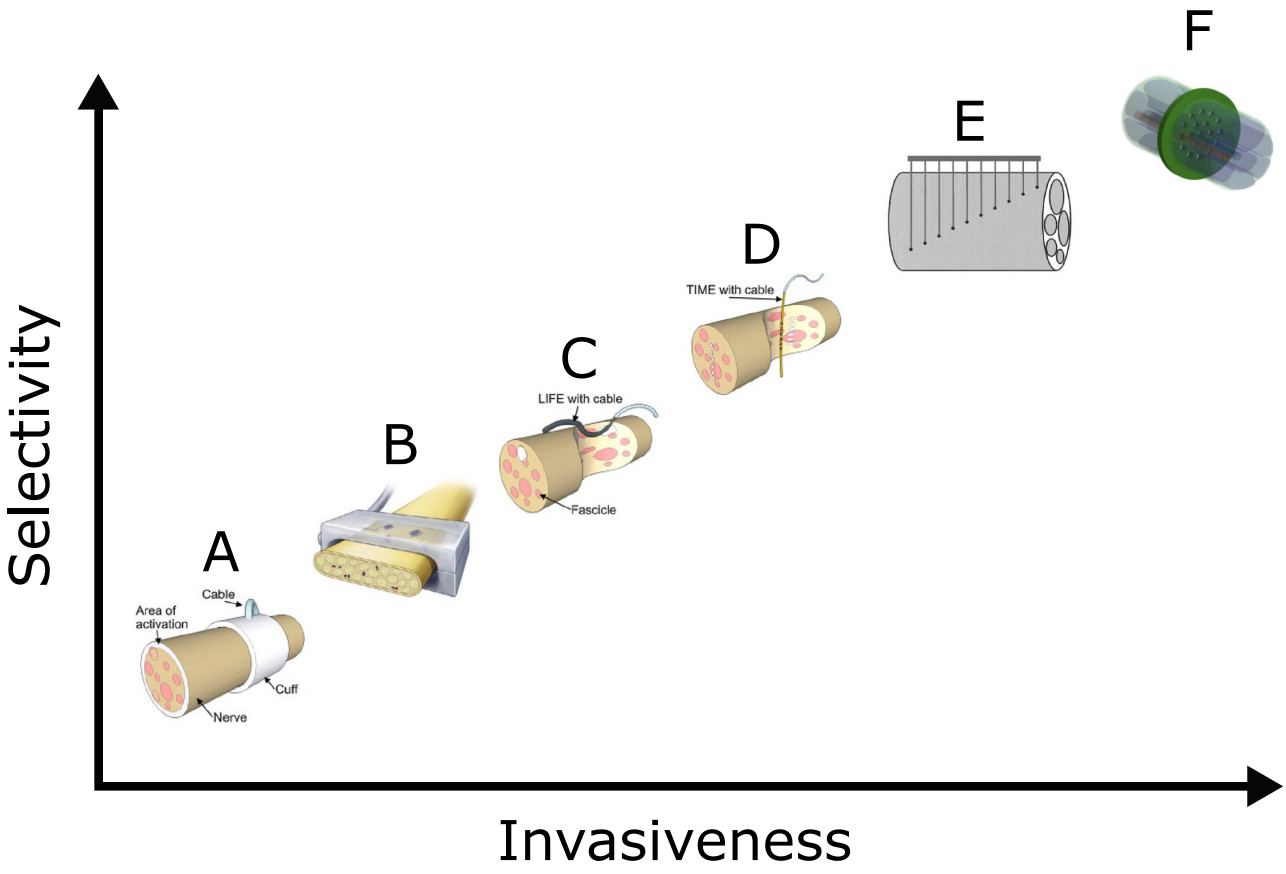


Figure 2.11: Graph showing the selectivity and invasiveness relationship for different stimulation and recording electrodes used in the peripheral nervous system. (A): Cuff electrode. (B): Flat Interface Nerve Electrode (FINE). (C): Longitudinal Inter-Fascicular Electrode (LIFE). (D): Transverse Intrafascicular Mutichannel Electrode (TIME). (E): Utah Slanted Electrode Array (USEA). (F): Sieve or regenerative electrode. A, C and D are from [55], B is from [56], E is from [57], F is from [54].

contacts outside of the nerve tissue. It is also this property that makes them the least invasive and the most reliable over long periods of implantation [60]–[62].

- Flat Interface Nerve Electrodes (FINEs) are extraneural electrodes like the cuff that reshape the nerve to enable higher selectivity when activating 'deep' fascicles compared to the cylindrical cuff. Studies using FINE electrodes over chronic timescales have shown there is a limit to how much the nerve can be reshaped before damage occurs, likely as a result of compression injury or disruption of the nerve blood supply [63].

- Longitudinal Inter-fascicular Electrodes (LIFEs) weave a polyamide ribbon with platinum electrode contacts inside of the nerve, penetrating the perineurium and epineurium but not the endoneurium. Chronic experiments indicate that implants cause chronic, albeit

very localized, inflammation [64]. Additional refinements and further studies are likely to be needed before this type of electrode is approved for human use.

- Transverse Intrafascicular Mutichannel Electrodes (TIMEs) are thin ribbon multichannel electrodes inserted transversally into the nerve. Studies indicate a high level of selectivity and chronic studies indicate good stability [65], however few studies have been conducted and the electrode has been known to cause issues with micromotion resulting from pulling on the lead.

- Utah Slanted Electrode Arrays (USEAs) are arrays of sharp insulated electrodes with an uninsulated tip inserted into the nerve much like TIMEs. They are typically arranged in a square with different rows having a different length to access as much of the nerve cross section as possible with individual electrodes. Chronic implantation evidence has not yet shown they are suitable for long-term implantation, with issues related to stability of signals and the amount of nerve tissue inflammation they cause [53].

- Sieve electrodes or more generally regenerative electrodes are electrode arrays which require the cutting and subsequent regeneration of nerves through the interface in order to establish interfaces very close to the nerve fibers proper. They have unparalleled selectivity[66] however are the most invasive due to their requirement of nerve regeneration. There is evidence that regeneration of the nerve, while providing a very selective interface that has successfully been used for long time scales, does not lead to complete regeneration of the nerve when compared to a healthy specimen[67], [68].

In the context of this work, the goal is to provide a stimulation protocol which is compatible with existing electrodes that have already been approved for human use, as this is likely to lead to more impact and direct improvement of existing stimulation therapies. Many of these therapies use cuff electrodes as this type of electrode has been shown to be the most robust and reliable over time [61]. There is also evidence that this electrode's initially poor stimulation selectivity can be improved [53], and novel stimulation protocols can further enhance this spatial selectivity with functional selectivity, the concept that electrodes can selectively stimulate one nerve target over another, rather than a specific nerve region. In this regard the cuff electrode seems the

most appropriate choice as it stands to have the most improvement in terms of selectivity from a different stimulation protocol, while the same will likely not be able to improve the drawbacks of the other designs which are related to the long-term reaction of the body to the implant. For this reason the work focuses on improving the selectivity of cuff and potentially FINE electrodes as they are both extraneural and well-tolerated by the body.

## 2.5 Electrochemical theory for stimulation electrodes

Stimulation can only be carried out successfully by an electronic stimulator if the designer understands what kind of electrical load the electrode is like when connected to the output of such a device. Electrodes are electrically nonlinear loads, and their characteristics can change over time as a consequence of degradation [69] or fibrous encapsulation [61]. The nonlinearity stems from the electrode-electrolyte interface which is created when a metal electrode is put into contact with a conductive liquid, which is the case in all neural interfaces as extracellular fluids occupy the space between metal contacts and the tissue proper. The electrode-electrolyte interface for neural stimulators can be electrically modeled as in the model proposed by Randles [70], a representation of which is shown in figure 2.12. Randles' model was developed to explain fast reaction kinetics at electrodes subjected to short alternating current pulses and is therefore of particular interest for neural stimulators.

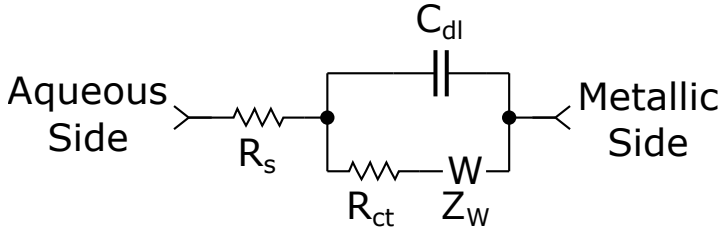


Figure 2.12: Randles circuit as an electrical model for electrode-electrolyte interfaces subjected to short pulses of alternating current. The component represented by a W is a nonlinear impedance similar to a capacitor and is also called a Warburg impedance or Constant Phase Element.

Randles' electrical model can be tied to the physical processes occurring at the electrode-electrolyte interface, namely the formation of the double-layer capacitance by positive ions in solution being attracted to electrons in the electrode itself [71], [72], as shown in figure 2.13.

Faradaic charge transfer has a corresponding resistance and capacitive element tied to the diffusion dynamics of ions near the electrode. It is particularly interesting to note that Randles tested the influence of colloids on interface kinetics and found them to slow certain reactions, which is important for neuroprosthetics as colloids are inherently present in biological systems such as the interfaces between implanted electrodes and living tissues. As many electrode characterizations are carried out in-vitro, possibly to improve the consistency of results, relatively little work has been done to study the effects of the presence of colloids at electrode-tissue interfaces.

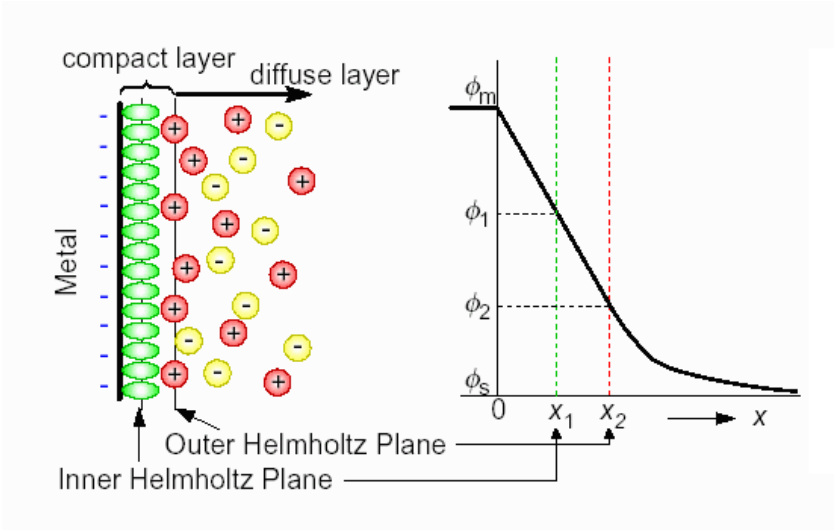


Figure 2.13: Schematic representation of the electric double layer at the electrode-electrolyte interface. Source: `https://web.nmsu.edu/~snsm/classes/chem435/Lab14/double_layer.html`

In addition to nonlinearity, the electrical characteristics of electrodes can drift over time due to two major processes: corrosion and fibrous encapsulation. The human body, and living tissues in general are aggressive environments for most metals and the susceptibility of metal implants to corrosion damage is well known [73]. In neuroprosthetics this has driven the use of platinum or platinum-iridium for stimulation electrodes as platinum is a biocompatible metal that does not readily oxidise in the body, even when current is driven through it. However, this has not completely solved the corrosion problem as high strength stimulation can still corrode platinum, and electrode leads are often made from other more corrosion-susceptible materials [74]. Furthermore, implantation of electrodes into nervous tissue leads to their progressive encapsulation as part of the immune response of the body to foreign objects [75]. The

resulting capsule is composed primarily of electrically resistive tissue and may penetrate the space between the electrodes and nerve tissue, increasing the impedance of the interface and lowering its stimulation efficacy [62].

Whether the capacitive component in the impedance of the electrode-electrolyte interface is significant depends on the polarizability of the electrode, which in turn depends on the physico-chemical properties and geometry of the interface material. Platinum electrodes are highly polarizable and also store charge using pseudocapacitive processes related to the adsorption of oxygen at their surface [76]. An example of the opposite type of electrode is the non-polarizable silver-silver chloride electrode, which does not polarize due to the fast kinetics of its oxidoreduction couple, and the relative insolubility of silver chloride in aqueous solutions. Because silver-silver chloride is not biocompatible chronically, and that platinum electrodes are standard in implantable stimulators, a stimulator circuit has to tolerate highly capacitive loads.

## 2.6 Electrode Materials

Historically the most common material used in stimulation electrodes in the PNS has been platinum, due to its biocompatibility and resistance to corrosion [77]. However, the charge injection limit of bare platinum as it is used in most commercially available electrodes is quite low [69], and this is an issue for stimulation therapies requiring high charge injection [78]. Improvement of its charge injection limit follows two strategies: roughening or coating the platinum surface to increase its charge injection limit [69], [79], or outright replacing the bulk material with another such as a conductive polymer [80] or a hydrogel [81]. Surface roughening of platinum has yielded modest improvements in performance, however few studies have investigated the stability of these improvements chronically *in-vivo*. In terms of coatings substantial improvements to the charge injection of stimulation electrodes have been measured *in-vitro* and acutely *ex-vivo* and *in-vivo*, however similarly to platinum surface roughening few studies have tested these new materials chronically. Previous attempts at using certain forms of PEDOT a.k.a. poly(3,4-ethylenedioxythiophene) or an oxidized form of platinum called platinum

black as a coating on top of platinum or gold, both promising materials electrochemically, have been hindered by their brittleness which significantly reduces the longevity of the coating once implanted [82], [83][4].

The key concept behind new material approaches for coating or bulk use is to avoid toxic species produced by electrochemical reactions at the electrodes from coming into contact with sensitive nerve tissue. In order to prevent this one can either change the material to change the electrochemistry, or move the metal-electrolyte part of the interface away from the tissue and transfer charge using a liquid interface. As the electronic circuits in a stimulator are made out of metal, either of these two approaches essentially boils down to the same scenario somewhere between the stimulator output contacts and the nerve tissue.

## 2.7 Premise for selective stimulation using combined stimulation and block

### 2.7.1 Bladder control after Spinal Cord Injury as a clinical scenario that could benefit from enhanced cuff electrode selectivity

The work of Rijkhoff et al [84] identifies the loss of bladder control after Spinal Cord Injury (SCI) as a significant loss of patient quality of life with limited pharmaceutical options for treatment. Common treatment procedures involve catheterization which can lead to damage of the lower urinary tract (LUT), urinary infections and further complications up to rehospitalization. Loss of the natural reflex pathways for continence and micturition can occur for both paraplegic and tetraplegic patients as much of the neural circuitry is located in the lumbar and sacral spine regions but also rely on communication links with circuits higher up in the spine.

As of today the condition can be treated by electrical stimulation, for example using a Finetech-Brindley stimulator [85]. Direct stimulation of the sacral nerve roots causes contraction of

[4]This being said, substantial work has been done to improve the toughness and longevity of both these materials for chronic implantation as the aforementioned sources detail

two antagonistic muscles, the bladder detrusor responsible for voiding and micturition, and the external urethral sphincter (EUS) responsible for continence, a condition called Detrusor-Sphincter-Dissynergia (DSD). When these stimulators are implanted a rhyzotomy interrupting sensory fibres proximal to the implantation site prevents the reflex responsible for DSD, however it also abolishes reflex sexual function as a side effect.

Rijkhoff et al identified several possible locations for the implantation of stimulating electrodes for this condition [84]; the intradural ventral sacral roots, extradural ventral sacral roots, the pelvic nerve and bladder wall as shown figure 2.14. Stimulating the detrusor muscle directly through the bladder wall is problematic because the resulting motion often leads to dislocation of the stimulating leads, and stimulating the pelvic nerve, while an attractive proposition in terms of neurophysiology, is made difficult by the local neuroanatomy, wherein the nerve splits early into multiple branches that are difficult to access surgically and make stimulation using a cuff impractical. Finally, the most promising implant location is identified as the extradural ventral sacral roots, however these contain fibers leading to both the detrusor and EUS. Motor fibers innervating the EUS have a larger diameter than those innervating the detrusor, and therefore stimulation of the detrusor motor units results in unavoidable activation of the EUS motor units when using conventional stimulation. Another candidate location for stimulation is the pudendal nerve with evidence that specific stimulation protocols can evoke continence or micturition [86], with evidence that either response is the result of direct activation of the detrusor or EUS muscles. Similarly to stimulating the sacral roots, the stimulation protocol resulting in bladder contraction also leads to EUS contraction. When stimulating to evoke a voiding response in cats, in the pudendal nerve bursts of 20-50 Hz monophasic stimuli can be used. A substantial improvement of the therapy could consist in ensuring this burst of stimuli only activates the detrusor muscle.

Finding a means to prevent EUS activation during the stimulation of either of these two locations could lead to more natural voiding and better clinical outcomes for SCI patients. One method to do this is to reverse the recruitment order of nerve fibers when stimulating in order to ensure that the the bladder wall can be stimulated without activating the EUS. For the purposes of explaining the design choices made for the stimulator in chapter 3 and the exper-

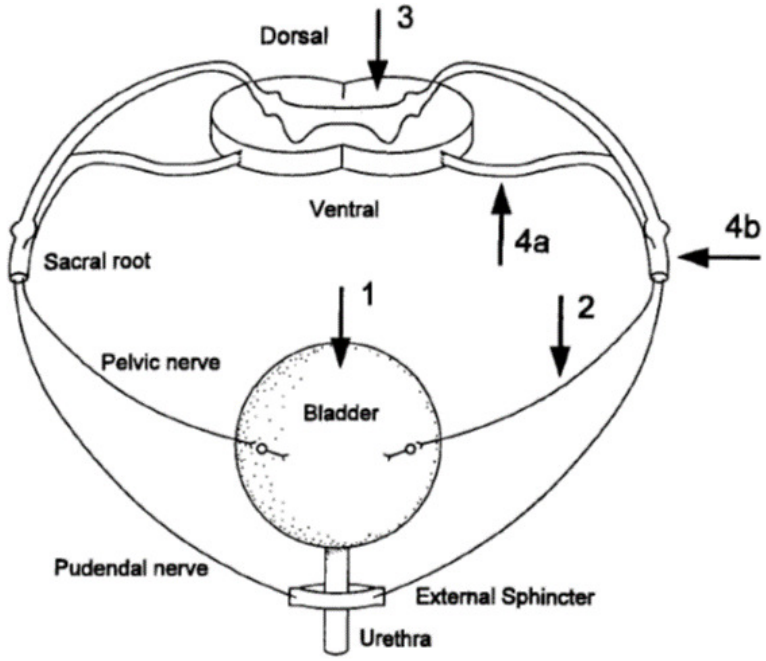


Figure 2.14: Drawing of several candidate implant locations for bladder control after SCI. This figure appears in [84].

iments in chapters 4 and 5 the application of combined block and stimulation to selectively recruit small fibers in a compound nerve will be described here. The idea of combining block and stimulation to enhance stimulation therapies for bladder control is not new, and is still the subject of active research [87]. However the specific approach here is not only to block undesired activity as in Peh et al's work, but to selectively stimulate the target organ so that antagonistic activation of other targets does not occur.

### 2.7.2 Simulation of combined block and stimulation for selective activation of small fibers in a compound nerve

Many early attempts at reversing the recruitment order for nerve fibers when using electrical stimulation relied on electrode designs and stimulation protocols that simultaneously stimulated the nerve in one location and prevented action potentials in large fibers from propagating, and this will be detailed in chapter 5. These methods all use extracellular anodic current to some extent to block large-diameter fibers. A very detailed use of the technique was described by Kuffler [88], in which selective stimulation of small myelinated fibers in frog nerve is achieved by

using two electrodes. The cathode is used to stimulate the nerve, and the current return anode is also placed on the nerve but more proximally, such that its current blocks action potentials propagating in the larger axons. The technique is very well described by a figure in his paper, reproduced as figure 2.15 here.

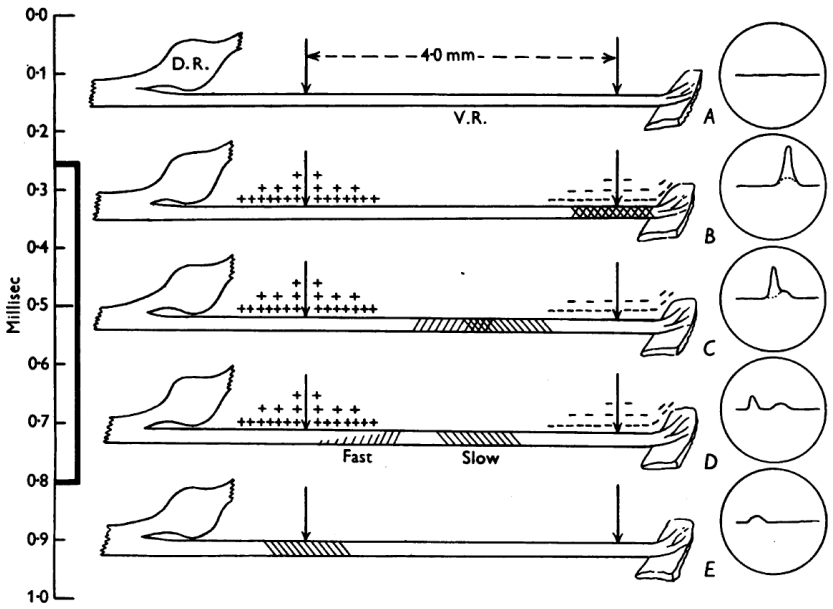


Figure 2.15: Drawing showing the stimulation technique used by Kuffler on frog motor nerves to selectively activate small nerve fibres for study. Cathodic stimulation of the nerve at the distal (right side) end generates action potentials travelling towards the proximal end (left side) at different speeds in compound nerve. Precise positioning of the anode allows selective block of fast action potentials by anodal block. This figure appears in [88].

While elegant in this case, this technique is not compatible with chronic use due to its reliance on long-pulse monophasic stimulation for DC nerve block. In chronic applications the use of short-pulse biphasic waveforms is necessary [89], as it was shown that DC block causes nerve damage even at low doses [90]. However directly replacing monophasic stimulation with biphasic stimulation would not be successful as it would interfere with the blocking action of the technique - the return cathodic phase could cause low-level activation of large fibers within the nerve and defeat the purpose of this selective stimulation protocol. A different technique for block is available however: high-frequency block as described in [91]. This block technique has been shown to be quick acting and is reversible even after substantial use, and is under active research [92]–[94]. The specifics of this technique will be described in chapter 5 however here it is important to note that it is the most promising technique for an adaptation of Kuffler's technique to mammalian nerves, that is compatible with chronic use and can be used with cuff

electrodes. The principle of the technique is slightly different from Kuffler's however, in that due to the mechanics of HFAC as detailed in chapter 5 it is necessary to first establish block distally in the nerve, and then to stimulate proximally. As in Kuffler's system fast and slow action potentials will be created at the stimulation location and propagate towards the end organ at different speeds. By timing the removal of HFAC block such that the fast-propagating action potentials are annihilated as in Kuffler's technique, and the slow-propagating potentials travel through, the same effect can be achieved: only slow-conducting fibres are then allowed to stimulate the end organ. In the case of bladder control, this would result in the selective stimulation of the detrusor muscle. This made combined stimulation and high-frequency block a promising stimulation protocol to enable selective stimulation with existing non-selective electrodes approved for human use. Furthermore, some work has been carried out in the literature to explore how high frequency block of the pudendal nerve could prevent DSD [95], [96].

To test an adaptation of Kuffler's technique using HFAC block, a simulation project was undertaken during the author's engineering master to determine whether selective stimulation of smaller motor fibres was possible in a compound nerve model [97], [98]. At the time the initial line of inquiry pointed to the African clawed toad *Xenopus Laevis* as a promising animal model to test simulation predictions and therefore simulation were carried out using the Frankenhaeuser-Huxley model for amphibian nerves [99] in the NEURON simulation environment [100].

### 2.7.3 Block thresholds in the FH model

Results from simulations first suggested that HFAC block was only effective when the stimulating signal was over a certain threshold frequency and a certain threshold amplitude. The two are related as can be seen in figure 2.16. There is a minimum frequency below which block will not be achieved no matter the stimulation signal amplitude, and vice-versa for the minimum amplitude. In a broad sense higher blocking signal frequencies will require higher amplitude to be used to achieve block, a result which has been reported in a number of papers studying

block [95], [101], [102] both with modelling and in-vivo.

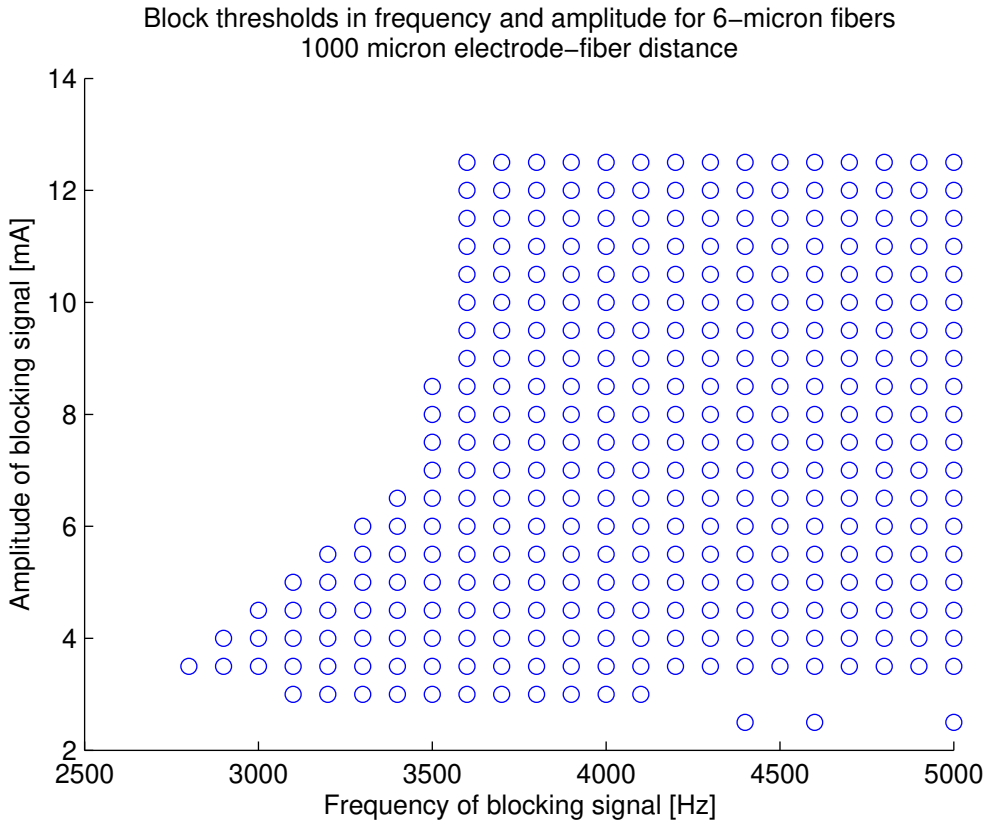


Figure 2.16: Graph showing block thresholds for high frequency block in the FH model for 6 micron diameter nerve fibres located 1000 µm away from a stimulating cuff electrode. Resolution of the simulation result is 100 Hz in the horizontal axis and 0.5 mA in the vertical axis. Circles represent parameter combinations for which nerve block was achieved. The data used to make this figure was previously published in [97].

These results provided a first-order approximation of the conditions in which HFAC block could be used for selective stimulation and recording. It is essential for the technique that all fibers in the nerve be blocked by the HFAC signal and therefore thresholds for block must be exceeded. Further work during the project established constraints on timing and positioning of the blocking and stimulation electrodes.

### 2.7.4 Relationship between inter-electrode spacing and technique selectivity

The first and principal result from the simulation work was the relationship between the distance separating the stimulation and blocking electrodes, assuming both were monopolar, and the

ability for the timed stimulation and block technique to discriminate between nerve fibres of different sizes. A minimum of 8 mm distance between electrodes was required for the timed stimulation and block technique to successfully discriminate between large and small nerve fibres with 2 µm of diameter difference. More distance only resulted in very minor gains beyond this resolution as shown figure 2.17.

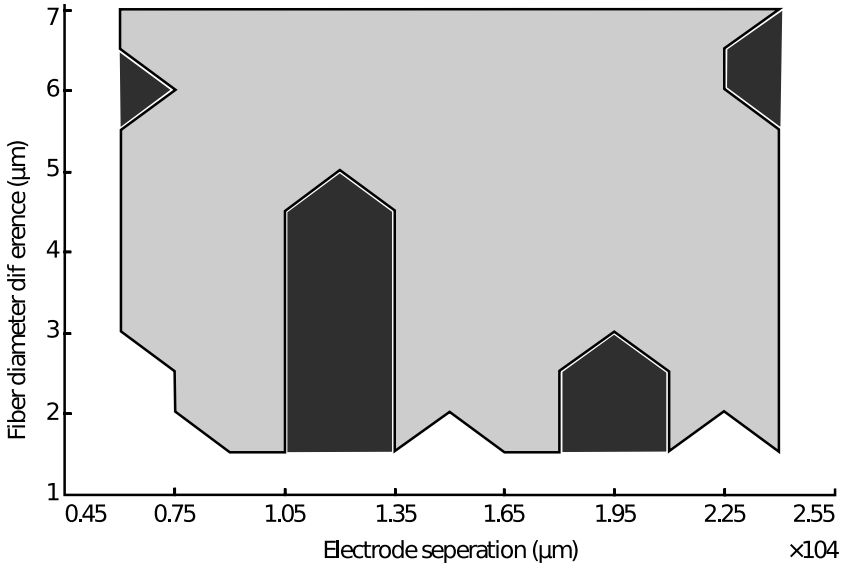


Figure 2.17: Plot showing nerve fibre diameter differences for which selective stimulation of the small nerve was successful at specific inter-electrode distances. Light gray areas represent parameter combinations for successful selective stimulation and dark gray areas for unsuccessful applications of the technique. This figure appears in [97].

These results were obtained for nerve fibres with diameters ranging from 5 to 12 µm. In the human sacral roots and pudendal nerve, fibre diameters range from 5 to 14 µm in diameter [103], with α-1 and α-2 motoneurons innervating the EUS and smaller α and β-motoneurons innervating the detrusor muscle, the former having diameters in the range 10.3-14.4 µm and the latter, 7.1-8.2 µm. This makes an application of the results from the simulation possible as nerve fibres with similar diameters were simulated in the previous work.

### 2.7.5 Compared performance of monopolar block and bipolar block

A second result from the simulation work was that monopolar block performed similarly to bipolar block in terms of frequency and amplitude thresholds. Here monopolar and bipolar block refers to the electrode configuration used to deliver block, respectively where one or two

electrodes are in proximity to the nerve tissue. In monopolar block, current return is at infinity, and in bipolar block, current flows between the two electrodes placed near the nerve.

Blocking signal frequency and amplitude were swept for monopolar and bipolar blocking electrode configurations, with combinations resulting in block identified with blue circles in figure 2.18 and 2.19.

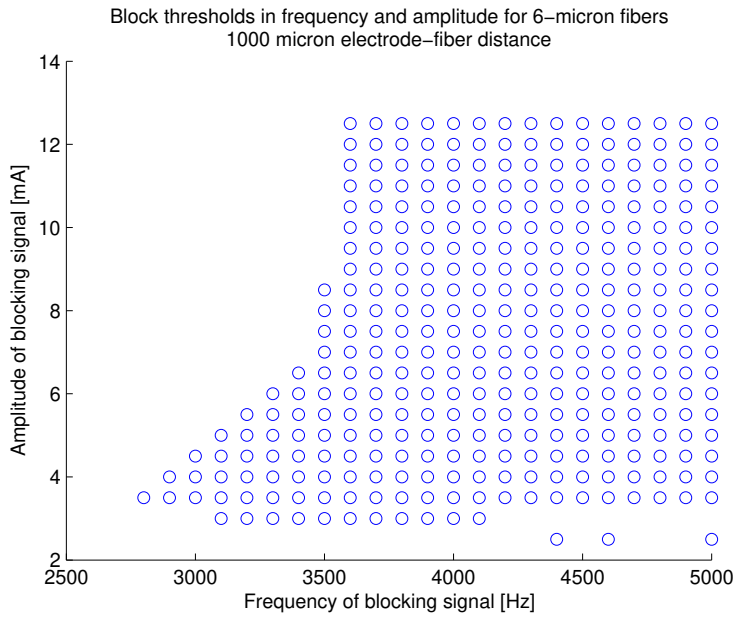


Figure 2.18: Plot showing blocking signal amplitude and frequency combinations for which block was successful in Frankenhaeuser-Huxley model simulations for monopolar blocking electrode configurations. Blue circles identify parameter combinations for which block was successful. This figure appears in [98].

Results from simulation suggest that performance for monopolar and bipolar block is similar for myelinated nerve fibres, however there are slight differences for very low diameter fibres in favor of bipolar block [98]. Furthermore, it has been reported that bipolar block can be achieved at lower amplitudes than monopolar block [104] with certain interelectrode distances for bipolar electrode configurations. Nevertheless, both monopolar and bipolar blocking electrode configurations can be used for the proposed selective stimulation technique.

### 2.7.6 Compatibility of the proposed technique with existing stimulation therapies for bladder control

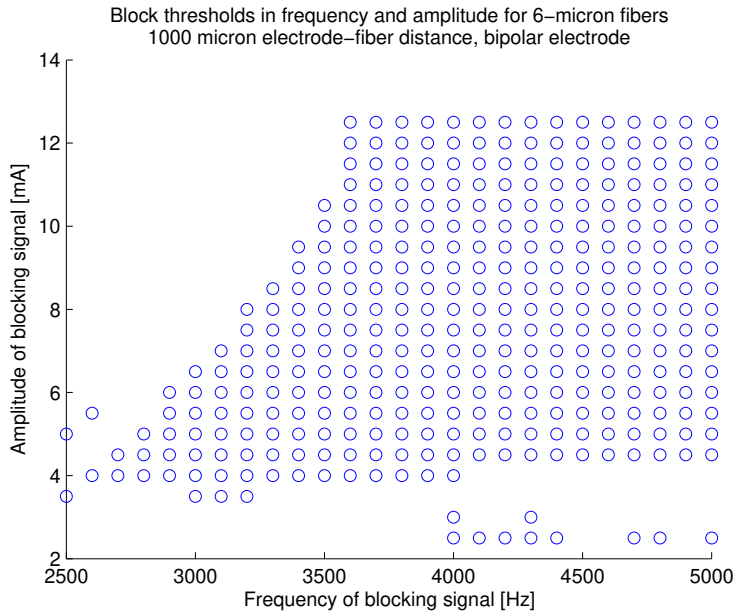


Figure 2.19: Plot showing blocking signal amplitude and frequency combinations for which block was successful in Frankenhaeuser-Huxley model simulations for bipolar blocking electrode configurations. Blue circles identify parameter combinations for which block was successful. This figure appears in [98].

Previous work on stimulation of the pudendal nerve to evoke micturition noted that 20-50 Hz stimulation produced effective results [86]. In the simulation work presented, blocking signal amplitude and frequency parameters were only considered to result in block if the onset response was shorter than 20 ms, and the selective stimulation technique was designed with this assumption in mind. Therefore, provided the model predictions are accurate the resulting selective stimulation technique using timed stimulation and block is compatible with the proposed stimulation protocol for micturition by stimulation of the pudendal nerve. Even accounting for timing overhead, it is possible to establish block, carry out selective stimulation, and wait for the nerve to return to the resting state within 50 ms, therefore making it possible to use selective stimulation at the rate of 20 Hz.

However, one remaining problem is that of the onset response itself, which activates most if not all fibers in the nerve at the start of HFAC block. While a broader overview of the underlying mechanics of HFAC block, problems with the technique and mitigating strategies are given in chapter 5, here we will emphasize the work carried out to nullify the onset response [105], [106]. The principle relies on applying near-DC currents to suppress the onset response when block is

first established using specially designed electrodes with large capacitance, and is promising as a solution to the aforementioned issue since it does not interfere with the selective stimulation protocol itself.

Finally, the simulation does not make any assumptions on the amplitude of conventional or blocking stimulation, insofar as the target fibres in the nerve are activated or blocked respectively. Precise calibration of stimulation or block amplitude is therefore not required, making the technique more robust towards variations in stimulation and block threshold over time in a clinical scenario involving fibrous encapsulation of stimulation electrodes.

Combined timed stimulation and block requires no calibration as the entire nerve is stimulated or blocked, and it is the timing between the two and the propagation speed of action potentials that determines which fibers are allowed to conduct action potentials to their terminal. This is a different approach to the precise calibration of anodic stimulation amplitude such as that used in some studies for selective stimulation using pre-pulses [107]. As such, theoretically, the technique is resistant to changes in stimulation thresholds due to fibrous encapsulation.

## 2.8 Conclusion

This chapter has laid out the context of the work both in terms of potential therapeutic targets in the peripheral nervous system that can benefit from using cuff electrodes with enhanced selectivity, but also a promising stimulation protocol that could be used to achieve this selectivity with an application for bladder control after spinal cord injury. The technique should be robust to changes in stimulation thresholds over time and therefore be useful at chronic timescales, where it could be translated to the clinic. The goal is to improve existing and future neural stimulation therapies by enhancing the selectivity of stimulation delivered using reliable and well-tolerated electrodes. The context provided here will serve as a base for many decisions made in further chapters of this thesis, such as the design of an electronic stimulator in chapter 3 and the experimental approach to determine the feasibility of using timed stimulation and block for selective stimulation in chapter 5.

# References


[1] A. L. Benabid, "Deep brain stimulation for Parkinson's disease," en, *Current Opinion in Neurobiology*, vol. 13, no. 6, pp. 696–706, Dec. 2003, ISSN: 0959-4388. DOI: 10.1016/j.conb.2003.11.001. [Online]. Available: http://www.sciencedirect.com/science/article/pii/S0959438803001739 (visited on 03/18/2020).

[2] J. A. Bamford and V. K. Mushahwar, "Intraspinal microstimulation for the recovery of function following spinal cord injury," en, in *Progress in Brain Research*, vol. 194, Elsevier, 2011, pp. 227–239, ISBN: 978-0-444-53815-4. [Online]. Available: http://linkinghub.elsevier.com/retrieve/pii/B9780444538154000042 (visited on 09/21/2015).

[3] G. H. Creasey, J. H. Grill, M. Korsten, H. S. U, R. Betz, R. Anderson, and J. Walter, "An implantable neuroprosthesis for restoring bladder and bowel control to patients with spinal cord injuries: A multicenter trial," en, *Archives of Physical Medicine and Rehabilitation*, vol. 82, no. 11, pp. 1512–1519, Nov. 2001, ISSN: 00039993. DOI: 10.1053/apmr.2001.25911. [Online]. Available: http://linkinghub.elsevier.com/retrieve/pii/S000399930128229X (visited on 09/21/2015).

[4] P. H. Peckham and J. S. Knutson, "Functional Electrical Stimulation for Neuromuscular Applications," *Annual Review of Biomedical Engineering*, vol. 7, no. 1, pp. 327–360, 2005, _eprint: https://doi.org/10.1146/annurev.bioeng.6.040803.140103. DOI: 10.1146/annurev.bioeng.6.040803.140103. [Online]. Available: https://doi.org/10.1146/annurev.bioeng.6.040803.140103 (visited on 03/05/2020).

[5] G. H. Creasey, K. L. Kilgore, D. L. Brown-Triolo, J. E. Dahlberg, P. H. Peckham, and M. W. Keith, "Reduction of Costs of Disability Using Neuroprostheses," *Assistive Technology*, vol. 12, no. 1, pp. 67–75, Jun. 2000, ISSN: 1040-0435. DOI: 10.1080/10400435.2000.10132010. [Online]. Available: https://doi.org/10.1080/10400435.2000.10132010 (visited on 01/27/2020).

[6] D. Guiraud, D. Andreu, S. Bonnet, G. Carrault, P. Couderc, A. Hagège, C. Henry, A. Hernandez, N. Karam, V. L. Rolle, P. Mabo, P. Maciejasz, C.-H. Malbert, E. Marijon, S. Maubert, C. Picq, O. Rossel, and J.-L. Bonnet, "Vagus nerve stimulation: State of the art

of stimulation and recording strategies to address autonomic function neuromodulation," en, *Journal of Neural Engineering*, vol. 13, no. 4, p. 041 002, Jun. 2016, ISSN: 1741-2552. DOI: 10.1088/1741-2560/13/4/041002. [Online]. Available: https://doi.org/10.1088%2F1741-2560%2F13%2F4%2F041002 (visited on 12/12/2019).

[7] N. L. Strominger, R. J. Demarest, and L. Laemle, *Noback's human nervous system: structure and function*, en, 7th ed. Totowa, N.J: Humana Press, 2012, OCLC: ocn778327350, ISBN: 978-1-61779-778-1.

[8] G. Chai, X. Sui, S. Li, L. He, and N. Lan, "Characterization of evoked tactile sensation in forearm amputees with transcutaneous electrical nerve stimulation," en, *Journal of Neural Engineering*, vol. 12, no. 6, p. 066 002, Sep. 2015, Publisher: IOP Publishing, ISSN: 1741-2552. DOI: 10.1088/1741-2560/12/6/066002. [Online]. Available: https://doi.org/10.1088%2F1741-2560%2F12%2F6%2F066002 (visited on 03/19/2020).

[9] K. L. Meadmore, T. A. Exell, E. Hallewell, A.-M. Hughes, C. T. Freeman, M. Kutlu, V. Benson, E. Rogers, and J. H. Burridge, "The application of precisely controlled functional electrical stimulation to the shoulder, elbow and wrist for upper limb stroke rehabilitation: A feasibility study," *Journal of NeuroEngineering and Rehabilitation*, vol. 11, no. 1, p. 105, Jun. 2014, ISSN: 1743-0003. DOI: 10.1186/1743-0003-11-105. [Online]. Available: https://doi.org/10.1186/1743-0003-11-105 (visited on 03/19/2020).

[10] D. W. Tan, M. A. Schiefer, M. W. Keith, J. R. Anderson, J. Tyler, and D. J. Tyler, "A neural interface provides long-term stable natural touch perception," en, *Science Translational Medicine*, vol. 6, no. 257, 257ra138–257ra138, Oct. 2014, ISSN: 1946-6234, 1946-6242. DOI: 10.1126/scitranslmed.3008669. [Online]. Available: http://stm.sciencemag.org/content/6/257/257ra138 (visited on 05/17/2016).

[11] B. S. Wilson and M. F. Dorman, "Cochlear implants: A remarkable past and a brilliant future," *Hearing research*, vol. 242, no. 0, pp. 3–21, Aug. 2008, ISSN: 0378-5955. DOI: 10.1016/j.heares.2008.06.005. [Online]. Available: https://www.ncbi.nlm.nih.gov/pmc/articles/PMC3707130/ (visited on 03/19/2020).

[12] B. staff (2014), "Medical gallery of blausen medical 2014," *WikiJournal of Medicine*, vol. 1, p. 2, 2014, ISSN: 2002-4436. DOI: 10.15347/wjm/2014.010. [Online]. Available: https://en.wikipedia.org/wiki/Cochlear_implant#/media/File:Blausen_0244_CochlearImplant_01.png (visited on 03/19/2020).

[13] L. Robles and M. A. Ruggero, "Mechanics of the Mammalian Cochlea," *Physiological reviews*, vol. 81, no. 3, pp. 1305–1352, Jul. 2001, ISSN: 0031-9333. [Online]. Available: https://www.ncbi.nlm.nih.gov/pmc/articles/PMC3590856/ (visited on 03/19/2020).

[14] Y.-C. Chang, D. H. Ghaffari, R. H. Chow, and J. D. Weiland, "Stimulation strategies for selective activation of retinal ganglion cell soma and threshold reduction," en, *Journal of Neural Engineering*, vol. 16, no. 2, p. 026 017, Feb. 2019, Publisher: IOP Publishing, ISSN: 1741-2552. DOI: 10.1088/1741-2552/aaf92b. [Online]. Available: https://doi.org/10.1088%2F1741-2552%2Faaf92b (visited on 03/19/2020).

[15] K. Dunning, M. W. O'Dell, P. Kluding, and K. McBride, "Peroneal Stimulation for Foot Drop After Stroke: A Systematic Review," en-US, *American Journal of Physical Medicine & Rehabilitation*, vol. 94, no. 8, pp. 649–664, Aug. 2015, ISSN: 0894-9115. DOI: 10.1097/PHM.0000000000000308. [Online]. Available: https://journals.lww.com/ajpmr/Abstract/2015/08000/Peroneal_Stimulation_for_Foot_Drop_After_Stroke__A.9.aspx (visited on 03/19/2020).

[16] H. C. Stronks and G. Dagnelie, "The functional performance of the Argus II retinal prosthesis," *Expert review of medical devices*, vol. 11, no. 1, pp. 23–30, Jan. 2014, ISSN: 1743-4440. DOI: 10.1586/17434440.2014.862494. [Online]. Available: https://www.ncbi.nlm.nih.gov/pmc/articles/PMC3926652/ (visited on 03/19/2020).

[17] A. Dalton, C. Mermier, and M. Zuhl, "Exercise influence on the microbiome–gut–brain axis," *Gut Microbes*, vol. 10, no. 5, pp. 555–568, Jan. 2019, ISSN: 1949-0976. DOI: 10.1080/19490976.2018.1562268. [Online]. Available: https://www.ncbi.nlm.nih.gov/pmc/articles/PMC6748614/ (visited on 03/19/2020).

[18] J. A. Waxenbaum and M. Varacallo, "Anatomy, Autonomic Nervous System," eng, in *StatPearls*, Treasure Island (FL): StatPearls Publishing, 2020. [Online]. Available: http://www.ncbi.nlm.nih.gov/books/NBK539845/ (visited on 03/19/2020).

[19] J. P. O'Reardon, P. Cristancho, and A. D. Peshek, "Vagus Nerve Stimulation (VNS) and Treatment of Depression: To the Brainstem and Beyond," *Psychiatry (Edgmont)*, vol. 3, no. 5, pp. 54–63, May 2006, ISSN: 1550-5952. [Online]. Available: https://www.ncbi.nlm.nih.gov/pmc/articles/PMC2990624/ (visited on 03/19/2020).

[20] C. C. Horn, J. L. Ardell, and L. E. Fisher, "Electroceutical Targeting of the Autonomic Nervous System," *Physiology*, vol. 34, no. 2, pp. 150–162, Mar. 2019, ISSN: 1548-9213. DOI: 10.1152/physiol.00030.2018. [Online]. Available: https://www.ncbi.nlm.nih.gov/pmc/articles/PMC6586833/ (visited on 03/19/2020).

[21] J. Hoffmann, H. E. Jensen, J. Christiansen, A. Olesen, F. B. Loud, and O. Hauch, "Prospective controlled vagotomy trial for duodenal ulcer. Results after 11-15 years.," *Annals of Surgery*, vol. 209, no. 1, pp. 40–45, Jan. 1989, ISSN: 0003-4932. [Online]. Available: https://www.ncbi.nlm.nih.gov/pmc/articles/PMC1493889/ (visited on 03/19/2020).

[22] R. L. Johnson and C. G. Wilson, "A review of vagus nerve stimulation as a therapeutic intervention," *Journal of Inflammation Research*, vol. 11, pp. 203–213, May 2018, ISSN: 1178-7031. DOI: 10.2147/JIR.S163248. [Online]. Available: https://www.ncbi.nlm.nih.gov/pmc/articles/PMC5961632/ (visited on 03/19/2020).

[23] M. Costa, S. J. H. Brookes, and G. W. Hennig, "Anatomy and physiology of the enteric nervous system," en, *Gut*, vol. 47, no. suppl 4, pp. iv15–iv19, Dec. 2000, Publisher: BMJ Publishing Group Section: Chapter 2, ISSN: 0017-5749, 1468-3288. DOI: 10.1136/gut.47.suppl_4.iv15. [Online]. Available: https://gut.bmj.com/content/47/suppl_4/iv15 (visited on 03/17/2020).

[24] B. B. Yoo and S. K. Mazmanian, "The Enteric Network: Interactions between the Immune and Nervous Systems of the Gut," *Immunity*, vol. 46, no. 6, pp. 910–926, Jun. 2017,

ISSN: 1074-7613. DOI: 10.1016/j.immuni.2017.05.011. [Online]. Available: https://www.ncbi.nlm.nih.gov/pmc/articles/PMC5551410/ (visited on 03/23/2020).

[25] B. B. Barth, C. S. Henriquez, W. M. Grill, and X. Shen, "Electrical stimulation of gut motility guided by anin silicomodel," en, *Journal of Neural Engineering*, vol. 14, no. 6, p. 066 010, Nov. 2017, ISSN: 1741-2552. DOI: 10.1088/1741-2552/aa86c8. [Online]. Available: https://doi.org/10.1088%2F1741-2552%2Faa86c8 (visited on 02/06/2020).

[26] Y.-K. Lo, P.-M. Wang, G. Dubrovsky, M.-D. Wu, M. Chan, J. Dunn, and W. Liu, "A Wireless Implant for Gastrointestinal Motility Disorders," en, *Micromachines*, vol. 9, no. 1, p. 17, Jan. 2018, ISSN: 2072-666X. DOI: 10.3390/mi9010017. [Online]. Available: http://www.mdpi.com/2072-666X/9/1/17 (visited on 03/23/2020).

[27] A. K. Chow and B. D. Gulbransen, "Potential roles of enteric glia in bridging neuroimmune communication in the gut," *American Journal of Physiology - Gastrointestinal and Liver Physiology*, vol. 312, no. 2, G145–G152, Feb. 2017, ISSN: 0193-1857. DOI: 10.1152/ajpgi.00384.2016. [Online]. Available: https://www.ncbi.nlm.nih.gov/pmc/articles/PMC5338608/ (visited on 03/23/2020).

[28] H. E. Lebovitz, "Interventional treatment of obesity and diabetes: An interim report on gastric electrical stimulation," *Reviews in Endocrine & Metabolic Disorders*, vol. 17, pp. 73–80, 2016, ISSN: 1389-9155. DOI: 10.1007/s11154-016-9350-7. [Online]. Available: https://www.ncbi.nlm.nih.gov/pmc/articles/PMC4882354/ (visited on 03/23/2020).

[29] C. E. Capener, H. J. Kim, Y. Arinaminpathy, and M. S. P. Sansom, "Ion channels: Structural bioinformatics and modelling," en, *Human Molecular Genetics*, vol. 11, no. 20, pp. 2425–2433, Oct. 2002, ISSN: 0964-6906, 1460-2083. DOI: 10.1093/hmg/11.20.2425. [Online]. Available: http://hmg.oxfordjournals.org/content/11/20/2425 (visited on 10/09/2015).

[30] A. L. Hodgkin and A. F. Huxley, "A quantitative description of membrane current and its application to conduction and excitation in nerve," en, *The Journal of Physiology*,

vol. 117, no. 4, pp. 500–544, 1952, ISSN: 1469-7793. DOI: 10.1113/jphysiol.1952.sp004764. [Online]. Available: https://physoc.onlinelibrary.wiley.com/doi/abs/10.1113/jphysiol.1952.sp004764 (visited on 02/11/2020).

[31] A. S. Pivovarov, F. Calahorro, and R. J. Walker, "Na+/K+-pump and neurotransmitter membrane receptors," en, *Invertebrate Neuroscience*, vol. 19, no. 1, p. 1, Nov. 2018, ISSN: 1439-1104. DOI: 10.1007/s10158-018-0221-7. [Online]. Available: https://doi.org/10.1007/s10158-018-0221-7 (visited on 03/16/2020).

[32] G. J. Kress and S. Mennerick, "Action potential initiation and propagation: Upstream influences on neurotransmission," *Neuroscience*, vol. 158, no. 1, pp. 211–222, Jan. 2009, ISSN: 0306-4522. DOI: 10.1016/j.neuroscience.2008.03.021. [Online]. Available: https://www.ncbi.nlm.nih.gov/pmc/articles/PMC2661755/ (visited on 03/16/2020).

[33] S. W. Kuffler and J. G. Nicholls, *From neuron to brain: a cellular approach to the function of the nervous system*, en. Sinauer Associates, 1976, Google-Books-ID: fTFwWl15nZ4C, ISBN: 978-0-87893-441-6.

[34] C. M. Armstrong, "Na channel inactivation from open and closed states," en, *Proceedings of the National Academy of Sciences*, vol. 103, no. 47, pp. 17 991–17 996, Nov. 2006, Publisher: National Academy of Sciences Section: Biological Sciences, ISSN: 0027-8424, 1091-6490. DOI: 10.1073/pnas.0607603103. [Online]. Available: https://www.pnas.org/content/103/47/17991 (visited on 03/16/2020).

[35] D. A. McCormick, "Chapter 5 - Membrane Potential and Action Potential," en, in *Fundamental Neuroscience (Fourth Edition)*, L. R. Squire, D. Berg, F. E. Bloom, S. du Lac, A. Ghosh, and N. C. Spitzer, Eds., San Diego: Academic Press, Jan. 2013, pp. 93–116, ISBN: 978-0-12-385870-2. DOI: 10.1016/B978-0-12-385870-2.00005-6. [Online]. Available: http://www.sciencedirect.com/science/article/pii/B9780123858702000056 (visited on 03/16/2020).

[36] *Action potential*, en, Page Version ID: 945592328, Mar. 2020. [Online]. Available: https://en.wikipedia.org/w/index.php?title=Action_potential&oldid=945592328 (visited on 03/16/2020).

[37] L. Conforti, "Chapter 20 - Patch-Clamp Techniques," en, in *Cell Physiology Source Book (Fourth Edition)*, N. Sperelakis, Ed., San Diego: Academic Press, Jan. 2012, pp. 369–381, ISBN: 978-0-12-387738-3. DOI: 10.1016/B978-0-12-387738-3.00020-2. [Online]. Available: http://www.sciencedirect.com/science/article/pii/B9780123877383000202 (visited on 03/17/2020).

[38] F. Rattay, "The basic mechanism for the electrical stimulation of the nervous system," en, *Neuroscience*, vol. 89, no. 2, pp. 335–346, Mar. 1999, ISSN: 0306-4522. DOI: 10.1016/S0306-4522(98)00330-3. [Online]. Available: http://www.sciencedirect.com/science/article/pii/S0306452298003303 (visited on 01/20/2020).

[39] B. Hille, *Ion channels of excitable membranes*, English. Sunderland, Mass.: Sinauer, 2001, OCLC: 57287448, ISBN: 978-0-87893-321-1.

[40] N. A. Pelot, B. J. Thio, and W. M. Grill, "Modeling Current Sources for Neural Stimulation in COMSOL," English, *Frontiers in Computational Neuroscience*, vol. 12, 2018, ISSN: 1662-5188. DOI: 10.3389/fncom.2018.00040. [Online]. Available: https://www.frontiersin.org/articles/10.3389/fncom.2018.00040/full (visited on 02/06/2020).

[41] H. Taghipour-Farshi, J. Frounchi, N. Ahmadiasl, P. Shahabi, and Y. Salekzamani, "Effect of contacts configuration and location on selective stimulation of cuff electrode," *Bio-Medical Materials and Engineering*, vol. 25, no. 3, pp. 237–248, Jun. 2015, ISSN: 18783619, 09592989. DOI: 10.3233/BME-151281. [Online]. Available: http://www.medra.org/servlet/aliasResolver?alias=iospress&doi=10.3233/BME-151281 (visited on 09/21/2015).

[42] I. Delgado-Martínez, J. Badia, A. Pascual-Font, A. Rodríguez-Baeza, and X. Navarro, "Fascicular Topography of the Human Median Nerve for Neuroprosthetic Surgery," *Frontiers in Neuroscience*, vol. 10, Jul. 2016, ISSN: 1662-4548. DOI: 10.3389/fnins.

2016.00286. [Online]. Available: https://www.ncbi.nlm.nih.gov/pmc/articles/PMC4929846/ (visited on 01/20/2020).

[43] J. Castro, P. Negredo, and C. Avendaño, "Fiber composition of the rat sciatic nerve and its modification during regeneration through a sieve electrode," en, *Brain Research*, vol. 1190, pp. 65–77, Jan. 2008, ISSN: 0006-8993. DOI: 10.1016/j.brainres.2007.11.028. [Online]. Available: http://www.sciencedirect.com/science/article/pii/S0006899307027941 (visited on 02/11/2020).

[44] M. Campero, J. Serra, and J. L. Ochoa, "Peripheral projections of sensory fascicles in the human superficial radial nerve," en, *Brain*, vol. 128, no. 4, pp. 892–895, Apr. 2005, ISSN: 0006-8950. DOI: 10.1093/brain/awh438. [Online]. Available: https://academic.oup.com/brain/article/128/4/892/284347 (visited on 01/20/2020).

[45] D. Arslantunali, T. Dursun, D. Yucel, N. Hasirci, and V. Hasirci, "Peripheral nerve conduits: Technology update," English, *Medical Devices: Evidence and Research*, vol. 7, pp. 405–424, Dec. 2014. DOI: 10.2147/MDER.S59124. [Online]. Available: https://www.dovepress.com/peripheral-nerve-conduits-technology-update-peer-reviewed-fulltext-article-MDER (visited on 03/17/2020).

[46] A. Weerasuriya, R. A. Spangler, S. I. Rapoport, and R. E. Taylor, "AC impedance of the perineurium of the frog sciatic nerve.," *Biophysical Journal*, vol. 46, no. 2, pp. 167–174, Aug. 1984, ISSN: 0006-3495. [Online]. Available: http://www.ncbi.nlm.nih.gov/pmc/articles/PMC1435024/ (visited on 09/28/2016).

[47] A. G. Richardson, C. C. McIntyre, and W. M. Grill, "Modelling the effects of electric fields on nerve fibres: Influence of the myelin sheath," en, *Medical and Biological Engineering and Computing*, vol. 38, no. 4, pp. 438–446, Jul. 2000, ISSN: 0140-0118, 1741-0444. DOI: 10.1007/BF02345014. [Online]. Available: http://link.springer.com/article/10.1007/BF02345014 (visited on 09/22/2016).

[48] F. T. Dun, "The Length and Diameter of the Node of Ranvier," *IEEE Transactions on Biomedical Engineering*, vol. BME-17, no. 1, pp. 21–24, Jan. 1970, ISSN: 0018-9294. DOI: 10.1109/TBME.1970.4502680.

[49] S. G. Waxman, "Determinants of conduction velocity in myelinated nerve fibers," *Muscle & Nerve*, vol. 3, no. 2, pp. 141–150, 1980, ISSN: 1097-4598. DOI: 10.1002/mus.880030207.

[50] G. Matsumoto and I. Tasaki, "A study of conduction velocity in nonmyelinated nerve fibers," en, *Biophysical Journal*, vol. 20, no. 1, pp. 1–13, Oct. 1977, ISSN: 00063495. DOI: 10.1016/S0006-3495(77)85532-X. [Online]. Available: https://linkinghub.elsevier.com/retrieve/pii/S000634957785532X (visited on 03/23/2020).

[51] D. Kernell, "Principles of Force Gradation in Skeletal Muscles," *Neural Plasticity*, vol. 10, no. 1-2, pp. 69–76, 2003, ISSN: 2090-5904. DOI: 10.1155/NP.2003.69. [Online]. Available: https://www.ncbi.nlm.nih.gov/pmc/articles/PMC2565421/ (visited on 03/24/2020).

[52] C. L. Lynch and M. R. Popovic, "Functional Electrical Stimulation," en, *IEEE Control Systems*, vol. 28, no. 2, pp. 40–50, Apr. 2008, ISSN: 1066-033X, 1941-000X. DOI: 10.1109/MCS.2007.914689. [Online]. Available: https://ieeexplore.ieee.org/document/4472378/ (visited on 03/24/2020).

[53] E. H. Rijnbeek, N. Eleveld, and W. Olthuis, "Update on Peripheral Nerve Electrodes for Closed-Loop Neuroprosthetics," English, *Frontiers in Neuroscience*, vol. 12, 2018, Publisher: Frontiers, ISSN: 1662-453X. DOI: 10.3389/fnins.2018.00350. [Online]. Available: https://www.frontiersin.org/articles/10.3389/fnins.2018.00350/full (visited on 03/19/2020).

[54] C. Russell, A. D. Roche, and S. Chakrabarty, "Peripheral nerve bionic interface: A review of electrodes," en, *International Journal of Intelligent Robotics and Applications*, vol. 3, no. 1, pp. 11–18, Mar. 2019, ISSN: 2366-598X. DOI: 10.1007/s41315-019-00086-3. [Online]. Available: https://doi.org/10.1007/s41315-019-00086-3 (visited on 03/24/2020).

[55] T. Boretius, J. Badia, A. Pascual-Font, M. Schuettler, X. Navarro, K. Yoshida, and T. Stieglitz, "A transverse intrafascicular multichannel electrode (TIME) to interface with the peripheral nerve," en, *Biosensors and Bioelectronics*, vol. 26, no. 1, pp. 62–69, Sep.

2010, ISSN: 0956-5663. DOI: 10.1016/j.bios.2010.05.010. [Online]. Available: http://www.sciencedirect.com/science/article/pii/S0956566310002496 (visited on 03/24/2020).

[56] E. L. Graczyk, M. A. Schiefer, H. P. Saal, B. P. Delhaye, S. J. Bensmaia, and D. J. Tyler, "The neural basis of perceived intensity in natural and artificial touch," *Science translational medicine*, vol. 8, no. 362, 362ra142, Oct. 2016, ISSN: 1946-6234. DOI: 10.1126/scitranslmed.aaf5187. [Online]. Available: https://www.ncbi.nlm.nih.gov/pmc/articles/PMC5713478/ (visited on 03/24/2020).

[57] A. Branner, R. B. Stein, and R. A. Normann, "Selective Stimulation of Cat Sciatic Nerve Using an Array of Varying-Length Microelectrodes," *Journal of Neurophysiology*, vol. 85, no. 4, pp. 1585–1594, Apr. 2001, Publisher: American Physiological Society, ISSN: 0022-3077. DOI: 10.1152/jn.2001.85.4.1585. [Online]. Available: https://journals.physiology.org/doi/full/10.1152/jn.2001.85.4.1585 (visited on 03/24/2020).

[58] W. F. Agnew and D. B. McCreery, "Considerations for Safety with Chronically Implanted Nerve Electrodes," en, *Epilepsia*, vol. 31, no. s2, S27–S32, 1990, ISSN: 1528-1167. DOI: 10.1111/j.1528-1157.1990.tb05845.x. [Online]. Available: https://onlinelibrary.wiley.com/doi/abs/10.1111/j.1528-1157.1990.tb05845.x (visited on 02/07/2020).

[59] V. S. Polikov, P. A. Tresco, and W. M. Reichert, "Response of brain tissue to chronically implanted neural electrodes," en, *Journal of Neuroscience Methods*, vol. 148, no. 1, pp. 1–18, Oct. 2005, ISSN: 01650270. DOI: 10.1016/j.jneumeth.2005.08.015. [Online]. Available: http://linkinghub.elsevier.com/retrieve/pii/S0165027005002931 (visited on 09/21/2015).

[60] B. P. Christie, M. Freeberg, W. D. Memberg, G. J. C. Pinault, H. A. Hoyen, D. J. Tyler, and R. J. Triolo, ""Long-term stability of stimulating spiral nerve cuff electrodes on human peripheral nerves"," *Journal of NeuroEngineering and Rehabilitation*, vol. 14, Jul.

2017, ISSN: 1743-0003. DOI: 10.1186/s12984-017-0285-3. [Online]. Available: https://www.ncbi.nlm.nih.gov/pmc/articles/PMC5504677/ (visited on 03/05/2020).

[61] C. Günter, J. Delbeke, and M. Ortiz-Catalan, "Safety of long-term electrical peripheral nerve stimulation: Review of the state of the art," *Journal of NeuroEngineering and Rehabilitation*, vol. 16, no. 1, p. 13, Jan. 2019, ISSN: 1743-0003. DOI: 10.1186/s12984-018-0474-8. [Online]. Available: https://doi.org/10.1186/s12984-018-0474-8 (visited on 01/27/2020).

[62] G. E. Loeb and R. A. Peck, "Cuff electrodes for chronic stimulation and recording of peripheral nerve activity," *Journal of Neuroscience Methods*, vol. 64, no. 1, pp. 95–103, Jan. 1996, ISSN: 0165-0270. DOI: 10.1016/0165-0270(95)00123-9. [Online]. Available: https://www.sciencedirect.com/science/article/pii/0165027095001239 (visited on 02/08/2017).

[63] D. K. Leventhal, M. Cohen, and D. M. Durand, "Chronic histological effects of the flat interface nerve electrode," en, *Journal of Neural Engineering*, vol. 3, no. 2, pp. 102–113, Apr. 2006, Publisher: IOP Publishing, ISSN: 1741-2552. DOI: 10.1088/1741-2560/3/2/004. [Online]. Available: https://doi.org/10.1088%2F1741-2560%2F3%2F2%2F004 (visited on 03/24/2020).

[64] N. Lago, K. Yoshida, K. P. Koch, and X. Navarro, "Assessment of Biocompatibility of Chronically Implanted Polyimide and Platinum Intrafascicular Electrodes," *IEEE Transactions on Biomedical Engineering*, vol. 54, no. 2, pp. 281–290, Feb. 2007, Conference Name: IEEE Transactions on Biomedical Engineering, ISSN: 1558-2531. DOI: 10.1109/TBME.2006.886617.

[65] J. Badia, T. Boretius, A. Pascual-Font, E. Udina, T. Stieglitz, and X. Navarro, "Biocompatibility of Chronically Implanted Transverse Intrafascicular Multichannel Electrode (TIME) in the Rat Sciatic Nerve," *IEEE Transactions on Biomedical Engineering*, vol. 58, no. 8, pp. 2324–2332, Aug. 2011, Conference Name: IEEE Transactions on Biomedical Engineering, ISSN: 1558-2531. DOI: 10.1109/TBME.2011.2153850.

[66] R. M. Bradley, X. Cao, T. Akin, and K. Najafi, "Long term chronic recordings from peripheral sensory fibers using a sieve electrode array," *Journal of neuroscience methods*, vol. 73, no. 2, pp. 177–186, 1997. [Online]. Available: http://www.sciencedirect.com/science/article/pii/S0165027097022255 (visited on 09/21/2015).

[67] M. R. MacEwan, E. R. Zellmer, J. J. Wheeler, H. Burton, and D. W. Moran, "Regenerated Sciatic Nerve Axons Stimulated through a Chronically Implanted Macro-Sieve Electrode," English, *Frontiers in Neuroscience*, vol. 10, 2016, Publisher: Frontiers, ISSN: 1662-453X. DOI: 10.3389/fnins.2016.00557. [Online]. Available: https://www.frontiersin.org/articles/10.3389/fnins.2016.00557/full (visited on 03/24/2020).

[68] N. Lago, E. Udina, A. Ramachandran, and X. Navarro, "Neurobiological Assessment of Regenerative Electrodes for Bidirectional Interfacing Injured Peripheral Nerves," *IEEE Transactions on Biomedical Engineering*, vol. 54, no. 6, pp. 1129–1137, Jun. 2007, ISSN: 0018-9294. DOI: 10.1109/TBME.2007.891168.

[69] R. A. Green, P. B. Matteucci, C. W. D. Dodds, J. Palmer, W. F. Dueck, R. T. Hassarati, P. J. Byrnes-Preston, N. H. Lovell, and G. J. Suaning, "Laser patterning of platinum electrodes for safe neurostimulation," en, *Journal of Neural Engineering*, vol. 11, no. 5, p. 056 017, 2014, ISSN: 1741-2552. DOI: 10.1088/1741-2560/11/5/056017. [Online]. Available: http://stacks.iop.org/1741-2552/11/i=5/a=056017 (visited on 10/01/2015).

[70] J. E. B. Randles, "Kinetics of rapid electrode reactions," en, *Discussions of the Faraday Society*, vol. 1, pp. 11–19, Jan. 1947, ISSN: 0366-9033. DOI: 10.1039/DF9470100011. [Online]. Available: https://pubs.rsc.org/en/content/articlelanding/1947/df/df9470100011 (visited on 01/22/2020).

[71] M. S. Uddin, H. Tanaya Das, T. Maiyalagan, and P. Elumalai, "Influence of designed electrode surfaces on double layer capacitance in aqueous electrolyte: Insights from standard models," en, *Applied Surface Science*, 4th International Conference on Nanoscience and Nanotechnology, vol. 449, pp. 445–453, Aug. 2018, ISSN: 0169-4332. DOI: 10.1016/j.

apsusc.2017.12.088. [Online]. Available: http://www.sciencedirect.com/science/article/pii/S0169433217336760 (visited on 01/22/2020).

[72] J. Huang, T. Zhou, J. Zhang, and M. Eikerling, "Double layer of platinum electrodes: Non-monotonic surface charging phenomena and negative double layer capacitance," *The Journal of Chemical Physics*, vol. 148, no. 4, p. 044 704, Jan. 2018, ISSN: 0021-9606. DOI: 10.1063/1.5010999. [Online]. Available: https://aip.scitation.org/doi/full/10.1063/1.5010999 (visited on 01/22/2020).

[73] C. f. D. a. R. H. FDA, "Biological Responses to Metal Implants," English, United States Food and Drug Administration, Tech. Rep., Sep. 2019, p. 149. [Online]. Available: https://www.fda.gov/media/131150/download.

[74] R. A. Green, N. H. Lovell, G. G. Wallace, and L. A. Poole-Warren, "Conducting polymers for neural interfaces: Challenges in developing an effective long-term implant," en, *Biomaterials*, vol. 29, no. 24, pp. 3393–3399, Aug. 2008, ISSN: 0142-9612. DOI: 10.1016/j.biomaterials.2008.04.047. [Online]. Available: http://www.sciencedirect.com/science/article/pii/S0142961208003220 (visited on 01/22/2020).

[75] W. F. Agnew, D. B. McCreery, T. G. H. Yuen, and L. A. Bullara, "Histologic and physiologic evaluation of electrically stimulated peripheral nerve: Considerations for the selection of parameters," en, *Annals of Biomedical Engineering*, vol. 17, no. 1, pp. 39–60, Jan. 1989, ISSN: 1573-9686. DOI: 10.1007/BF02364272. [Online]. Available: https://doi.org/10.1007/BF02364272 (visited on 02/07/2020).

[76] A. M. Dymond, "Characteristics of the Metal-Tissue Interface of Stimulation Electrodes," *IEEE Transactions on Biomedical Engineering*, vol. BME-23, no. 4, pp. 274–280, Jul. 1976, ISSN: 0018-9294. DOI: 10.1109/TBME.1976.324585.

[77] M. C. Wetzel, L. G. Howell, and K. J. Bearie, "Experimental Performance of Steel and Platinum Electrodes with Chronic Monophasic Stimulation of the Brain," English, *Journal of Neurosurgery*, vol. 31, no. 6, pp. 658–669, Dec. 1969, Publisher: Journal of Neurosurgery Publishing Group. DOI: 10.3171/jns.1969.31.6.0658. [Online].

Available: https://thejns.org/view/journals/j-neurosurg/31/6/article-p658.xml (visited on 03/24/2020).

[78] R. K. Shepherd, P. M. Carter, Y. L. Enke, A. K. Wise, and J. B. Fallon, "Chronic intracochlear electrical stimulation at high charge densities results in platinum dissolution but not neural loss or functional changes in vivo," en, *Journal of Neural Engineering*, vol. 16, no. 2, p. 026 009, Jan. 2019, Publisher: IOP Publishing, ISSN: 1741-2552. DOI: 10.1088/1741-2552/aaf66b. [Online]. Available: https://doi.org/10.1088%2F1741-2552%2Faaf66b (visited on 03/23/2020).

[79] C. M. Frost, P. S. Cederna, D. C. Martin, Bong Sup Shim, and M. G. Urbanchek, "Decellular biological scaffold polymerized with PEDOT for improving peripheral nerve interface charge transfer," en, in *2014 36th Annual International Conference of the IEEE Engineering in Medicine and Biology Society*, Chicago, IL: IEEE, Aug. 2014, pp. 422–425, ISBN: 978-1-4244-7929-0. DOI: 10.1109/EMBC.2014.6943618. [Online]. Available: http://ieeexplore.ieee.org/document/6943618/ (visited on 03/06/2020).

[80] E. Cuttaz, J. Goding, C. Vallejo-Giraldo, U. Aregueta-Robles, N. Lovell, D. Ghezzi, and R. A. Green, "Conductive elastomer composites for fully polymeric, flexible bioelectronics," en, *Biomaterials Science*, vol. 7, no. 4, pp. 1372–1385, 2019. DOI: 10.1039/C8BM01235K. [Online]. Available: https://pubs.rsc.org/en/content/articlelanding/2019/bm/c8bm01235k (visited on 01/06/2020).

[81] N. A. Staples, J. A. Goding, A. D. Gilmour, K. Y. Aristovich, P. Byrnes-Preston, D. S. Holder, J. W. Morley, N. H. Lovell, D. J. Chew, and R. A. Green, "Conductive Hydrogel Electrodes for Delivery of Long-Term High Frequency Pulses," English, *Frontiers in Neuroscience*, vol. 11, 2018, ISSN: 1662-453X. DOI: 10.3389/fnins.2017.00748. [Online]. Available: https://www.frontiersin.org/articles/10.3389/fnins.2017.00748/full (visited on 01/22/2020).

[82] T. D. Y. Kozai, K. Catt, Z. Du, K. Na, O. Srivannavit, R.-u. M. Haque, J. Seymour, K. D. Wise, E. Yoon, and X. T. Cui, "Chronic In Vivo Evaluation of PEDOT/CNT for Stable Neural Recordings," en, *IEEE Transactions on Biomedical Engineering*, vol. 63, no. 1,

pp. 111–119, Jan. 2016, ISSN: 0018-9294, 1558-2531. DOI: 10.1109/TBME.2015.2445713. [Online]. Available: http://ieeexplore.ieee.org/document/7123592/ (visited on 03/23/2020).

[83] S. Arcot Desai, J. D. Rolston, L. Guo, and S. M. Potter, "Improving impedance of implantable microwire multi-electrode arrays by ultrasonic electroplating of durable platinum black," English, *Frontiers in Neuroengineering*, vol. 3, 2010, Publisher: Frontiers, ISSN: 1662-6443. DOI: 10.3389/fneng.2010.00005. [Online]. Available: https://www.frontiersin.org/articles/10.3389/fneng.2010.00005/full (visited on 03/23/2020).

[84] N. J. M. Rijkhoff, H. Wijkstra, P. E. V. V. Kerrebroeck, and F. M. J. Debruyne, "Urinary bladder control by electrical stimulation: Review of electrical stimulation techniques in spinal cord injury," en, *Neurourology and Urodynamics*, vol. 16, no. 1, pp. 39–53, 1997, ISSN: 1520-6777. DOI: 10.1002/(SICI)1520-6777(1997)16:1<39::AID-NAU6>3.0.CO;2-F. (visited on 03/05/2020).

[85] M. J. McGee, C. L. Amundsen, and W. M. Grill, "Electrical stimulation for the treatment of lower urinary tract dysfunction after spinal cord injury," en, *The Journal of Spinal Cord Medicine*, vol. 38, no. 2, pp. 135–146, Mar. 2015, ISSN: 1079-0268, 2045-7723. DOI: 10.1179/2045772314Y.0000000299. [Online]. Available: http://www.tandfonline.com/doi/full/10.1179/2045772314Y.0000000299 (visited on 06/10/2020).

[86] C. Tai, J. Wang, X. Wang, W. C. d. Groat, and J. R. Roppolo, "Bladder inhibition or voiding induced by pudendal nerve stimulation in chronic spinal cord injured cats," en, *Neurourology and Urodynamics*, vol. 26, no. 4, pp. 570–577, 2007, _eprint: https://onlinelibrary.wiley.com/doi/pdf/10.1002/nau.20374, ISSN: 1520-6777. DOI: 10.1002/nau.20374. [Online]. Available: https://onlinelibrary.wiley.com/doi/abs/10.1002/nau.20374 (visited on 06/10/2020).

[87] W. Y. X. Peh, R. Mogan, X. Y. Thow, S. M. Chua, A. Rusly, N. V. Thakor, and S.-C. Yen, "Novel Neurostimulation of Autonomic Pelvic Nerves Overcomes Bladder-Sphincter Dyssynergia," English, *Frontiers in Neuroscience*, vol. 12, 2018, Publisher:

Frontiers, ISSN: 1662-453X. DOI: 10.3389/fnins.2018.00186. [Online]. Available: https://www.frontiersin.org/articles/10.3389/fnins.2018.00186/full (visited on 06/12/2020).

[88] S. W. Kuffler and E. M. V. Williams, "Small-nerve junctional potentials. The distribution of small motor nerves to frog skeletal muscle, and the membrane characteristics of the fibres they innervate*," en, *The Journal of Physiology*, vol. 121, no. 2, pp. 289–317, 1953, ISSN: 1469-7793. DOI: 10.1113/jphysiol.1953.sp004948. [Online]. Available: https://physoc.onlinelibrary.wiley.com/doi/abs/10.1113/jphysiol.1953.sp004948 (visited on 02/11/2020).

[89] J. C. Lilly, J. R. Hughes, E. C. Alvord, and T. W. Galkin, "Brief, Noninjurious Electric Waveform for Stimulation of the Brain," en, *Science*, vol. 121, no. 3144, pp. 468–469, Apr. 1955, ISSN: 0036-8075, 1095-9203. DOI: 10.1126/science.121.3144.468. [Online]. Available: https://science.sciencemag.org/content/121/3144/468 (visited on 01/27/2020).

[90] N. Bhadra and K. Kilgore, "Direct current electrical conduction block of peripheral nerve," *IEEE Transactions on Neural Systems and Rehabilitation Engineering*, vol. 12, no. 3, pp. 313–324, Sep. 2004, ISSN: 1558-0210. DOI: 10.1109/TNSRE.2004.834205.

[91] D. K. L. Kilgore and N. Bhadra, "Nerve conduction block utilising high-frequency alternating current," en, *Medical and Biological Engineering and Computing*, vol. 42, no. 3, pp. 394–406, May 2004, ISSN: 0140-0118, 1741-0444. DOI: 10.1007/BF02344716. [Online]. Available: http://link.springer.com/article/10.1007/BF02344716 (visited on 09/29/2015).

[92] N. Bhadra, T. L. Vrabec, N. Bhadra, and K. L. Kilgore, "Reversible conduction block in peripheral nerve using electrical waveforms," *Bioelectronics in Medicine*, vol. 1, no. 1, pp. 39–54, Jan. 2018, ISSN: 2059-1500. DOI: 10.2217/bem-2017-0004. [Online]. Available: https://www.ncbi.nlm.nih.gov/pmc/articles/PMC5811084/ (visited on 09/03/2019).

[93] Y. A. Patel and R. J. Butera, "Challenges associated with nerve conduction block using kilohertz electrical stimulation," en, *Journal of Neural Engineering*, vol. 15, no. 3, p. 031 002, 2018, ISSN: 1741-2552. DOI: 10.1088/1741-2552/aaadc0. [Online]. Available: http://stacks.iop.org/1741-2552/15/i=3/a=031002 (visited on 09/25/2018).

[94] N. A. Pelot and W. M. Grill, "In vivo quantification of excitation and kilohertz frequency block of the rat vagus nerve," en, *Journal of Neural Engineering*, 2020, ISSN: 1741-2552. DOI: 10.1088/1741-2552/ab6cb6. [Online]. Available: http://iopscience.iop.org/10.1088/1741-2552/ab6cb6 (visited on 02/06/2020).

[95] N. Bhadra, N. Bhadra, K. Kilgore, and K. J. Gustafson, "High frequency electrical conduction block of the pudendal nerve," en, *Journal of Neural Engineering*, vol. 3, no. 2, p. 180, 2006, ISSN: 1741-2552. DOI: 10.1088/1741-2560/3/2/012. [Online]. Available: http://stacks.iop.org/1741-2552/3/i=2/a=012 (visited on 09/29/2015).

[96] R. A. Gaunt and A. Prochazka, "Transcutaneously Coupled, High-Frequency Electrical Stimulation of the Pudendal Nerve Blocks External Urethral Sphincter Contractions," en, *Neurorehabilitation and Neural Repair*, vol. 23, no. 6, pp. 615–626, Jul. 2009, ISSN: 1545-9683. DOI: 10.1177/1545968308328723. [Online]. Available: https://doi.org/10.1177/1545968308328723 (visited on 12/03/2019).

[97] A. Rapeaux, K. Nikolic, I. Williams, A. Eftekhar, and T. G. Constandinou, "Fiber size-selective stimulation using action potential filtering for a peripheral nerve interface: A simulation study," in *2015 37th Annual International Conference of the IEEE Engineering in Medicine and Biology Society (EMBC)*, Aug. 2015, pp. 3411–3414. DOI: 10.1109/EMBC.2015.7319125.

[98] A. Rapeaux, "Final Year Project Report Imperial College Bioengineering," en, Imperial College London, MEng Thesis, 2014, p. 102. [Online]. Available: https://github.com/rapeauxa/RapeauxA_MEng_thesis (visited on 06/15/2020).

[99] B. Frankenhaeuser and A. F. Huxley, "The action potential in the myelinated nerve fibre of Xenopus laevis as computed on the basis of voltage clamp data," en, *The Journal of Physiology*, vol. 171, no. 2, pp. 302–315, 1964, ISSN: 1469-7793. DOI: 10.1113/jphysiol.

1964.sp007378. [Online]. Available: https://physoc.onlinelibrary.wiley.com/doi/abs/10.1113/jphysiol.1964.sp007378 (visited on 02/14/2020).

[100] M. L. Hines and N. T. Carnevale, "The NEURON Simulation Environment," *Neural Computation*, vol. 9, no. 6, pp. 1179–1209, Aug. 1997, ISSN: 0899-7667. DOI: 10.1162/neco.1997.9.6.1179. [Online]. Available: https://doi.org/10.1162/neco.1997.9.6.1179 (visited on 02/11/2020).

[101] Y. A. Patel and R. J. Butera, "Differential fiber-specific block of nerve conduction in mammalian peripheral nerves using kilohertz electrical stimulation," en, *Journal of Neurophysiology*, vol. 113, no. 10, pp. 3923–3929, Jun. 2015, ISSN: 0022-3077, 1522-1598. DOI: 10.1152/jn.00529.2014. [Online]. Available: http://jn.physiology.org/content/113/10/3923 (visited on 09/20/2016).

[102] R. P. Williamson and B. J. Andrews, "Localized electrical nerve blocking," *IEEE Transactions on Biomedical Engineering*, vol. 52, no. 3, pp. 362–370, Mar. 2005, ISSN: 0018-9294. DOI: 10.1109/TBME.2004.842790.

[103] G. Schalow, G. Zäch, and R. Warzok, "Classification of human peripheral nerve fibre groups by conduction velocity and nerve fibre diameter is preserved following spinal cord lesion," en, *Journal of the Autonomic Nervous System*, vol. 52, no. 2-3, pp. 125–150, Apr. 1995, ISSN: 01651838. DOI: 10.1016/0165-1838(94)00153-B. [Online]. Available: https://linkinghub.elsevier.com/retrieve/pii/016518389400153B (visited on 06/12/2020).

[104] D. M. Ackermann, E. L. Foldes, N. Bhadra, and K. L. Kilgore, "Effect of Bipolar Cuff Electrode Design on Block Thresholds in High-Frequency Electrical Neural Conduction Block," *IEEE Transactions on Neural Systems and Rehabilitation Engineering*, vol. 17, no. 5, pp. 469–477, Oct. 2009, ISSN: 1534-4320. DOI: 10.1109/TNSRE.2009.2034069.

[105] M. Franke, T. Vrabec, J. Wainright, N. Bhadra, N. Bhadra, and K. Kilgore, "Combined KHFAC + DC nerve block without onset or reduced nerve conductivity after block," en, *Journal of Neural Engineering*, vol. 11, no. 5, p. 056 012, 2014, ISSN: 1741-2552. DOI:

10.1088/1741-2560/11/5/056012. [Online]. Available: http://stacks.iop.org/1741-2552/11/i=5/a=056012 (visited on 10/01/2015).

[106] T. L. Vrabec, N. Bhadra, J. S. Wainright, N. Bhadra, and K. L. Kilgore, "A novel waveform for No-Onset nerve block combining direct current and kilohertz frequency alternating current," in *2013 6th International IEEE/EMBS Conference on Neural Engineering (NER)*, Nov. 2013, pp. 283–286. DOI: 10.1109/NER.2013.6695927.

[107] W. Grill and J. Mortimer, "Stimulus waveforms for selective neural stimulation," en, *IEEE Engineering in Medicine and Biology Magazine*, vol. 14, no. 4, pp. 375–385, Aug. 1995, ISSN: 07395175. DOI: 10.1109/51.395310. [Online]. Available: http://ieeexplore.ieee.org/document/395310/ (visited on 03/02/2020).

# Chapter 3

# A multi-channel, block capable, modular stimulator for acute neurophysiology experiments

## 3.1 Introduction

In this chapter we describe the design of a stimulator that is specifically able to combine both conventional and high frequency stimulation. The requirements of high frequency stimulation are high bandwidth and maximum output current, leading to high output voltage compliance. These two constraints alone place the resulting design on the high power end of the spectrum, as opposed to implantable stimulators which must maximise the life of their battery. As such more emphasis was placed on stimulator performance than power efficiency during the design process, despite the fact that the resulting stimulator is also battery powered due to the constraints of the experimental setup in which it is used.

After a review of electrode and stimulator technology this chapter will focus on the design process for the aforementioned block-capable stimulator and its characterization to ensure it will be suitable for multichannel stimulation and block.

Original stimulators were simple devices injecting current into tissue using voltage waveforms. Laboratory equipment such as the Grass S88 shown in figure 3.1, an advanced design in its own right capable of outputting finely tuned voltage-mode pulse trains using analog controls is a testament to this paradigm. Some older stimulator designs still use voltage waveforms to deliver therapy, such as for DBS [1].

Two key ideas changed this initial paradigm completely: the notion that charge is the determining factor for the level of neural activation [2] meant that current was more reliable than voltage for stimulating nervous tissue, and the fact that electrodes polarise as a result of charge accumulation which allows potentially toxic electrochemical reactions to occur at their surface led to changes in the stimulation protocol to prevent this [3], [4].


Figure 3.1: Grass S88 Voltage-Mode Stimulator as sold by Grass Instruments. Source: `https://www.a-msystems.com/t-grass_stimulators.aspx`

## 3.2 Stimulator topologies for control of injected charge

The fact that electrodes are nonlinear loads as detailed in chapter 2 has led the development of stimulators with better control of the charge that is injected, so that consistent results can be obtained from stimulation. These can be separated into two categories, current-controlled and switched capacitor-based stimulators. There has been considerable focus on the development of current-controlled stimulators as they offer better control of injected charge despite their higher power consumption compared to either voltage or charge-controlled stimulators.

### 3.2.1 Current-controlled stimulators

Current-control point to using controllable current sources as the main analog element in a stimulator. Stimulators have to tradeoff important characteristics such as voltage swing and output impedance, maximum output current, bandwidth and slew rate. In each case higher is better and priority will be given to one or more properties depending on the electrode interface and stimulation regime. Topologies chosen tend to depend on whether the stimulator is made using integrated or discrete components.

Integrated stimulators are designed for small size, enabling implantability close to the target site, such as for retinal stimulators [5], [6], or for small animal science [7]. Typically a current steering DAC topology is coupled with a cascode output stage. Combining the two enables good precision and linearity from the DAC by using well-matched conventional CMOS structures, and high output impedance from the cascode, trading off voltage compliance and therefore lowering either maximum output current, or maximum load impedance. High output node voltages can be reached with high voltage CMOS technology options [8], [9]. However this type of circuit alone can only output current in one direction, sinking when the output stage is made using NMOS, and sourcing when the output stage is made with PMOS. When optimising the tradeoff between output swing and impedance, a regulated cascode topology can be used at the cost of additional power consumption and complexity.

When designing stimulators using discrete components, the same topologies aren't available due to the inherent mismatch between discrete components and the fact that current DACs with high voltage output stages aren't sold commercially as discrete devices. However, the wide range of op-amps available make powerful transimpedance circuits an option, where a voltage output from a conventional DAC is then converted to current output, with several examples shown in figure 3.2.

The simple transimpedance current source has been implemented several times [10], [11] for use in neural stimulators made with commercially available parts. While straightforward to implement and requiring few components, its main drawback is that the load is inside the

feedback loop, leading to potential instability issues when stimulating using large electrodes with correspondingly high capacitances.

The Howland current pump isolates its load from the feedback loop by using a current-sensing resistor, $R_S$ preventing the instability issues seen by the first circuit. The 'improved' version of the circuit is shown here as it has a better output voltage swing with respect to output impedance, although the original version has been used for neural stimulation when this is less of a concern as in [12]. The resistor network inside the circuit must be carefully matched, for example using specific matched resistor network components, in order to achieve high output impedance. Output impedance for this circuit rolls off at the same rate as the op-amp's open-loop gain with frequency, making wide bandwidth op-amps preferable. An excellent review of this circuit and tradeoffs that a designer can consider is given in [13], with example optimizations given in [14].

A second type of circuit isolating the load from the feedback loop uses an instrumentation amplifier with a set gain of A to measure the current flowing across the current-sensing resistor. While providing better CMRR than either of the other circuits thanks to the instrumentation amplifier, the damping network formed by $R_f$ and $C_f$ must be carefully designed to prevent instability in the circuit, as using op-amps with similar bandwidths will lead to insufficient closed-loop phase margins. In this case it is better to use a fast instrumentation amplifier and slow down the response of the main amplifier, though this may lead to tradeoffs on speed compared to the other two circuits.

### 3.2.2 Switched capacitor stimulators

To reduce power consumption compared to integrated current sources, and yet retain some control over injected charge, charge-mode stimulators were designed that essentially use switched capacitor topologies to inject charge into tissue [15] as shown in figure 3.3. The voltage used to charge the stimulating capacitor bounds the maximum amount of charge injected into the tissue, and the voltage-mode nature of this charging helps with energy efficiency compared to current-mode stimulators for which the current mirror DACs and output stages are not energy

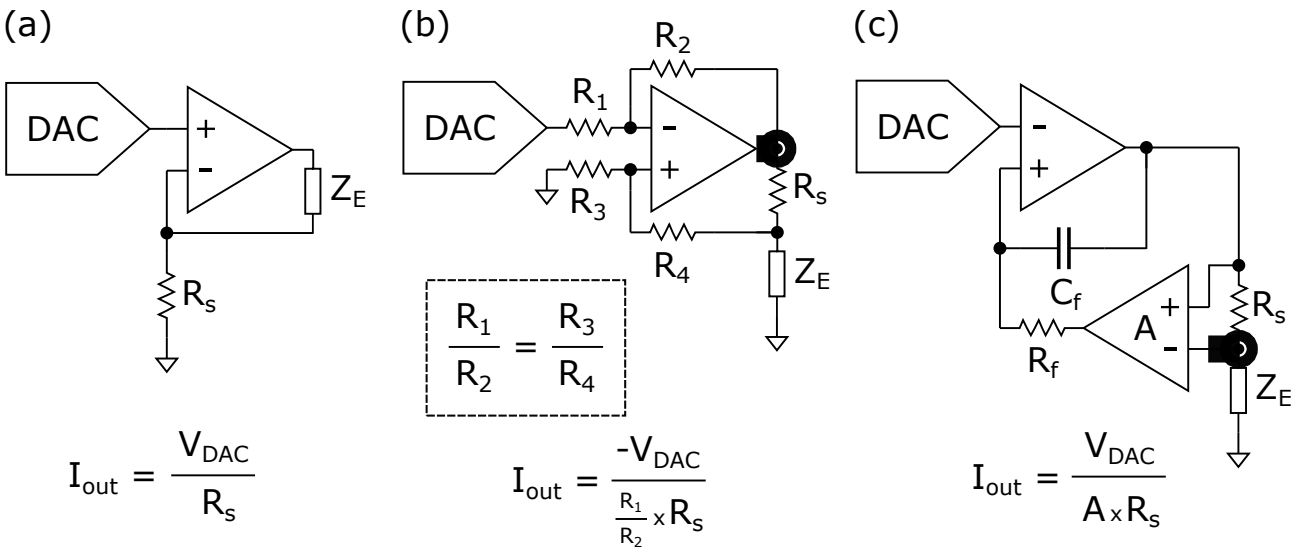


Figure 3.2: Several transimpedance circuits that can be implemented for stimulators using discrete electronics. (a) Simple transimpedance circuit. (b) Improved Howland Current Pump. (c) Instrumentation amplifier transimpedance circuit.

efficient. This topology is only seen in integrated stimulator designs where power consumption is a significant constraining factor.

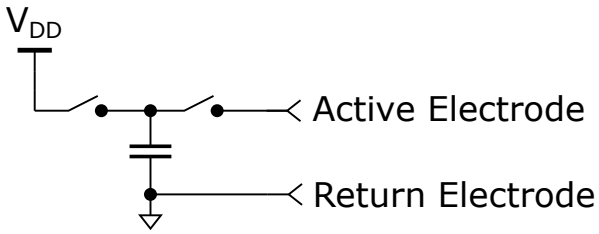


Figure 3.3: A simplified schematic for a charge controlled stimulator. The stimulator capacitor is first charged to the desired voltage (or a set of different capacitors may be charged to the supply voltage) and then the current source is discharged to the stimulation electrodes. This enables good charge control while allowing optimisation of power use due to knowing how the stimulator capacitor behaves.

## 3.3 Charge Balance

Control over injected charge, while important to ensure consistency of stimulation, also has a significant role in the safety of neural stimulation. As early as the 1950s it was already known that current sourced into neural tissue unidirectionally could cause damage [4], presumably as a consequence of faradaic currents producing cytotoxic species at the electrode-electrolyte interface and therefore in the vicinity of sensitive neural tissue [3], [16]. The paper by Lilly [4]

also proposes that quick 'charge-balanced' pulses could prevent these reactions from occurring or reverse them to prevent damage. The analysis by Shannon of empirical data on tissue damage caused by stimulation in cat brain led to the well-known plot and Shannon limit imposed on stimulators using platinum electrodes [17] shown in figure 3.4. The limit is expressed as a relationship between charge density $D$ at the electrode in [µC.cm$^{-2}$] and $Q$ the charge injected by the electrode by stimulation cycle phase in [µC] as shown in equation 3.1. The area unit in charge density refers to the surface area of the electrode. The parameter $k$ was empirically determined to have a value of 1.75 [17]. As a result most stimulators today use and even enforce charge-balanced stimulation.

$$\log(D) = k - \log(Q) \tag{3.1}$$

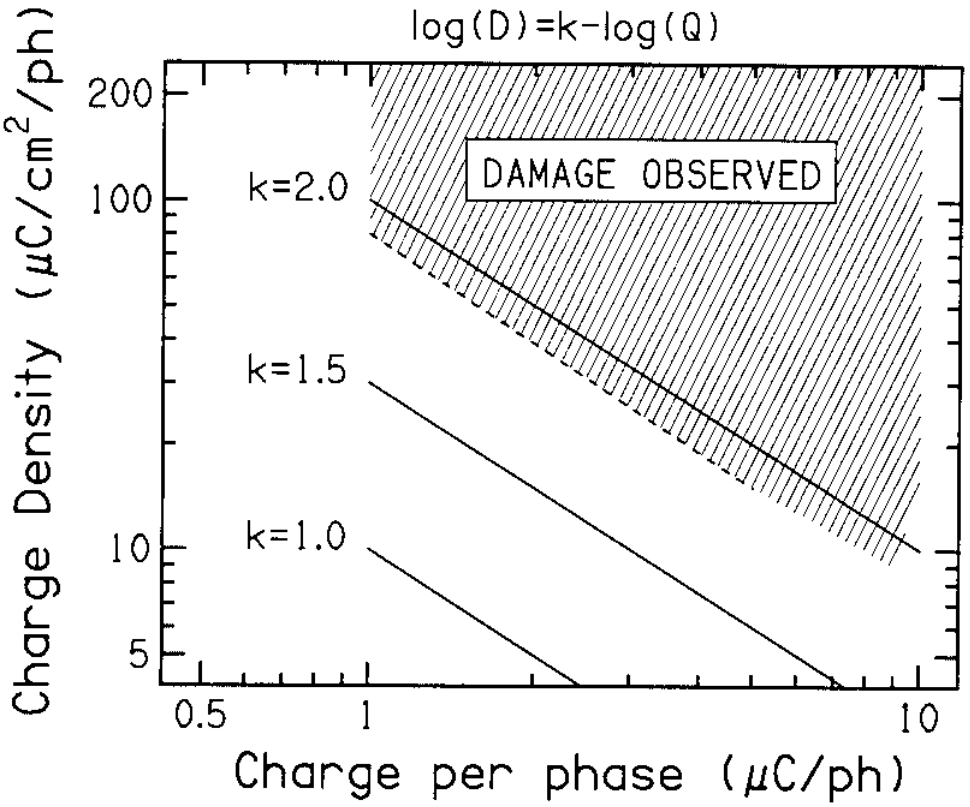


Figure 3.4: Plot showing empirically-determined limits on the amount of charge that can be injected per stimulation cycle by platinum electrodes located in cat brain as shown in [17]. Data is based on [18].

### 3.3.1 Electrode polarisation and the water window

The underlying mechanisms behind the toxicity of unbalanced stimulation are varied and complex as they relate to electrochemistry at the electrode-tissue interface. This interface is in contact with a number of organic molecules such as proteins and fatty acids which can adsorb onto the electrode surface and modify its properties [19]. The presence of these proteins as well as a number of different ions in the extracellular fluid enable a diverse set of electrochemical reactions to take place at the interface depending on electrode voltage with respect to the medium [20]. For platinum electrodes, despite the near-ideal polarisability of the material slowing interfacial faradaic reaction kinetics, two of the most important faradaic reactions that can take place are the oxidation and reduction of water to form dioxygen and dihydrogen gases respectively. These reactions can locally change the pH of the medium and produce reactive oxygen species that cause permanent damage by denaturing or modifying other important organic molecules. These water-splitting reactions can only occur when the polarization voltage of platinum electrodes shifts outside of a potential range called the *water window*. Most often this is due to the passing of current through the electrode during stimulation. The water window for platinum spans approximately -0.6 V to +0.9 V as shown in figure 3.5 relative to silver silver-chloride at physiological pH, approximately 7.2 [21], however this can change with the presence of dissolved oxygen facilitating some reactions over others.

### 3.3.2 DC leakage in current-mode stimulators

The nature of current-mode stimulators as high output impedance current sources leads to specific issues when there is not a clear '0' output setting. When the output of a current source is dependent on an input voltage and this voltage can span both positive and negative current output values, small deviations away from the '0' output voltage can lead to DC current output. As output impedance is high, the source can then charge highly polarisable electrodes until significant voltages are reached, potentially enabling water-splitting reactions to occur in the case of platinum electrodes.

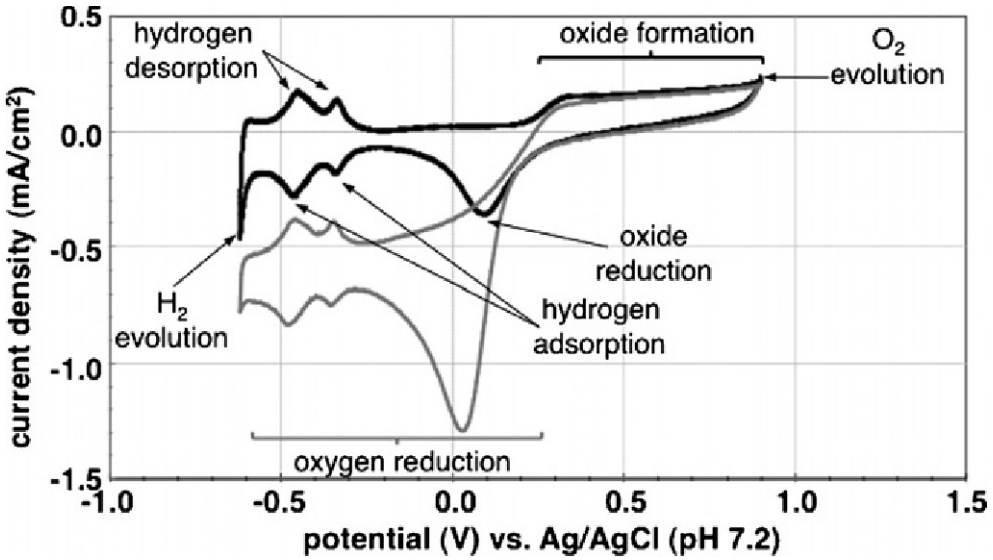


Figure 3.5: Electrochemical characterisation of platinum by voltammetry as shown in [21], where the platinum water window can be identified by the peaks near -0.6 and +0.9 V indicating the occurrence of specific reactions that lower the electrode's impedance significantly as voltage is decreased or increased respectively.

## 3.4 Compensation techniques for charge accumulation

As it was established that stimulators must not allow electrodes to be polarized outside the bounds of the water window, a number of techniques can be used at the circuit design phase to prevent this condition from occurring, or to minimise the amount of time electrodes are outside the water window. These techniques go beyond the use of biphasic stimulation to balance charge in which a stimulation pulse is followed by a pulse of opposite polarity that seeks to return the potential of the electrode to the resting state. Many designs use a combination of active and passive charge equalisation techniques to supplement or even replace biphasic pulsing [5].

### 3.4.1 Passive discharge and DC filtering

Passive components can help maintain the potential of stimulation electrodes within the water window by preventing the buildup of charge through 'unbalanced' stimulation, or by discharging electrodes through a parallel resistive pathway [22]–[24] with examples shown in figure 3.6.

As biphasic stimulation cannot guarantee balanced injection of charge during stimulation due

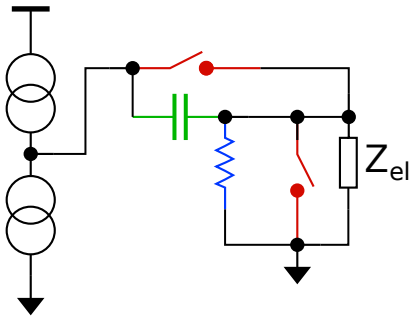


Figure 3.6: Schematic representation of passive charge-balancing circuit elements such as blocking capacitors (green), shunting resistors (blue) and discharging switches (red) attached to a dual current source stimulator. A design may use one or more of these elements for passive charge balance.

to non-idealities in current source circuits and stimulation electrode self-discharge, these can become polarized over the course of multiple stimulation cycles [3], [4]. To prevent this capacitors can be placed between the output nodes of the current source and the stimulation electrode themselves, and in this way charge which is not balanced is kept stimulator-side. To prevent charge accumulation across the blocking and decoupling capacitor, passive or active devices can be used to discharge the capacitor [25].

### 3.4.2 Active charge balancing

When bidirectional current output is required, two techniques can be used to provide this functionality. The first and most often used is the H-bridge [26], a simplified schematic of which is shown in figure 3.7, which allows the direction of current output to the load to be reversed by toggling SPDT switches.

H-bridges have the distinct advantage of allowing the use of the same current output circuit for both sourcing and sinking current to the load. This means that current sourced into the load will be very well matched with current sunk from the load, assuming that the cathodic and anodic phases of the stimulation cycle are of the same amplitude and that the output resistance of the stimulator current source is high enough to make the influence of the load impedance negligible. For applications where the stimulation cycle must be asymmetric to mitigate electrode dissolution or other undesirable effects [27], the linearity of the DAC will be

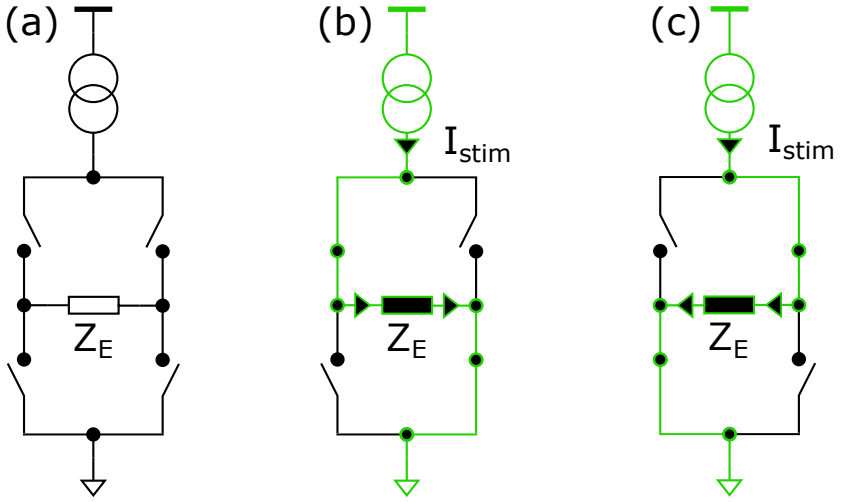


Figure 3.7: Schematic representation of an h-bridge as a set of two Single-Pole Double Throw (SPDT) switches used to invert the polarity of current moving through the stimulation electrode load. (a) Schematic representation. (b) Forward operation state. (c) Reverse operation state.

much more important for precision and control of injected charge.

The main drawback of h-bridges is that much like a capacitive charge pump [7], the voltage between the output nodes connected to the stimulation electrode may be outside the power rails when the polarity of the load is inverted by the h-bridge switches. This is due to the capacitive nature of the load when polarisable electrodes are used. As most integrated circuits use ESD diodes tied to the power rails to prevent damage from application of large potentials to any input or output, these diodes will bleed charge from the load, resulting in current going through the load being uncontrolled. To prevent this, an additional power rail must be implemented to accommodate all possible voltages that can be reached at the stimulator outputs, despite no current being sourced from this extra rail as shown in figure 3.8.

To avoid this problem, some designs have instead opted to implement two independent current sources, one for sinking and the other for sourcing current into the load [28]–[30] as shown in figure 3.9. A drawback of this strategy is that careful calibration of both current sources must be carried out to ensure that charge does not accumulate on the electrode over time with trains of stimulation pulses, as the two independent sources cannot benefit from integrated circuit matching techniques.

A second active charge balancing technique is to first measure the electrode potential at the end

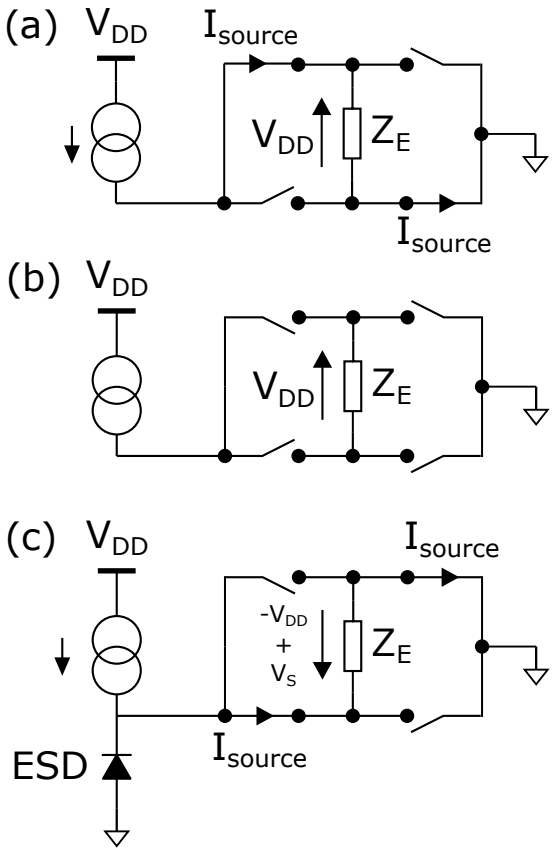


Figure 3.8: Schematics explaining how h-bridges can develop voltages outside the bounds of the stimulator power supply. (a) First pulse: the electrode is charged up to the voltage supply. (b) End of the first pulse. The electrode's double layer capacitance retains the supply voltage. (c) Reverse pulse: due to H-bridge action the stimulator sees $-V_{DD} + V_S$ with $V_S$ being the series resistance across the two electrodes. The overall voltage is negative and outside of the supply rails. Any ESD diodes connected to the current source outputs can then source or sink an unknown amount of charge from the electrodes.

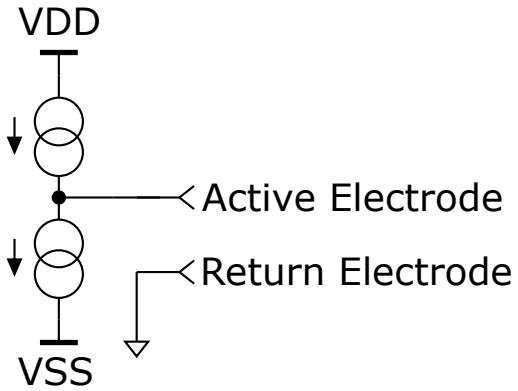


Figure 3.9: Simplified schematic representation of a stimulator current source using two sources. The return electrode is generally connected to ground, at a potential between the positive and negative supply.

of a stimulation cycle and then adjust it by injecting charge in very short bursts that will not stimulate the nerve [30], [31] to ensure electrode potential is within a specific window, generally

narrower than the water window itself.

Finally, with biphasic pulsing the duration of the anodic phase of stimulation can be adjusted to compensate for electrode and stimulator non idealities to ensure that electrode potential stays within the water window [32]–[34].

It is important to note that in implantable systems circuits that measure residual electrode polarization to determine whether to inject additional current to active balance charge do so using the stimulation electrodes. In some cases the stimulator uses a monopolar electrode arrangement with many individual stimulating or active electrodes all returning current through a common return or counter electrode. It is assumed that the potential of the counter electrode remains stable since it is much larger than the stimulating electrodes and therefore its capacitance is also much larger [5], however since it is generally made of platinum it is also polarizable and the potential between the active and return electrodes may not reflect the potential between the active electrode and bulk solution, which is the determining factor for hazardous redox reactions. In order to obtain an accurate measurement of such a potential, a three-electrode setup akin to that used by a potentiostat must be used, with a non-polarizable reference electrode such as Silver Silver-Chloride being used to measure the potential between the active stimulation electrode and the bulk solution. Unfortunately as silver silver-chloride is not biocompatible this technique cannot be used for chronically implanted devices.

### 3.4.3 Ongoing research on charge balance for safe neural stimulation

The key idea behind the adoption of charge balancing is that potentially toxic processes occurring at the electrode-electrolyte interface during stimulation can be prevented or reversed provided that the electrode potential relative to the medium is brought back to the equilibrium state as quickly as possible [20]. It should be noted however, that with continuing investigation the paradigm of perfect charge balance in neural stimulation is being challenged [21], [27], [35]. While purely monophasic stimulation is still considered unsuitable for chronic use, strict balancing of charge has also been found to be deleterious under some conditions [27]. In addition to this, a lot of the initial research establishing the need for charge balance was carried out

using studies of intracortical stimulation [17], [36]. It is likely that extraneural interfaces to peripheral nerves can sustain higher injected charge per phase and charge densities than invasive intracortical interfaces without causing damage, due to the greater distance between the electrodes and sensitive neural tissue. Apart from an initial review in 1990 [37], literature that specifically looks at the safety of peripheral nerve stimulation has been sparse. More recently focus seems to be moving towards that area with the publication of an updated review [38].

Another important note is recognizing the limitations of blocking capacitors for charge balance. It is often assumed that placing blocking capacitors between stimulation current sources and electrodes is sufficient to prevent damage, as the electrodes will not be able to source DC currents into the tissue. While these capacitors will prevent damage arising from a hypothetical fault in a system shorting supply voltages to the electrodes [25], it is not the DC current per se that is the cause of damage, but the fact that it polarizes the electrodes to a state where certain electrochemical reactions can occur. The products and effects from these reactions are harmful and nerve damage is their direct consequence. If a stimulator with DC-blocking capacitors sources current into connected electrodes, the DC-blocking capacitor and the electrode's electrical double-layer capacitance will initially be charged. The electrode can still be polarized to levels that allow harmful electrochemical reactions to occur. If enough time elapses between this initial phase and the phase of opposite polarity used to balance charge, the electrode will have returned to an equilibrium state by discharging its double layer capacitance through its faradaic charge transfer resistance according to Randles' model [3], [32]. This faradaic charge transfer represents the occurrence of irreversible electrochemical reactions that may result in harmful products for the nerve tissue. The balancing of charge with a stimulation pulse of opposite polarity will then discharge the blocking capacitor while not preventing harmful reactions from occurring at the electrode. This simple thought experiment explains why blocking capacitors alone are not sufficient to prevent nerve damage arising out of electrode polarization and self-discharge. It is only by controlling the level of electrode polarization with respect to the aqueous medium, and the time the electrodes are polarized enough to allow harmful electrochemical reactions to occur, that nerve damage can be avoided. Even then, there is evidence that nerve damage can occur purely as a result of excessive stimulation [39], [40], possibly as

a result of other processes at the level of the nerve cell such as oxygen or ATP depletion as a result of cell hyperactivity [3].

## 3.5 Designing for High Frequency Stimulation

In order to combine both conventional stimulation and high frequency block capabilities in a single stimulator, the stimulator must comply with the requirements of both interfacing methods. A stimulator that is suitable for high-frequency alternative current stimulation as described in [41] comes with specific requirements for large bandwidth and high voltage compliance due to the large currents needed for block as compared to conventional stimulation [42]. High frequency block typically requires several milliamps for small peripheral nerves and possibly higher current values when translating applications from small laboratory animals such as the rat to non-human primates [43]. Despite the use of low-impedance electrodes with cuff and hook configurations [44], this requires stimulators to have high output compliance voltages of 10V or more to source enough current. As the signal is alternating, the stimulator must be able to both source and sink current.

Many published stimulator designs do not fulfill necessary requirements for HFAC stimulation, lacking sufficient compliance voltage [12], [22], [45], [46] or having low output current, having been designed solely for conventional stimulation, potentially for low nerve recruitment thresholds enabled by invasive high impedance electrodes.

As high frequency block requires a duty cycle of 100% during operation, this leaves no time to short electrodes or passively discharge them, nor to actively balance charge by charge bolus injection at the end of block, since applications of block can require the signal to be injected for several minutes [47], [48] in certain applications. This means that even minute DC offsets in the alternating signal can lead to significant injection of DC current into the electrode, and corresponding deleterious effects. Therefore, not only is high precision required of the current source, but also a means to dynamically balance charge, such as adjusting the length of anodic and cathodic phases in the signal to compensate for DC leakage [33].

Some previous published stimulator designs can make for great alternating current stimulators, such as the Neurodyne [49], however these designs are not suitable for all types of conventional stimulation, as for example the Neurodyne's transformer core, while affording it excellent DC leakage rejection, also impacts its ability to precisely deliver short or long conventional stimulation pulses. Stimulators used in experimental work for block have typically been commercial voltage to current converters such as the DS5 (Digitimer), A360 (World Precision Instruments), or Model 2200 (A-M Systems) connected to Arbitrary Waveform Generators (AWGs). These are open-loop systems with no means to sample electrode voltage during stimulation and adjust accordingly to compensate for DC leakage. Despite careful calibration, small DC leaks can affect results in high frequency block studies [50] owing to the powerful and destructive effect of DC block [51]. The outputs of these systems can be filtered as described in [50], however fundamentally they remain single channel systems with no specific mechanism to precisely time the start and end of stimulation, which can be important when combining conventional stimulation and block for highly selective neural interfacing [52]–[54]. This makes their integration into an experimental setup difficult, and they represent a significant financial investment for the laboratory.

Multichannel stimulation capability was considered essential as a single device could then be used to precisely time stimulation on multiple locations on a nerve as required by the timed stimulation and block for selective stimulation protocol developed *in-silico*. As mentioned previously there is evidence that bipolar block is more effective in some scenarios than monopolar block, however simulation results indicated that monopolar electrode configurations could be used successfully for HFAC block. The circuitry for completely electrically isolated channels for a single stimulator is far more complex as each channel requires its own isolated power supply, digital to analog converter (DAC) and digital isolator at a minimum. This makes for an unattractive tradeoff in terms of device complexity, size and cost to manufacture considering that monopolar block is effective, therefore a key design decision was to build a multichannel stimulator with monopolar stimulation channels having a common current return to system ground. Each channel being an independent current source ensures that the current flowing through each stimulation electrode is tightly controlled while reducing system complexity. The

effect of the common return electrode can be ignored as long as it is kept at a sufficient distance from the nerve tissue where its electric field will not affect it.

When designing the following stimulator system, emphasis was placed not only on its ability to effectively carry out high frequency block stimulation as well as conventional stimulation, but also to specific features. The ability to dynamically sample electrode voltage and balance charge, handle multiple channels concurrently, and signal other devices that stimulation was occurring were all integrated into the design. The next step was to determine whether a discrete or integrated approach was most appropriate.

## 3.6 Development paradigm: discrete vs integrated electronics

The choice between discrete and integrated electronics to design a multichannel block-capable stimulator is actually quite simple. Only commercial voltage to current converters or stimulus isolators are used for high-frequency block studies in the literature. These are fundamentally discrete electronics systems where implantability is outside the scope of use due to the much higher power consumption requirements, as the duty cycle during use is 100% for several minutes at a time. However this does not prevent the use of batteries to effectively isolate the stimulator from earth and any instruments connected to the setup and using mains power supplies.

Compliance voltages of 10 V or more, while achievable using high-voltage specific integrated circuit technologies, increase the design effort. High voltage op-amps necessary for any op-amp based current sources also require specific technologies such as BiCMOS. From a logistical and time management perspective, the design, manufacturing and testing of a high frequency block-capable integrated circuit is a time-consuming process even during the three years of a doctorate degree. Knowing that several iterations would most likely be needed, and factoring into this the time needed to develop a suitable experimental setup to use the device, the quicker turnaround time of PCB design makes designing using discrete electronics a much more attractive prospect.

The key advantages of designing an integrated system for stimulation are the savings on area and power and the potential for implantability that comes with them. Implantability is an asset for chronic studies, however doing a chronic study of conventional high frequency stimulation and block would have been outside the scope of this thesis, since the primary research question is about the feasibility of using high frequency block to enhance the selectivity of peripheral nerve interfaces, and not the reliability of this hypothetical technique over the long term.

## 3.7 Embedded system design with electrically isolated modules

The consequences of choosing a discrete electronics approach is that current DACs are not readily available; design has to focus on voltage to current conversion for stimulation, with the voltage signal being generated from a tightly controlled source. Embedded systems such as microcontrollers enable the control of a voltage source with high precision in time and ensure maximum reliability by remaining independent from external devices during operation. Once programmed by an external PC, timers and peripherals within the microcontroller IC can drive the DAC voltage source that will determine the current output of each channel of the stimulator with guaranteed timing. Another advantage with using an embeded system to drive a stimulator is that controlling PCs can be electrically isolated from this system using digital isolators, allowing the microcontroller and stimulator to be powered from the same battery and simplifying power supply design.

Having a microcontroller drive the system also provides an opportunity to use it to capture neural signals, meaning that the stimulator can become a bidirectional interface. For protocols requiring fast feedback from recording to adjust stimulation parameters this can be valuable and could potentially further reduce the cost of setting up a dedicated neural recording system in the laboratory. In this case, the recording system needs to be isolated from the stimulator to help suppress stimulation artefacts [55]. This requires an external DAC to be used for the stimulator, or an external ADC for neural recording. For our use case, true concurrent

multichannel stimulation requires a multi-channel DAC, while several neural recording channels can be adequately sampled via multiplexing provided the sampling rate is high enough. In addition, microcontroller systems generally use low-voltage supplies which are compatible with those used for neural recording, while the stimulator requires much higher supply voltages. This makes the use of an external multi-channel DAC, digitally isolated from the microcontroller, an attractive choice to drive the stimulator analog front-end. Due to its multiple powerful peripherals including 32-bit timers, an enhanced DMA engine, independent SPI and UART pins on a single development board, the Kinetis K64 (NXP) was chosen as the microcontroller core for the stimulator, using the Freedom-K64F development platform shown in figure 3.10. The stimulator front-end would then directly interface with the development board by plugging into the available pin headers to provide isolated power and data to the microcontroller. Further expansion of the system is possible by stacking additional boards onto the assembly.

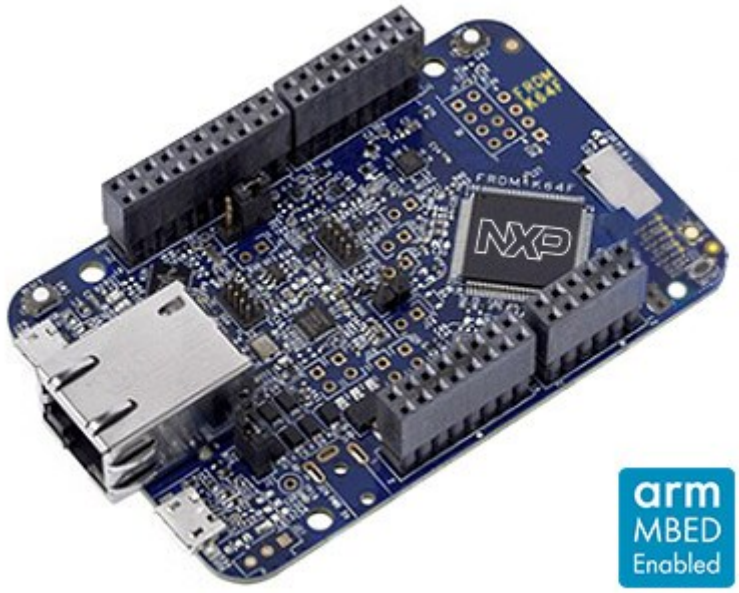


Figure 3.10: Picture of the Freedom-K64F development board used for the project, as shown on `www.nxp.com`.

The end result is a modular system comprising a stimulator front-end digitally isolated from a microcontroller module with neural recording capabilities, as shown in figure 3.11. The microcontroller module is itself programmed or controlled by a PC running a suitable interface, for example a set of MATLAB scripts accessing a PC-side UART, to program stimulation

protocols into the microcontroller. A command can then be used to start stimulation, and the microcontroller carries out the protocol without intervention from the PC, guaranteeing timing and reliability whatever the processing load is on the PC itself. This allows the PC to carry out signal processing during stimulation, for example analysing incoming neural recording data, without disturbing the operation of the stimulator. If needed stimulation parameters can be adjusted on the fly by using microcontroller interrupts. Power to the stimulator is provided by a 5 V USB battery pack or similar isolated power source that is then converted to ±18 V for the stimulator and passed through an isolating 5V-5V converter to provide power to the microcontroller board.

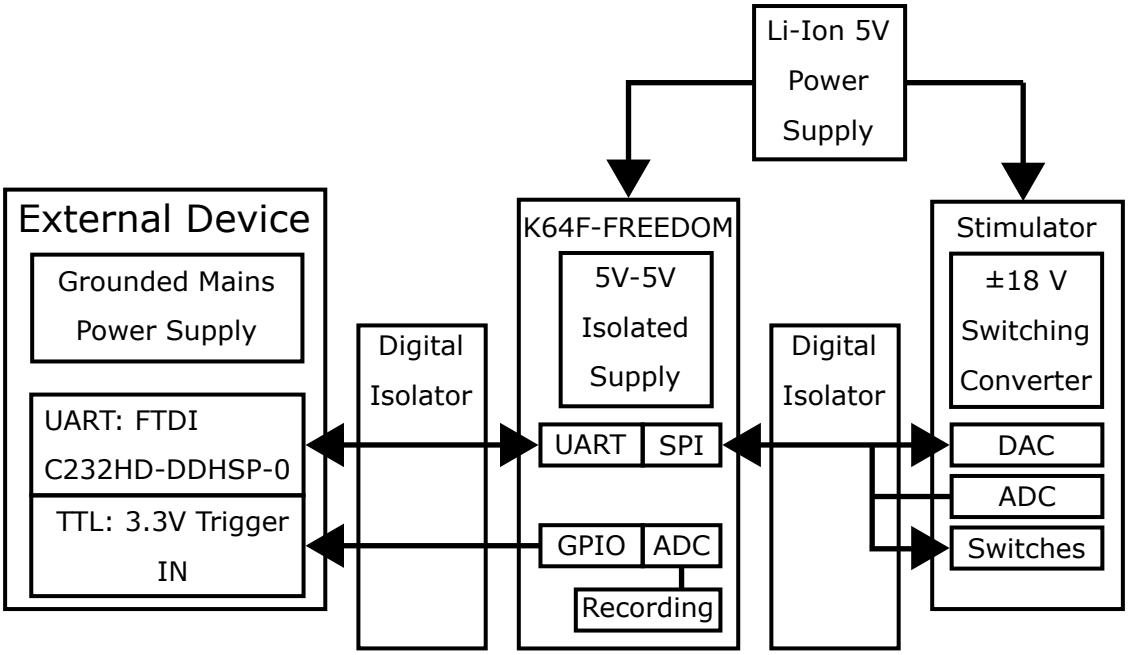


Figure 3.11: Block diagram showing the different modules included in the stimulator system, the isolated power domains and communication interfaces between them.

## 3.8 Address-event representation of stimulation commands

Usage of a microcontroller platform enables a powerful and versatile programming technique to be used to drive stimulation, ensuring timing reliability regardless of the computing load on the microcontroller processor. In essence timer peripherals can be used to trigger DMA transfers from the memory to communication interfaces such as an SPI. The same timers can be used to trigger DMA transfers from the memory to their own configuration registers, which

allow variable timer periods to be used without any processor intervention. This combination allows DAC values to be input to the multichannel DAC at specific, guaranteed times with clock cycle precision and leaving the processor free to service interrupts from a PC controlling the stimulator, or to process neural recording data with realtime latency during stimulation. A key peripheral enabling this strategy is the K64 microcontroller's Periodic Interrupt Timers (PITs), for which each independent timer channel can be used to drive one current output channel of the stimulator. The process is outlined in figure 3.12. Due to how the PIT timer operates, changes to its period register are only taken into account on the next trigger of the timer. Due to this when starting a new stimulation protocol the transfer of the first non-timing-critical period change is carried out by the processor. The DMA engine then takes over for the remainder of the stimulation protocol by alternating between transfers to the SPI, which change the DAC output value, and changes to the PIT timer period register to change the time between triggers to the DMA. In this way complete control over cathodic pulse, interphase, anodic pulse and interpulse duration can be achieved. Since the PIT timer registers are 32 bits long on the K64, knowing that the bus clock used to clock peripherals runs at 60 MHz, the maximum time between PIT triggers is approximately 71 seconds, which is more than enough for the vast majority of stimulation protocols, and the minimum time is shorter than the time needed to transfer values by SPI to the DAC.

## 3.9 Stimulator integration into experimental platforms

While some commercial stimulus isolators provide an electrode monitor allowing an external device to record the voltage between electrodes passing current into the tissue, they do not use this signal as feedback information to balance charge. Furthermore, if the goal of balancing charge is to control electrode voltages with respect to the tissue medium, as stimulation electrodes are often polarisable platinum this signal is less informative than a measure of electrode potential between a stimulation electrode and an electrochemical reference such as silver silver-chloride. In order to address this drawback, dedicated circuits were designed to allow the sampling of electrode voltage by the stimulator system. These circuits share power supplies

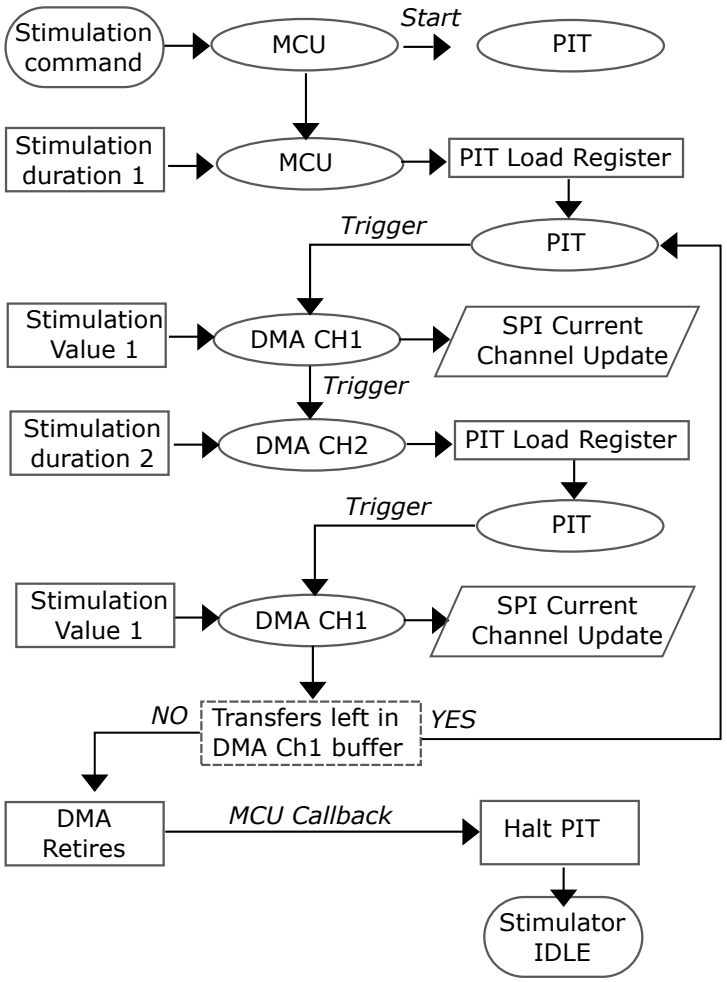


Figure 3.12: Flow diagram describing how microcontroller peripherals can be used to single-handedly drive stimulation with processor interaction only being required at the start of the stimulation protocol for configuration. describing how stimulation is carried out without processor intervention. The processor is only used at the start and end to configure the DMA and timers and to halt the timers and reset the DMA when timing is not critical.

with the rest of the stimulator, and thus require an external ADC to digitise the signal which is then communicated back to the microcontroller. The electrode monitor can be referenced to the stimulation current return electrode, or to an external silver silver-chloride reference which does not conduct any current, providing a good reference for measuring electrode voltage with respect to the medium. Measurement of voltage between the two electrodes sourcing and sinking current into the tissue can inform the stimulator as to whether compliance has been exceeded, at which point the current flowing through the electrodes may be significantly different than what has been requested by the user. This functionality can be used to stop and warn the user or dynamically adjust stimulation amplitude to prevent over-compliance conditions.

A further important feature is the ability of the stimulator to concurrently source current into multiple independent channels. These channels may have different outputs at the same DAC input due to component mismatch, and require calibration. For this purpose a specific dummy electrode circuit was designed that together with the electrode monitor provides a way for the stimulator to self-calibrate and track output drift over time and temperature to prevent errors. Only one dummy circuit and electrode monitor was implemented due to constraints on space, as the stimulator module was designed to have the same form factor as the development board housing the microcontroller. With a total of 16 SPST switches it was possible to route current channel output to electrodes or to the dummy, and route the electrode monitor input to each channel, as well as provide two different reference inputs as shown in figure 3.13. Component values are detailed in table 3.1.

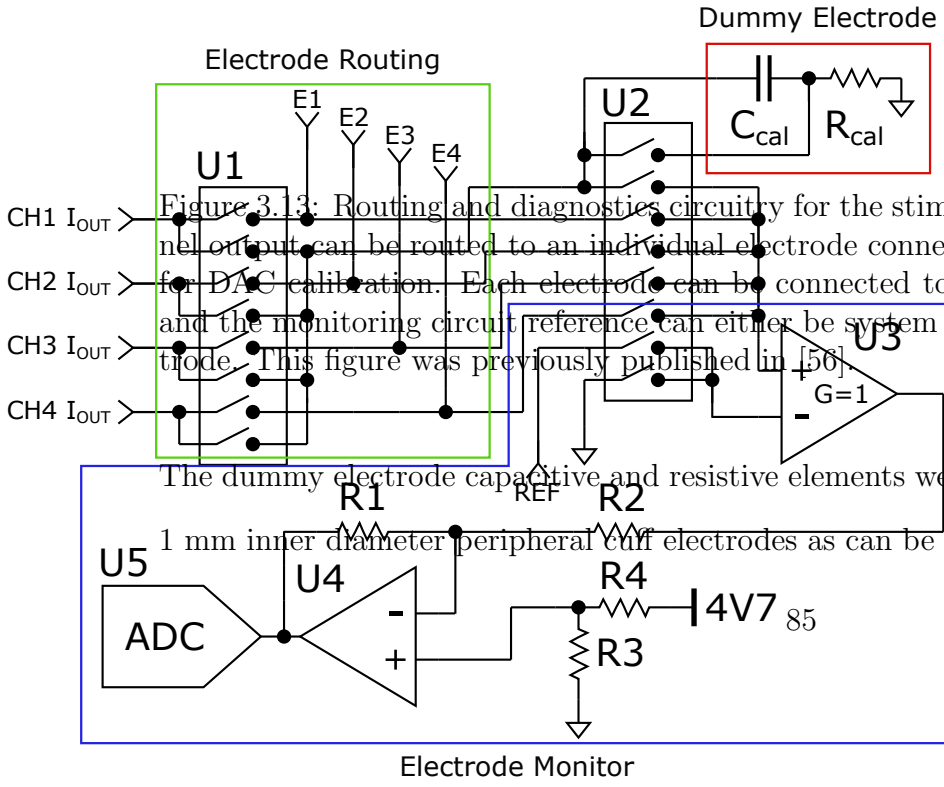


Figure 3.13: Routing and diagnostics circuitry for the stimulator front-end. Each c
nel output can be routed to an individual electrode connector or to the dummy el
for DAC calibration. Each electrode can be connected to the monitoring circuit
and the monitoring circuit reference can either be system ground or an external re
trode. This figure was previously published in [56].

The dummy electrode capacitive and resistive elements were chosen to reflect typic
1 mm inner diameter peripheral cuff electrodes as can be purchased standard in in

Table 3.1: Component values for the diagnostics module. Part of this table was previously published in [56].

| Component | Value | Component | Value |
|---|---|---|---|
| R1 | 1 kΩ | U1 | ADGS5414 |
| R2 | 9.09 kΩ | U2 | ADGS5414 |
| R3 | 2 kΩ | U3 | AD8422 |
| R4 | 3.24 kΩ | U4 | OPA211 |
| $R_{cal}$ | 1 kΩ | U5 | LTC2313ITS8-14 |
| $C_{cal}$ | 100 nF | | |

electrode monitor was made to accomodate all possible voltages across the electrodes within the supply rails and then scaled down to a suitable input voltage for a 16-bit SPI-driven ADC, sharing an SPI link with the DAC driving current output channels.

## 3.10 HFAC-capable current source using discrete components

To provide block-capable stimulation capabilities, the stimulator current source has to be able to source and sink alternating current waveforms at tens of kilohertz without distortion or attenuation as it can be an issue for some voltage to current converters [57]. The compliance voltage available to the stimulator must be maximised to accomodate for the large currents needed for HFAC block. To speed up the circuit, ideally the effect of the large capacitance of extraneural electrodes such as cuff electrodes must be minimised, i.e. having the load within the feedback loop should be avoided as this will lead to worse tradeoffs between speed and stability.

For this reason the Howland Current Pump was chosen as the most suitable current source for stimulation. The feedback paths are independent of the load at the electrode and allow fast settling for the circuit even with large capacitances at the output. However its output impedance is directly tied to the matching of the resistor network and the CMRR of the error or primary amplifier. Combining high CMRR, low offset, wide bandwidth and large output current is difficult in a single amplifier. For this reason a compound amplifier approach was

chosen based on the work of Jiang [14] in which a secondary wide bandwidth, current feedback amplifier with large output current capability was used to complement a low offset, high gain amplifier, with the resulting circuit shown in figure 3.14, and component values detailed in 3.2.

These channels each have a current source driven by a DAC voltage input. DACs with multiple output channels that can be driven by a single communication interface and are a good choice for this role. An ideal DAC will have multiple output channels driven by a single $I^2C$ or SPI interface, fast settling time and enough resolution to bound the maximum current output error to safe levels for stimulation. The MAX5580 (Maxim Integrated) DAC was chosen for its combination of 12-bit accuracy and full-scale settling within 3 µs, in addition to having 4 independent channels driven by a single SPI interface.

Closely matched resistor networks are available commercially nowadays enabling the use of this kind of circuit with high output impedance and minimal potentiometer-based trimming. The real implementation of this circuit does contain some trim potentiometers in series with R2, R4 and R7 to maximise output impedance. As the Howland Current Pump uses both positive and negative feedback paths, if the gain of the positive feedback branch outstrips that of the negative branch, a unique operating condition results in which the output impedance of the circuit is negative [13].

In line with what happens to the output of a current source with finite output resistance, changes in the output node voltage also change the output current. In the case of a negative resistance, output current increases with increasing output node voltage when the voltage is positive, and vice versa when the voltage is negative. If the stimulator is operating close to its compliance limits assuming infinite output resistance, there will be significant distortion of the current waveform in a real-world scenario, wherein the electrode will be highly polarized and likely to cause damage to the nerve tissue. To account for this, trimming is necessary to ensure that the output of the circuit stays stable with varying output node voltage.

Biasing of the input is carried out using R6 and R7 trimmed with R10 so that even though the mid-scale voltage output of the DAC is 2.048 V[1], the resulting voltage at the input of the circuit

[1]The resistor values used in the circuit reflect the assumption that the mid-scale voltage is 2.5, which is in

is 0V and the primary amplifier does not have to sink current sourced by the DAC when the Howland Pump is set to output 0 A, at which point we assume that the output node voltage is 0 V.

The circuit gain is specified in equation 3.2. Component values were chosen for the gain-setting resistor network such that the full scale current output spanned ±10 mA output could be achieved despite the nonidealities of the DAC and op-amps. As the DAC LSB is 1 mV, the ratio between the gain resistors is 0.1, and the sense resistor is 20 Ω, each DAC step theoretically corresponds to an output step of 5 µA, which was considered an acceptable maximum error for the dynamic range required.

$$I_{OUT} = -\frac{1}{R_S \times \frac{R1}{R2}} V_{in} \tag{3.2}$$

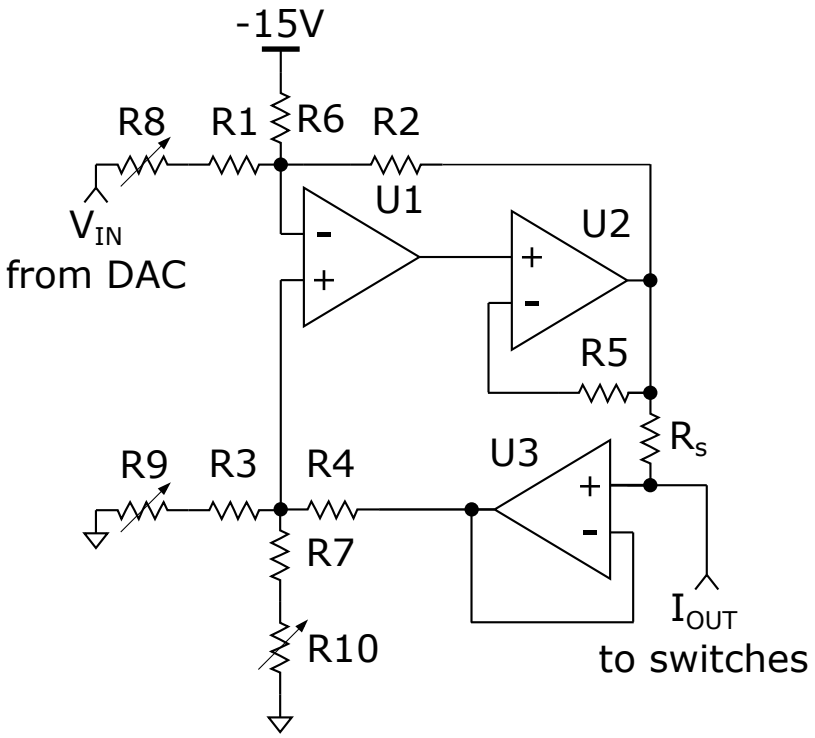


Figure 3.14: Schematic for the Howland Current Pump circuit used as the voltage to current converter for each channel of the stimulator. Variable resistors are trim potentiometers (BOURNS). Adapted from [56].

error. This was corrected by adjusting the mid-scale voltage in software after assembly.

Table 3.2: Component values for the current output channel. This table was adapted from [56].

| Component | Value | Component | Value |
|---|---|---|---|
| R1 | 10 kΩ | R6 | 64.2 kΩ |
| R2 | 1 kΩ | R7 | 64.2 kΩ |
| R3 | 10 kΩ | R8 | 3224 50 Ω |
| R4 | 1 kΩ | R9 | 3224 50 Ω |
| R5 | 1 kΩ | R10 | 3224 5 kΩ |
| $R_S$ | 20Ω | U1 | OPA211 |
| U2 | AD844 | U3 | OPA211 |
| DAC | MAX5580AEUP+ | | |

## 3.11 Use of Triphasic Waveforms to reduce electrode polarization

One limitation of many current source devices used for HFAC block is the inability to avoid electrode polarization by bleeding through the faradaic charge transfer resistance of connected electrodes. Even with DC blocking capacitors, injecting a square wave into an electrode will cause a substantial amount of charge to bleed through the faradaic charge transfer resistance at the start and end of the waveform as shown in [50], [58], [59]. This phenomenon can be mitigated by using zero-mean charge waveforms as suggested by [59]. this was implemented for the proposed stimulator by halving the duration of the first and last half-cycles of block, effectively making the waveform zero-mean and limiting electrode polarization at the start and end of the waveform. Measurements taken of the voltage across the capacitor component of a mock electrode circuit is shown figures 3.15 and 3.16 for biphasic and triphasic or zero-mean operation respectively. The mock electrode circuit is detailed further below, figure 3.20.

It is evident from the graphs that when using a purely biphasic waveform the electrode capacitor will be polarized in only one direction at the start of the waveform. This will occur whether or not there are DC blocking capacitors and will lead the electrode to self-discharge preferentially in one direction until equilibrium has been achieved with respect to the average charge level on the electrode capacitor during one cycle of the square wave, which will tend towards zero. This will lead to long DC-like pulses of current being sourced into the tissue, once during the start of the block waveform and once at the end. This does not occur when using a zero-mean

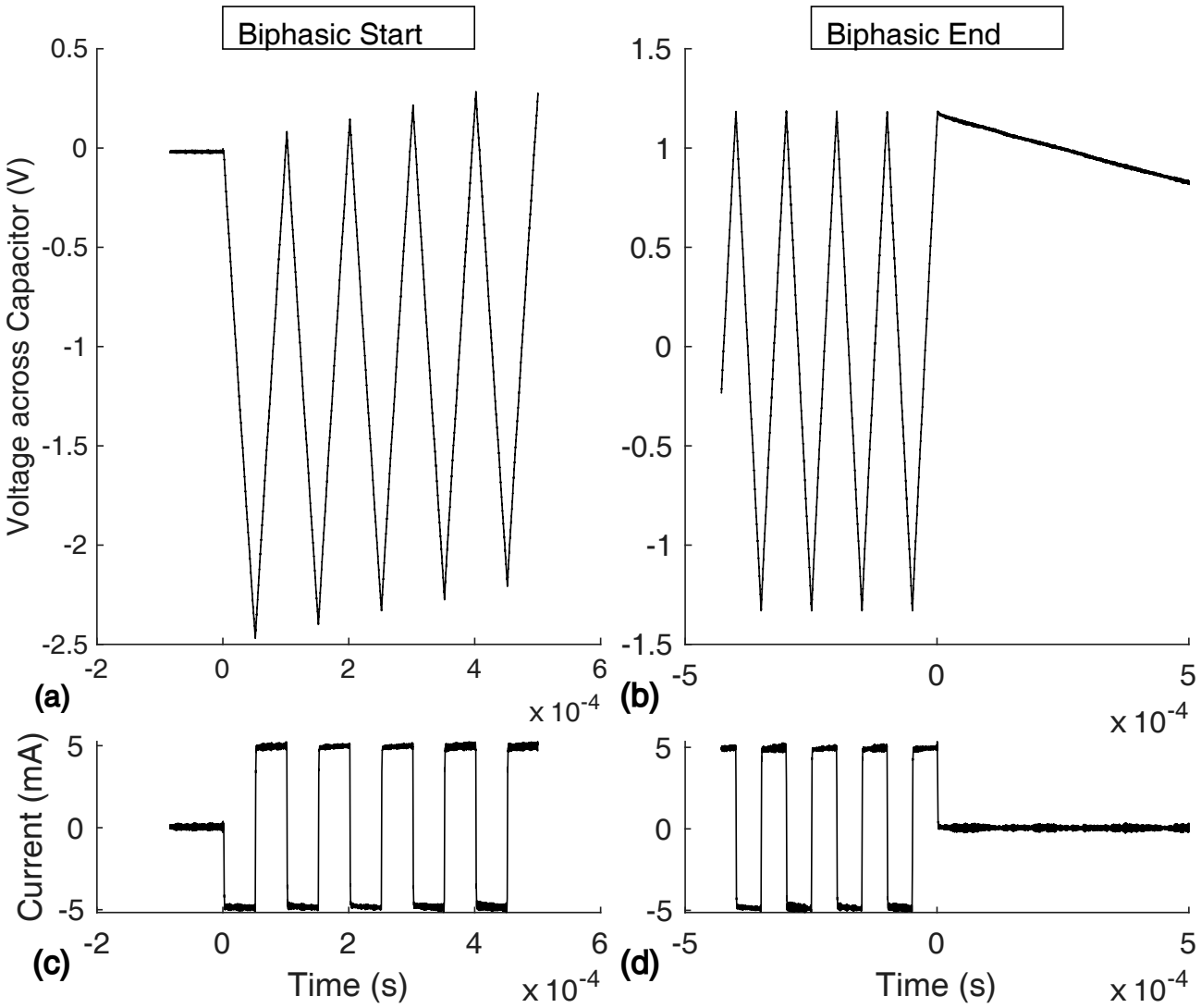


Figure 3.15: (a): Voltage across the mock electrode circuit capacitor at the start of biphasic HFAC block. (b) Voltage across the mock electrode circuit capacitor at the end of biphasic block. (c) and (d) corresponding current output from the stimulator as measured by a current sensing resistor.

waveform as the charge on the capacitor is ensured to be close to zero by the waveform itself. The zero-mean waveform is achieved by halving the length of the first and last cathodic and anodic phase in the signal respectively. At that point the only means for charge to accumulate on the electrode capacitor is by imbalance between the anodic and cathodic phases, which has a much smaller effect at the start and end of HFAC block waveforms. By default, the stimulator uses such a zero-mean waveform for HFAC block.

The same phenomenon occurs during conventional stimulation however its effect is much smaller as these events have short durations that prevent the electrode capacitor from discharging

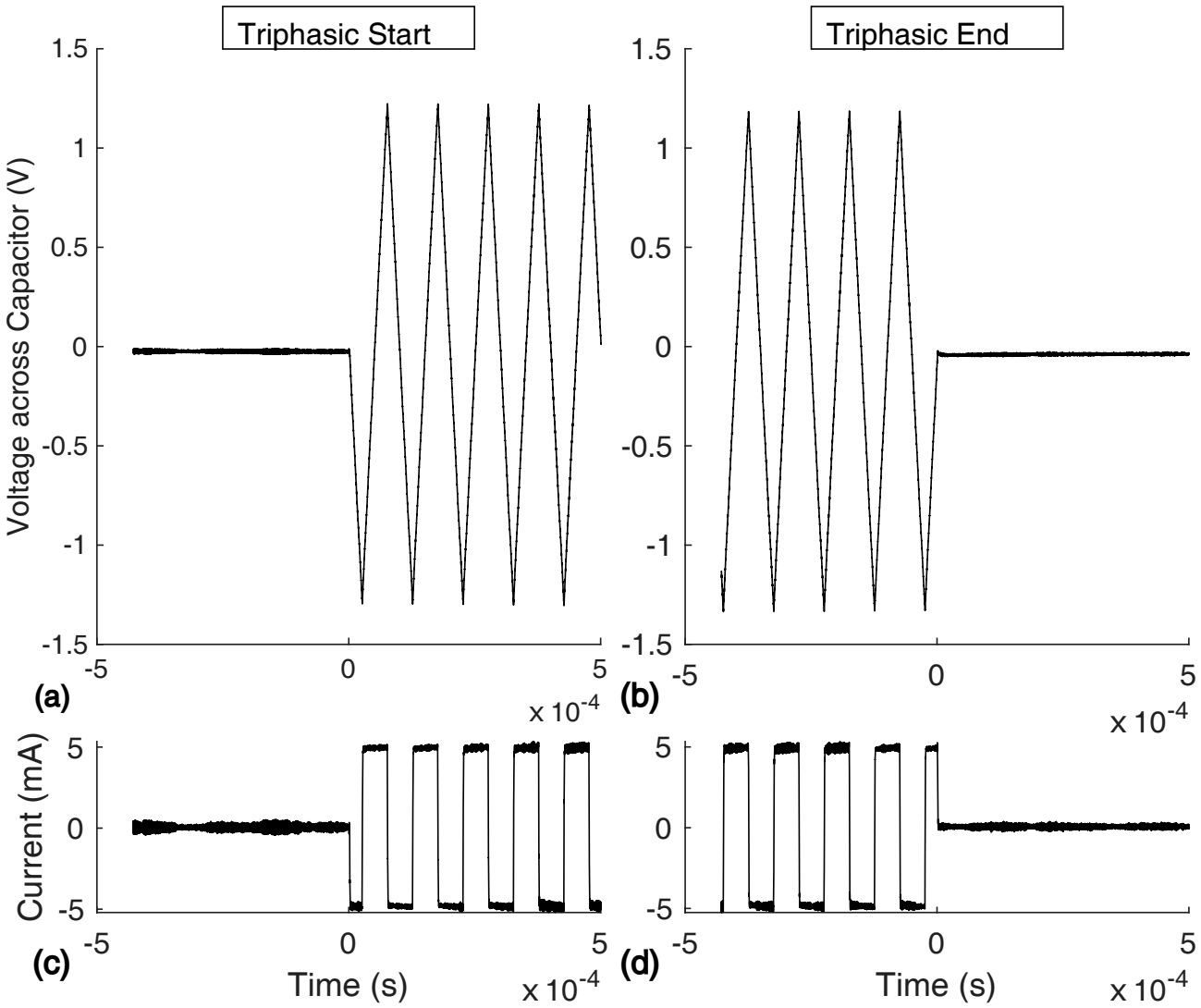


Figure 3.16: (a): Voltage across the mock electrode circuit capacitor at the start of triphasic HFAC block. (b) Voltage across the mock electrode circuit capacitor at the end of triphasic block. (c) and (d) corresponding current output from the stimulator as measured by a current sensing resistor.

significantly, as the corresponding time constant is quite long for both the mock and real electrodes. The effect is much stronger for HFAC block waveforms lasting several seconds and with a duty cycle of 100%.

## 3.12 Stimulator Characterization

To ensure that the stimulator would comply with requirements for high frequency block, a number of tests were carried out to measure output impedance and compliance and how well the

complete circuit preserved the DAC's manufacturer-specified resolution and linearity. Further tests were carried out to ensure the stimulator behaved as expected when injecting charge into lumped sum 'mock electrode' models as well as real electrode in phosphate-buffered saline.

### 3.12.1 Output Impedance

To measure compliance, output node voltage was swept from -18 V to +18 V in 100 mV steps using a Keithley 2635B Sourcemeter at 10 mA current output from the stimulator both for sinking and sourcing cases. Keithley received current was measured as a function of stimulator output node voltage to determine the compliance limits of the stimulator, with results shown in figure 3.18 showing voltage compliance of ±15 V before noticeable output error.

To measure output impedance magnitude over frequency, the setup shown on figure 3.17 was used. The output impedance plot is shown figure 3.18 with a cut-off frequency of approximately 1 kHz. The DC output impedance magnitude is approximately 2 MΩ. Assuming the series resistance of the arbitrary waveform generator (AFG3102, Tektronix) is negligible compared to the 15 kΩ measurement resistance, the latter and the output impedance can be considered in parallel. The output impedance magnitude was calculated using the following equation:

$$|Z_{out}| = \frac{R_m * (U_{AFG} - U_{measure})}{U_{measure}}$$

where $U_{AFG}$ is the amplitude of the AFG output sine wave and $U_{measure}$ is the amplitude of the sine wave measured at the terminals of the measuring resistance. A simulation of the circuit was also carried out in LTspice XVII for comparison.

### 3.12.2 Resolution and Linearity

All DAC output values were swept and the resulting output current measured through a 819 Ω resistor using a 434-series Wavesurfer Oscilloscope (LeCroy). A resistor below 1 kΩ had to be used in order to improve the measurement accuracy by using lower voltage per division and

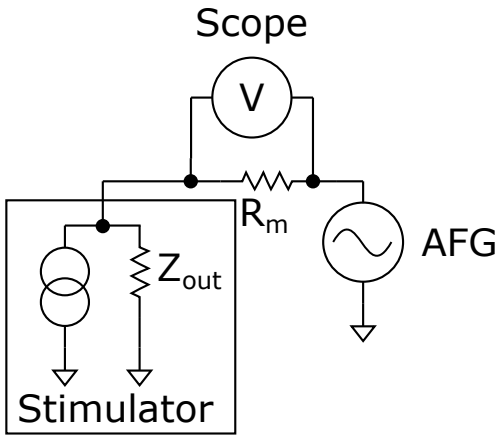


Figure 3.17: Instrument setup used to measure the output impedance of the Howland current pump. This figure was previously published in [56].

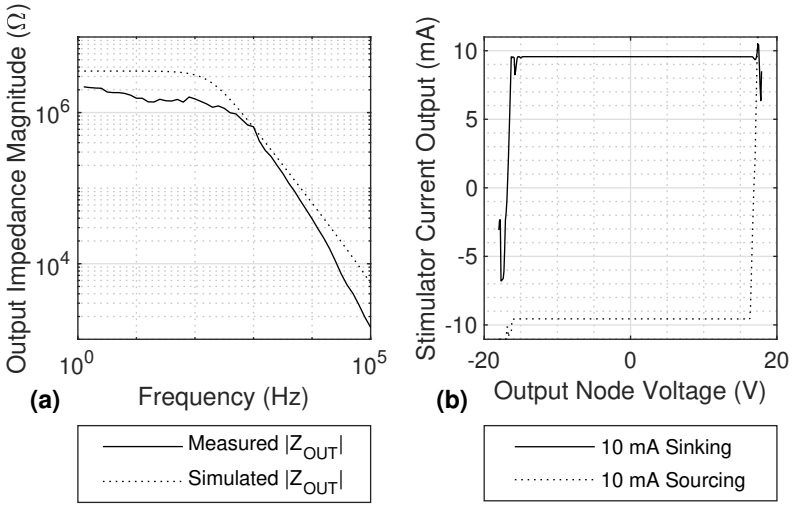


Figure 3.18: (a) Output impedance magnitude over frequency for one current output channel of the stimulator, comparing simulated and measured results; (b) measured current output of the stimulator when sweeping the output node voltage in maximum current sourcing and sinking scenarios.

analog offset settings on the oscilloscope. Data was filtered by averaging at each step. Step size was on average -5.6784 µA/LSB. DNL and INL are plotted on figure 3.19. As output displayed non-linearity at the extremes of the range the INL plot was cropped accordingly to reflect performance in the linear range of the circuit. The output range of the circuit spans ±10 mA as shown in figure 3.18.

### 3.12.3 Average Bias Current during Block

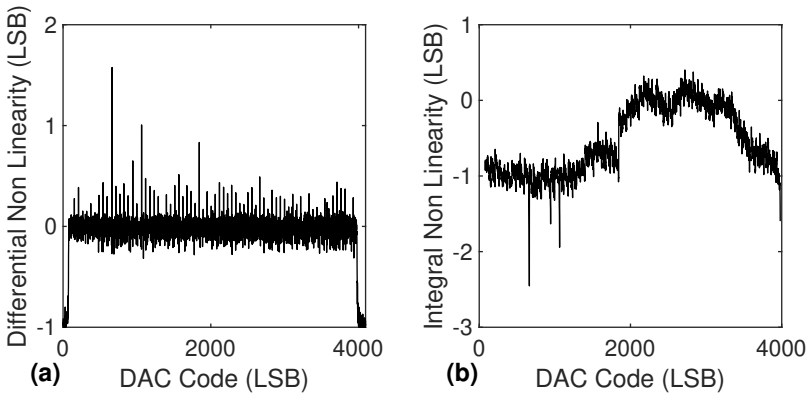


Figure 3.19: (a) Differential non linearity (DNL), normalised to LSBs; (b) Integral non-linearity, normalised to LSBs. Note that the INL plot in (b) has been cropped to display values in the linear operating range of the circuit.

As some charge imbalance is unavoidable, especially when considering the 100% duty cycle used during HFAC block, it is important to know the equivalent levels of DC current sourced by the device when it is used for block.

For this and the following two tests described in this section, the mock electrode consisted in a parallel resistor-capacitor element in series with another simple resistance to approximate an electrode, as shown figure 3.20. In this circuit, $R_S$ is used as a current-sensing resistor and a differential probe is connected to both terminals to measure the current flowing through the mock electrode circuit. The value of $R_S$ is 100˙ Ω. $R_P$ is used as an equivalent for the faradaic charge transfer resistance of real electrodes with a comparatively high value of 15˙ kΩ. Finally the capacitor C representing the capacitance of the electrode-electrolyte interface is of the value 100 nF, approximating that of typical cuff electrodes.

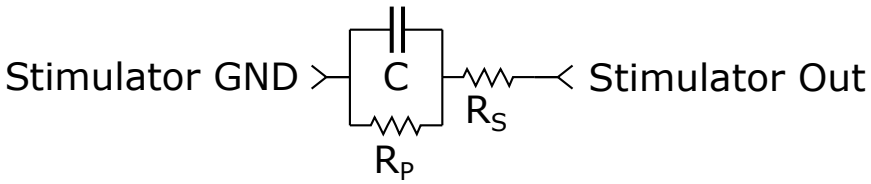


Figure 3.20: Lumped mock electrode circuit schematic.

Blocking signals were injected into the model circuit and the voltage and current recorded. Amplitudes and frequencies used were 1, 3, 5, 8 and 10 mA and 10, 20, 30, 40, 50 kHz respec-

tively. Average DC current sourced by the stimulator during block was determined by analysis residual voltage at the end of the block cycle. The block duration was extended until no change was seen in the level of charge at the end of block, indicating the steady state had been reached and was representative of the average DC current sourced. Results are shown in figure 3.21.

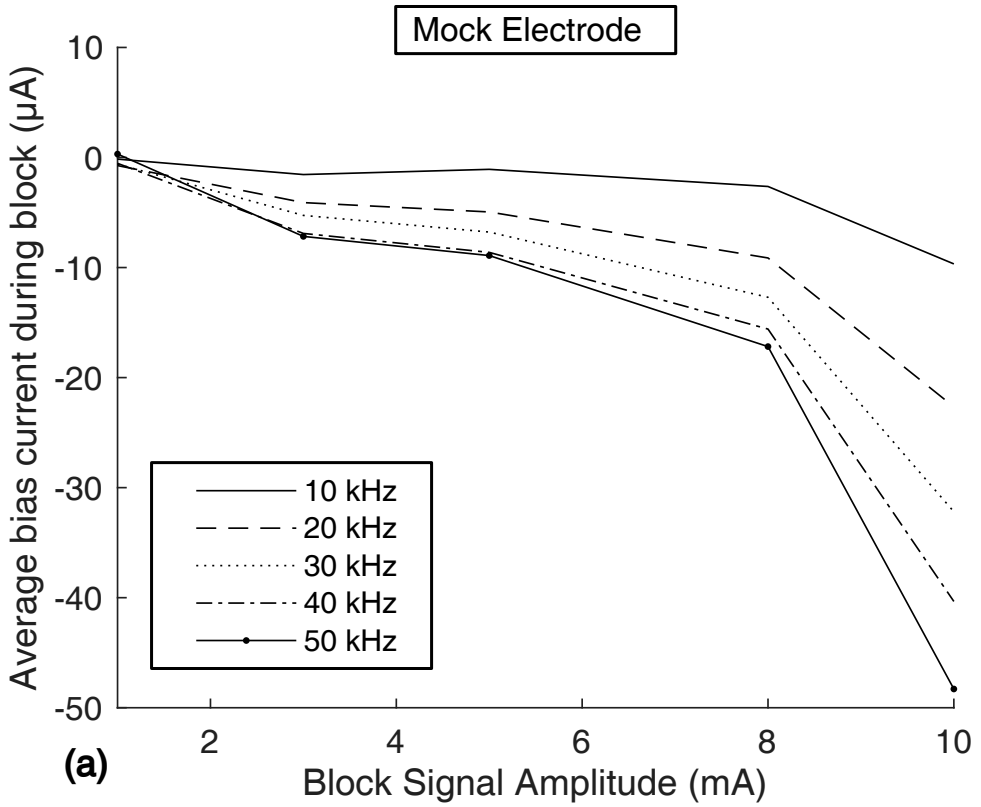


Figure 3.21: Average bias current sourced by the device during HFAC block for a range of frequencies and amplitudes, measured using a mock electrode test circuit.

The results show that with higher block amplitudes and frequencies, the average DC current sourced by the device increases. For 10 kHz average DC is kept under 5 µA except for the highest possible amplitude at 10 mA of block. These results suggest that to prevent high levels of electrode polarization, very high stimulation amplitudes such as 10 mA or higher frequencies should be avoided, and therefore stimulation protocols using the device will focus on using 10 kHz blocking signals where possible. Due to resolution limitations with the measuring equipment it was not possible to precisely measure the current flowing through a real electrode and provide results for this, however subsection 3.12.5 deals with measurements of residual voltage after block which can provide related insight as to how polarized a real electrode becomes.

### 3.12.4 Measured versus Expected Charge Injected during Block

A test measuring actual injected charge per phase of block relative to the expectation from the stimulation parameters was carried out with the same parameters as the previous test. Results are shown in figure 3.22, both for the mock electrode test circuit and for a real cuff electrode (Cortec) of 1 mm inner diameter in phosphate-buffered saline.

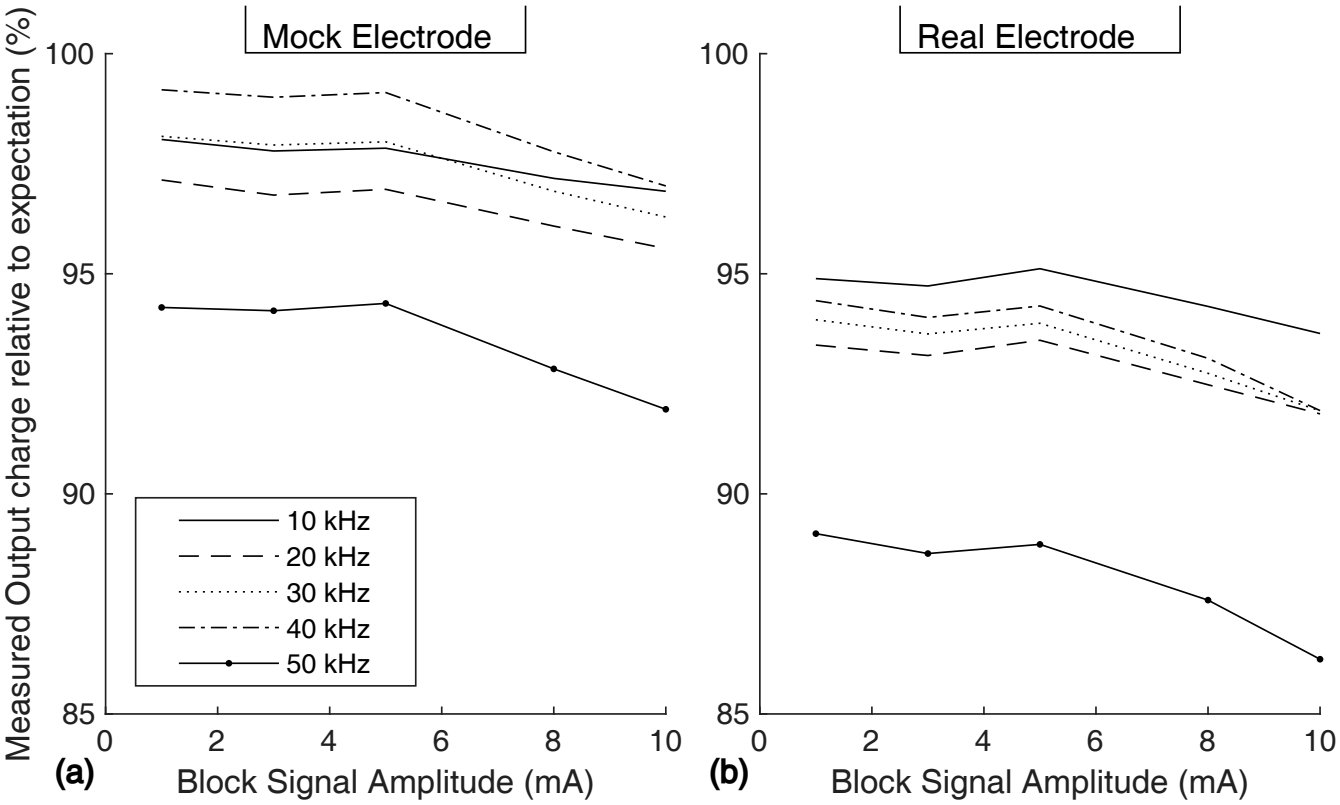


Figure 3.22: Relative measured charge injected compared to expectation for the stimulator during HFAC block for both the mock electrode test circuit and a real cuff electrode in saline.

The results indicate that broadly speaking the stimulator is accurate for block frequencies at 40 kHz and below where the error is less than 5% between actual injected charge and the expectation. The error is larger at 50 kHz and this is likely due to gradually worsening output impedance with increasing frequency. The performance for the real electrode is somewhat lower than for the mock circuit, likely due to the higher series resistance of the real electrode compared to the mock circuit.

### 3.12.5 Post-Block Residual Voltage

A useful metric to ascertain whether an electrode has been polarized to levels outside the water window is to measure the residual voltage at the end of the block waveform. Outside of the water window, water-splitting reactions start occurring which change the local pH and cause damage to tissue. The residual voltage after the end of the block waveform as shown in figures 3.16 and 3.15 reflect the average electrode polarization during block. A value above 800 mV or below -600 mV indicates the electrode was outside of the water window for a significant amount of time when HFAC block was used.

This measure was carried out for both the mock electrode circuit and the same real electrode in saline as mentioned in the previous subsection. The results of the measurement are shown in figure 3.23.

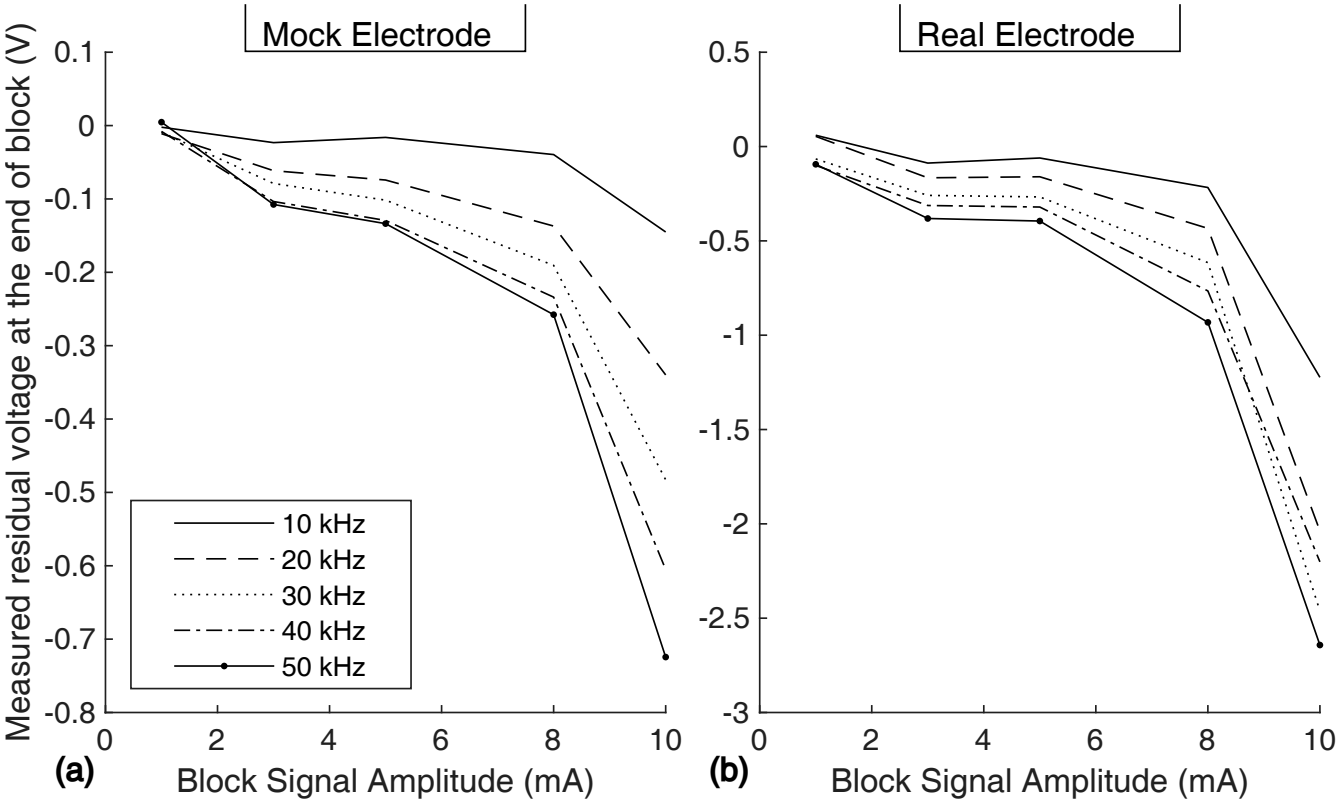


Figure 3.23: Residual voltage measured after the end of block for both the mock electrode test circuit and a real cuff electrode in saline.

The results are qualitatively quite similar between the mock circuit and the real electrode, indicating that for the most part a scaling factor can be used to predict the behaviour of real electrodes from measurements carried out on a mock electrode circuit. Quantitatively electrode polarization out of the water window is reached for high block amplitudes of 8 mA or more

at certain higher frequencies, otherwise these levels of polarization are only reached for the maximum output amplitude of 10 mA, which will be avoided during HFAC block protocols where possible to prevent damage to the nervous tissue. These results confirm it is preferable to use lower frequencies of block to avoid electrode polarization, however a wide span of block amplitudes is still possible to use safely.

### 3.12.6 Channel-Channel Crosstalk

Due to using a single current return electrode, it is possible for stimulator channels to bleed current into each other when operating at the same time, for example during concurrent conventional stimulation and high-frequency block. The amount of current sourced in this manner depends on the frequency and amplitude of another channel's output waveform as seen from the perspective of the receiving channel. In the worst case scenario assuming the outputs of two channels are connected together, a 10 kHz input voltage waveform of 15 V amplitude will see an input impedance close to 40 kΩ which will result in a maximum of 375 µA of leakage, which will not affect block thresholds as these are more than an order of magnitude higher at several mA. Inversely stimulation amplitudes used during block trials to ensure complete recruitment of nerve fibres are also at this order of magnitude in amplitude and will therefore not be significantly affected. In actual experiments the impedance between channels will in fact be much higher due to the separation between electrodes connected to different channels active at the same time, e.g. 2-3 cm of distance between conventional stimulation and block electrodes, which will further reduce channel-channel crosstalk.

## 3.13 Discussion

When taking into account the initial goals of creating a stimulator capable of concurrent high frequency block and conventional stimulation, the proposed system complies. A comparison of the performance of system with other designs from the literature is given table 3.3.

Table 3.3: Measured performance specifications for the stimulator compared to other similar designs. Table previously published in [56].

| Parameter | [60] | [8] | [12] | [61] | [56] |
|---|---|---|---|---|---|
| Device Type | CMOS | CMOS | COTS | COTS | COTS |
| Compliance Voltage (V) | N/A | 17 | 18 | 120 | ±15 |
| Full-scale Current (mA) | 1 | 0.31 | 0.250 | 10 | ±10 |
| Current Resolution (µA) | N/A | 10 | 1 | analog | 5.6784 |
| Stimulation Timing Resolution (µs) | N/A | 0.8 | 2 | 5 | 4 |
| Channel Number | 4 | 8 | 1 | 1 | 4 |
| Power Consumption (W) | 0.0189 mW | 0.029 | 0.165 | 1.8 | $\leq 4$ |
| Size (cm) | $3 \times 1.5 \times 0.5$ | N/A | $2 \times 4 \times 0.5$ | N/A | $9 \times 6 \times 5$ |

While concurrent stimulation is possible using multiple independent channels, the proposed design relies on a specific monopolar stimulation electrode configuration, i.e. an electrode connected to system ground is used as a common return for all stimulation currents, and must be held away from electrically excitable tissues in an experimental setup. Individually isolating each channel would have been possible only when providing isolated high-voltage supplies and a dedicated DAC for each channel, and significantly higher system complexity from a communications perspective. Together with existing size constraints for the device to preserve the form factor of the microcontroller development board, the tradeoff was not considered viable. In the event that bipolar stimulation is needed on several channels, multiple stimulators can be controlled from one PC and stimulation protocols can be started on several devices with very low latency.

In terms of AC and DC performance, **the system is very accurate and linear over the output range of interest and features high output impedance compared to cuff electrode impedances at DC.** At AC frequencies, output impedance begins to roll off at 1 kHz despite using a wide-bandwidth amplifier, and this in turn results in output error that increases with output amplitude and frequency. Output error is kept at minimum levels for 10 kHz block output and therefore this frequency will be prioritized in experiments with real tissue. Fortunately, as the output impedance of the circuit decreases for higher frequencies, so does the impedance of most electrodes until the electrode impedance magnitude is dominated by the bulk electrolyte resistance of Randles' model. Possible adjustments to the circuit topology include using an inverted configuration for op-amp U2, trading power for speed as this topology would

require a feedback resistor network sinking current from U1. Differences between the simulated and measured output impedance over frequency suggest there may be additional optimisations that can be carried out to improve the speed of the design for the highest frequencies, most likely at the level of the PCB where size constraints forced tradeoffs on signal isolation, which could have lead to larger parasitic capacitances on some sensitive nodes (see Appendix for layout).

**It is important to note with this design that power efficiency was not a design constraint** and that this allowed more freedom when choosing components optimised for speed and precision. As such power consumption compared to other stimulators is quite high at around 4W. A significant portion of this power is actually consumed by the microcontroller board running at maximum clock speed. This clock speed is not necessary for operation of the stimulator, however it does provide more timing precision and enables the use of a very fast SPI interface to minimise the lag between the sending of a DAC output voltage change command, and seeing this change on the current output of a channel, which can make a difference for very short stimulation pulses or the higher frequencies of HFAC block such as 40 kHz block. As it is the system cannot turn off unused channels which is not power efficient, but adding more switches for this functionality was not possible due to size constraints on the board.

Some experience using this design in experimental scenarios has identified potential areas for improvement that rely on modest increases of the PCB size. With such an increase, more reliable connectors can be used and several more power-saving features can also be implemented. In addition, moving power supplies off the board and using a shielded enclosure for the switch-mode regulators should help further reduce noise, especially in the context of using the microcontroller board power domain for ENG recording. Initially output current noise was quite high as a result of the proximity between an unshielded converter inductor L1 and the feedback nodes connected to the inputs of U1 in channel 0 and 1 (see figure 7.1). Replacing this inductor with a shielded version significantly reduced noise however greater gains are likely if there was more space between it and the affected nodes, and if these nodes were better shielded with grounded copper on the board.

## 3.14 Conclusion

**To conclude a powerful and versatile stimulator was designed and implemented for acute experimental use. It is the only stimulator of its type to be capable of electrically blocking nerves using high-frequency waveforms, and gives complete control to the user over this waveform using a flexible and reliable address-event representation for stimulation.** As stimulation does not rely on the processor, the stimulator is responsive to commands during a stimulation trial and these commands do not disrupt the operation of the stimulator even though it uses only one processing core. The design was extensively tested both conventionally and during *ex-vivo* and *in-vivo* trials and was found to perform to specification in every case. As suggested by results measuring residual voltage after usage of HFAC block, protocols involving block will use signals at 10 kHz frequency along with the lowest possible amplitude to reduce residual electrode polarization. As a result of using zero-mean waveforms for block, polarization of the electrode at the start and end is minimized and this reduces the amount of charge sourced faradaically into nerve tissue compared to stimulators using regular biphasic waveforms, especially for HFAC block. A number of stimulators were assembled[2] and used successfully in experiments and further development work by several students and another research group at Imperial working on novel electrode materials [62]. Work using this stimulator is ongoing and will likely lead to further adjustments and optimizations of the design.

The key strengths of the proposed stimulator design are:

1. Based on Commercial Off-The-Shelf (COTS) components.
2. Space-saving design at less than $6 \times 8 \times 5$ cm volume.
3. Cheap to source and assemble (less than GBP 350 or USD 450 for components and board).
4. Flexible powering options, including the controlling computer through a dedicated 5W USB port.

[2]Special thanks to Jieni Wang, Charalampos Mastrokostas and Deland Liu for their assistance assembling multiple copies of this more-than-200-component board, without a pick and place machine.

5. **Complete control of output waveform**, scripted using any program and hardware that can interface with the microcontroller UART.

6. High current output combined with high resolution and voltage compliance.

7. Multiple independent channels that are driven with accurate timing.

8. Feature extendability using additional PCB modules, such as for recording, that can be driven by the microcontroller processor independently from stimulation.

**The overall vision is to provide a reliable and affordable tool for neurophysiology** that allows researchers to experiment with both conventional and HFAC block stimulation without any builtin limiters such as blocking capacitors, which can be connected externally to the stimulator if needed. The use of this tool in experiments to determine the feasibility of using HFAC block to improve stimulation selectivity of cuff electrodes will be described in the following chapters.

# References


[1] A. Chaturvedi, T. J. Foutz, and C. C. McIntyre, "Current steering to activate targeted neural pathways during deep brain stimulation of the subthalamic region," eng, *Brain Stimulation*, vol. 5, no. 3, pp. 369–377, Jul. 2012, ISSN: 1876-4754. DOI: 10.1016/j.brs.2011.05.002.

[2] J. T. Mortimer, "Motor prosthesis," en, in *Handbook of Physiology, section 1: the nervous system*, vol. 2, Bethesda, USA: American Physiology Society, 1981, pp. 155–187.

[3] D. R. Merrill, M. Bikson, and J. G. R. Jefferys, "Electrical stimulation of excitable tissue: Design of efficacious and safe protocols," *Journal of Neuroscience Methods*, vol. 141, no. 2, pp. 171–198, Feb. 2005, ISSN: 0165-0270. DOI: 10.1016/j.jneumeth.2004.10.020. [Online]. Available: http://www.sciencedirect.com/science/article/pii/S0165027004003826 (visited on 06/13/2019).

[4] J. C. Lilly, J. R. Hughes, E. C. Alvord, and T. W. Galkin, "Brief, Noninjurious Electric Waveform for Stimulation of the Brain," en, *Science*, vol. 121, no. 3144, pp. 468–469, Apr. 1955, ISSN: 0036-8075, 1095-9203. DOI: 10.1126/science.121.3144.468. [Online]. Available: https://science.sciencemag.org/content/121/3144/468 (visited on 01/27/2020).

[5] M. Ortmanns, "Charge Balancing in Functional Electrical Stimulators: A Comparative Study," in *IEEE International Symposium on Circuits and Systems, 2007. ISCAS 2007*, May 2007, pp. 573–576. DOI: 10.1109/ISCAS.2007.378802.

[6] N. Tran, S. Bai, J. Yang, H. Chun, O. Kavehei, Y. Yang, V. Muktamath, D. Ng, H. Meffin, M. Halpern, and E. Skafidas, "A Complete 256-Electrode Retinal Prosthesis Chip," *IEEE Journal of Solid-State Circuits*, vol. 49, no. 3, pp. 751–765, Mar. 2014, ISSN: 0018-9200. DOI: 10.1109/JSSC.2014.2298037.

[7] E. Pepin, D. Micheletti, S. Perlmutter, and J. C. Rudell, "High-voltage compliant, capacitive-load invariant neural stimulation electronics compatible with standard bulk-CMOS integration," in *2014 IEEE Biomedical Circuits and Systems Conference (BioCAS) Proceedings*, ISSN: 2163-4025, Oct. 2014, pp. 260–263. DOI: 10.1109/BioCAS.2014.6981712.

[8] L. Bisoni, C. Carboni, L. Raffo, N. Carta, and M. Barbaro, "An HV-CMOS Integrated Circuit for Neural Stimulation in Prosthetic Applications," *IEEE Transactions on Circuits and Systems II: Express Briefs*, vol. 62, no. 2, pp. 184–188, Feb. 2015, ISSN: 1558-3791. DOI: 10.1109/TCSII.2014.2387679.

[9] I. Williams, A. Rapeaux, Y. Liu, S. Luan, and T. G. Constandinou, "A 32-ch. bidirectional neural/EMG interface with on-chip spike detection for sensorimotor feedback," in *2016 IEEE Biomedical Circuits and Systems Conference (BioCAS)*, ISSN: null, Oct. 2016, pp. 528–531. DOI: 10.1109/BioCAS.2016.7833848.

[10] D. Loi, C. Carboni, G. Angius, G. N. Angotzi, M. Barbaro, L. Raffo, S. Raspopovic, and X. Navarro, "Peripheral Neural Activity Recording and Stimulation System," *IEEE Transactions on Biomedical Circuits and Systems*, vol. 5, no. 4, pp. 368–379, Aug. 2011,

ISSN: 1932-4545, 1940-9990. DOI: 10.1109/TBCAS.2011.2123097. [Online]. Available: http://ieeexplore.ieee.org/lpdocs/epic03/wrapper.htm?arnumber=5750065 (visited on 09/21/2015).

[11] N. Fernando, D. Macklin, M. Hsu, and J. Judy, "An Embedded Wireless Neural Stimulation and Recording System," in *3rd International IEEE/EMBS Conference on Neural Engineering, 2007. CNE '07*, May 2007, pp. 333–336. DOI: 10.1109/CNE.2007.369678.

[12] M. Alam, X. Chen, and E. Fernandez, "A low-cost multichannel wireless neural stimulation system for freely roaming animals," en, *Journal of Neural Engineering*, vol. 10, no. 6, p. 066 010, 2013, ISSN: 1741-2552. DOI: 10.1088/1741-2560/10/6/066010. [Online]. Available: http://stacks.iop.org/1741-2552/10/i=6/a=066010 (visited on 02/09/2017).

[13] "A Comprehensive Study of the Howland Current Pump," en, Texas Instruments, Application Report AN-1515, Apr. 2013, p. 17. [Online]. Available: http://www.ti.com/lit/an/snoa474a/snoa474a.pdf.

[14] N. Jiang, "A Large Current Source with High Accuracy and Fast Settling," en, *Analog Dialogue*, vol. 52, no. 10, p. 4, 2018. [Online]. Available: https://www.analog.com/en/analog-dialogue/articles/a-large-current-source-with-high-accuracy-and-fast-settling.html#.

[15] W.-Y. Hsu and A. Schmid, "Compact, Energy-Efficient High-Frequency Switched Capacitor Neural Stimulator With Active Charge Balancing," *IEEE Transactions on Biomedical Circuits and Systems*, vol. 11, no. 4, pp. 878–888, Aug. 2017, ISSN: 1940-9990. DOI: 10.1109/TBCAS.2017.2694144.

[16] C. f. D. a. R. H. FDA, "Biological Responses to Metal Implants," English, United States Food and Drug Administration, Tech. Rep., Sep. 2019, p. 149. [Online]. Available: https://www.fda.gov/media/131150/download.

[17] R. Shannon, "A model of safe levels for electrical stimulation," *IEEE Transactions on Biomedical Engineering*, vol. 39, no. 4, pp. 424–426, Apr. 1992, ISSN: 1558-2531. DOI: 10.1109/10.126616.

[18] D. B. McCreery, W. F. Agnew, T. G. H. Yuen, and L. A. Bullara, "Comparison of neural damage induced by electrical stimulation with faradaic and capacitor electrodes," en, *Annals of Biomedical Engineering*, vol. 16, no. 5, pp. 463–481, Sep. 1988, ISSN: 1573-9686. DOI: 10.1007/BF02368010. [Online]. Available: https://doi.org/10.1007/BF02368010 (visited on 02/05/2020).

[19] K. Nakanishi, T. Sakiyama, and K. Imamura, "On the adsorption of proteins on solid surfaces, a common but very complicated phenomenon," en, *Journal of Bioscience and Bioengineering*, vol. 91, no. 3, pp. 233–244, Jan. 2001, ISSN: 1389-1723. DOI: 10.1016/S1389-1723(01)80127-4. [Online]. Available: http://www.sciencedirect.com/science/article/pii/S1389172301801274 (visited on 03/17/2020).

[20] D. R. Merrill, "The Electrochemistry of Charge Injection at the Electrode/Tissue Interface," en, *inp*, p. 85, 2010. DOI: 10.1007/978-0-387-98120-8_4. [Online]. Available: https://ui.adsabs.harvard.edu/abs/2010inp..book...85M/abstract (visited on 12/04/2019).

[21] E. M. Hudak, J. T. Mortimer, and H. B. Martin, "Platinum for neural stimulation: Voltammetry considerations," en, *Journal of Neural Engineering*, vol. 7, no. 2, p. 026 005, Mar. 2010, ISSN: 1741-2552. DOI: 10.1088/1741-2560/7/2/026005. [Online]. Available: https://doi.org/10.1088%2F1741-2560%2F7%2F2%2F026005 (visited on 01/27/2020).

[22] U. Bihr, T. Ungru, H. Xu, J. Anders, J. Becker, and M. Ortmanns, "A bidirectional neural interface with a HV stimulator and a LV neural amplifier," in *2013 IEEE International Symposium on Circuits and Systems (ISCAS2013)*, May 2013, pp. 401–404. DOI: 10.1109/ISCAS.2013.6571865.

[23] K. Chen, Z. Yang, L. Hoang, J. Weiland, M. Humayun, and W. Liu, "An Integrated 256-Channel Epiretinal Prosthesis," *IEEE Journal of Solid-State Circuits*, vol. 45, no. 9, pp. 1946–1956, Sep. 2010, ISSN: 1558-173X. DOI: 10.1109/JSSC.2010.2055371.

[24] D. Boinagrov, X. Lei, G. Goetz, T. I. Kamins, K. Mathieson, L. Galambos, J. S. Harris, and D. Palanker, "Photovoltaic Pixels for Neural Stimulation: Circuit Models and

Performance," *IEEE Transactions on Biomedical Circuits and Systems*, vol. 10, no. 1, pp. 85–97, Feb. 2016, ISSN: 1940-9990. DOI: 10.1109/TBCAS.2014.2376528.

[25] X. Liu, A. Demosthenous, and N. Donaldson, "Five valuable functions of blocking capacitors in stimulators," 2008.

[26] W.-M. Chen, H. Chiueh, T.-J. Chen, C.-L. Ho, C. Jeng, M.-D. Ker, C.-Y. Lin, Y.-C. Huang, C.-W. Chou, T.-Y. Fan, M.-S. Cheng, Y.-L. Hsin, S.-F. Liang, Y.-L. Wang, F.-Z. Shaw, Y.-H. Huang, C.-H. Yang, and C.-Y. Wu, "A Fully Integrated 8-Channel Closed-Loop Neural-Prosthetic CMOS SoC for Real-Time Epileptic Seizure Control," *IEEE Journal of Solid-State Circuits*, vol. 49, no. 1, pp. 232–247, Jan. 2014, ISSN: 0018-9200, 1558-173X. DOI: 10.1109/JSSC.2013.2284346. [Online]. Available: http://ieeexplore.ieee.org/lpdocs/epic03/wrapper.htm?arnumber=6637111 (visited on 09/21/2015).

[27] D. Kumsa, E. M. Hudak, F. W. Montague, S. C. Kelley, D. F. Untereker, B. P. Hahn, C. Condit, M. Cholette, H. Lee, D. Bardot, and P. Takmakov, "Electrical neurostimulation with imbalanced waveform mitigates dissolution of platinum electrodes," en, *Journal of Neural Engineering*, vol. 13, no. 5, p. 054 001, Sep. 2016, ISSN: 1741-2552. DOI: 10.1088/1741-2560/13/5/054001. [Online]. Available: https://doi.org/10.1088%2F1741-2560%2F13%2F5%2F054001 (visited on 01/27/2020).

[28] E. Greenwald, C. Chen, N. Thakor, C. Maier, and G. Cauwenberghs, "A CMOS neurostimulator with on-chip DAC calibration and charge balancing," in *2013 IEEE Biomedical Circuits and Systems Conference (BioCAS)*, Oct. 2013, pp. 89–92. DOI: 10.1109/BioCAS.2013.6679646.

[29] D. Osipov, S. Paul, S. Strokov, and A. Kreiter, "A new current stimulator architecture for visual cortex stimulation," Nov. 2015. DOI: 10.1109/NORCHIP.2015.7364399.

[30] M. Ortmanns, A. Rocke, M. Gehrke, and H.-J. Tiedtke, "A 232-Channel Epiretinal Stimulator ASIC," *IEEE Journal of Solid-State Circuits*, vol. 42, no. 12, pp. 2946–2959, Dec. 2007, ISSN: 1558-173X. DOI: 10.1109/JSSC.2007.908693.

[31] L. Yao, J. Zhao, P. Li, R. Xue, Y. P. Xu, and M. Je, "A 20V-compliance implantable neural stimulator IC with closed-loop power control, active charge balancing, and electrode impedance check," in *2014 IEEE Asian Solid-State Circuits Conference (A-SSCC)*, Nov. 2014, pp. 201–204. DOI: 10.1109/ASSCC.2014.7008895.

[32] V. M. Woods, I. F. Triantis, and C. Toumazou, "Offset prediction for charge-balanced stimulus waveforms," en, *Journal of Neural Engineering*, vol. 8, no. 4, p. 046 032, Aug. 2011, ISSN: 1741-2560, 1741-2552. DOI: 10.1088/1741-2560/8/4/046032. [Online]. Available: http://stacks.iop.org/1741-2552/8/i=4/a=046032?key=crossref.095292dc9efbecc8ebb706a2a9a6e225 (visited on 02/03/2020).

[33] R. Ranjandish and A. Schmid, "A design methodology for charge-balanced stimulators based on anodic current variation monitoring," en, *Analog Integrated Circuits and Signal Processing*, vol. 101, no. 2, pp. 341–350, Nov. 2019, ISSN: 1573-1979. DOI: 10.1007/s10470-019-01462-6. [Online]. Available: https://doi.org/10.1007/s10470-019-01462-6 (visited on 02/03/2020).

[34] Y.-K. Lo, R. Hill, K. Chen, and W. Liu, "Precision control of pulse widths for charge balancing in functional electrical stimulation," in *2013 6th International IEEE/EMBS Conference on Neural Engineering (NER)*, ISSN: 1948-3546, Nov. 2013, pp. 1481–1484. DOI: 10.1109/NER.2013.6696225.

[35] G. Fridman and C. Della Santina, "Safe Direct Current Stimulation to Expand Capabilities of Neural Prostheses," *IEEE Transactions on Neural Systems and Rehabilitation Engineering*, vol. 21, no. 2, pp. 319–328, Mar. 2013, ISSN: 1534-4320. DOI: 10.1109/TNSRE.2013.2245423.

[36] V. S. Polikov, P. A. Tresco, and W. M. Reichert, "Response of brain tissue to chronically implanted neural electrodes," en, *Journal of Neuroscience Methods*, vol. 148, no. 1, pp. 1–18, Oct. 2005, ISSN: 01650270. DOI: 10.1016/j.jneumeth.2005.08.015. [Online]. Available: http://linkinghub.elsevier.com/retrieve/pii/S0165027005002931 (visited on 09/21/2015).

[37] W. F. Agnew and D. B. McCreery, "Considerations for Safety with Chronically Implanted Nerve Electrodes," en, *Epilepsia*, vol. 31, no. s2, S27–S32, 1990, ISSN: 1528-1167. DOI: 10.1111/j.1528-1157.1990.tb05845.x. [Online]. Available: https://onlinelibrary.wiley.com/doi/abs/10.1111/j.1528-1157.1990.tb05845.x (visited on 02/07/2020).

[38] C. Günter, J. Delbeke, and M. Ortiz-Catalan, "Safety of long-term electrical peripheral nerve stimulation: Review of the state of the art," *Journal of NeuroEngineering and Rehabilitation*, vol. 16, no. 1, p. 13, Jan. 2019, ISSN: 1743-0003. DOI: 10.1186/s12984-018-0474-8. [Online]. Available: https://doi.org/10.1186/s12984-018-0474-8 (visited on 01/27/2020).

[39] D. B. McCreery, W. F. Agnew, T. G. H. Yuen, and L. A. Bullara, "Relationship between stimulus amplitude, stimulus frequency and neural damage during electrical stimulation of sciatic nerve of cat," en, *Medical and Biological Engineering and Computing*, vol. 33, no. 3, pp. 426–429, May 1995, ISSN: 1741-0444. DOI: 10.1007/BF02510526. [Online]. Available: https://doi.org/10.1007/BF02510526 (visited on 02/07/2020).

[40] W. F. Agnew, D. B. McCreery, T. G. H. Yuen, and L. A. Bullara, "Histologic and physiologic evaluation of electrically stimulated peripheral nerve: Considerations for the selection of parameters," en, *Annals of Biomedical Engineering*, vol. 17, no. 1, pp. 39–60, Jan. 1989, ISSN: 1573-9686. DOI: 10.1007/BF02364272. [Online]. Available: https://doi.org/10.1007/BF02364272 (visited on 02/07/2020).

[41] N. Bhadra, T. L. Vrabec, N. Bhadra, and K. L. Kilgore, "Reversible conduction block in peripheral nerve using electrical waveforms," *Bioelectronics in Medicine*, vol. 1, no. 1, pp. 39–54, Jan. 2018, ISSN: 2059-1500. DOI: 10.2217/bem-2017-0004. [Online]. Available: https://www.ncbi.nlm.nih.gov/pmc/articles/PMC5811084/ (visited on 09/03/2019).

[42] K. Singh, F. J. R. Richmond, and G. E. Loeb, "Recruitment Properties of Intramuscular and Nerve-Trunk Stimulating Electrodes," en, *IEEE TRANSACTIONS ON REHABILITATION ENGINEERING*, vol. 8, no. 3, p. 10, 2000.

[43] D. M. Ackermann, C. Ethier, E. L. Foldes, E. R. Oby, D. Tyler, M. Bauman, N. Bhadra, L. Miller, and K. L. Kilgore, "Electrical conduction block in large nerves: High-frequency current delivery in the nonhuman primate," en, *Muscle & Nerve*, vol. 43, no. 6, pp. 897–899, Jun. 2011, ISSN: 1097-4598. DOI: 10.1002/mus.22037. [Online]. Available: http://onlinelibrary.wiley.com/doi/10.1002/mus.22037/abstract (visited on 02/14/2017).

[44] G. E. Loeb and R. A. Peck, "Cuff electrodes for chronic stimulation and recording of peripheral nerve activity," *Journal of Neuroscience Methods*, vol. 64, no. 1, pp. 95–103, Jan. 1996, ISSN: 0165-0270. DOI: 10.1016/0165-0270(95)00123-9. [Online]. Available: https://www.sciencedirect.com/science/article/pii/0165027095001239 (visited on 02/08/2017).

[45] C. Carboni, L. Bisoni, N. Carta, R. Puddu, S. Raspopovic, X. Navarro, L. Raffo, and M. Barbaro, "An integrated interface for peripheral neural system recording and stimulation: System design, electrical tests and in-vivo results," en, *Biomedical Microdevices*, vol. 18, no. 2, p. 35, Mar. 2016, ISSN: 1572-8781. DOI: 10.1007/s10544-016-0043-5. [Online]. Available: https://doi.org/10.1007/s10544-016-0043-5 (visited on 12/04/2019).

[46] A. T. Nguyen, J. Xu, W.-k. Tam, W. Zhao, T. Wu, and Z. Yang, "A programmable fully-integrated microstimulator for neural implants and instrumentation," in *2016 IEEE Biomedical Circuits and Systems Conference (BioCAS)*, ISSN: null, Oct. 2016, pp. 472–475. DOI: 10.1109/BioCAS.2016.7833834.

[47] H. Liu, L. Zhu, S. Sheng, L. Sun, H. Zhou, H. Tang, and T. Qiu, "Post stimulus effects of high frequency biphasic electrical current on a fibre's conductibility in isolated frog nerves," en, *Journal of Neural Engineering*, vol. 10, no. 3, p. 036 024, 2013, ISSN: 1741-2552. DOI: 10.1088/1741-2560/10/3/036024. [Online]. Available: http://stacks.iop.org/1741-2552/10/i=3/a=036024 (visited on 04/11/2017).

[48] G. Yang, Z. Xiao, J. Wang, B. Shen, J. R. Roppolo, W. C. de Groat, and C. Tai, "Post-stimulation block of frog sciatic nerve by high-frequency (kHz) biphasic stimulation,"

en, *Medical & Biological Engineering & Computing*, vol. 55, no. 4, pp. 585–593, Apr. 2017, ISSN: 1741-0444. DOI: 10.1007/s11517-016-1539-0. [Online]. Available: https://doi.org/10.1007/s11517-016-1539-0 (visited on 12/12/2019).

[49] J. Millar, T. G. Barnett, and S. J. Trout, "The neurodyne: A simple mains-powered constant-current stimulus isolator," en, *Journal of Neuroscience Methods*, vol. 55, no. 1, pp. 53–57, Nov. 1994, ISSN: 0165-0270. DOI: 10.1016/0165-0270(94)90040-X. [Online]. Available: http://www.sciencedirect.com/science/article/pii/016502709490040X (visited on 11/20/2019).

[50] M. Franke, N. Bhadra, N. Bhadra, and K. Kilgore, "Direct Current Contamination of Kilohertz Frequency Alternating Current Waveforms," *Journal of neuroscience methods*, vol. 232, pp. 74–83, Jul. 2014, ISSN: 0165-0270. DOI: 10.1016/j.jneumeth.2014.04.002. [Online]. Available: http://www.ncbi.nlm.nih.gov/pmc/articles/PMC4069243/ (visited on 10/01/2015).

[51] N. Bhadra and K. Kilgore, "Direct current electrical conduction block of peripheral nerve," *IEEE Transactions on Neural Systems and Rehabilitation Engineering*, vol. 12, no. 3, pp. 313–324, Sep. 2004, ISSN: 1558-0210. DOI: 10.1109/TNSRE.2004.834205.

[52] A. Rapeaux, K. Nikolic, I. Williams, A. Eftekhar, and T. G. Constandinou, "Fiber size-selective stimulation using action potential filtering for a peripheral nerve interface: A simulation study," in *2015 37th Annual International Conference of the IEEE Engineering in Medicine and Biology Society (EMBC)*, Aug. 2015, pp. 3411–3414. DOI: 10.1109/EMBC.2015.7319125.

[53] I. J. Ungar, D. J. T. Mortimer, and J. D. Sweeney, "Generation of unidirectionally propagating action potentials using a monopolar electrode cuff," en, *Annals of Biomedical Engineering*, vol. 14, no. 5, pp. 437–450, Sep. 1986, ISSN: 0090-6964, 1573-9686. DOI: 10.1007/BF02367364. [Online]. Available: http://link.springer.com/article/10.1007/BF02367364 (visited on 09/21/2015).

[54] Z.-P. Fang and J. Mortimer, "Selective activation of small motor axons by quasitrapezoidal current pulses," *IEEE Transactions on Biomedical Engineering*, vol. 38, no. 2, pp. 168–174, Feb. 1991, ISSN: 1558-2531. DOI: 10.1109/10.76383.

[55] E. J. Peterson, D. A. Dinsmoor, D. J. Tyler, and T. J. Denison, "Stimulation artifact rejection in closed-loop, distributed neural interfaces," in *ESSCIRC Conference 2016: 42nd European Solid-State Circuits Conference*, ISSN: null, Sep. 2016, pp. 233–236. DOI: 10.1109/ESSCIRC.2016.7598285.

[56] A. Rapeaux and T. G. Constandinou, "A Block-Capable and Module-Extendable 4-Channel Stimulator for Acute Neurophysiology," en, *bioRxiv*, p. 2020.01.28.923474, Jan. 2020. DOI: 10.1101/2020.01.28.923474. [Online]. Available: https://www.biorxiv.org/content/10.1101/2020.01.28.923474v1 (visited on 02/07/2020).

[57] Y. A. Patel and R. J. Butera, "Differential fiber-specific block of nerve conduction in mammalian peripheral nerves using kilohertz electrical stimulation," en, *Journal of Neurophysiology*, vol. 113, no. 10, pp. 3923–3929, Jun. 2015, ISSN: 0022-3077, 1522-1598. DOI: 10.1152/jn.00529.2014. [Online]. Available: http://jn.physiology.org/content/113/10/3923 (visited on 09/20/2016).

[58] M. N. van Dongen and W. A. Serdijn, "Does a coupling capacitor enhance the charge balance during neural stimulation? An empirical study," en, *Medical & Biological Engineering & Computing*, vol. 54, no. 1, pp. 93–101, Jan. 2016, ISSN: 1741-0444. DOI: 10.1007/s11517-015-1312-9. [Online]. Available: https://doi.org/10.1007/s11517-015-1312-9 (visited on 02/03/2020).

[59] I. Williams, "Zero mean waveforms for neural stimulation," en, engrXiv, preprint, Mar. 2018. DOI: 10.31224/osf.io/m24kt. [Online]. Available: https://osf.io/m24kt (visited on 07/16/2020).

[60] B. Lee, M. K. Koripalli, Y. Jia, J. Acosta, M. S. E. Sendi, Y. Choi, and M. Ghovanloo, "An Implantable Peripheral Nerve Recording and Stimulation System for Experiments on Freely Moving Animal Subjects," en, *Scientific Reports*, vol. 8, no. 1, pp. 1–12, Apr.

2018, ISSN: 2045-2322. DOI: 10.1038/s41598-018-24465-1. [Online]. Available: https://www.nature.com/articles/s41598-018-24465-1 (visited on 02/11/2020).

[61] F. .-.-S. Jaw, S. .-.-J. Liu, T. .-.-S. Kuo, and C. .-.-Y. Wang, "Microcomputer-based pulse stimulator," en, *Journal of Neuroscience Methods*, vol. 62, no. 1, pp. 193–197, Nov. 1995, ISSN: 0165-0270. DOI: 10.1016/0165-0270(95)00076-3. [Online]. Available: http://www.sciencedirect.com/science/article/pii/0165027095000763 (visited on 11/20/2019).

[62] E. Cuttaz, J. Goding, C. Vallejo-Giraldo, U. Aregueta-Robles, N. Lovell, D. Ghezzi, and R. A. Green, "Conductive elastomer composites for fully polymeric, flexible bioelectronics," en, *Biomaterials Science*, vol. 7, no. 4, pp. 1372–1385, 2019. DOI: 10.1039/C8BM01235K. [Online]. Available: https://pubs.rsc.org/en/content/articlelanding/2019/bm/c8bm01235k (visited on 01/06/2020).

# Chapter 4

# Preliminary *in-silico* and *in-vivo* work exploring the properties of HFAC block

## 4.1 Foreword and Motivation

While the objective was always to determine whether selective stimulation was possible with the use of timed stimulation and block, the first step towards exploring this question in living nerve tissue was to characterise HFAC block in a better model for human nerves than the African Clawed Toad *Xenopus Laevis*. This became possible when an opportunity presented itself to carry out acute *in-vivo* experiments on rat sciatic nerves at Newcastle University in partnership with researchers there. The work described in this chapter was possible thanks to these collaborations as detailed in the footnote [1].

## 4.2 Introduction

[1] Acute *in-vivo* work in the rat sciatic nerve model was carried out at Newcastle University in partnership with Emma Brunton, Carolina Silveira and Kianoush Nazarpour. Carolina Silveira and Emma Brunton are at School of Engineering, Newcastle University. Kianoush Nazarpour is currently at School of Engineering and Biosciences Research Institute, Newcastle University. The work was carried out as part of project Senseback (EPSRC Grant EP/M025977/1). Simulation work was carried out in collaboration with Emanuele Perra and Dr. Konstantin Nikolic, with funding from ERC Synergy Grant no.139818 i2MOVE.

With initial simulation work in the Frankenhaeuser-Huxley model showing promising initial results on whether it was possible to selectively stimulate smaller fibres in a compound nerve trunk by timing conventional stimulation and HFAC block, it was essential at this point to move towards validating these predictions in live tissue. A purely *in-vitro* approach featuring a neural cell culture would not have been adequate as cell suspensions do not retain the structural organisation of peripheral nerves which is essential for studying their behaviour in relation to stimulation, therefore an *ex-vivo* or *in-vivo* approach was required. An opportunity to investigate HFAC block *in-vivo* came first. The motivation for these experiments was primarily in characterising block in living mammalian tissue and determining how accurate model predictions were. A secondary objective was the design of a suitable experimental protocol to test whether selective stimulation could be carried out using a similar technique as previously presented in Chapter 2.

This chapter will first detail preliminary work on HFAC block *in-silico*, followed by the choice of a more translatable model for HFAC block experiments, the rat sciatic nerve. *In-vivo* experiments to charaterize HFAC block in the rat sciatic nerve are described and a specific mechanism of HFAC block is identified as an opportunity for selective stimulation, albeit with limitations. After discussion of the results the chapter concludes by detailing further steps to improve the quality of collected neural data and the practicality of using HFAC block for selective stimulation.

## 4.3 Preliminary Investigations on stimulation and high frequency block for fibre-size selective stimulation *in-silico*

### 4.3.1 Simulations of frog nerve in NEURON

Initial work as described in Chapter 2, subsection 2.7.3 suggested that High Frequency Block was only effective when the stimulating signal was over a certain threshold frequency and a certain threshold amplitude. However, as mentioned in a recent review [1], studies of high-frequency block report different frequency and amplitude thresholds depending on a number of parameters. The type and shape of the electrode used to interface with the nerve, the size of the nerve and the type of the fibres being blocked, the temperature of the system all have significant impact. For example, the threshold frequency has been reported to be in the lower kHz or higher than 20 kHz depending on the case. Furthermore, it is important to note that there seem to be discrepancies between what *in-silico* models predict and what is actually observed, taking the duration of the onset response as an example. While most models predict that a single action potential will be generated at the onset of block before complete block is established, experimentally the onset response of block is of variable duration and can last several seconds [2], [3]. Conversely, models predict that under certain high frequency block parameters outside of the thresholds of frequency or amplitude, constant activation of nerves will result. In practice, secondary mechanisms that regulate nerve cell activity prevent this as part of accomodation [4]. As block is carried out over timescales of several seconds it is possible these mechanisms have a role in block experimentally, that is not captured in models used to study block *in-silico*. Of particular interest is changes in the concentration of intracellular and extracellular ions as a result of prolonged voltage-gated ion channel activity, which is not generally simulated as computational models as used in the literature specify extracellular and intracellular ion concentrations as constant parameters [5]–[7].

### 4.3.2 HFAC block simulations using the MRG mammalian nerve model

A further step to characterise block *in-silico* but in a mammalian nerve model that is more translatable for human clinical applications of a selective stimulation technique, work was carried out in partnership with Emanuele Perra and Konstantin Nikolic to investigate the mechanisms of block in the McIntyre-Richardson-Grill model [8]. A key result of the work was that for HFAC block thresholds there was agreement between the FH and MRG models as shown figure 4.1. In the figure, noting the differences in x and y-axis scales, the frequency threshold at which blocking signals become effective is roughly the same for the FH and MRG models. Due to differences in how the blocking signal was modeled for the two simulation studies, it is however not possible to truly compare the amplitude thresholds as the units are different.

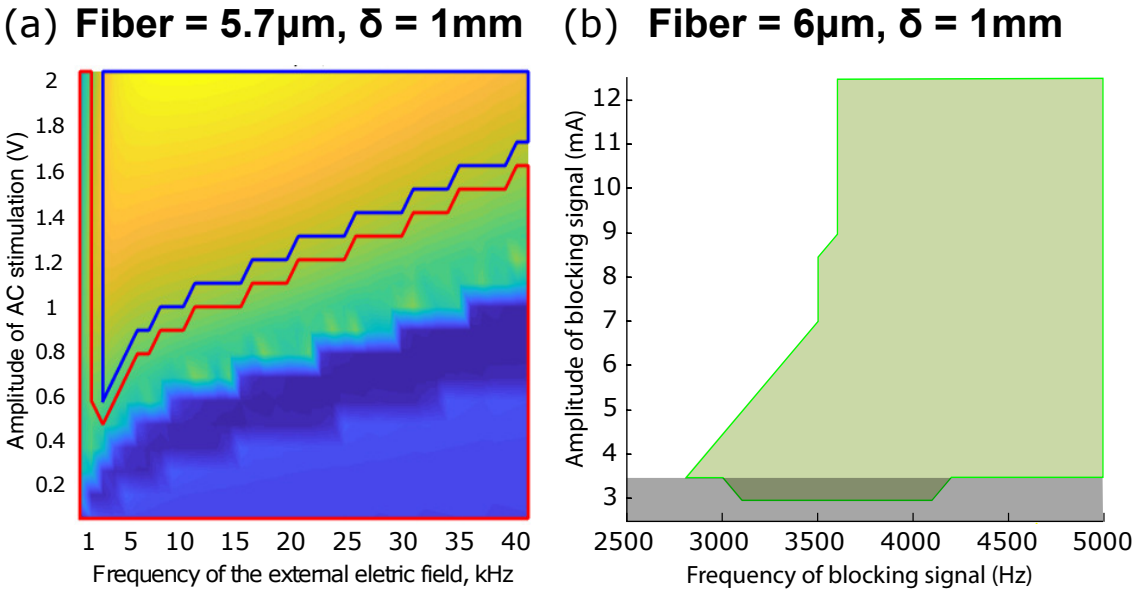


Figure 4.1: (a): Block thresholds over frequencies spanning 1 to 40 kHz HFAC block in the MRG mammalian nerve model. Part of this figure was previously published in [8] (b): Block thresholds over frequencies spanning 2.5 to 5 kHz HFAC block in the FH amphibian nerve model. Part of this figure was previously published in [9].

Returning to the analysis of the initial timed block and stimulation simulation work for selective activation of small nerve fibres [9], the conclusion was that *in-silico* models suggest that the technique is feasible and able to differentiate between fibre diameters of about 2 µm. However taking into account the fact that models did not capture all phenomena observed in acute experiments using living tissue, it was evident that further investigation using live tissue was

necessary to confirm model predictions and determine whether timed stimulation and block was translatable. If any mechanism that would prevent the technique from working was occurring in real nerves, it was expected it would be revealed by acute *in-vivo* experiments.

### 4.3.3 The rat sciatic nerve as a more translatable model for investigation of stimulation and block

To improve translatability a first step was to choose a mammalian nerve model which would be more relevant than the FH model which represents amphibian nerves. Studies on high-frequency block in the literature cite several animal models including cats [10], rats [11] and non-human primates [3] (see [1] for a more extensive list). Due to the availability of the rat animal model and the extensive information on the anatomy of its sciatic nerve [12]–[14], it was chosen as a promising model for further experiments on timed stimulation and block for selective stimulation of small nerve fibres.

The nerve fibres in the rat sciatic nerve are divided into motor neurons, myelinated and unmyelinated sensory fibres, and unmyelinated sympathetic fibres according to [12], with reported percentages in table 4.1. The presence of several fibre populations with distinct functions tied to different fibre diameters provides a good experimental model to verify whether selective stimulation using block as in Kuffler's technique is feasible.

Table 4.1: Fibre composition of the rat sciatic nerve as reported in [12] for the whole sciatic nerve and specific branches.

| Dataset | Myelinated Motor | | Myelinated Sensory | | Unmyelinated Sensory | | Unmyelinated Sympathetic | |
|---|---|---|---|---|---|---|---|---|
| | Count | Percent | Count | Percent | Count | Percent | Count | Percent |
| Total | 1620 | 6% | 6210 | 23% | 6210 | 48% | 12960 | 23% |
| Tibial | 1000 | 7.3% | 3500 | 25.7% | 5400 | 39.7% | 3700 | 27.2% |
| Peroneal | 600 | 10% | 1300 | 21.6% | 3000 | 50% | 1100 | 18.3% |
| Sural | 0 | 0% | 1100 | 20.37% | 2800 | 51.8% | 1500 | 27.7% |
| Cutaneous | 0 | 0% | 400 | 18.2% | 1800 | 81.8% | 0 | 0% |

Furthermore, the rat sciatic nerve model is uniquely placed as a nerve for which many electrode types have a standard design. Suppliers of cuff electrodes such as CorTec, Microprobes and Microleads all have standard cuffs with an inner diameter of approximately 1 mm which

corresponds to the size of the rat sciatic nerve, shown in figure 4.2 with a cuff from Microprobes implanted on a rat sciatic nerve. From the point of view of the experimenter, nerves of this size can tolerate the handling required for electrode implantation without damage, which might not be the case for smaller mouse nerves for example, or nerves located near organs with less myelination and connective tissue to preserve their structural integrity. This makes the rat sciatic nerve model both robust to handling and for which it is easy to source commercial stimulation electrodes that closely match those used clinically in humans.

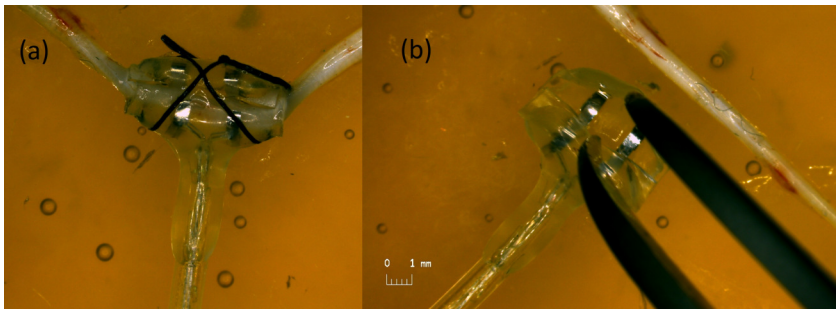


Figure 4.2: (a):Photograph taken using a macroscope of a nerve cuff (Microprobes for Life Science) implanted onto a rat sciatic nerve and closed using 6-0 suturing thread. (b): Photograph of the same cuff opened with tweezers to see the inside electrode configuration (two flat wires threaded through the inside of the cuff). The scale bar applies to both photographs.

## 4.4 *In-vivo* experiments in rat sciatic nerve at Newcastle University

During the course of this project there were a number of opportunities to carry out experiments with HFAC block acutely on Sprague-Dawley rat sciatic nerves *in-vivo* at Newcastle University. A first objective for these experiments were to confirm predictions made by simulations in the FH model, to determine whether these findings were translatable to an *in-vivo* mammalian model. More specifically, to measure block effectiveness in terms of amplitude and frequency so as to ensure complete block was possible as required by the selective stimulation protocol developed in the model, and potentially to investigate any mechanisms that were not captured by simulations *in-silico*.

### 4.4.1 Experimental Setup

Initial *in-vivo* experiments sought to replicate a setup similar to the one described in [15], where the activity of the rat gastrocnemius muscle is measured before, during and after block to determine block efficacy, and block signal parameters such as frequency and amplitude are swept. Due to the existing experience of collaborators with EMG recording at Newcastle University, this measurement modality was chosen instead of force transducer-based measurements as in the aforementioned paper.

The setup used is described in [16] and shown in figure 4.3.

For stimulation and block a custom nerve cuff was designed that allowed maximum flexibility in choosing where on the nerve the blocking signal was delivered, while providing separate proximal and distal stimulating contacts for baseline and control measurements. This cuff was manufactured by Microprobes for Life Science, as described in [17], and pictured in figure 4.4. The total length of the cuff was 24mm, with stimulation tripoles on both ends with contact spacing of 0.5 mm and a ladder of 8 contacts in the middle of the cuff, with inter-contact distance of 1 mm. The distance between the tripoles and ladder was 3 mm. The wire diameter was 0.1 mm.

Stimulation was carried out using a custom stimulator for high-frequency block stimulation and a Cerestim stimulator (Blackrock Microsystems, USA) for conventional stimulation, such that the two were electrically isolated. The custom stimulator was a predecessor design to the one described in Chapter 3, with details of the implementation in [16], [17]. Recording was carried out using an A-M Systems model 1700 amplifier, with recording set to:

- Low-pass Second Order 10 kHz
- High-pass Second Order 10 Hz
- 50 Hz notch filter (line noise removal)
- Amplifier gain 100

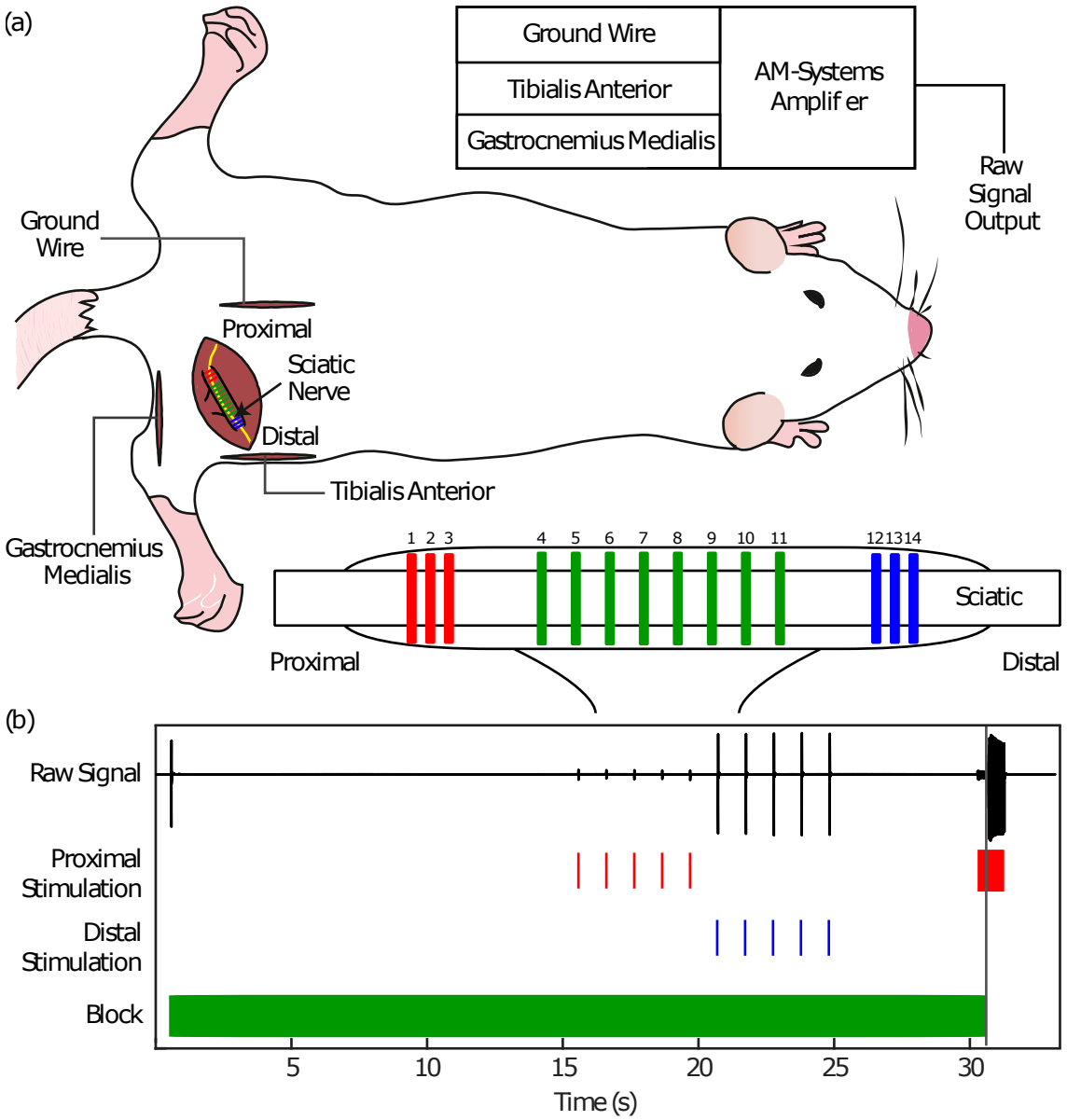


Figure 4.3: (a): Schematic representation of the experimental setup used for *in-vivo* experiments at Newcastle University (see collaborators on chapter first page footnote). (b): Timeline of a typical combined block and stimulation trial to evaluate block thresholds. This figure was previously published in [17].

Initial attempts to record neural activity directly were unsuccessful due to the level of noise injected by the stimulation, notably HFAC stimulation, into the system, which would saturate recording amplifiers. As there was no means at the time to isolate the recording from the stimulation enough to enable direct measurement of the ENG, neural activity was measured by proxy by using EMG recording of the *gastrocnemius medialis* (GM) and *tibialis anterior* (TA) muscles as described in the next section.

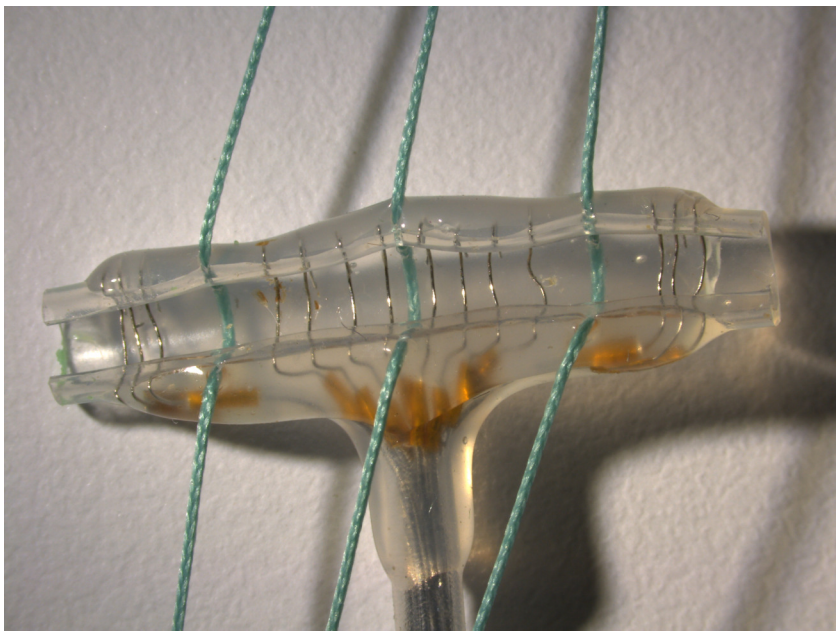

Figure 4.4: Photograph of the custom 14-contact custom cuff electrode used during the acute *in-vivo* experiments at Newcastle University.

### 4.4.2 Surgical Methods

All procedures described in the following paragraphs were performed under licenses issued by the UK Home Office under the Animals (Scientific Procedures) Act 1986 and were approved by the Animal Welfare and Ethical Review Board (AWERB) of Newcastle University.

Briefly, 3 Sprague-Dawley (SD) rats weighing between 350 and 450 grams were anaesthetized according to a protocol detailed in [18] using isoflurane and intraperitoneal injections of medazolam and hypnorm (fentanyl/fluanisone) to maintain anaesthesia level. Notably, isoflurane levels were kept low by using the other anaesthetics so as to avoid its effects on neural conduction and activity at high levels [19]. Each rat was kept warm using a heating pad, however this heating pad had to be turned off during some recordings as it was a strong noise source when powered. Fluids were maintained using a tail-vein cannula dispensing a mixture composed of 0.05 mL potassium chloride, 10 mL of 0.18% saline with 8% glucose concentration in 10 mL of water, delivered at the rate of 2 mL per hour. Incisions were made on the dorsal aspect of the right leg to expose the sciatic nerve trunk, which was then implanted with the cuff electrode. Subsequent incisions were made to place tungsten wire electrodes into the *gastrocnemius medialis* (GM) and *tibialis anterior* (TA) muscles. Finally, as the differential EMG recording amplifier

required a reference electrode far from the stimulation electrodes, an additional tungsten wire was wrapped around a spinous process and secured using dental cement[17].

### 4.4.3 *In-Vivo* Block Thresholds

In order to determine block thresholds *in-vivo*, EMG signals were captured before, during and after block as shown in figure 4.3 (b). Briefly, for each trial measuring block efficacy for a combination of amplitude and frequency parameters, block was first turned on at the start of the trial and maintained for 30 seconds (green bar). 15 seconds were reserved for the onset response of variable duration to subside, at which point stimulation proximal to the blocking electrode was applied, and corresponding EMG recorded. To ensure that the neuromuscular junction was not fatigued, which would make it appear as though block were successful regardless of its actual efficacy, stimulation distal to the block electrode was applied as a control and expected to result in baseline muscle activation. Finally, a train of high frequency conventional stimulation was applied proximally at the rate of 100 Hz to measure the speed of recovery from block of both the *gastrocnemius medialis* and *tibialis anterior* muscles.

EMG responses were processed to obtain a single value from each response as shown in figure 4.5, in order to quantify the response relative to a baseline value obtained without block active. In this way the activity of the muscle as a result of stimulation during the experiment could be monitored and the degree of block quantified. In addition, any damage to the nerve as a result of block could also be measured if there were differences between the EMG responses from proximal and distal stimulation that changed over time.

Results obtained by processing the EMG response of the GM and TA muscles are shown in figures 4.6 and 4.7, with each curve representing the data from one rat. In a qualitative sense for a specific blocking signal frequency a progressive reduction in the EMG signal relative to baseline was observed with increasing blocking signal amplitude as previously reported in a number of block studies both *in-silico* and *in-vivo*. Furthermore, the results suggest a relationship between block signal frequency and reliability of the block when comparing across animals. For low frequencies such as 10 kHz and 15 kHz, block was achieved for specific ranges of

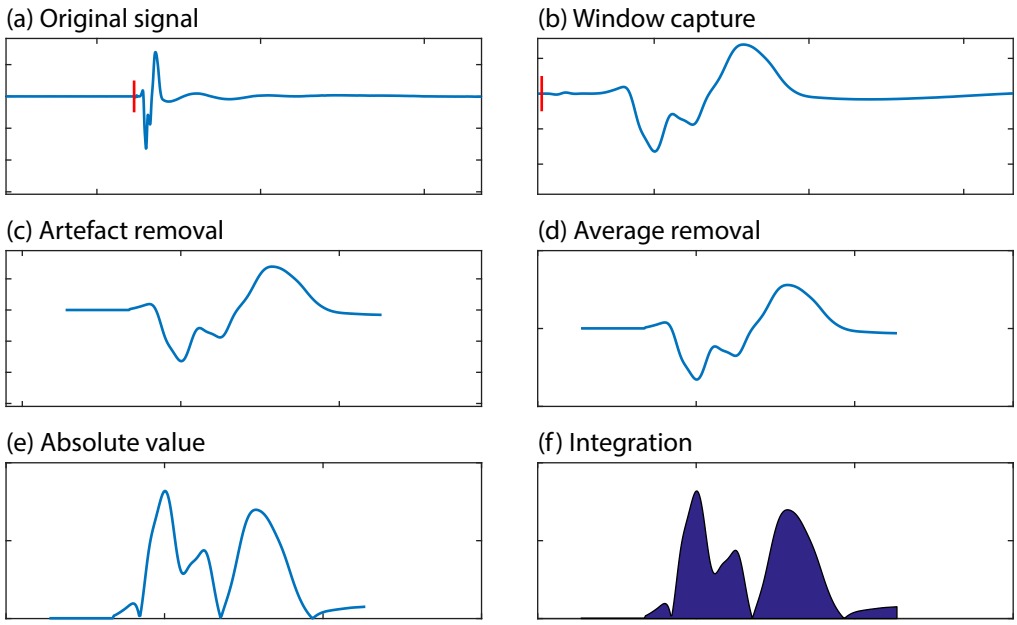


Figure 4.5: Diagrammatic representation of the EMG processing carried out to evaluate the strength of the response relative to a baseline response during *in-vivo* EMG measurements. The vertical red bar represents the time at which stimulation was delivered. This figure was previously published in [17].

amplitudes that changed depending on the animal, however results were much more consistent across animals when considering higher frequencies, particularly 20 to 30 kHz. At still higher frequencies, while results were more consistent than at low frequencies, complete block was not achieved, as expected with reports in literature describing an increase in block threshold with block signal frequency [20].

However, it is difficult to draw definite conclusions by looking at these curves alone, which prompted an analysis that reduces the two parameters of block signal amplitude and frequency to a single one, block charge per cycle (CPC). This corresponds to charge delivered by the electrode during a cathodic or anodic phase of block. CPC will be higher for lower frequencies and high amplitudes, and lower for high frequencies and low amplitudes. There is precedent within the literature that suggests such a derived variable could be useful for measuring the effect of stimulation, as has been reported using strength-duration curves for measurements of nerve excitability [21]. Such a single variable provides a useful method to compare data statistically according to how much charge per cycle was seen by the nerve during a trial.

For each of the following analyses, data from all rats were grouped into two fractions, one

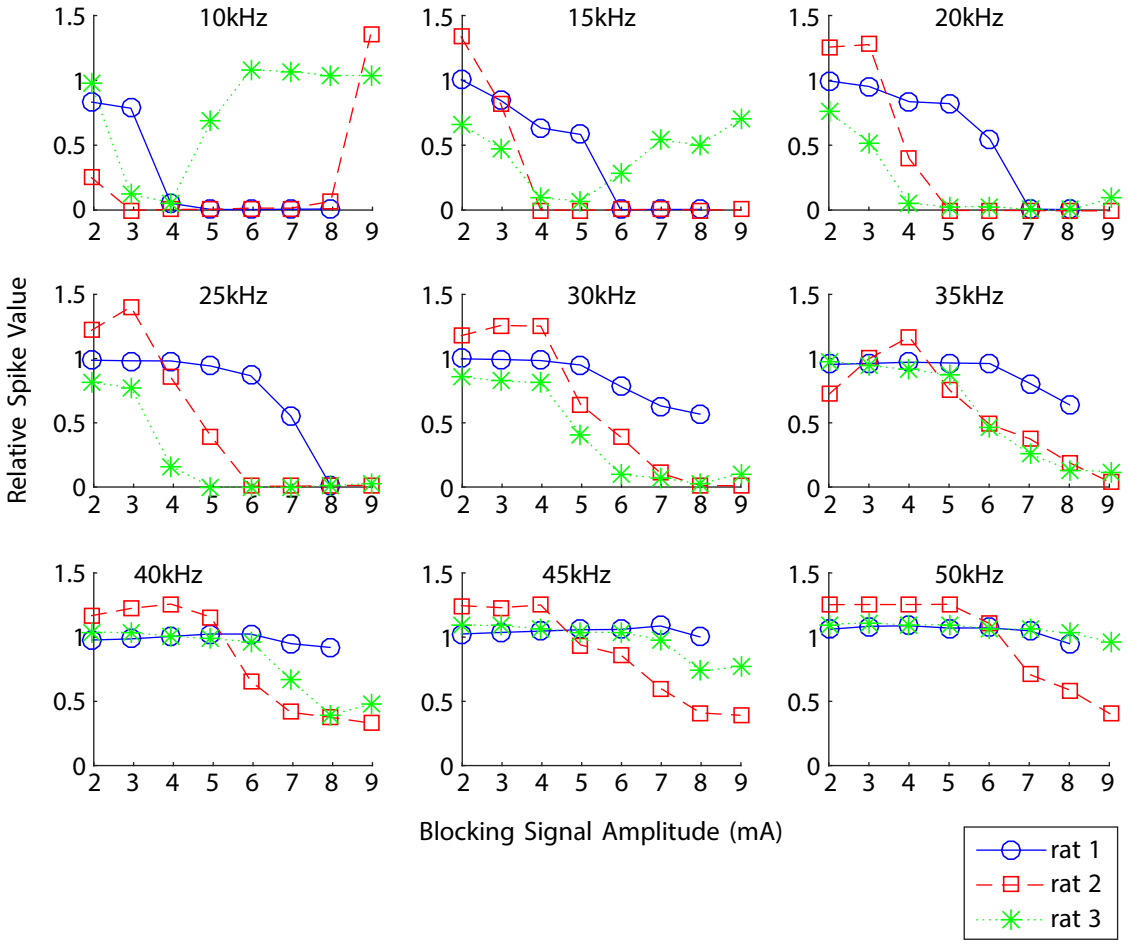


Figure 4.6: Plots of the normalized EMG response of the Sprague Dawley rat *gastrocnemius medialis* muscle during concurrent stimulation and block of the sciatic nerve as a function of blocking signal amplitude. Each plot corresponds to a trialled blocking signal frequency. This figure was previously published in [17].

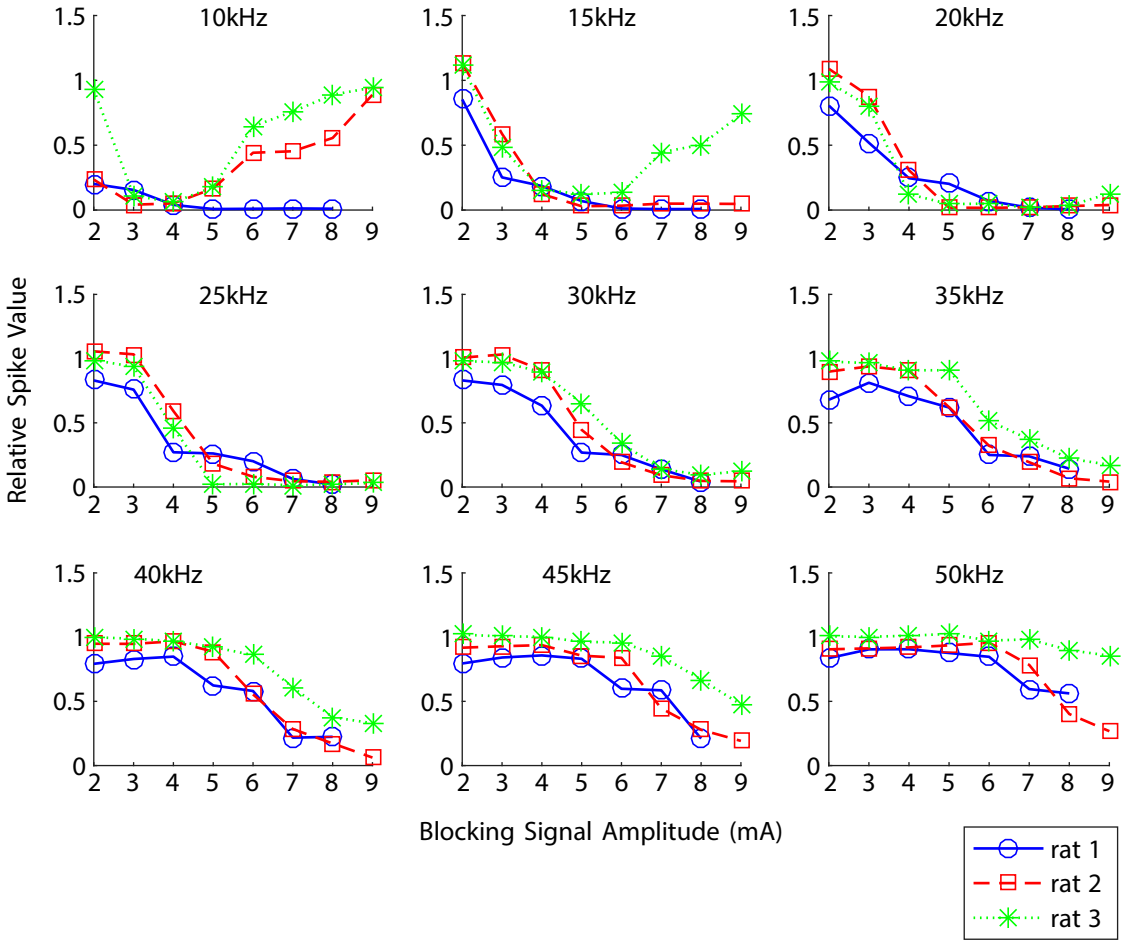


Figure 4.7: Plots of the normalized EMG response of the Sprague Dawley rat *tibialis anterior* muscle during concurrent stimulation and block of the sciatic nerve as a function of blocking signal amplitude. Each plot corresponds to a trialled blocking signal frequency. This figure was previously published in [17].

corresponding to CPC above the median of the CPC distribution during the experiments, and one corresponding to CPC below the median of that same distribution. This maximises the size of each group before further filtering out of invalid trials as specified in rejection criteria for each analysis. If sub-groups are observed in the resulting distributions then alternative categorization methods are considered.

Block charge per cycle is displayed in table 4.2 for the block amplitudes and frequencies used in the trials. The median CPC is 1.9 nC.

Table 4.2: Charge per cycle depending on block amplitude and frequency in nanocoulombs (nC).

| Frequency (kHz) | Amplitude (mA) | | | | | | | |
|---|---|---|---|---|---|---|---|---|
| | 2 | 3 | 4 | 5 | 6 | 7 | 8 | 9 |
| 10 | 2.00 | 3.00 | 4.00 | 5.00 | 6.00 | 7.00 | 8.00 | 9.00 |
| 15 | 1.33 | 2.00 | 2.66 | 3.33 | 4.00 | 4.66 | 5.33 | 6.00 |
| 20 | 1.00 | 1.50 | 2.00 | 2.50 | 3.00 | 3.50 | 4.00 | 4.50 |
| 25 | 0.80 | 1.20 | 1.60 | 2.00 | 2.40 | 2.80 | 3.20 | 3.60 |
| 30 | 0.66 | 1.00 | 1.33 | 1.66 | 2.00 | 2.33 | 2.66 | 3.00 |
| 35 | 0.57 | 0.86 | 1.14 | 1.43 | 1.71 | 2.00 | 2.29 | 2.57 |
| 40 | 0.50 | 0.75 | 1.00 | 1.25 | 1.50 | 1.75 | 2.00 | 2.25 |
| 45 | 0.44 | 0.66 | 0.88 | 1.11 | 1.33 | 1.55 | 1.77 | 2.00 |
| 50 | 0.40 | 0.60 | 0.80 | 1.00 | 1.20 | 1.40 | 1.60 | 1.80 |

A first analysis to confirm the relationship between high block efficacy and either low frequencies or high amplitude is carried out by plotting block efficacy versus CPC for CPC below median and CPC above median as previously explained. The result is shown figure 4.8.

The figure shows that for both muscles there is a significant effect of block on relative EMG activity when considering trials for which block CPC is above the median value of 1.9 nC. To be precise block is far more effective for trials where block CPC is above the median For both muscles in some trials where block CPC is below the median (and more rarely for when CPC is above the median), a number of trials show relative EMG substantially above the baseline, however this observation was too inconsistent to be accurately characterized. Instead, a further analysis was undertaken to determine whether block CPC had any effect on fibre conduction or recovery speeds from block as such effects could be used for selective stimulation as per Kuffler's method.

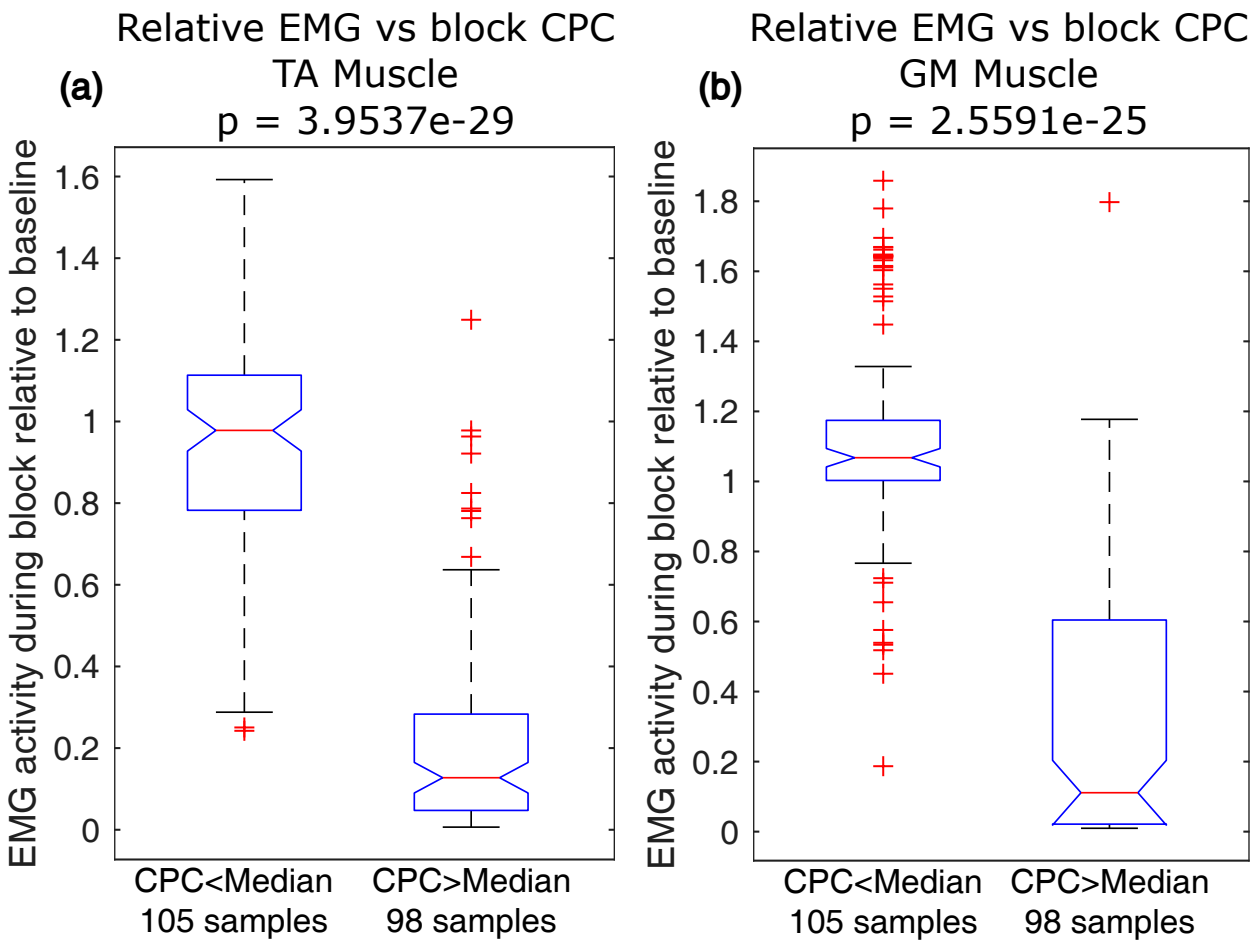


Figure 4.8: Boxplots of block efficacy data aggregated across all rats and separated according to whether block charge per cycle was above or below median, with one comparison per muscle. P-values reported on figure correspond to 2-sided Wilcoxon Rank-Sum test testing for difference in median between the two distributions.

### 4.4.4 Effect of block Charge Per Cycle on time between stimulation and EMG waveform arrival

EMG signals from both muscles were analysed to measure the time between stimulation and the arrival of the EMG. Initial analysis suggested that the first negative peak of the EMG waveform was the most consistent for measuring the time between stimulation and EMG response, at least when considering EMG recordings of the *tibialis anterior* muscle. The key question underlying the analysis was whether block had any effect on the timing of the EMG that could be interpreted as selective block, particularly when the muscle starts recovering from block as this is the crucial period when simulations predict a window exists to carry out fibre-size selective stimulation. During complete block the EMG signal is not strong enough such that

time between stimulation and EMG arrival can be measured accurately, therefore we focused on EMG recorded after block cutoff for which the respective muscle had recovered at least 5% of activity relative to baseline in order to have sufficient amplitude for a reliable timing measurement to be made. The time delays between stimulation and EMG arrival at block cutoff were substracted from those recorded during baseline trials in order to obtain a measure of the difference, and the resulting dataset was separated into trials corresponding to a CPC of block below and above the median as above. Results of the analysis are plotted in boxplots on figure 4.9.

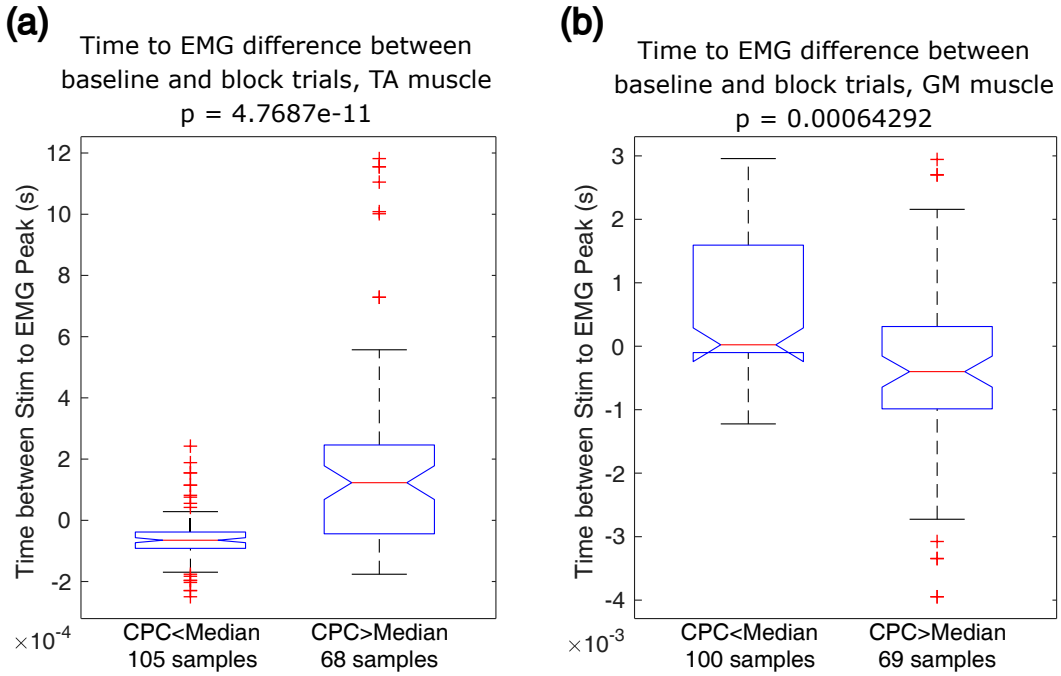


Figure 4.9: Boxplots of time to EMG arrival difference between baseline and block trials for block CPC below and above the median. (a): data for the *tibialis anterior* muscle. (b): data for the *gastrocnemius medialis* muscle. p-values correspond to a 2-sided Wilcoxon Rank-Sum test applied to determine whether the medians of the two distributions were different.

The results show that for TA there was a small yet significant effect of block CPC on time between stimulation and EMG signal arrival at the recording electrodes placed on the muscle, however for GM the result is less consistent and despite having a p-value low enough to reject the null hypothesis for the two-sided Wilcoxon Rank-Sum test, it is likely the measure is not reliable enough to draw a conclusion. The measured effect is more significant for TA and we can say with higher confidence that the timing measures for TA are valid (see section 4.5 for discussion of the results). Overall for TA the time between stimulation and EMG response

increases when considering block trials with CPC above the median compared to block trials for which CPC is below the median. Interestingly, compared to baseline recordings the trials with block CPC below median show a small effect on timing (p = 1.008717e-10 for a Wilcoxon single-sided rank sign test) indicating that the time between stimulation and EMG response is slightly shorter, though the results suggest the effect is not as large as the difference between the two distributions when considering block trials only. For GM, carrying out the same test type on both distributions returns p-values of 1.66e-04 and 0.0502 respectively for block trials below and above median CPC respectively. The latter test cannot reject the null hypothesis and therefore indicates that it's not possible to tell whether there is an effect for GM for high CPC trials, and while the p-value for trials with CPC below the median can reject the null hypothesis, the variability of EMG recording for GM specifically and its effect on the reliability of the timing measurement reduces confidence in a conclusion for that specific result.

## 4.5 Discussion

We can first attempt to interpret the effects on timing due to block, when looking at the difference in terms of CPC. An increase in the time to EMG response can be explained two different ways. Fundamentally the increase in the time between stimulation and arrival of the EMG for block CPC above the median indicates that for those trials, it appears the EMG is slower to arrive. The EMG itself is a compound action potential and therefore several fibre groups within a muscle are contributing. One explanation for the effect is that the action potential has been slowed down. Another explanation is that slower fibres recover first from block, as then their peak would be recognised as the EMG peak as the fast fibres are not active enough to cross the detection threshold. It is not possible to tell which of the two effects is being observed with the dataset, as we would require single unit recordings of either ENG or EMG to determine whether the signal is being slowed or whether certain fibres are recovering before others.

In terms of effect impact on function, if we make the hypothesis that the effect is due to a slowing

of the signal and that this slowing is in the nerve, as that is where the blocking signal is being applied, then we can determine the relative effect on the speed of the neural action potential. The speed of the fastest A fibres in the rat sciatic nerve is approximately 100 $m.s^{-1}$. The distance between the stimulation electrode and the neuromuscular junction is approximately 3 cm based on the anatomical location of the cuff stimulation contacts after implantation. A delay of 0.15 ms as per the median of the distribution corresponding to $CPC > Median$ for the *tibialis anterior* muscle would then correspond to an average speed of 66.6 $m.s^{-1}$, a reduction of 33%. However, it is quite possible this reduction is not on average speed but at the specific location of the block, and correspondingly stronger.

On that note and going back to section 4.3.3 describing the composition of the rat sciatic nerve, it is important to note here that capturing EMG signals is somewhat limiting in terms of interpreting neural activity within the sciatic nerve itself, which is the end goal as high-frequency block acts on the nerve itself and not the muscle. In effect, only activity from the efferent motor units comprising 6% of the total fibre population can be recorded, with possible indirect activity from afferent fibres through proprioceptive reflexes not involving the brain. However, EMG recording was still attractive in this context because of the noise and filtering challenges associated with direct electroneurogram (ENG) recording from the sciatic nerve *in-vivo*. In effect, high frequency block *in-vivo* would generate a large amount of noise in the recording as impedance between the recording and stimulation electrodes was in the kilo-ohm range and the stimulation signal had a high amplitude. Using EMG signals with significantly greater amplitudes than ENG signals, coupled with the greater distance between the recording electrodes placed in the muscle, and the stimulating electrodes placed on the nerve, effectively increased the SNR and made filtering the coupled HFAC signal out of the recording possible.

A further note is on the variability of the *gastrocnemius medialis* muscle response. It is possible that movement of the muscle due to stimulation led to more noise and artefact for this muscle more than for *tibialis anterior*. Overall *tibialis anterior* was more stable than *gastrocnemius medialis* over all experiments and therefore more reliable for measurements. EMG electrodes are more susceptible to movement artefacts, especially when considering the onset response to high-frequency block which initially causes tetanic muscle contraction [22]. Another element

to consider is the fact *gastrocnemius medialis* also displayed quick fatigue when subjected to high-frequency stimulation that was not blocking, as shown in figure 4.10.

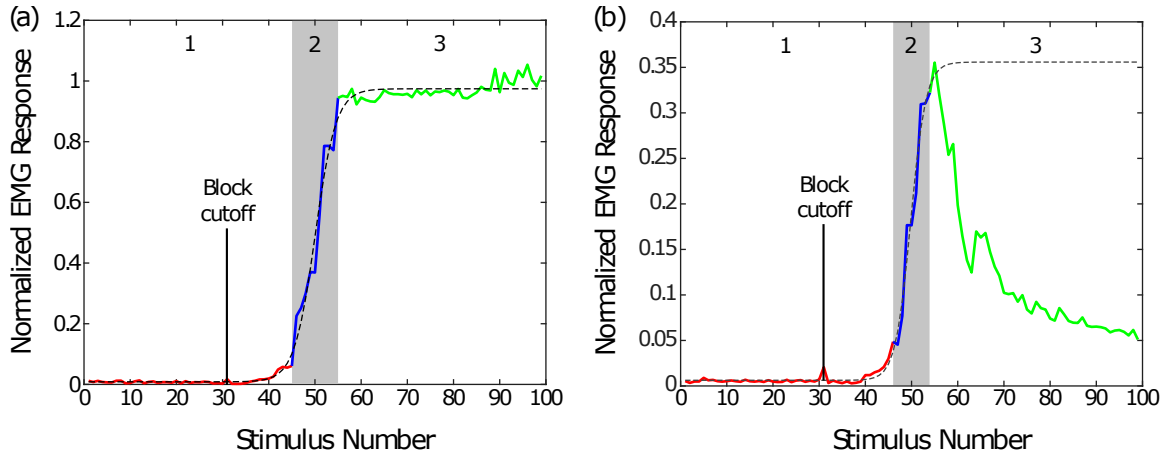


Figure 4.10: Curves showing EMG response to 100 Hz stimulation at the end of block, used to measure muscle recovery from block. (a) is for *tibialis anterior*, (b) is for *gastrocnemius medialis*. Numbers on the x-axis correspond to the stimulus number in the train.

Finally, there were notable differences between predictions from the computational model and observations made during the experiments, when looking at predictions made by the FH model, and this validates the need for verification using live tissue models. While the FH model predicted that block signal frequencies between 2.5 and 5 kHz would be broadly successful at blocking neural activity as shown in figure 2.16, in practice block was not achievable under 10 kHz and was most reliable at frequencies between 20 and 30 kHz during these experiments, with high blocking signal amplitudes being ineffective at suppressing the conduction of action potentials at lower frequencies. In terms of amplitude block thresholds were reached between 4 and 7 mA during experiments while the model predicted 3 to 4 mA for a generous distance of 1 mm between the blocking electrode and nerve fibres, which would have been lower in experiments as the diameter of the nerve is approximately 1 mm.

## 4.6 Conclusions

Experiments at Newcastle University sought to combine block and stimulation in the *in-vivo* rat sciatic nerve model to determine whether selective activation of 'slow-twitch' motor units was feasible. The key idea was that the EMG response of 'fast-twitch' and 'slow-twitch' motor

units would be different in a way that would enable simple signal processing techniques such as frequency analysis or template-based correlation filters to classify EMG response as 'fast-twitch', 'slow-twitch' or a combination of the two. Block efficacy was measured by recording EMG activity from both the *gastrocnemius medialis* and *tibialis anterior* muscles.

The results suggest that block effect can be measured using a single CPC variable rather than a combination of frequency and amplitude, which makes comparisons between datasets more straightforward. Block efficacy effects dependent on this variable were measured, and are also associated with a change in the timing of the EMG signal. Interpretations of this timing indicate either a slowing of the ENG action potential, as no effect could be seen on EMG according to distal stimulation controls, or different recovery speeds for fibres of different sizes, as larger fibres tend to innervate faster motor units. Depending on the root cause of the effect, there could be applications in selective stimulation, for example by enabling stimulation of slow-twitch fibres after block without activation of fast-twitch fibres, due to them recovering more slowly.

However, another conclusion to draw is the difficulty in interpreting neural phenomena from EMG recordings alone. Ideally, direct ENG recordings would increase confidence in conclusions made from measurements, and also enable the study of how nerve fibres that do not innervate muscles react to block, for example C fibres. As detailed in the next chapter (chapter 5), this drove the search for and development of a means to carry out ENG recordings during block so as to better understand what happens to the neural action potential when it crosses through the blocked portion of nerve.

# References

[1] J. Avendaño-Coy, D. Serrano-Muñoz, J. Taylor, C. Goicoechea-García, and J. Gómez-Soriano, "Peripheral Nerve Conduction Block by High-Frequency Alternating Currents: A Systematic Review," *IEEE Transactions on Neural Systems and Rehabilitation Engi-*

*neering*, vol. 26, no. 6, pp. 1131–1140, Jun. 2018, ISSN: 1534-4320. DOI: 10.1109/TNSRE.2018.2833141.

[2] R. P. Williamson and B. J. Andrews, "Localized electrical nerve blocking," *IEEE Transactions on Biomedical Engineering*, vol. 52, no. 3, pp. 362–370, Mar. 2005, ISSN: 0018-9294. DOI: 10.1109/TBME.2004.842790.

[3] D. M. Ackermann, C. Ethier, E. L. Foldes, E. R. Oby, D. Tyler, M. Bauman, N. Bhadra, L. Miller, and K. L. Kilgore, "Electrical conduction block in large nerves: High-frequency current delivery in the nonhuman primate," en, *Muscle & Nerve*, vol. 43, no. 6, pp. 897–899, Jun. 2011, ISSN: 1097-4598. DOI: 10.1002/mus.22037. [Online]. Available: http://onlinelibrary.wiley.com/doi/10.1002/mus.22037/abstract (visited on 02/14/2017).

[4] J. E. Arle, L. Mei, and K. W. Carlson, "Fiber Threshold Accommodation as a Mechanism of Burst and High-Frequency Spinal Cord Stimulation," en, *Neuromodulation: Technology at the Neural Interface*, vol. n/a, no. n/a, Nov. 2019, ISSN: 1525-1403. DOI: 10.1111/ner.13076. [Online]. Available: https://onlinelibrary.wiley.com/doi/abs/10.1111/ner.13076 (visited on 02/17/2020).

[5] A. G. Richardson, C. C. McIntyre, and W. M. Grill, "Modelling the effects of electric fields on nerve fibres: Influence of the myelin sheath," en, *Medical and Biological Engineering and Computing*, vol. 38, no. 4, pp. 438–446, Jul. 2000, ISSN: 0140-0118, 1741-0444. DOI: 10.1007/BF02345014. [Online]. Available: http://link.springer.com/article/10.1007/BF02345014 (visited on 09/22/2016).

[6] H. Liu, J. Roppolo, W. de Groat, and C. Tai, "The Role of Slow Potassium Current in Nerve Conduction Block Induced by High-Frequency Biphasic Electrical Current," *IEEE Transactions on Biomedical Engineering*, vol. 56, no. 1, pp. 137–146, Jan. 2009, ISSN: 0018-9294. DOI: 10.1109/TBME.2008.2006013.

[7] N. Bhadra, E. A. Lahowetz, S. T. Foldes, and K. L. Kilgore, "Simulation of high-frequency sinusoidal electrical block of mammalian myelinated axons," en, *Journal of Computational Neuroscience*, vol. 22, no. 3, pp. 313–326, Jan. 2007, ISSN: 0929-5313,

1573-6873. DOI: 10.1007/s10827-006-0015-5. [Online]. Available: http://link.springer.com/article/10.1007/s10827-006-0015-5 (visited on 09/20/2016).

[8] E. Perra, A. Rapeaux, and K. Nikolic, "The Crucial Role of Nerve Depolarisation in High Frequency Conduction Block in Mammalian Nerves: Simulation Study," in *2018 40th Annual International Conference of the IEEE Engineering in Medicine and Biology Society (EMBC)*, ISSN: 1557-170X, Jul. 2018, pp. 2214–2217. DOI: 10.1109/EMBC.2018.8512759.

[9] A. Rapeaux, K. Nikolic, I. Williams, A. Eftekhar, and T. G. Constandinou, "Fiber size-selective stimulation using action potential filtering for a peripheral nerve interface: A simulation study," in *2015 37th Annual International Conference of the IEEE Engineering in Medicine and Biology Society (EMBC)*, Aug. 2015, pp. 3411–3414. DOI: 10.1109/EMBC.2015.7319125.

[10] K. L. Kilgore and N. Bhadra, "High Frequency Mammalian Nerve Conduction Block: Simulations and Experiments," in *28th Annual International Conference of the IEEE Engineering in Medicine and Biology Society, 2006. EMBS '06*, Aug. 2006, pp. 4971–4974. DOI: 10.1109/IEMBS.2006.259254.

[11] L. Joseph and R. J. Butera, "High-Frequency Stimulation Selectively Blocks Different Types of Fibers in Frog Sciatic Nerve," *IEEE Transactions on Neural Systems and Rehabilitation Engineering*, vol. 19, no. 5, pp. 550–557, Oct. 2011, ISSN: 1534-4320. DOI: 10.1109/TNSRE.2011.2163082.

[12] H. Schmalbruch, "Fiber composition of the rat sciatic nerve," en, *The Anatomical Record*, vol. 215, no. 1, pp. 71–81, 1986, ISSN: 1097-0185. DOI: 10.1002/ar.1092150111. [Online]. Available: https://onlinelibrary.wiley.com/doi/abs/10.1002/ar.1092150111 (visited on 01/23/2020).

[13] J. Castro, P. Negredo, and C. Avendaño, "Fiber composition of the rat sciatic nerve and its modification during regeneration through a sieve electrode," en, *Brain Research*, vol. 1190, pp. 65–77, Jan. 2008, ISSN: 0006-8993. DOI: 10.1016/j.brainres.2007.11.

028. [Online]. Available: http://www.sciencedirect.com/science/article/pii/S0006899307027941 (visited on 02/11/2020).

[14] S. Raspopovic, M. Capogrosso, and S. Micera, "A Computational Model for the Stimulation of Rat Sciatic Nerve Using a Transverse Intrafascicular Multichannel Electrode," en, *IEEE Transactions on Neural Systems and Rehabilitation Engineering*, vol. 19, no. 4, pp. 333–344, Aug. 2011, ISSN: 1534-4320, 1558-0210. DOI: 10.1109/TNSRE.2011.2151878. [Online]. Available: http://ieeexplore.ieee.org/document/5898424/ (visited on 03/02/2020).

[15] N. Bhadra and K. L. Kilgore, "High-frequency electrical conduction block of mammalian peripheral motor nerve," en, *Muscle & Nerve*, vol. 32, no. 6, pp. 782–790, Dec. 2005, ISSN: 1097-4598. DOI: 10.1002/mus.20428. [Online]. Available: http://onlinelibrary.wiley.com/doi/10.1002/mus.20428/abstract (visited on 09/20/2016).

[16] A. Rapeaux, E. Brunton, K. Nazarpour, and T. G. Constandinou, "Preliminary Study of Time to Recovery of Rat Sciatic Nerve from High Frequency Alternating Current Nerve Block," in *2018 40th Annual International Conference of the IEEE Engineering in Medicine and Biology Society (EMBC)*, ISSN: 1557-170X, Jul. 2018, pp. 2671–2674. DOI: 10.1109/EMBC.2018.8512832.

[17] A. Rapeaux, E. Brunton, K. Nazarpour, and T. G. Constandinou, "Recovery Dynamics of the High Frequency Alternating Current Nerve Block," *bioRxiv*, p. 235 135, Dec. 2017. DOI: 10.1101/235135. [Online]. Available: https://www.biorxiv.org/content/10.1101/235135v1 (visited on 02/19/2020).

[18] E. Brunton, C. W. Blau, and K. Nazarpour, "Separability of neural responses to standardised mechanical stimulation of limbs," en, *Scientific Reports*, vol. 7, no. 1, pp. 1–14, Sep. 2017, ISSN: 2045-2322. DOI: 10.1038/s41598-017-11349-z. [Online]. Available: https://www.nature.com/articles/s41598-017-11349-z (visited on 02/18/2020).

[19] J. Kortelainen, H. Al-Nashash, A. Vipin, X. Y. Thow, and A. All, "The effect of anaesthesia on somatosensory evoked potential measurement in a rat model," en, *Laboratory Animals*, vol. 50, no. 1, pp. 63–66, Feb. 2016, ISSN: 0023-6772. DOI: 10.1177/

0023677215589514. [Online]. Available: https://doi.org/10.1177/0023677215589514 (visited on 02/18/2020).

[20] N. Bhadra, T. L. Vrabec, N. Bhadra, and K. L. Kilgore, "Reversible conduction block in peripheral nerve using electrical waveforms," *Bioelectronics in Medicine*, vol. 1, no. 1, pp. 39–54, Jan. 2018, ISSN: 2059-1500. DOI: 10.2217/bem-2017-0004. [Online]. Available: https://www.ncbi.nlm.nih.gov/pmc/articles/PMC5811084/ (visited on 09/03/2019).

[21] W. Friedli and M. Meyer, "Strength-duration curve: A measure for assessing sensory deficit in peripheral neuropathy," en, p. 6,

[22] D. M. Ackermann, E. L. Foldes, N. Bhadra, and K. L. Kilgore, "Conduction Block of Peripheral Nerve Using High Frequency Alternating Currents Delivered through an Intrafascicular Electrode," *Muscle & nerve*, vol. 41, no. 1, pp. 117–119, Jan. 2010, ISSN: 0148-639X. DOI: 10.1002/mus.21496. [Online]. Available: http://www.ncbi.nlm.nih.gov/pmc/articles/PMC2947328/ (visited on 10/01/2015).

# Chapter 5

# Enhancing the selectivity of extraneural electrodes with precisely timed conventional stimulation and high-frequency block

## 5.1 Foreword

Having described a custom block-capable stimulator in chapter 3, and initial experiments to characterise block *in-silico* and *in-vivo* in chapter 4, initial results for using block suggest that the period during which the nerve is recovering from block could be used for selective stimulation. However, several limitations remain. It is not possible to interpret activity from fibres other than the ones innervating muscle from an *in-vivo* preparation due to ENG recording not being possible during block in that specific experimental setup. Another limitation is the duration of the recovery period is very small which reduces the practical usability of the technique.

The next logical step was to find an experimental setup for which ENG recording was possible during block, as this gives us direct access to the activity happening inside the nerve before, during and after block such that the effects of block can be accurately described. This will also make it possible to record non-somatic neural activity. A second step is to extend the duration of the recovery period during which not all fibres in the nerve are excitable, which represents the most likely opportunity to carry out selective stimulation. The end goal is to determine whether high-frequency block can be used to enhance the selectivity of nerve cuff electrodes[1].

## 5.2 Motivation

The holy grail of neural interfaces is often thought of as "one to one" interfacing with nerve cells such that perfect control of the interface between the nervous system and a therapeutic or communication device can be achieved. It is evident that the field is still a long way from this goal; current stimulation-based therapies all have side-effects tied to the non-selective nature of the interface used to deliver the therapy. The tradeoff between selectivity and invasiveness, and the challenges associated with invasive interfaces has been described previously in chapter 2. Much work has been carried out to attempt to optimize this tradeoff and benefit from the body's tolerance of less invasive interfaces as well as more control over which parts of the nervous system are activated by stimulation, however each have their drawbacks which reduce their usefulness in a clinical context.

It can be argued that the origin for the drive towards more selectivity comes from issues with FES, an early application of neural stimulation to recover muscle function after neural injury. Typical applications of FES include corrections for foot drop [1], bladder control [2] and hand grasp [3], often as means of recovering muscle function after spinal cord injury [4]. As electrical nerve stimulation preferentially activates large diameter fibers, this leads larger fast-twitch,

[1]In this chapter, animal experiments were carried out with the approval of the Animal Welfare and Ethical Review Board (AWERB) of Imperial College London. These experiments were made possible by partnerships with the research group of Dr. Rylie Green (Imperial College Bioengineering) and more specifically contributions from Dr. Omaer Syed and Estelle Cuttaz. Omaer Syed assisted with animal Schedule 1 procedures and measurements during experiments. Estelle Cuttaz designed and fabricated the custom conductive elastomer cuff electrodes used for some experiments with block as will be described later in this chapter.

fatigue-prone motor units to be activated first when grades stimulation is used. In healthy bodies slow-twitch, fatigue-resistant motor-units are recruited first. This leads FES to cause premature muscle fatigue. An early goal for improving FES implants was to reverse the motor unit recruitment order during stimulation, requiring fiber-size selectivity. Further work refined this concept to a more generalized definition of selectivity that is well described in [5] when neural stimulation was applied to nerves not connected to muscles but to other organs, such as the vagus nerve.

This chapter will first detail techniques and electrodes specifically designed to improve selectivity, essentially describing attempts to optimize the selectivity and invasiveness tradeoff, before focusing on high frequency block as a new and powerful tool for enhancing selectivity. An analysis of the mechanics of block at the ion channel level will be given with tentative explanations for some of the processes observed in *ex-vivo* and *in-vivo* experiments that are not captured by computational models of nerve.Section 5.5 will detail the development of an ex-vivo platform to enable the recording of ENG during HFAC block and place it in the context of experimental platforms for neurophysiology. Finally *ex-vivo* experiments to characterise and validate the platform for HFAC block experiments are described in section 5.7, and experiments exploring HFAC carryover, an extension of he recovery period from block, to enable selective stimulation are detailed in section 5.8. After discussing the results, the chapter will conclude with an analysis of the requirements for using high-frequency block for selective stimulation using cuff electrodes.

## 5.3 Selective Stimulation Paradigms

Selective stimulation strategies approach selectivity from three directions: using specially designed waveforms to stimulate specific fiber types, using selective electrodes to activate specific fascicles within a nerve, and finally using block to filter out unwanted activity from stimulation.

### 5.3.1 Selective stimulation waveforms: leveraging ion channel dynamics and nerve microanatomy

An early approach to improve the selectivity of electrodes was to change the waveform used to stimulate nerves. Traditionally square pulses are used for stimulation since this waveform allows straightforward calculation of injected charge; the injected charge is equal to the constant output current times the duration of the pulse. However this pulse shape does not utilize the dynamics of membrane ion channels in any way. A number of studies proposed the use of different stimulation waveforms that utilized voltage-gated ion channel dynamics to influence which fibers were in effect stimulated, most with the goal of inverting the motor unit recruitment order allowing slow-twitch and most importantly fatigue-resistant motor units to be activated, thereby improving the useability of motor prostheses for spinal cord injury patients.

One of the earliest techniques used to achieve selectivity was a polarization block leveraging the difference in conduction speeds between fast and slow motor units. As larger nerve fibers conduct action potentials faster, and are more sensitive to anodal currents blocking these signals, an bipolar stimulation electrode configuration arranged such that during stimulation, the anode is active when the action potential propagating in the larger fibers reaches it, and action potentials propagating in smaller fibers are located between the cathode and anode, results in the selective anodal block of the action potentials in the larger fibers and therefore in the selective activation of the smaller fibers. This technique was pioneered by Kuffler [6] in frog nerve as has been previously mentioned in this thesis, but is based on the work of Pflüger [7] who first noticed this effect. The technique requires a long distance between the stimulating cathode and blocking anode, and uses long pulses which may be harmful to the nerve, both drawbacks for clinical applications. In addition, Kuffler's technique does not work as well in mammalian nerve due to anode break excitation; when using rectangular pulses if an anode is in contact with mammalian nerve tissue the membrane will be hyperpolarized and the inactivation component of depolarizing sodium channels will be fully open instead of partially closed. This means that when the anodic current is suddenly switched off the small current that can then flow through the sodium channel can be enough to depolarize the membrane to the

stimulation threshold and generate an action potential, nullifying the selective nature of this stimulation technique [8]. Accornero [9] proposed using triangular-shaped pulses with an exponential decay instead to compensate for this, however the technique could still cause unwanted activation of nerves distal to the stimulation site, and likely required extensive nerve-specific calibration before use, such as adjusting stimulation amplitudes and inter-electrode distance. Fang and Mortimer [10] suggest using quasi-trapezoidal pulses, also with an exponential decay to prevent anodal break excitation, but with the difference of requiring the use of a tripolar cuff electrode. The significant difference between the two techniques is the plateau phase of the latter, which essentially combines a square wave with the triangular wave of the former. Finally, van Bolhuis [11] used two separate stimulators, one to excite all fibers within the nerve and the second to selectively block activity in fast fibers.

### 5.3.2 Collision block as a selective stimulation tool

A different approach entirely is to stimulate the entire nerve, but generate action potentials propagating in only one direction. Cathodic currents applied to peripheral nerve fibers generate action potentials propagating both distally and proximally. Conversely anodic currents can block these action potentials, when an action potential attempts to propagate through a section of membrane that has been hyperpolarized by anodic current. If the stimulating cathode and blocking anode are placed such that action potentials generated in one direction are completely blocked during the stimulation cycle, the result is unidirectional stimulation.

Unidirectional stimulation is generally achieved by careful design of cuff electrodes [12]–[14] and calibration of stimulus pulse duration to optimize the anodal block of action potentials propagating in the opposite direction to what is desired. Achieving this provides an interface that can selectively excite motor or sensory nerve fibers, but that can also be used for collision block of unwanted action potentials when multiple populations of nerve fibers are activated by therapeutic stimulation. Collision block occurs when two action potentials travelling in opposite directions in the same nerve fiber collide: both action potentials are annihilated due to the refractory period of sodium ion channels, which prevents them from opening twice in

quick succession. Since these channels are closed in both directions when action potentials collide, there are no ion channels that can be opened to continue the action potential in either direction, and therefore both action potentials are annihilated, resulting in a form of block. This block can be used to selectively filter out unwanted activity arising out of therapeutic stimulation. For example, when stimulating slow-twitch motor units, fast-twitch motor units are also activated. Fast-twitch motor units have lower activation thresholds than slow-twitch motor units. By activating both fast-twitch and slow-twitch proximally, and stimulating in the afferent direction distally, to prevent activation of fast-twitch muscle fibers when stimulating slow-twitch motor units Overall collision block and recruitment order reversal all aim to address the problem of fast-onset fatigue that is common in FES therapies.

### 5.3.3 Selective electrode designs: current steering to selectively activate regions of the nerve

In a more general sense and as mentioned in [5], these selective stimulation techniques all use differences in action potential conduction speed or stimulation threshold of different fibers based on the size of the fiber or its distance to the stimulating electrode to more precisely control which fibers are activated at the end of a stimulation cycle. However, these techniques have drawbacks, such as the requirement for a large distance between stimulating electrodes, precise calibration of thresholds which can change over time in chronic implants, or requirements for long stimulation pulses that may not be suitable for chronic use.

A different approach to selectivity is instead to target specific subpopulations of fibers within a region in the cross-section of a nerve. As described in chapter 2, peripheral nerves are organized in fascicles which eventually branch out distally to reach specific targets. This enables electrodes to target these fascicles selectively for stimulation, even when interfacing with the entire nerve trunk.

There are many electrode geometries and configurations available for use experimentally, at different locations on the spectrum of invasiveness correlated with selectivity, though in general

only extraneural electrodes that do not penetrate the epineurium are approved for chronic human use. These are all cuff electrodes in some form, with three main categories.

- Conventional cuff electrodes: This is the oldest cuff design and consist of a split silastic tube with woven wire or pad electrodes on the inside [15]. The cross-section is in the shape of a 'C' which is typically closed around the nerve using suturing thread. Suppliers of this electrode design as of this writing include Microprobes for Life Science (USA) and Microleads (UK). Cuff size has to be carefully chosen before experiments as they may be too tight, leading to nerve damage by compression, or too loose, increasing stimulation thresholds, variability and severely impacting any recording that can be done of neural activity.

- Spiral cuff electrodes: A pre-stressed silicone sheet backing makes these electrodes curl upon themselves, obviating the need for suturing thread to maintain the cuff closed. Generally pad electrodes are placed on the inside for stimulation, as wire stimulating contacts are often too stiff to allow the cuff to close by itself. The closing action also allow them to adjust their size according to the implanted nerve, making them more versatile as they can be implanted on a wider range of nerve diameters. They apply an amount of pressure on nerves due to this closing action [16], and therefore there may be a risk of nerve damage due to constraining the blood supply without careful design. A supplier of this type of electrode is Cortec (Germany)

- Flat Interface Nerve Electrodes: This type of cuff, also called a 'book electrode' due to its distinctive shape, attempts to improve the selectivity of conventional cuffs by improving access to nerve fascicles at the centre of a nerve. This is done by making the nerve conform to a more oval shape within the electrode, while avoiding any damage from compression of the blood supply [17]. By flattening the nerve fascicles are arranged in one or more rows that can be more readily interfaced with several electrodes within the implant.

These cuffs can be made more selective by increasing the number of contacts at each position along the length of the cuff [18], [19], essentially enabling current-steering within cuffs to target

regions within the nerve for stimulation. As shown in figure 7.3, fascicles can be configured differently within nerves from individual to individual, and electrode contacts can be split to have more control over which fascicles are stimulated using one contact. the different positions of fascicles explains the challenge of trying to activate one fascicle within a nerve without activating others reliably using extraneural electrodes - it is not possible to see whether contacts align with fascicles inside the nerve at implantation time. Even in an ideal contact positioning case it is unlikely that the electric field generated by one contact of the cuff only activates one fascicle, though some encouraging results have been obtained in the past [18], [20], [21]. Overall, the variation between fascicle configurations from individual to individual can make selective cuff configurations unreliable when applied in a clinical setting.

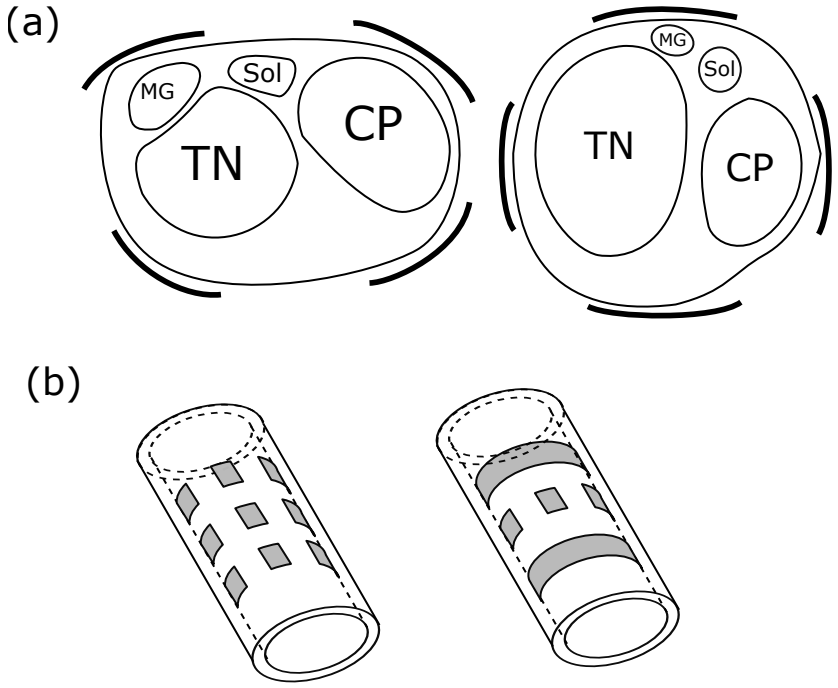


Figure 5.1: (a): Two different possible configurations for fascicles within cat sciatic nerve, adapted from [20]. Thicker lines represent stimulating contact positions for a cuff around the nerve. (b): drawing of two possible configurations for contacts of a multipolar nerve cuff, with split or complete rings at different locations around the implanted nerve, adapted from [18].

It is these drawbacks that motivated the search for a selective stimulation technique that would be suitable for chronic use, with minimal calibration requirements, and could be used with cuff electrodes approved for human use.

## 5.4 Analysis of block *in-silico*, *in-vivo* and *ex-vivo*

When it was discovered, high-frequency block was immediately recognized as a potentially chronically usable tool for nerve block as opposed to DC nerve block, due to using alternative current that would prevent harmful reactions from occurring at the electrode-electrolyte interface. However despite a number of studies several aspects of high-frequency block are still poorly understood. It is possible this is due to computational models not capturing all observed processes related to high frequency block in nerve, but also due to the difficulty in directly recording single fiber neural activity when injecting high amplitude, high frequency signals into the nerve tissue.

### 5.4.1 Quantification of nerve block and experimental controls

Part of the reason why interpretation of results in difficult when considering HFAC block studies is the diversity of measurands used to evaluate block efficacy, and the number of variables that can influence this efficacy.

The measurands used in studies depend primarily on the experimental setup used to carry out the measurements. Measurands are detailed in the following list:

- Force transduction: early studies used motor output to evaluate block efficacy. Briefly, an animal's hind leg was suspended in a custom fixture at the knee and a major muscle, generally the *gastrocnemius-soleus* was cut at the achilles tendon and the end attached to an in-line force transducer [22], which was used to measure the force generated by the muscle as a result of sciatic nerve stimulation. Relative changes in force due to block could then be recorded to evaluate block efficacy. A similar approach was used in the nonhuman primate [23]. An approach using direct EMG recording yields similar amounts of information. However information on block is incomplete with this approach as results can be confounded by processes specific to the neuromuscular junction and muscle itself. In effect the activity of only a small fraction of nerve fibers within a nerve

trunk is measured: for example this method ignores the contribution of any afferent sensory fibers.

- Direct ENG measurements are used when it is necessary to evaluate the activity of nerves not connected to muscles, such as when measuring block in the vagus nerve [24], [25]. This approach measures the CAP resulting from stimulation and interprets block efficacy based on relative difference in the CAP before, during and after block. CAPs are measured based on peak-peak amplitude [24] or area under the curve [26] for each signal component arising from the activity of different types of fibers.

- Counting action potentials propagating in fibers can be done in the case of simulation studies [27], [28]. Some studies simulate individual fibers while others simulate whole nerve with many axons in order to determine the effect of electrode geometry on block efficacy[29]. There are no known studies where stimulation and block outcome in computational modelling is tied to predicted CAP amplitude and shape if it were recorded *in-vivo* or *ex-vivo*, making comparison of model predictions and experimental results more difficult.

A number of parameters that can have an effect on block efficacy have been identified and are listed here:

- Block amplitude: This parameter affects overall block efficacy and the length of the secondary onset response [30]–[32].

- Block frequency: This parameter has a distinct threshold behaviour wherein block cannot be achieved if the blocking signal is delivered below a certain frequency [33], [34]. As frequency is increased the amplitude threshold for block increases.

- Duration of block: as block causes an onset response before resulting in the cessation of action potential conduction, duration has an effect on efficacy, with many variables influencing the exact behaviour over time

- Fiber diameter: larger diameter fibers can be blocked with lower block amplitudes, at least at lower block frequencies [25], [34], [35]

- Electrode-fiber distance: nerve fibers farther away from the blocking electrode require higher currents to be blocked [35], [36].

- Electrode size and configuration: contact size and inter-electrode distance when using bipolar electrodes has an effect on block efficacy, for example there is evidence that block electrodes must be tightly fitting and circumferential to the entire nerve in order to be effective [29], [36], [37].

- Ramping of frequency and amplitude: changing waveform parameters during block has an effect, whether it be on the onset response, or being able to reduce the waveform amplitude while maintaining block once it has been established. This is related to block duration [31], [38], [39].

It is important to note that as new studies are published, new parameters that have an effect on block efficacy, such as the 'dose' of HFAC injected into the nerve in the course of an experimental trial [40] are discovered. As such protocols are constantly being refined to account for these new parameters in order to isolate effects from each other.

Experimental trials using block and stimulation use a number of controls to avoid confounding effects such as muscle fatigue when force transducer measurements are used. Stimulation is delivered using multiple electrodes, one proximal and one distal to the blocking electrode [22]. During block trials both electrodes are used for stimulation. In the proximal case action potentials are blocked by the signal injected at the blocking electrode, while action potentials generated by the distal electrode propagate unhindered. Differences in response between stimulation delivered proximal or distal to the blocking electrode enables comparative measures of block efficacy to be carried out, as well as tracking any decrease in nerve function at the location of the block. This type of control can also be used both *in-vivo* and *ex-vivo*, for EMG, force transducer and ENG recordings and is used in trials in this work.

### 5.4.2 Drawbacks of High Frequency Block and existing solutions

Here a number of drawbacks of high-frequency block that would hinder its adoption in the clinic must be detailed, as well as work that has been carried out to mitigate these drawbacks.

- High Power Consumption: contrary to conventional stimulation modalities, high-frequency block seems to require high duty cycles. Interestingly, to the author's knowledge there have been no studies investigating specifically whether high frequency block can be achieved using waveforms with lower duty cycles[2], and therefore all studies to date have used HFAC block with 100% duty cycle waveforms. This leads to very high power consumption, especially considering that HFAC generally requires higher current waveform amplitudes than conventional stimulation. Power consumption has generally not been the focus of studies since experiments have generally relied on non-implantable hardware with access to large-capacity power supplies, save for the notable exception of the Enteromedics vBloc®system [41], however simulation studies have shown that this system is unlikely to be actually performing block [29], even though it has demonstrated clinical benefit. The device delivers blocking signals at a frequency of 5 kHz and an amplitude of 1 mA, typically for 2 minutes followed by 1 minute of no delivery during active therapy [42]. Expected electrode impedance is less than or equal to 1 kΩ. Assuming 1 kΩ resistive electrode impedance, the device would consume at least 1W during delivery of the signal, not including any overheads. For comparison, modern cardiac pacemakers consume 10-40 µW [43], requiring implanted HFAC block devices such as the Enteromedics Maestro®system delivering vBlock therapy to use rechargeable batteries and be recharged regularly [42].

- Onset Response: High Frequency Block is characterised by a strong onset response when first delivered before nerve conduction is effectively arrested [22]. This corresponds to a period during which the nerve fires at the maximum frequency as constrained by the refractory period. Evidently in clinical application of block this is undesirable as it would lead, in the best case, to discomfort for the patient, and in the worst to potentially

[2]The author acknowledges Dr. Ian Williams of Imperial College for this observation.

deleterious effects arising from strong off-target stimulation [36]. In the specific case of using block as a selectivity-enhancing modality, it would nullify any selectivity gained as simulation studies show whichever part of the nerve is blocked displays an onset response, and successful HFAC block delivery generally requires the entire nerve to be blocked [29]. As such a number of studies were carried out to investigate how this response might be mitigated or even eliminated. Strategies focus on modifying the envelope of the HFAC block signal, such as ramping the amplitude or frequency of the waveform [31], [39], [44], or combining HFAC block with bursts of DC block using specially designed electrodes to prevent DC current-induced nerve damage [45], [46]. The latter strategy has been the most successful at eliminating the onset response and is promising for application with the selectivity-enhancing HFAC block and stimulation protocol.

- Electrode Geometry Requirements: There is evidence in the literature that HFAC block efficacy and duration of onset response are sensitive to stimulation electrode geometry, such that selective multi-contact electrodes are unlikely to be successful if used for the delivery of HFAC block [29], [36], [47]. In this case the most effective stimulation electrode geometry has been a circumferential contact such as that used in simple nerve cuffs, with extra contact width to increase the electrode charge injection capacity and avoid nerve damage. However, there is evidence that HFAC block was delivered successfully using a non-circumferential electrode [48], however it is the only study of its type so far and has not demonstrated any specific advantages fore block compared to the use of circumferential cuff electrodes.

### 5.4.3 DC and near-DC block in recent literature

Despite the longstanding move away from DC nerve block due to evidence of nerve damage even with limited use [49], more recently interest in DC nerve block has been rekindled with the development of specially designed electrodes and materials enabling the use of this technique without causing nerve damage.

DC nerve block does not have several of the drawbacks of high frequency AC block, notably

its onset response and high power consumption. Anodal DC block can be delivered with relatively small currents and without any nerve activation before the block is active, providing a straightforward neuromodulation technique for therapy or as part of a combinatorial stimulation approach to enhance selectivity.

Work on DC block in the literature has focused either on using DC block in short bursts to negate the onset response of high frequency block, or to enable the prolonged use of DC block using special materials and electrodes. In terms of materials work has focused on improving the charge injection limit of stimulation electrodes, which represents the maximum amount of charge per stimulation cycle that can be safely injected with the material. While conventional stimulation and high frequency block do not in general require very high charge injection limits, DC block does require it as a result of using very long stimulation pulses, even with smaller currents.

### 5.4.4 HFAC Block Carryover

Recently in the literature, there has been an increasing amount of reports describing a period of time after block cutoff during which blocked nerve fibres remain suppressed. This period is called block carryover, and could be an important tool in extending the recovery response of A fibres such that stimulation becomes selective for a period of time after block cutoff.

Originally in 2011 Waataja et al. [24] reported that applying high-frequency block to the rat vagus nerve, which is composed primarily of smaller, unmyelinated axons, resulted in a reversible nerve block. Apart from recording C fiber block for the first time since previous studies primarily used measurements derived from muscular activity, a second and intriguing result is that nerve conduction remained suppressed after block cutoff. This was in contradiction with previous studies specifically stating that recovery of nerves from HFAC block was near-instantaneous [22]. However the same or similar effects were reported thereafter [25], [40], [50], [51] and work started on characterization of this relatively new phenomenon which had not been reported in any simulation study. Crucially, if block carryover for A fibres is longer than for C fibres, or if C fibres are not blocked at all and A fibres experience carryover, this would

theoretically result in a window of time during which conventional stimulation is selective for C fibres. Waataja et al. reported that C fibers in the rat vagus nerve recovered from block before A-delta fibers, a larger fiber type. If this can be reproduced in the rat sciatic nerve it would show that timed stimulation and block to enhance selectivity could be feasible.

The duration of block carryover varies substantially depending on the report, with Pelot and Grill [25] citing tens of seconds, and Bhadra et al. [38] citing hours in some cases. This seems to be dependent on the amount of HFAC block that was applied to the nerve before cutoff [24]. Furthermore nerve activity returns to baseline, indicating that this process is not the result of nerve damage, at least not damage affecting nerve conduction. Waataja's initial work used an experimental setup very similar to the one presented in chapter 4 to study the effects of HFAC block on the rat vagus nerve, and here similar experiments were carried out on the rat sciatic nerve, but using a cuff electrode instead of hook electrodes to deliver stimuli.

The fact that time to recovery of A fibres, while still relatively short in this trial, could potentially be changed by the amplitude or dose of block, warrants further investigation in the context of this work. Carryover itself points to a fundamental difference between the behaviour of mammalian nerve *in-silico* and *ex-vivo* that may be the key to using timed stimulation and block as a selective stimulation protocol, as detailed in sections 5.8.

## 5.5 Development of an ex-vivo experimental platform to improve reliability and consistency of results

### 5.5.1 Initial exposure to an *ex-vivo* experimental platform

The need for direct ENG recording as well as greater control over experimental variables pointed to an *in-vitro* or *ex-vivo* approach to experimentation with high frequency block and conventional stimulation. Fortunately, an opportunity to trial an *ex-vivo* experimental setup presented itself with the start of an internship at Galvani Bioelectronics that would last one year. As

Galvani Bioelectronics develops neuromodulation-based therapies they need a process to reduce the number of lengthy chronic *in-vivo* studies they have to undertake in animal models, by first evaluating electrodes and stimulation modalities acutely. As neuromodulation therapies influence how small unmyelinated fibres carry information between the brain and other organs within the body, EMG measurement modalities are not suitable to study the effects of stimulation targeting the autonomous nervous system. As part of electrode evaluation, it is necessary to measure the impact of an electrode on nerve health and function acutely and chronically. For this task ENG signals are more informative than EMG, and therefore an experimental setup allowing direct measurement of ENG signals as a result of stimulation is ideal.

As mentioned previously, the reason ENG signals can't be measured directly *in-vivo* is due to the noise produced by stimulation. This problem isn't specific to high-frequency stimulation, although it is made worse by it. In scenarios involving just conventional stimulation, the noise injected by stimulation, or stimulation artefact, can cause the recording amplifiers to saturate and be unable to capture low amplitude neural signals for several milliseconds after stimulation [52]. In many cases this is unacceptable as action potentials propagating within large nerve fibres such as α-motoneurons are expected to reach the recording electrodes in that timeframe, and are therefore lost. The primary challenge of reducing stimulation-induced noise can be solved by increasing the impedance between the stimulation and recording electrodes, and combining this increase with differential recording so as to eliminate common-mode noise. In this way, even large signals at the stimulation electrodes are attenuated by resistive division and effectively filtered, allowing small ENG signals to be captured with good signal to noise ratio (SNR). Another limitation of EMG recording is the lack of information on autonomous nervous system activity or sensory nerve fibre activity, for which only ENG recording is suitable.

### 5.5.2 Operating Principles

The most important aspect of the setup that allows measurement of ENG during stimulation, with manageable artefact levels, is to place the nerve in oil and carry out ENG measurements in that insulating medium. Stimulation currents then have only the nerve itself as a path to

the recording electrodes, substantially improving artefact rejection. Another positive outcome is that ambient electrical noise is also filtered out in the medium, improving the rejection of common noise sources such as line hum provided that the recording electrode leads are sufficiently shielded.

However to keep the tissue alive and maintain homeostasis, ion balance and oxygenation have to be kept constant externally. As the extracellular fluid in living tissue is aqueous, placing the nerve in a specifically formulated saline bath allows experiments to be carried out over several hours with consistent stimulation and recording performance. To replicate *in-vivo* studies as closely as possible, stimulation electrodes are implanted into the tissue in the saline compartment of the bath.

While the author originally learned about the modern *ex-vivo* platform during the internship at Galvani Bioelectronics, the idea is not new. Ironically enough an ancestor of this setup can be found in the same paper by Kuffler which originally inspired the use of timed blocking and stimulation [6] and which the author did not initially appreciate for its potential. This setup is shown in figure 5.2.

In Kuffler's setup the sciatic nerve and attached gastrocnemius muscle of a frog are placed in a single compartment bath with two phases: one aqueous, one oily. Stimulation and recording and carried out in the oily phase using hook electrodes. Stimulation is carried out in oil in this case as the current sourced by the hook electrodes would be dispersed in the aqueous phase, and therefore not participate in neural stimulation. In order to ensure all the current sourced by the stimulation electrode enters the nerve the stimulation is therefore carried out in the oily phase, although this is not representative of stimulation with clinically available electrodes. EMG is also recorded using a silver-silver chloride referenced micro-electrode and muscle force is recorded using a force transducer. The result is a powerful multi-modal recording setup to study the effects of stimulation on muscle activation.

The advantages of this kind of setup is the degree of control it affords on many experimental variables, and the elimination of other variables that can confound measurements. Placed in a saline bath outside the body, the tissue's environment is tightly controlled with specific

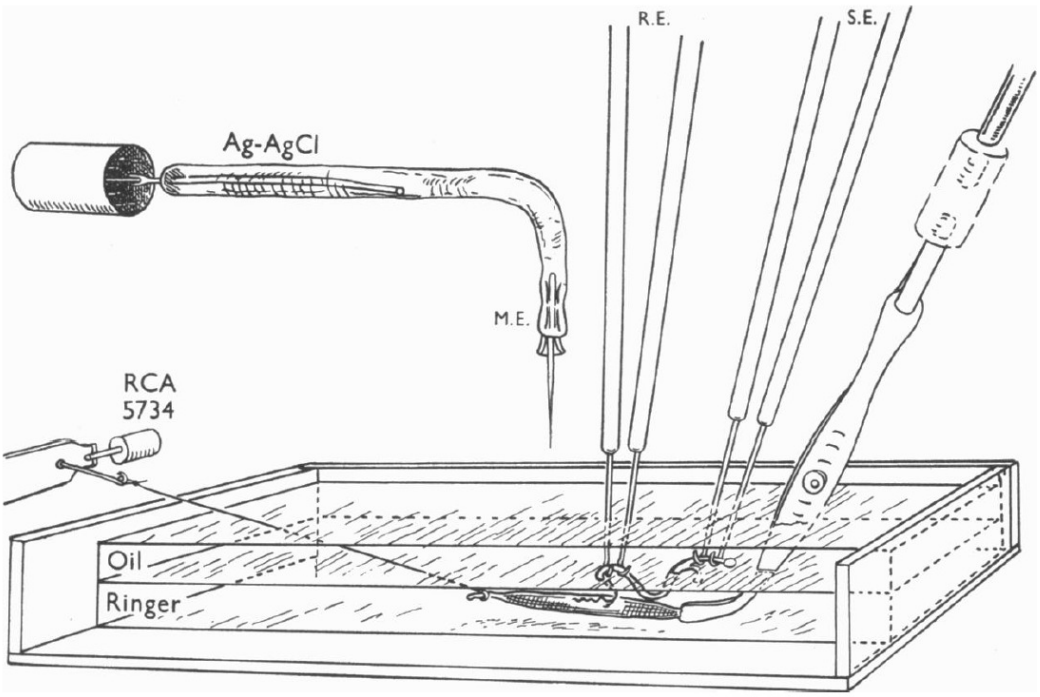


Figure 5.2: Drawing of the *ex-vivo* experimental setup used by Kuffler for studies with frog nerve in [6]. S.E. refers to the stimulation pair of hook electrodes. R.E. refers to the recording pair of hook electrodes, placed distally. M.E. refers to the microelectrode used to record muscle action potentials.

extracellular ion concentrations that replicate those found naturally, but that are also prevented from drifting over time, resulting in consistent, repeatable experiments. Sugar levels are set extracellularly and maintained with the assumption that the metabolic activity of the tissue does not cause the concentration of sugar within the saline solution to vary over time. There is no influence from hormones which might affect the tissue *in-vivo*. In contrast to *in-vitro* approaches, the structure of the tissue is preserved and clinically available electrodes can be used for recording and stimulation, which improves the translatability of results. The most important aspect is the possibility of recording low-noise ENG signals which gives us direct information about what is happening inside the nerve during high frequency block and stimulation. These strengths solve several of the problems associated with the previous *in-vivo* approach.

The model animal in Kuffler's setup is the frog, and therefore the aqueous phase must be suitable for homeostasis of frog nerve and muscle tissue. Ringer's solution (RS), as specified in the figure, is used for this purpose. RS was originally designed as a cardioplegic solution to keep a frog's heart beating while outside of the body by Sydney Ringer. It's role is to

stabilize extracellular ion concentrations as would be done by body processes *in-vivo* and to provide an osmotically compatible medium for tissue preparation - if a medium's osmolarity is too different from the tissue which is placed in it the tissue will die [53], [54]. It was found to preserve the viability of other tissues and became a base for most physiological saline buffers [55] and cardioplegic solutions for other species. Despite this, a number of changes are needed when moving from amphibian to mammalian tissue.

### 5.5.3 Control of ionic concentration, pH, oxygenation, and temperature: the modified Krebs-Henseleit buffering system

In Kuffler's setup the bath was most likely at room temperature, and this is suitable as frogs are cold-blooded. As mammals are homeotherms regulation of temperature above room temperature is required to better replicate actual conditions inside the body, and indeed some differences were observed in the response of rat nerve to stimulation as a function of temperature [56], [57]. Furthermore the metabolic and respiration rate of nerve tissue can be significantly affected by stimulation at high frequencies and therefore active infusion of oxygen into the saline is necessary to compensate for oxygen consumption by the tissue. It is surprising that Kuffler and Williams did not mention any kind of oxygenation method in the description of their setup, despite their stated requirement of "prolonged trials" in some cases to successfully carry out their experiment, and the presence of muscle in the preparation which no doubt needs oxygen to function.

Ringer's solution is not suitable for mammalian tissue, due to the different composition of the extracellular fluid in mammals. Fortunately a mammalian-optimized cardioplegic buffer exists - the Krebs-Henseleit buffer [58]. Comparative composition in terms of ion and glucose concentrations for Ringer's Solution (RS) and modified Krebs-Henseleit Buffer (mKHB) is given table 5.1 as reported in [55] and as used at Galvani Bioelectronics respectively. This buffer uses the carbonate-carbonic acid couple to buffer pH. There is a significant effect of pH on nerve excitability [59] and *in-vivo* pH is tightly controlled by the kidneys [60], therefore it is essential to accurately control the concentration of carbon dioxide [$CO_2$] for *ex-vivo* preparations using

this buffer [61]. For this reason a source of carbon dioxide is necessary to ensure the pH is adequately buffered, which leads to the use of carbogen, a mixture of 5% $CO_2$ and 95% $O_2$, to be used for both pH control of the buffer and oxygenation of the tissue contained within.

Table 5.1: Ion and sugar compositions of RS and mKHB in [mmol.$L^{-1}$]

| **Ion** | **RS** | **mKHB** |
|---|---|---|
| $Na^+$ | 135.76 | 138 |
| $Cl^-$ | 136.84 | 122.8 |
| $K^+$ | 1.34 | 6 |
| $Ca^{2+}$ | 1.25 | 2.5 |
| $PO_4^{2-}$ | 0 | 1.2 |
| $Mg^{2+}$ | 0 | 1.2 |
| $SO_4^{2-}$ | 0 | 1.2 |
| $CO_3^{2-}$ | 0 | 25 |
| Glucose | 0 | 5.55 |

As can be seen from the table RS contains only 4 of the 9 ions and no glucose; presumably the frog nerve preparations did not require this within the scope of their respective experiments *ex-vivo*. The additions of phosphate, sulfate and magnesium are to better reflect the composition of extracellular fluid in mammals, whereas carbonate is present just as in the living body to buffer pH. Glucose is included to enable mitochondria within cells to synthesize new ATP in order to compensate for its use during prolonged stimulation.

### 5.5.4 Adaptation of the setup for use at Imperial College

A number of adaptations had to be considered when importing the setup from the laboratory at Galvani to Imperial College. Briefly, at Galvani Bioelectronics piped carbogen gas was directly available from a wall tap, and temperature control of the buffer was carried out using a recirculating water bath connected to a jacketed container. The water jacket warmed the buffer inside the container which was then piped to and from a custom nerve bath using peristaltic pumps. This allowed the use of a small bath as the perfused bather was pre-oxygenated and warmed. The relevant equipment was not available in the laboratory at Imperial College, especially the gas source. Perhaps more importantly the laboratory at Imperial College did not have the space available to house all the required equipment even if it could have been

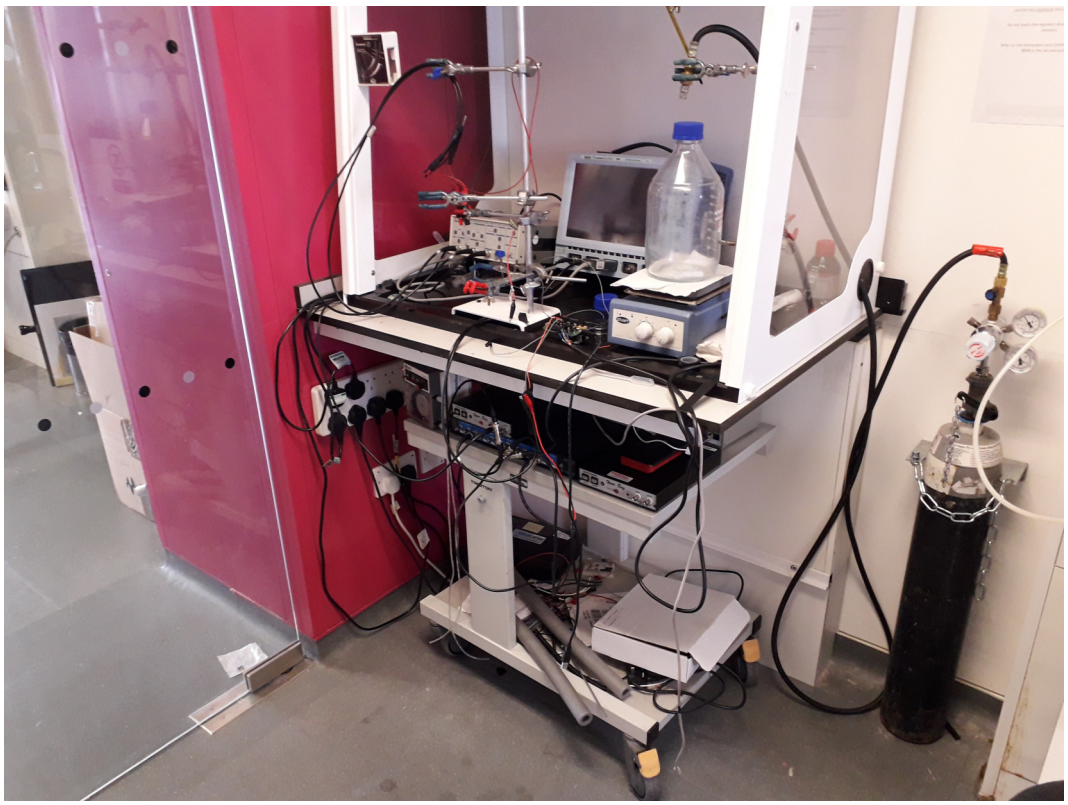

Figure 5.3: An annotated photograph of the *ex-vivo* experimental platform at Imperial College showing the equipment within and below a fume hood.

acquired, and this issue is common to all shared laboratory spaces: an experimental setup must be sufficiently compact so as not to place severe restrictions on where it can be implemented.

The setup at Imperial College was designed to fit within a floor area of $1 \times 0.75$ m$^2$ and is shown in an annotated photograph in figure 5.3. Carbogen gas is sourced from a canister located next to the setup and secured onto a wall-mounted bracket. An oxygen sensor can detect elevated oxygen concentrations in the air in the event of a carbogen leak. The buffer solution is kept in a 2 L bottle of the same volume as the jacketed container, and heated using a heating stirrer. Temperature is fixed such that the steady state temperature within the bottle is near 35 degrees Celsius as reported by thermometer; heating stirrers with integrated temperature controllers tend to behave erratically when heating large liquid volumes due to the thermal inertia of such systems.

A schematic representation of the setup is shown in figure 5.4, which shows how liquid flows during operation as well as the configuration of the nerve chamber, and how the nerve is connected to a recording amplifier and the multi-channel stimulation device described in chapter 3

during a typical experimental session. On the stimulator side each stimulator channel connects to one contact of a stimulation electrode, while a large platinum sheet is used as a common return in the bath with no influence on nerve activation. On the recording side differential measurements of nerve electrical activity are carried out using a pair of silver silver-chloride hook electrodes in contact with the nerve tissue in the oil. The ground reference for the differential measurement is an additional silver silver-chloride electrode in the aqueous phase. Stainless steel insect pins are used to secure the nerve to an inert silicone coating on the bottom of the bath, ensuring consistent contact of the nerve with the suspended recording electrodes. This however requires the oil and aqueous phases to be at the same level to allow the nerve to rest flat. For this purpose the nerve is threaded through a partition in the bath separating the oil and buffer compartments, and silicone grease is applied using a large bore syringe around the nerve on both sides of the partition to prevent leaks. The placement of multiple stimulation electrodes allows concurrent stimulation and block to be applied; generally the stimulation electrode is placed at the extremity of the nerve and the blocking electrode between the stimulating electrode and recording hooks. In this way the effect of block on evoked nerve action potentials can be accurately measured.

While buffer feeding to the chamber is carried out using a siphon[3], outflow to waste has to be regulated using a peristaltic pump to ensure consistent flow rate, which reduces recording noise arising out of large variations in the buffer level within the bath.

For recording, the setup uses an SRS-560 low-noise differential amplifier (Stanford Research Systems, USA) with gain set to 100 and a second order bandpass filter applied between 10 and 1OOO Hz. Further filtering may be needed in post-processing in order to facilitate the quantitative measurement of nerve response. The preamplifier signal is passed through a Humbug line-noise eliminator (Digitimer, UK) to remove most of the unavoidable 50 Hz pickup. This filter samples the noise and adaptively substracts the corresponding waveform to avoid distorting the resulting signal. The signal is then sent to an oscilloscope triggered by the stimulator and a Micro-1401 multichannel ADC (CED, UK) to capture the signal in real time over the course of the experiment. The stimulator used with the setup is the custom-made 4-channel

[3]Special thanks to Dr. G.E. Hunsberger for this elegant solution.

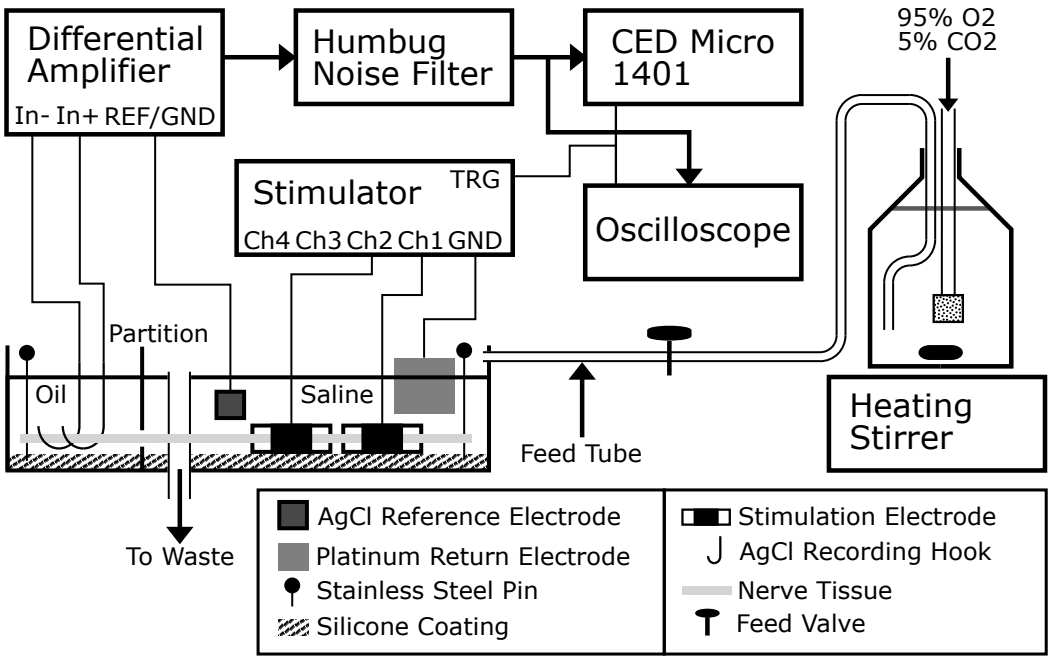


Figure 5.4: Drawing of the setup showing the piping to and from the nerve chamber, and configuration of recording and stimulation electrodes in the oily and aqueous phases respectively. This figure was previously published in [62].

block capable stimulator described in chapter 3.

## 5.6 Initial measurements and evaluation of the setup as an *ex-vivo* investigational platform

To validate the experimental platform for *ex-vivo* experiments using peripheral nerves, a number of trials measuring nerve function were carried out using the rat sciatic nerve model. In a more general sense these initial results also validate the setup for experiments using other small laboratory animal peripheral nerve models such as those of mouse, or other peripheral nerves of the rat.

All animal care and procedures were performed under appropriate licences issued by the UK Home office under the Animals (Scientific Procedures) Act (1986) and were approved by the Animal Welfare and Ethical Review Board of Imperial College London. In the following experiments, the following protocol was used for preparation of the rat sciatic nerve for recording and stimulation:

### 5.6.1 Tissue preparation protocol

Animals were anaesthetized using isoflurane. Once deep anaesthesia was obtained and verified by an absence of reflex to noxious toe pinch stimuli, animals were culled by cervical dislocation. Animals were placed dorsal side up. First the calcaneal tendon is cut to gain access to the space between the skin and leg muscles. Blunt dissection scissors are used to cut through the skin of the leg from the ankle upwards to the spine following the tibia and femur of the outstretched leg. The sciatic nerve was carefully exposed by cutting through the muscle planes, and the resulting cavity immediately moisturized using mKHB cooled on ice. The *gastrocnemius medialis* muscle is split to expose the complete tibial branch of the sciatic nerve. The nerve is then carefully removed from the leg, starting with the distal end of the tibial branch at the ankle, and upwards as close to the spine as timely dissection allows. This should yield a section of nerve approximately 5 cm long in about 5-10 minutes of dissection per leg, where speed is important for preservation of tissue integrity. All branches of the sciatic nerve except the tibial branch are cut and the nerve placed in cold mKHB. Under a dissection microscope the nerve is placed in a silicone-coated[4] petri dish and carefully cleaned of any residual fascia, blood vessels, muscle tissue and cut nerve branches are trimmed close to the trunk to prevent variation in contact quality with cuffs placed on the tibial branch. The nerve is then placed in the nerve bath with warmed oxygenated and pH controlled mKHB buffer in one compartment and mineral oil in the other to begin stimulation and recording. Nerve generally remain viable for experiments for up to 7-8 hours after dissection. Additional protocol details are given in chapter 7.

### 5.6.2 Baseline evaluation of nerve function: A and C fibre stimulation thresholds in the rat sciatic nerve

A strong validating test for the experimental platform is showing consistent results on benchmark nerve viability assays for stimulation. A typical assay is carried out by measuring the

[4]An example is sylgard but any biocompatible silicone is appropriate here

stimulation thresholds of nerves in the bath over time and over several experiments, over a range of stimulation pulse widths. These thresholds are specific to the nerve and the electrode used for the test. In this way if nerves are prepared in a consistent manner and the same electrode used and placed at the same general location on the nerve for each experiment in a series, consistent results can be expected for stimulation thresholds. The rat sciatic nerve is composed of several different types of fibres with different action potential propagation speeds. The two groups with the most difference in action potential propagation speed are the myelinated α-motoneurons and the unmyelinated C-type nociceptor nerve fibres, with conduction velocities of approximately 50-60 m.s$^{-}$1 [63], [64]. and 0.5-2 m.s$^{-}$1 respectively [65][5]. ENG signals from rat sciatic nerve therefore display two distinctive peaks when both A and C fibres are activated, as shown in figure 5.5. The data shown in figure 5.5 was captured using the *ex-vivo* experimental setup during a typical experiment at Imperial College. Monopolar biphasic stimulation was applied to the rat sciatic nerve using a commercially available bipolar cuff electrode (Cortec) of 800 µm inner diameter. Stimulation pulses were cathodic first biphasic symmetric with 20 µs of interphase and applied to the nerve using the cuff contact closest to the recording hooks in the bath. The other cuff contact was left unconnected and current return was done using a large platinum sheet away from the nerve in the bath. Stimulation amplitudes used were 1000 and 3000 µA. Only the 3000 µA amplitude pulse was able to activate the C fibre response.

The conduction speed for the two ENG peaks in the recording can be calculated based on the time between the stimulation pulse and the time of the start of the peak and estimations of the distance[6] between the stimulation electrode and recording electrodes, which was typically 3-4 cm. The time between the stimulation and start of the neural response is approximately 1 and 50 ms respectively for the A and C fibres, corresponding to speeds between 30-40 m.s$^{-}$1 and 0.6-0.8 m.s$^{-}$1 respectively. This is within the expected range for A and C fibre conduction speeds.

A second assay is consistency in terms of stimulation thresholds for A and C fibres across

[5]This reference measures C fibre conduction speeds in man however similarity is expected for C nociceptor conduction speeds in rat

[6]Accurate measurement of the distance was difficult using this setup as there was no means to place a measurement tool next to the nerve to determine stimulation to recording distance easily. Estimates are based on bath dimensions and typical positions for the recording and stimulation electrodes during experiments.

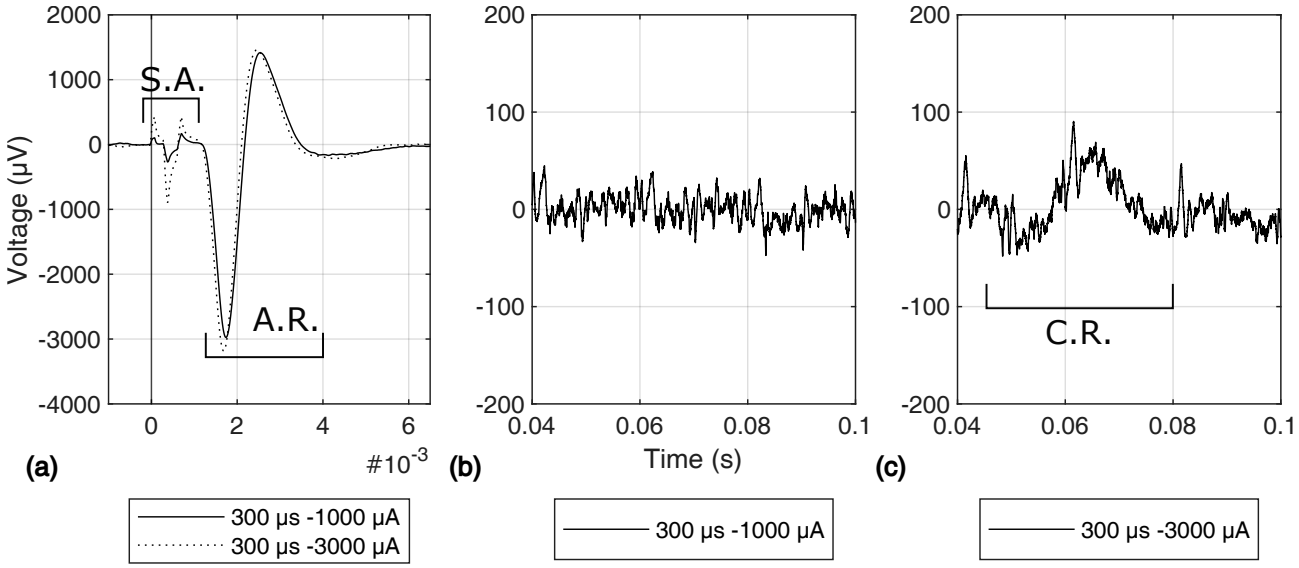


Figure 5.5: Neural waveforms obtained from stimulation using two sets of parameters detailed in the legend. (a) Portion of the waveform specific to the A fibre response. The vertical line shows when the stimulation pulse started. S.A. refers to the stimulation artefact. A.R. refers to the A fibre response in both waveforms. (b) Portion of waveform where the C fibre response is expected; in this case the stimulation was not strong enough to activate C fibres and the recording is baseline noise. (c) Portion of waveform where the C fibre response is expected. C.R. refers to the C fibre response. This figure was adapted from [62].

multiple experiments. The degree of control over experimental variables can be verified by ensuring these measures are in good agreement with each other. Stimulation thresholds for A and C fibres were measured three times using different sciatic nerves with the 800 µm inner diameter Cortec cuff electrode and presented in figure 5.6, for a range of stimulation pulse widths. Stimulation thresholds were determined without post-processing by the user using an oscilloscope to capture the ENG during the stimulation trial. The threshold was set slightly above the noise floor as observed during a specific experiment. As the stimulation amplitude resolution of the stimulator is 5 µA and A fibres have thresholds on the order of 10 µA for longer pulse widths it was not possible to precisely determine these thresholds, leading to apparent discontinuities in A fibre thresholds. A fibre thresholds data from experiment 3 is higher than expected due to the preparation having a slightly lower pH than normal.

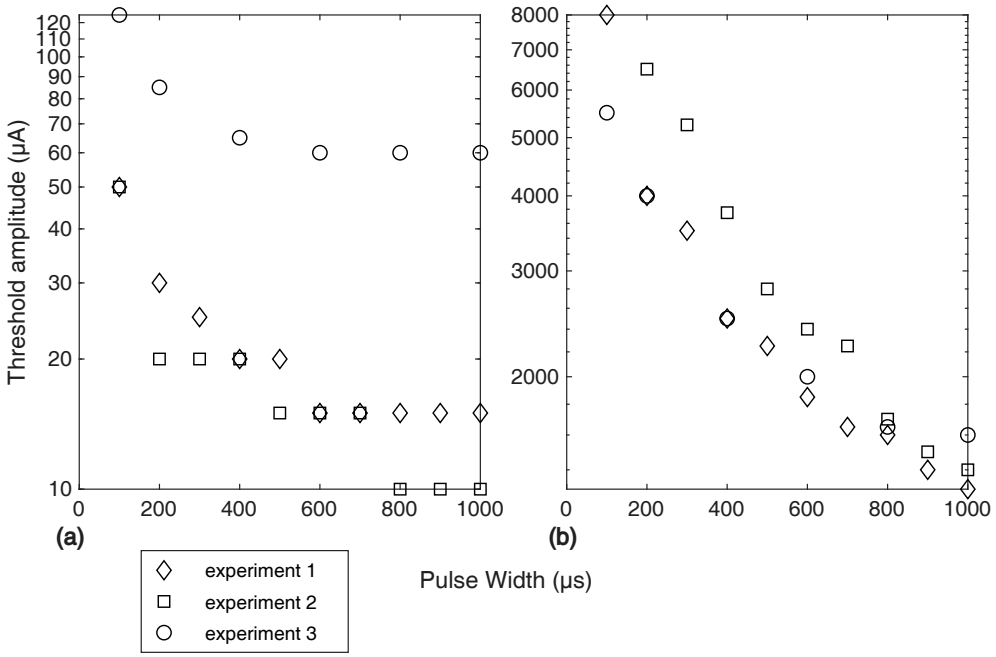


Figure 5.6: (a): Stimulation thresholds for A fibre of the rat sciatic nerve obtained using a Cortec 800 um bipolar cuff electrode, for a range of pulse widths. (b):Stimulation thresholds for C fibres of the rat sciatic nerve obtained using a Cortec 800 um bipolar cuff electrode, for a range of pulse widths.

## 5.7 Initial investigation of high frequency block *ex-vivo*

To characterize block *ex-vivo* a number of experiments were carried out, first to characterize block efficacy versus blocking signal amplitude and frequency, and then characterizing the recovery speed of nerve fibers from block to determine the feasibility of using timed block and stimulation for elective stimulation in the *ex-vivo* rat sciatic nerve model. In all experiments described below stimulation and block were delivered using monopolar electrode configurations due to how the multi-channel stimulator described in chapter 3 operates.

Trials generally followed a set structure:

1. A set of three to five stimulation pulses was delivered to the nerve at the rate of 1 Hz to record baseline A and C fibre nerve response at the start of a trial

2. Block was applied to the nerve for 15 seconds during which stimulation continued at a rate of 1 Hz to record nerve response during block.

3. At the end of the 15 second period block was cut off and stimulation continued for at

least 7 seconds at a rate of 1 Hz to measure nerve recovery from block

4. Whether or not the nerve had recovered to within 90% of baseline activity at the end of the trial, nerve activity was periodically measured and enough time was allowed to elapse for the nerve to return to at least 90% of baseline activity before the next block trial.

Nerve signals were recorded using silver silver-chloride hook electrodes with an interelectrode distance of approximately 2 mm. These were connected to the inputs of a differential amplifier (SRS-560, Stanford Research Systems, USA), with a gain of 100 and an input second order bandpass filter with a 10-1000 Hz pass band. The signal was further filtered by passing it through a Humbug Noise Eliminator (Digitimer, UK) to remove residual mains hum before digitisation with a Micro-1401 (CED, UK). The recorded signal was duplicated for separate filtering of A and C fiber signals. A fiber signals were filtered using a moving average filter with a window size of 0.14 ms and a DC Removal filter, calculated as the difference between the signal and its corresponding moving average with a window size of 20 ms. C fiber signals were filtered using the same filters with window sizes of 1 ms and 20 ms respectively.

Nerve response was evaluated by rectifying and integrating signals at specific time windows referenced by stimulation event triggers sent to the digitisation system by the stimulator. For A fiber signals the window was 1.23 ms to 7 ms after the stimulation trigger. For C fiber signals the window was 35 ms to 85 ms after the stimulation trigger. These settings were retained for all experiments with stimulation and block.

### 5.7.1 Experimental setup validation trials

As a further test to ensure the validity of the setup to study combined block and stimulation, a stimulation and block trial was conducted. Typical trials evaluating block first stimulate the nerve without applying block to measure the baseline response, then apply block and continue stimulating to measure how the ENG signal changes as the nerve becomes blocked. The blocking signal is turned off after a set number of seconds, and the stimulation continues to measure the recovery of the nerve from the blocked state.

In the trial shown in figure 5.7, cathodic first biphasic symmetric stimulation of 2500 µA amplitude is applied to the nerve to excite both A and C fibres as seen in figure 5.7 (b and e). In the blocking phase a square wave signal of 6 mA amplitude and with a frequency of 10 kHz is applied to the nerve and maintained for 15 seconds. During this time the peak to peak amplitude of the A fibre signal visibly decreases over time, and a zoomed capture of the signal at the last stimulation event before block cutoff reveals that the residual A fibre signal is actually smaller than the stimulation artefact. The C fibre signal is only partially blocked using these parameters. Results from these initial experiments suggest that contrary to the *in-vivo* experiments described in chapter 4, 10 kHz HFAC block here produces reliable block at 6 mA amplitude while not leading to nerve damage. Higher frequencies of block will not be as effective as previously reported in the literature, while lower frequencies were unreliable for block or caused damage. As a result 10 kHz was the preferred frequency of block to use for *ex-vivo* experiments going forward, especially considering the validation measurements detailed in chapter 3 for the stimulator which confirm that using 10 kHz block will be safe for the nerve at 6 mA amplitude.

### 5.7.2 Effect of blocking signal amplitude on block efficacy

To determine what block amplitudes were reliable for blocking A fibres in the rat sciatic nerve, 3 nerves from different rats were tested using a conductive elastomer cuff electrode for block and a conventional platinum cuff electrode (800 µm inner diameter, Cortec) for stimulation. The conductive elastomer cuff is described in [66] and pictured in the appendix, chapter 7. Block was delivered at 10 kHz for at least 10 seconds per trial, and nerve response for both A and C fibres were compared to baseline. For each trial baseline nerve response was obtained by averaging the response of the first 3 stimulation pulses during which no block was applied. Stimulation intensity was adjusted so that both A and C fibres were maximally recruited for each nerve. Between each trial the nerve was allowed to recover to at least 90% of baseline activity. Block amplitudes were swept from 1 to 6 mA with a step of 1 mA and the relative response of A and C fibers before, during and after the block was recorded. The response of A

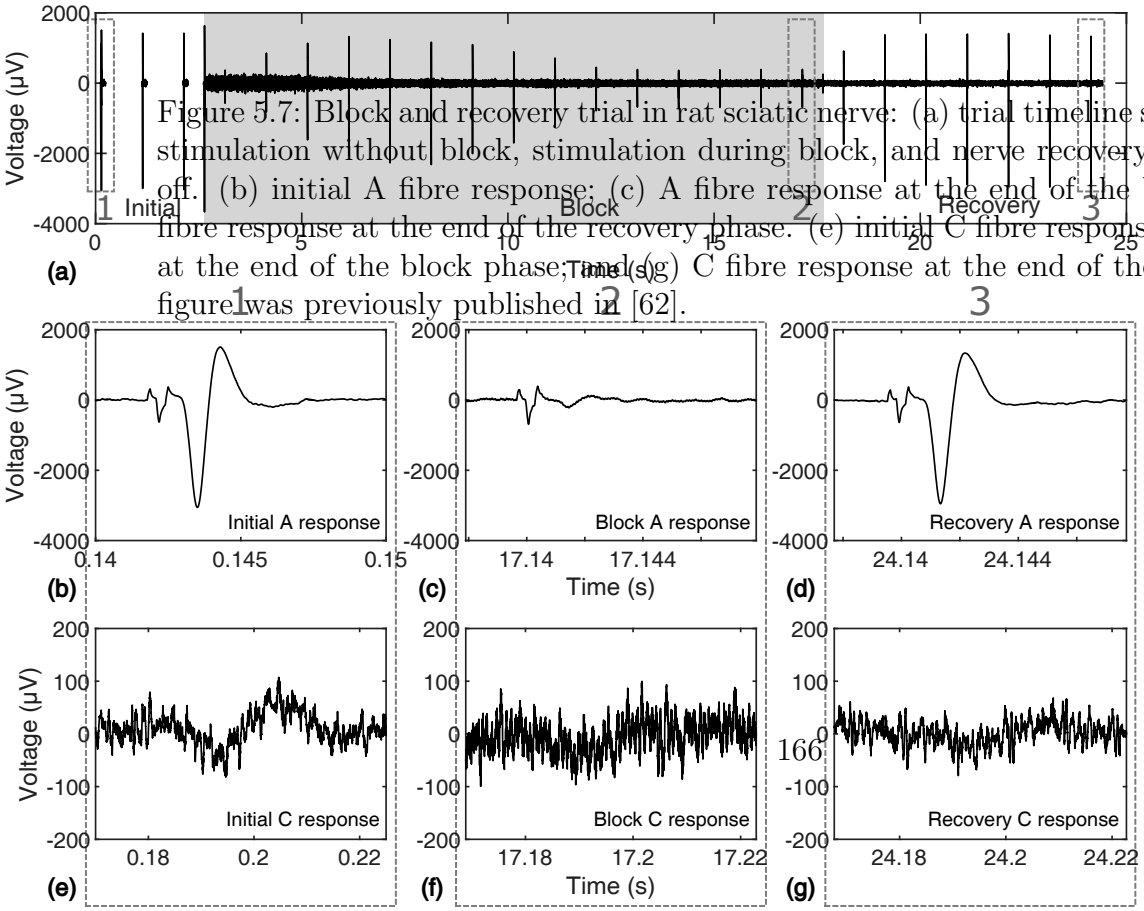


Figure 5.7: Block and recovery trial in rat sciatic nerve: (a) trial timeline split into three pl stimulation without block, stimulation during block, and nerve recovery after block is t off. (b) initial A fibre response; (c) A fibre response at the end of the blocking phase; fibre response at the end of the recovery phase. (e) initial C fibre response; (f) C fibre res at the end of the block phase; and (g) C fibre response at the end of the recovery phase figure was previously published in [62].

and C fibres relative to their respective baselines is plotted on figure 5.8.

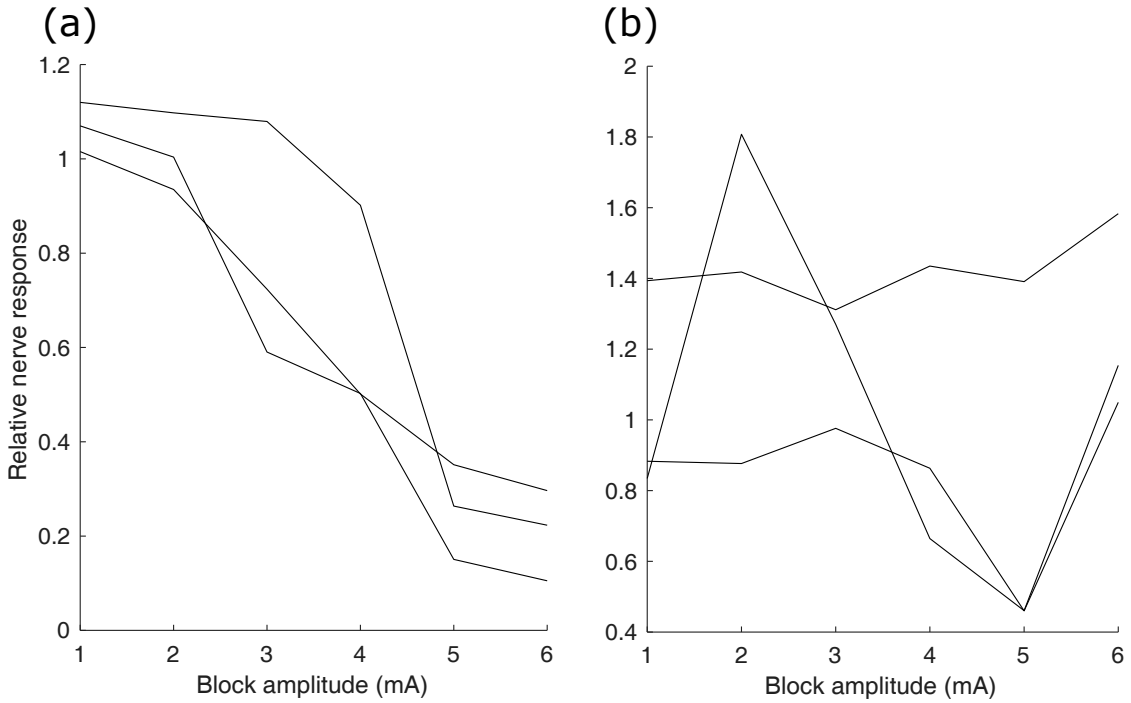


Figure 5.8: A and C fiber response during 10 kHz block relative to baseline for a range of block amplitudes.(a): A fibre response during block. (b): C fibre response during block.

As expected from previous literature [38], as block amplitude is increased the relative response of A fibres decreases until reaching a low point corresponding to minimum activity, where the compound action potential cannot be visually discerned above the noise. The reason the minimum relative activity is not zero is due to noise which contributes slightly to the integral used to measure the nerve response to stimulation. For all 3 nerves tested with the same block and stimulation electrodes, substantial block was achieved for 5 mA but 6 mA amplitude block was the most effective. Higher amplitudes were not trialled as gains in block efficacy were minor, it did not significantly change the relative C fibre activity, and there was less risk of damaging the nerve by blocking with moderate amplitudes. C fibre activity appears to change depending on block amplitude but this is not consistent and likely due to noise which makes a greater contribution to the integral despite more aggressive filtering. Overall C fibres were not blocked and their relative activity did not change during or after block compared to baseline.

In order to determine whether it was feasible to block C fibers, trials were carried out with a blocking signal frequency of 5 kHz on a single nerve, using a conductive elastomer electrode to deliver block and a standard 800 µm inner diameter platinum stimulation electrode (Cortec)

to stimulate with monophasic pulses. Pulse width was 300 µs and pulse amplitude was 5 mA. Relative nerve response for both A and C fibers over the course of the trials is plotted on figure 5.9.

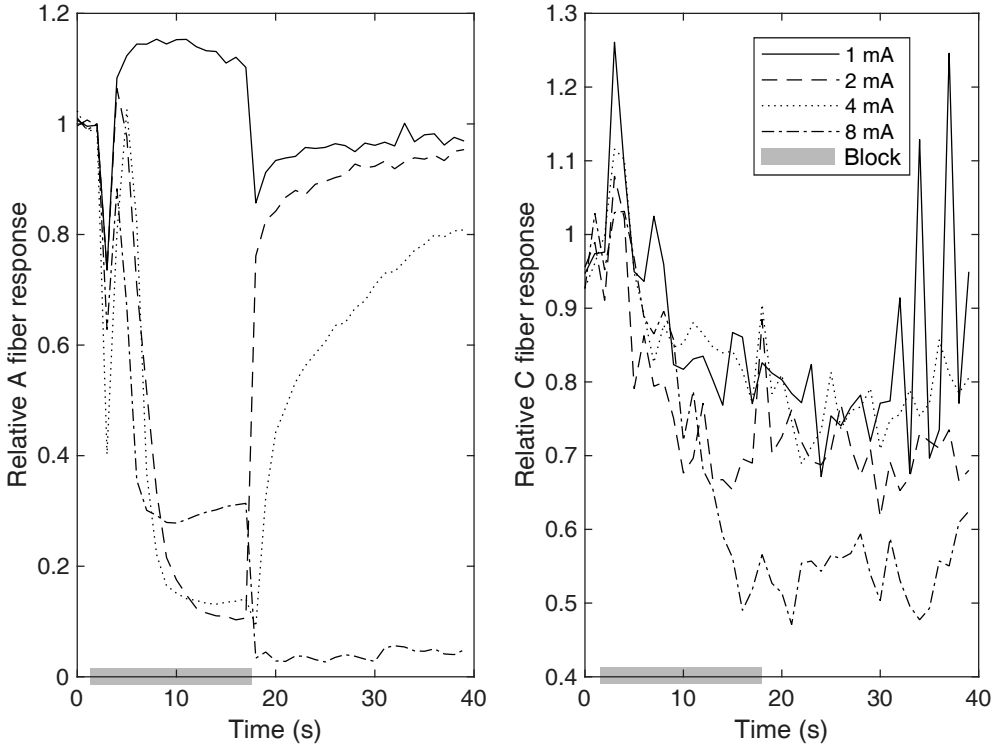


Figure 5.9: (a) Plot of relative A fiber activity before, during and after delivery of block at 5kHz for several block amplitudes. (b) Plot of relative C fiber activity before, during and after delivery of block at 5kHz for several amplitudes. The gray block on the time axis indicates the time at which block was active.

In all cases A fiber activity recovered to more than 90% of baseline after sufficient time had elapsed. For C fibers results indicate that block threshold may have been reached at 8 mA block amplitude when the blocking signal frequency is 5 kHz, however even at this high amplitude block was partial as the reduction in C fiber activity was only approximately 50%. Nerve activity for both fiber types recovered to 90% of baseline activity after sufficient time had elapsed. 5khz was the only block frequency for which a substantial reversible suppression of C fiber activity was achieved. As block of C fibres was not achieved reliably with any block parameter trialled, block characterisation continued using 10 kHz primarily as application of 5 kHz block made filtering of noise more difficult for no apparent benefit in terms of block performance.

Results for A fibers are quite interesting because as block amplitude is increased, the time

required for A fibres to recovery from block also increases. This is likely due to carryover as in every case A fibre excitability returned to baseline levels and there was no evidence of damage.

## 5.8 Characterization of HFAC block carryover as a tool to enable selective stimulation

A set of experiments was designed to investigate carryover for selective stimulation. The primary scientific question was whether carryover could be induced in A fibres but not C fibres, or whether C fibres would recover from carryover more quickly as reported by Waataja [24] but this time in the rat sciatic nerve.

From previous results it was known that 10 kHz 6mA block was effective for blocking A fibres but did not block C fibres. In total 5 experiments were carried out on 5 different nerves to characterise carryover in the rat sciatic nerve. Block was delivered using the conductive elastomer electrode previously described, and stimulation was delivered using a conventional cuff electrode with platinum contacts.

For each trial, stimulation was first carried out 5 times to establish a baseline for nerve excitability. Stimulation pulse width and amplitude were adjusted to recruit both A and C fibres. Block was delivered for 30 or 60 seconds depending on the trial to determine whether carryover duration depended on HFAC block dose independently of block signal amplitude and frequency. Block and carryover trials were repeated 3 or 4 times in order to determine whether carryover duration changed depending on accumulated dose of HFAC block. Subsequent sets of trials were delivered using other contacts of the three-contact conductive elastomer electrode to determine whether carryover duration was affected by contact location. Inter-contact distance was 2 mm. Recovery is achieved when A fibre activity recovers to at least 90% of baseline. Time to recovery is the time between block cutoff and reaching this threshold. Not all block trials led to measurable carryover due to limitations in how often the nerve was stimulated during the trials, which was once every 2 seconds. In total 26 out of 48 trials resulted in measurable

carryover i.e. the time between the end of block delivery and measuring relative A fibre activity above 90% of baseline was greater than 2 seconds.

### 5.8.1 Control measures: ensuring nerve damage did not occur during trials

Activity from A and C fibres was measured during block and at the end of the trial (after recovery) to ensure that the nerve had recovered to within 90% of baseline activity. Trials for which this did not occur were not considered in the analyses below and led to termination of the experiment. As the same block settings were used throughout each experiment, it is unlikely application of block itself was the underlying reason for non-recovery of nerve excitability, and the most likely reason is due to progressive loss of function of the nerve outside of the body, an inherent limitation of the *ex-vivo* preparation. Boxplots comparing A and C fibre activity relative to baseline during block and after recovery are plotted in figure 5.10. The results show a clear effect of block on A fibre activity while there is no consistent effect on C fibre activity. Measurements showing relative A or C fibre activity above 1 are due to noise, especially for C fibres as the longer integral is more susceptible to spurious noise spikes within the recordings. Statistical analysis of A and C fibre activity at the end of each trial, after sufficient time is allowed to elapse for fibres to recover from block, but during which conventional stimulation continues, shows no significant reduction, indicating delivery of block was safe for the nerve. Reported p-values reference left-tailed rank sign tests for each boxplot data set, relative to 1, i.e. testing whether the median of the dataset represented by each boxplot is lower than 1.

### 5.8.2 Characterization of A fiber block carryover: effect of HFAC block dosage

Trials where block was delivered for 30 and 60 seconds were separated into two sets and are compared statistically in figure 5.11 using two-sided right-tailed Rank-Sign tests. p-values are reported at the top of the figure, testing whether the median recovery time for 60s block

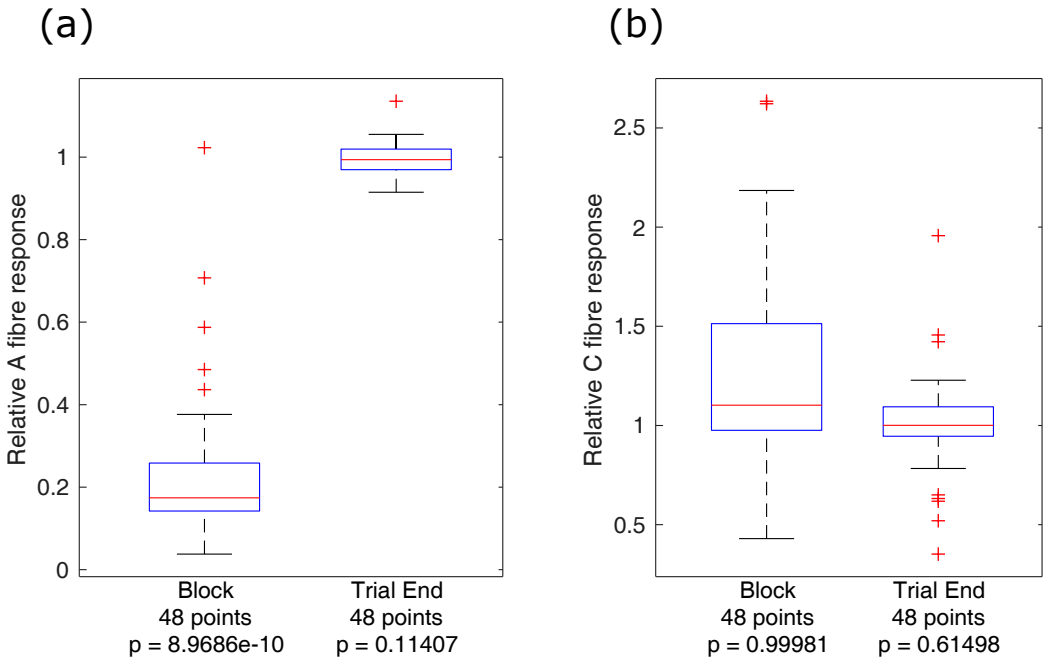


Figure 5.10: Boxplots comparing A and C fibre activity relative to their respective baselines during block and after recovery form block (trial end). Outliers from each set are identified using red crosses. The horizontal red line for each boxplot represents the median of the set, not including outliers. The number of data points in each set is specified below each boxplot. The p-value for a left-tailed sign-rank test relative to 1 is reported below each boxplot.(a): Boxplots representing A fibre activity.(b): Boxplots representing C fibre activity.

delivery is higher than that for 30s block delivery. The result indicates a statistically significant difference in duration when aggregating data across all trials in all experiments, suggesting that block carryover duration is dependent on the 'dose' of HFAC block delivered, and that duration of delivery is a variable in this dose. Importantly in the context of determining in which conditions block delivery led to carryover, in experiments where delivery of block for 30 seconds did not lead to measurable carryover, with recovery times less than or equal to 2 seconds, delivery of block for 60 seconds in the same experiment led to measurable carryover where recovery time was above this value, with one exception where recovery from 60s of block delivery was 'instantaneous' with recovery to above 90% baseline on the stimulation event immediately posterior to block cutoff.

### 5.8.3 Effect of accumulated dose on carryover duration

While the previous result suggests that block duration increases carryover duration, a further

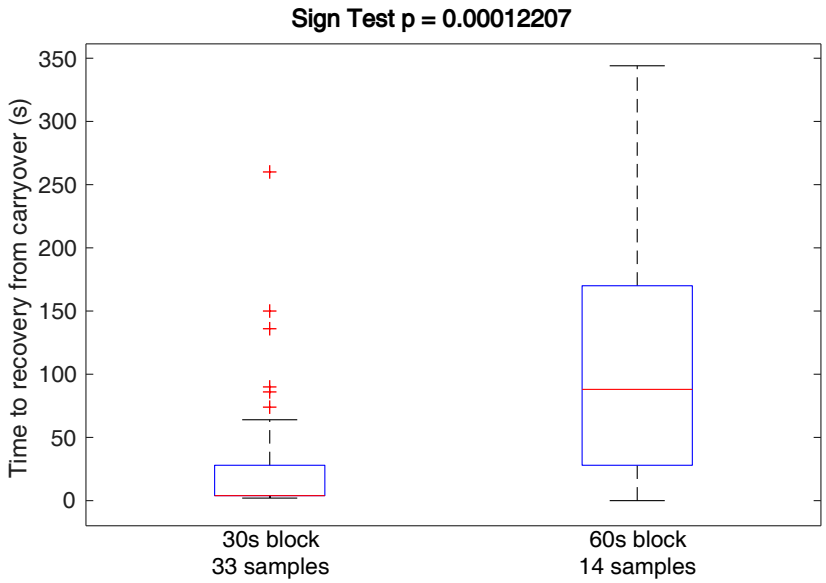


Figure 5.11: Boxplots comparing time to recovery from block for trials applying block for 30 seconds and 60 seconds. Outliers from each set are identified using red crosses. The horizontal red line for each boxplot represents the median of the set, not including outliers. The number of data points in each set is specified below each boxplot. The p-value for a 2-sided rank-sign test is reported at the top of the figure, testing whether the median of the right boxplot set is above the median of the left boxplot set.

analysis is then to determine whether this effect leads to differences in carryover duration when considering successive trials. For trials where carryover was measurable as described previously, within the same set, and therefore considering the same block and stimulation protocol on the same electrode contact, carryover duration was substracted from the n+1 trial from that measured in trial n, yielding a difference measure for any increase or decrease of carryover duration when repeating trials. Between each trial, A and C fibres were verified to have recovered to at least 90% of baseline activity. The resulting boxplot is shown figure 5.12.

The results show that for trials where block carryover is measurable, additional application of block following the same protocol increases the duration of carryover in every case. The increase in seconds spans values from 6 to 110 seconds. The reported p-value corresponds to that of a right-tailed rank-sign test relative to 0, testing whether the true median is above 0, rejecting the null hypothesis.

## 5.9 Discussion

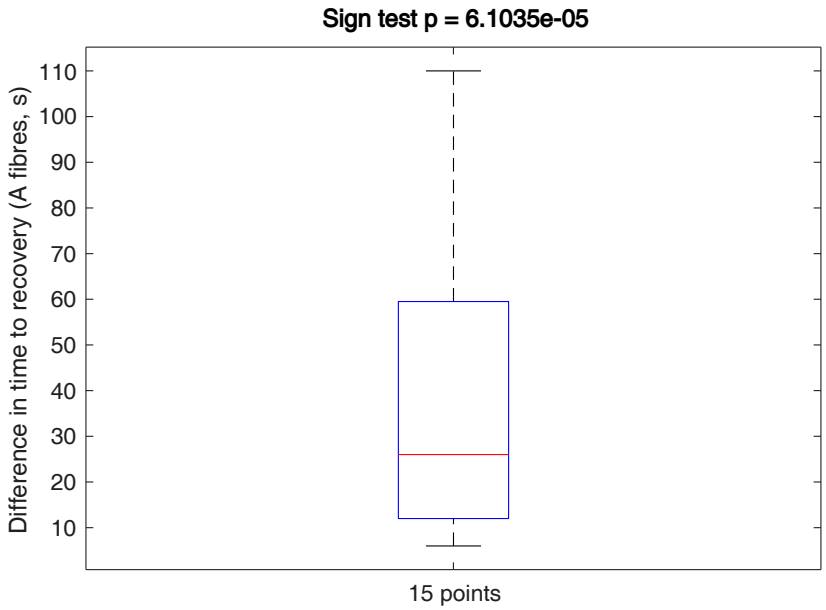


Figure 5.12: Boxplot of carryover block duration difference between subsequent block trials in the same set across all experiments. Outliers from the set are identified using red crosses. The horizontal red line for the boxplot represents the median of the set, not including outliers. The number of data points in the set is specified below the boxplot. The p-value for a right-tailed sign-rank test relative to 0 is reported at the top of the figure, testing whether the median of the boxplot set is above 0.

At the onset of experiments, the prevailing hypothesis was that conduction speed differences would allow selective stimulation of slowly-conducting fibers to be carried out by precisely timing high frequency block cutoff. After many trials searching for a parameter set including amplitude and frequency of the blocking signal that would block both A and C fibers, it became clear selective stimulation in this manner was not feasible: C fibres could not be blocked consistently, and often further increasing block amplitude beyond 6 mA for a 10 kHz frequency could cause permanent damage. **Leveraging the small window in time between the arrival of the 'fast' and 'slow' action potentials is not possible when nerve activity remains blocked several minutes after block cutoff** as was shown in results, especially considering the requirement for very high blocking signal amplitudes delivered at low frequencies to increase the charge delivered per cycle.

It was only by observing carryover for A fibres, confirming results from [24], that a means to use HFAC block to selectively stimulate A fibres without C fibres during a therapeutically useful time window was found. However there is an additional complication compared to the initial idea: block carryover is not independent from block parameters as conduction speed would be;

in order for stimulation to be selective the duration of block carryover for both A and C fibers has to be predicted. There is currently insufficient data to model nerve recovery from carryover in order to make these predictions, although it was shown that the duration is linked to in-trial and accumulated charge as well as block signal parameters such as amplitude.

Results also point to a possible limitation of the gold-standard measure to evaluate nerve excitability. Typically nerve excitability is measured by using peak to peak or integral measures such as the one used in experiments for this work and corresponds to a measure of nerve health. However results obtained during experiments show that despite nerve activity having fully recovered to baseline, a repetition of the stimulation protocol used in a previous trial yields different results, therefore there has to be some mechanism at work that is not adequately measured by this technique, that affects the time needed for nerve fibres to recover from block.

In several experiments it was observed that at times blocking signal parameters which would reduce A fiber activity to below the noise threshold for supramaximal stimulation parameters, would no longer do so if stimulation amplitude or pulse width was increased beyond the initial values, despite there being no measurable change in A fiber activity. This is in contradiction of results obtained in [22], where it is specifically asserted that once the block threshold was reached for supramaximal stimuli, any evoked action potentials would not be allowed to conduct. A similar result seems to have been reported in the work of Peh et al. [67], where block efficacy depended not simply on the block amplitude itself but on the ratio between block amplitude and stimulation amplitude. These observations were spurious and inconsistent between experiments, but occurred consistently within the same experiment, and as the stimulator was the same in every case this suggests it may be related to the interface between the nerve and stimulation electrode rather than the stimulator itself.

In terms of noise, despite the excellent filtering afforded by the oil partition of the setup and the analog filtering and differential recording setup, additional digital filtering of the signal was necessary to improve the quality of measurements such that the block feed-through did not significantly contribute to relative nerve activity. The author is confident the data is representative of actual signal values and not noise, however additional refinements could further

improve the quality of quantitative analysis, especially if additional data is collected.

In terms of protocol, at the time the experiments were carried out several features that were initially planned for the stimulator had not yet been implemented, such as real-time electrode polarization measurements, automatic calibration and drift cancellation. Additional projects are developing neural recording hardware that would directly integrate with the stimulator thanks to its modular nature[7]. The stimulator was carefully calibrated using Keithley instrumentation and drift was measured and attributed primarily to the stimulator warming up. Therefore during experiments the stimulator was turned on and given sufficient time to stabilize before starting trials. From trial to trial within the same experimental session very little drift has been observed in terms of block thresholds, although absolute nerve activity would decline slowly over time as the tissue inevitably lost viability out of the body after some 4 to 5 hours[8]. Additional time for development of these features would remove these limitations.

## 5.10 Conclusion

In this chapter, after describing the background for selective stimulation and how it has been achieved in the literature, a detailed analysis of high-frequency block was given from the perspective of three experimental paradigms. In each paradigm experiments enabled the characterization of block in terms of frequency and amplitude thresholds, moving from an initial amphibian model to a mammalian model. A number of findings qualitatively confirmed results published in the literature, although there are differences when considering quantitative data. These differences can potentially be traced to differences in stimulation protocol and in the electrodes used for stimulation as HFAC block experiments on rat sciatic nerve using standard CorTec, Microprobes or conductive elastomer electrodes have not previously been reported. **Results obtained using the *ex-vivo* approach validated the experimental setup for investigation of HFAC block in the rat sciatic nerve model as the same phenomena**

[7]This is a project led by Jieni Wang.

[8]It is still possible to record nerve activity some 8 hours after extraction from the body, though baseline nerve activity has to be sampled regularly.

**were observed as *in-vivo***, while affording greater control over variables compared to the latter approach. One essential conclusion is that **existing *in-silico* models of high-frequency block are only accurate for short-term applications of the technique**. They do not capture the secondary phase of the onset response or block carryover, which have been reliably observed in experiments and have a direct impact on how to apply block to enhance selectivity. There are also substantial quantitative differences in block thresholds in terms of frequency and amplitude between computational modelling and live tissue experiments that may be explained by corresponding differences between amphibian and mammalian nerves.

To work around the limitations of *in-vivo* experimentation as described in chapter 4, a dedicated *ex-vivo* experimentation platform was developed to study HFAC block at Imperial College and was validated for HFAC block experiments. Key results such as the relationship between block amplitude and its efficacy were repeated, as well as the observation of block carryover *ex-vivo*. This platform was used to show the relationship between block dosage in terms of duration of delivery within a single trial, and also accumulative effects of block leading to longer carryover times with repeated block delivery.

Despite their drawbacks in relation to the data that can be obtained using acute *ex-vivo* experimental setups, they are a very valuable research tool when considering the time required for any acute *in-vivo* work, let alone the time needed for results from chronic studies to be analysed. In this way **acute experiments carried out in idealized conditions can be a useful predictor of relative performance**, and pave the way for more focused and thorough investigation. Understanding which approach amongst those detailed at the start of this chapter is suitable at a given time in an investigation and for a specific scientific question is undeniably a key skill for researchers.

Initial exposure to multiple experimental paradigms was essential for developing an effective approach based on the advantages and weaknesses of each. While computer simulations give useful first order insight, further experiments with living tissue demonstrated they do not capture all relevant processes in the case of high-frequency block. It is likely some underlying mechanisms aren't represented and tentative explanations for which will be described in chap-

ter 5. *In-vivo* experiments not only indicated that more realistic experimental models than those available *in-silico* were required for investigation of block, but also many of the pitfalls of experimentation using living systems. Gaining appreciation for these challenges and realizing the necessity for greater control of many environmental variables is what drove the development of an effective *ex-vivo platform* for experiments that address the limitations of both *in-silico* and *in-vivo* paradigms.

**Furthermore this work has had significant impact by making a powerful experimental setup available for multiple research groups and students of Imperial College.** At the time of writing this thesis the setup is being used by a group in the department of Bioengineering for the evaluation of novel cuff electrode materials described in [66], other researchers within the Centre for Bioinspired Technology for evaluating ion-sensitive electrodes [68], a research group in Italy investigating selective recording techniques, and several Imperial College students developing a custom neural recording device, an improved single-container nerve bath, and modular fixtures for suspending electrodes over the bath, instead of using bulkier retort rods, boss-heads and grippers.

The setup is not only viable for the rat sciatic nerve, but also for other peripheral nerves of the rat, mouse or frog which could pave the way for useful comparative studies or nerve-specific experiments, such as with the vagus nerve, that can guide the development of new stimulation-based therapies.

Referring to the results obtained for block carryover specifically, the mechanisms underlying this process remain unknown at the time of this writing, and there is no clear relationship between block and carryover that would lead to a straightforward model capable of predicting block carryover duration. To make a selective stimulation technique utilizing carryover reliable, it is essential to be able to accurately predict how long carryover will last for each fiber group in the stimulated nerve which motivates future work. Potential applications of this technique include reducing painful A-delta fiber activation during vagus nerve stimulation which leads to unwanted contractions of the larynx muscles, for example. In the case of vagus nerve stimulation, the stimulation target is the C fibers in the nerve that regulate the activity of

internal organs, and therefore conventional stimulation will always lead to off-target effects. While carryover block was first reported nearly 10 years ago, very little is known about why it occurs, whether it can be accurately modelled and predicted, and even whether it is completely reversible. With the potential impact of better stimulation selectivity on existing and future stimulation-based therapies, it is exciting to consider the possibilities of future research on this topic.

# References


[1] C. Shendkar, P. K. Lenka, A. Biswas, R. Kumar, and M. Mahadevappa, "Design and development of a low-cost biphasic charge-balanced functional electric stimulator and its clinical validation," *Healthcare Technology Letters*, vol. 2, no. 5, pp. 129–134, Oct. 2015, ISSN: 2053-3713. DOI: 10.1049/htl.2015.0001. [Online]. Available: https://www.ncbi.nlm.nih.gov/pmc/articles/PMC4625831/ (visited on 03/05/2020).

[2] N. J. M. Rijkhoff, H. Wijkstra, P. E. V. V. Kerrebroeck, and F. M. J. Debruyne, "Urinary bladder control by electrical stimulation: Review of electrical stimulation techniques in spinal cord injury," en, *Neurourology and Urodynamics*, vol. 16, no. 1, pp. 39–53, 1997, ISSN: 1520-6777. DOI: 10.1002/(SICI)1520-6777(1997)16:1<39::AID-NAU6>3.0.CO;2-F. (visited on 03/05/2020).

[3] W. D. Memberg, K. H. Polasek, R. L. Hart, A. M. Bryden, K. L. Kilgore, G. A. Nemunaitis, H. A. Hoyen, M. W. Keith, and R. F. Kirsch, "An Implanted Neuroprosthesis for Restoring Arm and Hand Function in People with High Level Tetraplegia," *Archives of physical medicine and rehabilitation*, vol. 95, no. 6, 1201–1211.e1, Jun. 2014, ISSN: 0003-9993. DOI: 10.1016/j.apmr.2014.01.028. [Online]. Available: https://www.ncbi.nlm.nih.gov/pmc/articles/PMC4470503/ (visited on 03/05/2020).

[4] P. H. Peckham and J. S. Knutson, "Functional Electrical Stimulation for Neuromuscular Applications," *Annual Review of Biomedical Engineering*, vol. 7, no. 1, pp. 327–360, 2005, _eprint: https://doi.org/10.1146/annurev.bioeng.6.040803.140103. DOI: 10.1146/

annurev.bioeng.6.040803.140103. [Online]. Available: https://doi.org/10.1146/annurev.bioeng.6.040803.140103 (visited on 03/05/2020).

[5] W. Grill and J. Mortimer, "Stimulus waveforms for selective neural stimulation," en, *IEEE Engineering in Medicine and Biology Magazine*, vol. 14, no. 4, pp. 375–385, Aug. 1995, ISSN: 07395175. DOI: 10.1109/51.395310. [Online]. Available: http://ieeexplore.ieee.org/document/395310/ (visited on 03/02/2020).

[6] S. W. Kuffler and E. M. V. Williams, "Small-nerve junctional potentials. The distribution of small motor nerves to frog skeletal muscle, and the membrane characteristics of the fibres they innervate*," en, *The Journal of Physiology*, vol. 121, no. 2, pp. 289–317, 1953, ISSN: 1469-7793. DOI: 10.1113/jphysiol.1953.sp004948. [Online]. Available: https://physoc.onlinelibrary.wiley.com/doi/abs/10.1113/jphysiol.1953.sp004948 (visited on 02/11/2020).

[7] E. F. W. PFLUEGER, *Untersuchungen über die Physiologie des Electrotonus*, de. 1859, Google-Books-ID: mThWAAAAcAAJ.

[8] R. K. Hobbie and B. J. Roth, *Intermediate Physics for Medicine and Biology*, en, 4th ed. New York: Springer-Verlag, 2007, ISBN: 978-0-387-30942-2. DOI: 10.1007/978-0-387-49885-0. [Online]. Available: https://www.springer.com/gp/book/9780387309422 (visited on 03/05/2020).

[9] N. Accornero, G. Bini, G. L. Lenzi, and M. Manfredi, "Selective Activation of peripheral nerve fibre groups of different diameter by triangular shaped stimulus pulses.," en, *The Journal of Physiology*, vol. 273, no. 3, pp. 539–560, Dec. 1977, ISSN: 1469-7793. DOI: 10.1113/jphysiol.1977.sp012109. [Online]. Available: http://onlinelibrary.wiley.com/doi/10.1113/jphysiol.1977.sp012109/abstract (visited on 09/21/2015).

[10] Z.-P. Fang and J. Mortimer, "Selective activation of small motor axons by quasitrapezoidal current pulses," *IEEE Transactions on Biomedical Engineering*, vol. 38, no. 2, pp. 168–174, Feb. 1991, ISSN: 1558-2531. DOI: 10.1109/10.76383.

[11] A. I. van Bolhuis, J. Holsheimer, and H. H. C. M. Savelberg, "A nerve stimulation method to selectively recruit smaller motor-units in rat skeletal muscle," en, *Journal*

*of Neuroscience Methods*, vol. 107, no. 1, pp. 87–92, May 2001, ISSN: 0165-0270. DOI: 10.1016/S0165-0270(01)00355-7. [Online]. Available: http://www.sciencedirect.com/science/article/pii/S0165027001003557 (visited on 03/02/2020).

[12] C. v. d. Honert and J. T. Mortimer, "Generation of unidirectionally propagated action potentials in a peripheral nerve by brief stimuli," en, *Science*, vol. 206, no. 4424, pp. 1311–1312, Dec. 1979, Publisher: American Association for the Advancement of Science Section: Reports, ISSN: 0036-8075, 1095-9203. DOI: 10.1126/science.515733. [Online]. Available: https://science.sciencemag.org/content/206/4424/1311 (visited on 03/02/2020).

[13] I. J. Ungar, D. J. T. Mortimer, and J. D. Sweeney, "Generation of unidirectionally propagating action potentials using a monopolar electrode cuff," en, *Annals of Biomedical Engineering*, vol. 14, no. 5, pp. 437–450, Sep. 1986, ISSN: 0090-6964, 1573-9686. DOI: 10.1007/BF02367364. [Online]. Available: http://link.springer.com/article/10.1007/BF02367364 (visited on 09/21/2015).

[14] J. D. Sweeney and J. T. Mortimer, "An Asymmetric Two Electrode Cuf for Generation of Unidirectionally Propagated Action Potentials," en, *IEEE Transactions on Biomedical Engineering*, vol. BME-33, no. 6, pp. 541–549, Jun. 1986, ISSN: 0018-9294, 1558-2531. DOI: 10.1109/TBME.1986.325818. [Online]. Available: http://ieeexplore.ieee.org/document/4122341/ (visited on 02/25/2020).

[15] G. E. Loeb and R. A. Peck, "Cuff electrodes for chronic stimulation and recording of peripheral nerve activity," *Journal of Neuroscience Methods*, vol. 64, no. 1, pp. 95–103, Jan. 1996, ISSN: 0165-0270. DOI: 10.1016/0165-0270(95)00123-9. [Online]. Available: https://www.sciencedirect.com/science/article/pii/0165027095001239 (visited on 02/08/2017).

[16] G. Naples, J. Mortimer, A. Scheiner, and J. Sweeney, "A spiral nerve cuff electrode for peripheral nerve stimulation," en, *IEEE Transactions on Biomedical Engineering*, vol. 35, no. 11, pp. 905–916, Nov. 1988, ISSN: 00189294. DOI: 10.1109/10.8670. [Online]. Available: http://ieeexplore.ieee.org/document/8670/ (visited on 03/09/2020).

[17] D. Tyler and D. Durand, "Functionally selective peripheral nerve stimulation with a flat interface nerve electrode," en, *IEEE Transactions on Neural Systems and Rehabilitation Engineering*, vol. 10, no. 4, pp. 294–303, Dec. 2002, ISSN: 1534-4320. DOI: 10.1109/TNSRE.2002.806840. [Online]. Available: http://ieeexplore.ieee.org/document/1178100/ (visited on 03/09/2020).

[18] H. Taghipour-Farshi, J. Frounchi, N. Ahmadiasl, P. Shahabi, and Y. Salekzamani, "Effect of contacts configuration and location on selective stimulation of cuff electrode," *Bio-Medical Materials and Engineering*, vol. 25, no. 3, pp. 237–248, Jun. 2015, ISSN: 18783619, 09592989. DOI: 10.3233/BME-151281. [Online]. Available: http://www.medra.org/servlet/aliasResolver?alias=iospress&doi=10.3233/BME-151281 (visited on 09/21/2015).

[19] S. Lee, S. Sheshadri, Z. Xiang, I. Delgado-Martinez, N. Xue, T. Sun, N. V. Thakor, S.-C. Yen, and C. Lee, "Selective stimulation and neural recording on peripheral nerves using flexible split ring electrodes," *Sensors and Actuators B: Chemical*, vol. 242, pp. 1165–1170, Apr. 2017, ISSN: 0925-4005. DOI: 10.1016/j.snb.2016.09.127. [Online]. Available: http://www.sciencedirect.com/science/article/pii/S0925400516315520 (visited on 04/11/2017).

[20] C. Veraart, W. M. Grill, and J. T. Mortimer, "Selective control of muscle activation with a multipolar nerve cuff electrode," *IEEE Transactions on Biomedical Engineering*, vol. 40, no. 7, pp. 640–653, Jul. 1993, ISSN: 0018-9294. DOI: 10.1109/10.237694.

[21] J. Badia, T. Boretius, D. Andreu, C. Azevedo-Coste, T. Stieglitz, and X. Navarro, "Comparative analysis of transverse intrafascicular multichannel, longitudinal intrafascicular and multipolar cuff electrodes for the selective stimulation of nerve fascicles," en, *Journal of Neural Engineering*, vol. 8, no. 3, p. 036 023, 2011, ISSN: 1741-2552. DOI: 10.1088/1741-2560/8/3/036023. [Online]. Available: http://stacks.iop.org/1741-2552/8/i=3/a=036023 (visited on 06/08/2016).

[22] D. K. L. Kilgore and N. Bhadra, "Nerve conduction block utilising high-frequency alternating current," en, *Medical and Biological Engineering and Computing*, vol. 42, no. 3,

pp. 394–406, May 2004, ISSN: 0140-0118, 1741-0444. DOI: 10.1007/BF02344716. [Online]. Available: http://link.springer.com/article/10.1007/BF02344716 (visited on 09/29/2015).

[23] D. M. Ackermann, C. Ethier, E. L. Foldes, E. R. Oby, D. Tyler, M. Bauman, N. Bhadra, L. Miller, and K. L. Kilgore, "Electrical conduction block in large nerves: High-frequency current delivery in the nonhuman primate," en, *Muscle & Nerve*, vol. 43, no. 6, pp. 897–899, Jun. 2011, ISSN: 1097-4598. DOI: 10.1002/mus.22037. [Online]. Available: http://onlinelibrary.wiley.com/doi/10.1002/mus.22037/abstract (visited on 02/14/2017).

[24] J. J. Waataja, K. S. Tweden, and C. N. Honda, "Effects of high-frequency alternating current on axonal conduction through the vagus nerve," en, *Journal of Neural Engineering*, vol. 8, no. 5, p. 056 013, 2011, ISSN: 1741-2552. DOI: 10.1088/1741-2560/8/5/056013. [Online]. Available: http://stacks.iop.org/1741-2552/8/i=5/a=056013.

[25] N. A. Pelot and W. M. Grill, "In vivo quantification of excitation and kilohertz frequency block of the rat vagus nerve," en, *Journal of Neural Engineering*, 2020, ISSN: 1741-2552. DOI: 10.1088/1741-2552/ab6cb6. [Online]. Available: http://iopscience.iop.org/10.1088/1741-2552/ab6cb6 (visited on 02/06/2020).

[26] Y. A. Patel and R. J. Butera, "Differential fiber-specific block of nerve conduction in mammalian peripheral nerves using kilohertz electrical stimulation," en, *Journal of Neurophysiology*, vol. 113, no. 10, pp. 3923–3929, Jun. 2015, ISSN: 0022-3077, 1522-1598. DOI: 10.1152/jn.00529.2014. [Online]. Available: http://jn.physiology.org/content/113/10/3923 (visited on 09/20/2016).

[27] K. L. Kilgore and N. Bhadra, "High Frequency Mammalian Nerve Conduction Block: Simulations and Experiments," in *28th Annual International Conference of the IEEE Engineering in Medicine and Biology Society, 2006. EMBS '06*, Aug. 2006, pp. 4971–4974. DOI: 10.1109/IEMBS.2006.259254.

[28] C. Tai, W. de Groat, and J. Roppolo, "Simulation of nerve block by high-frequency sinusoidal electrical current based on the Hodgkin-Huxley model," *IEEE Transactions*

*on Neural Systems and Rehabilitation Engineering*, vol. 13, no. 3, pp. 415–422, Sep. 2005, ISSN: 1534-4320. DOI: 10.1109/TNSRE.2005.847356.

[29] N. A. Pelot, C. E. Behrend, and W. M. Grill, "Modeling the response of small myelinated axons in a compound nerve to kilohertz frequency signals," eng, *Journal of Neural Engineering*, vol. 14, no. 4, p. 046 022, 2017, ISSN: 1741-2552. DOI: 10.1088/1741-2552/aa6a5f.

[30] N. Bhadra, N. Bhadra, K. Kilgore, and K. J. Gustafson, "High frequency electrical conduction block of the pudendal nerve," en, *Journal of Neural Engineering*, vol. 3, no. 2, p. 180, 2006, ISSN: 1741-2552. DOI: 10.1088/1741-2560/3/2/012. [Online]. Available: http://stacks.iop.org/1741-2552/3/i=2/a=012 (visited on 09/29/2015).

[31] J. D. Miles, K. L. Kilgore, N. Bhadra, and E. A. Lahowetz, "Effects of ramped amplitude waveforms on the onset response of high-frequency mammalian nerve block," en, *Journal of Neural Engineering*, vol. 4, no. 4, p. 390, 2007, ISSN: 1741-2552. DOI: 10.1088/1741-2560/4/4/005. [Online]. Available: http://stacks.iop.org/1741-2552/4/i=4/a=005 (visited on 02/08/2017).

[32] E. L. Foldes, D. M. Ackermann, N. Bhadra, and K. L. Kilgore, "Counted cycles method to quantify the onset response in high-frequency peripheral nerve block," in *2009 Annual International Conference of the IEEE Engineering in Medicine and Biology Society*, Sep. 2009, pp. 614–617. DOI: 10.1109/IEMBS.2009.5332758.

[33] N. Bhadra, E. A. Lahowetz, S. T. Foldes, and K. L. Kilgore, "Simulation of high-frequency sinusoidal electrical block of mammalian myelinated axons," en, *Journal of Computational Neuroscience*, vol. 22, no. 3, pp. 313–326, Jan. 2007, ISSN: 0929-5313, 1573-6873. DOI: 10.1007/s10827-006-0015-5. [Online]. Available: http://link.springer.com/article/10.1007/s10827-006-0015-5 (visited on 09/20/2016).

[34] L. Joseph and R. J. Butera, "High-Frequency Stimulation Selectively Blocks Different Types of Fibers in Frog Sciatic Nerve," *IEEE Transactions on Neural Systems and Rehabilitation Engineering*, vol. 19, no. 5, pp. 550–557, Oct. 2011, ISSN: 1534-4320. DOI: 10.1109/TNSRE.2011.2163082.

[35] A. Rapeaux, K. Nikolic, I. Williams, A. Eftekhar, and T. G. Constandinou, "Fiber size-selective stimulation using action potential filtering for a peripheral nerve interface: A simulation study," in *2015 37th Annual International Conference of the IEEE Engineering in Medicine and Biology Society (EMBC)*, Aug. 2015, pp. 3411–3414. DOI: 10.1109/EMBC.2015.7319125.

[36] D. M. Ackermann, N. Bhadra, E. L. Foldes, X.-F. Wang, and K. L. Kilgore, "Effect of Nerve Cuff Electrode Geometry on Onset Response Firing in High-Frequency Nerve Conduction Block," *IEEE transactions on neural systems and rehabilitation engineering : a publication of the IEEE Engineering in Medicine and Biology Society*, vol. 18, no. 6, pp. 658–665, Dec. 2010, ISSN: 1534-4320. DOI: 10.1109/TNSRE.2010.2071882. [Online]. Available: http://www.ncbi.nlm.nih.gov/pmc/articles/PMC3467702/ (visited on 02/08/2017).

[37] D. M. Ackermann, E. L. Foldes, N. Bhadra, and K. L. Kilgore, "Effect of Bipolar Cuff Electrode Design on Block Thresholds in High-Frequency Electrical Neural Conduction Block," *IEEE Transactions on Neural Systems and Rehabilitation Engineering*, vol. 17, no. 5, pp. 469–477, Oct. 2009, ISSN: 1534-4320. DOI: 10.1109/TNSRE.2009.2034069.

[38] N. Bhadra, T. L. Vrabec, N. Bhadra, and K. L. Kilgore, "Reversible conduction block in peripheral nerve using electrical waveforms," *Bioelectronics in Medicine*, vol. 1, no. 1, pp. 39–54, Jan. 2018, ISSN: 2059-1500. DOI: 10.2217/bem-2017-0004. [Online]. Available: https://www.ncbi.nlm.nih.gov/pmc/articles/PMC5811084/ (visited on 09/03/2019).

[39] M. Gerges, E. L. Foldes, D. M. Ackermann, N. Bhadra, N. Bhadra, and K. L. Kilgore, "Frequency- and amplitude-transitioned waveforms mitigate the onset response in high-frequency nerve block," en, *Journal of Neural Engineering*, vol. 7, no. 6, p. 066 003, 2010, ISSN: 1741-2552. DOI: 10.1088/1741-2560/7/6/066003. [Online]. Available: http://stacks.iop.org/1741-2552/7/i=6/a=066003 (visited on 02/08/2017).

[40] N. Bhadra, E. Foldes, T. Vrabec, K. L. Kilgore, and N. Bhadra, "Temporary persistence of conduction block after prolonged Kilohertz Frequency Alternating Current (KHFAC)

on rat sciatic nerve.," en, *Journal of Neural Engineering*, 2017, ISSN: 1741-2552. DOI: 10.1088/1741-2552/aa89a4. [Online]. Available: http://iopscience.iop.org/10.1088/1741-2552/aa89a4.

[41] C. M. Apovian, S. N. Shah, B. M. Wolfe, S. Ikramuddin, C. J. Miller, K. S. Tweden, C. J. Billington, and S. A. Shikora, "Two-Year Outcomes of Vagal Nerve Blocking (vBloc) for the Treatment of Obesity in the ReCharge Trial," *Obesity Surgery*, vol. 27, no. 1, pp. 169–176, 2017, ISSN: 0960-8923. DOI: 10.1007/s11695-016-2325-7. [Online]. Available: https://www.ncbi.nlm.nih.gov/pmc/articles/PMC5187356/ (visited on 10/17/2017).

[42] *Maestro Instruction Manual*, en, 2015. (visited on 03/30/2020).

[43] A. Haeberlin, A. Zurbuchen, S. Walpen, J. Schaerer, T. Niederhauser, C. Huber, H. Tanner, H. Servatius, J. Seiler, H. Haeberlin, J. Fuhrer, and R. Vogel, "The first batteryless, solar-powered cardiac pacemaker," en, *Heart Rhythm*, vol. 12, no. 6, pp. 1317–1323, Jun. 2015, ISSN: 1547-5271. DOI: 10.1016/j.hrthm.2015.02.032. [Online]. Available: http://www.sciencedirect.com/science/article/pii/S1547527115002520 (visited on 03/30/2020).

[44] T. L. Vrabec, T. E. Eggers, E. L. Foldes, D. M. Ackermann, K. L. Kilgore, and N. Bhadra, "Reduction of the onset response in kilohertz frequency alternating current nerve block with amplitude ramps from non-zero amplitudes," *Journal of NeuroEngineering and Rehabilitation*, vol. 16, Jun. 2019, ISSN: 1743-0003. DOI: 10.1186/s12984-019-0554-4. [Online]. Available: https://www.ncbi.nlm.nih.gov/pmc/articles/PMC6599251/ (visited on 12/12/2019).

[45] M. Franke, T. Vrabec, J. Wainright, N. Bhadra, N. Bhadra, and K. Kilgore, "Combined KHFAC + DC nerve block without onset or reduced nerve conductivity after block," en, *Journal of Neural Engineering*, vol. 11, no. 5, p. 056 012, 2014, ISSN: 1741-2552. DOI: 10.1088/1741-2560/11/5/056012. [Online]. Available: http://stacks.iop.org/1741-2552/11/i=5/a=056012 (visited on 10/01/2015).

[46] T. L. Vrabec, N. Bhadra, J. S. Wainright, N. Bhadra, and K. L. Kilgore, "A novel waveform for No-Onset nerve block combining direct current and kilohertz frequency alternating current," in *2013 6th International IEEE/EMBS Conference on Neural Engineering (NER)*, Nov. 2013, pp. 283–286. DOI: 10.1109/NER.2013.6695927.

[47] N. A. Pelot, B. J. Thio, and W. M. Grill, "Modeling Current Sources for Neural Stimulation in COMSOL," English, *Frontiers in Computational Neuroscience*, vol. 12, 2018, ISSN: 1662-5188. DOI: 10.3389/fncom.2018.00040. [Online]. Available: https://www.frontiersin.org/articles/10.3389/fncom.2018.00040/full (visited on 02/06/2020).

[48] D. M. Ackermann, E. L. Foldes, N. Bhadra, and K. L. Kilgore, "Conduction Block of Peripheral Nerve Using High Frequency Alternating Currents Delivered through an Intrafascicular Electrode," *Muscle & nerve*, vol. 41, no. 1, pp. 117–119, Jan. 2010, ISSN: 0148-639X. DOI: 10.1002/mus.21496. [Online]. Available: http://www.ncbi.nlm.nih.gov/pmc/articles/PMC2947328/ (visited on 10/01/2015).

[49] N. Bhadra and K. Kilgore, "Direct current electrical conduction block of peripheral nerve," *IEEE Transactions on Neural Systems and Rehabilitation Engineering*, vol. 12, no. 3, pp. 313–324, Sep. 2004, ISSN: 1558-0210. DOI: 10.1109/TNSRE.2004.834205.

[50] H. Liu, L. Zhu, S. Sheng, L. Sun, H. Zhou, H. Tang, and T. Qiu, "Post stimulus effects of high frequency biphasic electrical current on a fibre's conductibility in isolated frog nerves," en, *Journal of Neural Engineering*, vol. 10, no. 3, p. 036 024, 2013, ISSN: 1741-2552. DOI: 10.1088/1741-2560/10/3/036024. [Online]. Available: http://stacks.iop.org/1741-2552/10/i=3/a=036024 (visited on 04/11/2017).

[51] G. Yang, Z. Xiao, J. Wang, B. Shen, J. R. Roppolo, W. C. de Groat, and C. Tai, "Post-stimulation block of frog sciatic nerve by high-frequency (kHz) biphasic stimulation," en, *Medical & Biological Engineering & Computing*, vol. 55, no. 4, pp. 585–593, Apr. 2017, ISSN: 1741-0444. DOI: 10.1007/s11517-016-1539-0. [Online]. Available: https://doi.org/10.1007/s11517-016-1539-0 (visited on 12/12/2019).

[52] K. C. McGill, K. L. Cummins, L. J. Dorfman, B. B. Berlizot, K. Luetkemeyer, D. G. Nishimura, and B. Widrow, "On the Nature and Elimination of Stimulus Artifact in Nerve Signals Evoked and Recorded Using Surface Electrodes," *IEEE Transactions on Biomedical Engineering*, vol. BME-29, no. 2, pp. 129–137, Feb. 1982, ISSN: 1558-2531. DOI: 10.1109/TBME.1982.325019.

[53] J. D. Finan and F. Guilak, "The effects of osmotic stress on the structure and function of the cell nucleus," *Journal of cellular biochemistry*, vol. 109, no. 3, pp. 460–467, Feb. 2010, ISSN: 0730-2312. DOI: 10.1002/jcb.22437. [Online]. Available: https://www.ncbi.nlm.nih.gov/pmc/articles/PMC3616882/ (visited on 02/24/2020).

[54] J. Tranum-Jensen, M. J. Janse, W. T. Fiolet, W. J. Krieger, C. N. D'Alnoncourt, and D. Durrer, "Tissue osmolality, cell swelling, and reperfusion in acute regional myocardial ischemia in the isolated porcine heart.," en, *Circulation Research*, vol. 49, no. 2, pp. 364–381, Aug. 1981, ISSN: 0009-7330, 1524-4571. DOI: 10.1161/01.RES.49.2.364. [Online]. Available: https://www.ahajournals.org/doi/10.1161/01.RES.49.2.364 (visited on 02/24/2020).

[55] D. J. Miller, "Sydney Ringer; physiological saline, calcium and the contraction of the heart," *The Journal of Physiology*, vol. 555, no. Pt 3, pp. 585–587, Mar. 2004, ISSN: 0022-3751. DOI: 10.1113/jphysiol.2004.060731. [Online]. Available: https://www.ncbi.nlm.nih.gov/pmc/articles/PMC1664856/ (visited on 02/21/2020).

[56] J. R. Schwarz and G. Eikhof, "Na currents and action potentials in rat myelinated nerve fibres at 20 and 37° C," en, *Pflügers Archiv*, vol. 409, no. 6, pp. 569–577, Aug. 1987, ISSN: 0031-6768, 1432-2013. DOI: 10.1007/BF00584655. [Online]. Available: https://link.springer.com/article/10.1007/BF00584655 (visited on 04/11/2017).

[57] P. F. Cranefield, F. Brink, and D. W. Bronk, "The Oxygen Uptake of the Peripheral Nerve of the Rat," en, *Journal of Neurochemistry*, vol. 1, no. 3, pp. 245–249, 1957, ISSN: 1471-4159. DOI: 10.1111/j.1471-4159.1957.tb12078.x. [Online]. Available: https://onlinelibrary.wiley.com/doi/abs/10.1111/j.1471-4159.1957.tb12078.x (visited on 02/21/2020).

[58] S. M. Minasian, M. M. Galagudza, Y. V. Dmitriev, D. I. Kurapeev, and T. D. Vlasov, "Myocardial protection against global ischemia with Krebs-Henseleit buffer-based cardioplegic solution," *Journal of Cardiothoracic Surgery*, vol. 8, p. 60, Apr. 2013, ISSN: 1749-8090. DOI: 10.1186/1749-8090-8-60. [Online]. Available: https://www.ncbi.nlm.nih.gov/pmc/articles/PMC3654955/ (visited on 02/21/2020).

[59] J. E. Lehmann, "The Effect of Changes in pH on the Action of Mammalian A Nerve Fibers," en, *American Journal of Physiology-Legacy Content*, vol. 118, no. 3, pp. 600–612, Feb. 1937, ISSN: 0002-9513. DOI: 10.1152/ajplegacy.1937.118.3.600. [Online]. Available: https://www.physiology.org/doi/10.1152/ajplegacy.1937.118.3.600 (visited on 02/21/2020).

[60] L. L. Hamm, N. Nakhoul, and K. S. Hering-Smith, "Acid-Base Homeostasis," *Clinical Journal of the American Society of Nephrology : CJASN*, vol. 10, no. 12, pp. 2232–2242, Dec. 2015, ISSN: 1555-9041. DOI: 10.2215/CJN.07400715. [Online]. Available: https://www.ncbi.nlm.nih.gov/pmc/articles/PMC4670772/ (visited on 12/06/2019).

[61] L. E. Bailey and S. D. Ong, "Krebs-Henseleit solution as a physiological buffer in perfused and superfused preparations," en, *Journal of Pharmacological Methods*, vol. 1, no. 2, pp. 171–175, Aug. 1978, ISSN: 0160-5402. DOI: 10.1016/0160-5402(78)90022-0. [Online]. Available: http://www.sciencedirect.com/science/article/pii/0160540278900220 (visited on 02/21/2020).

[62] A. Rapeaux and T. G. Constandinou, "A Block-Capable and Module-Extendable 4-Channel Stimulator for Acute Neurophysiology," en, *bioRxiv*, p. 2020.01.28.923474, Jan. 2020. DOI: 10.1101/2020.01.28.923474. [Online]. Available: https://www.biorxiv.org/content/10.1101/2020.01.28.923474v1 (visited on 02/07/2020).

[63] N. Huseyinoglu, I. Ozaydin, U. Huseyinoglu, S. Yayla, and O. Aksoy, "Minimally Invasive Motor Nerve Conduction Study of the Rat Sciatic and Tail Nerves," en, *Kafkas Universitesi Veteriner Fakultesi Dergisi*, 2013, ISSN: 1300-6045. DOI: 10.9775/kvfd.2013.9065. [Online]. Available: http://vetdergi.kafkas.edu.tr/extdocs/2013_6/943-948.pdf (visited on 02/26/2020).

[64] M. Ayaz, E. Kiziltan, S. Tuncer, N. Dalkilic, I. Demirel, H. Bariskaner, and F. Pehlivan, "Sexual Dependency of Rat Sciatic Nerve Fiber Conduction Velocity Distributions," *International Journal of Neuroscience*, vol. 117, no. 11, pp. 1537–1549, Jan. 2007, Publisher: Taylor & Francis _eprint: https://doi.org/10.1080/00207450701239244, ISSN: 0020-7454. DOI: 10.1080/00207450701239244. [Online]. Available: https://doi.org/10.1080/00207450701239244 (visited on 02/26/2020).

[65] E. Opsommer, E. Masquelier, and L. Plaghki, "Determination of nerve conduction velocity of C-fibres in humans from thermal thresholds to contact heat (thermode) and from evoked brain potentials to radiant heat (CO2 laser)," en, *Neurophysiologie Clinique/Clinical Neurophysiology*, vol. 29, no. 5, pp. 411–422, Oct. 1999, ISSN: 0987-7053. DOI: 10.1016/S0987-7053(00)87265-2. [Online]. Available: http://www.sciencedirect.com/science/article/pii/S0987705300872652 (visited on 02/26/2020).

[66] E. Cuttaz, J. Goding, C. Vallejo-Giraldo, U. Aregueta-Robles, N. Lovell, D. Ghezzi, and R. A. Green, "Conductive elastomer composites for fully polymeric, flexible bioelectronics," en, *Biomaterials Science*, vol. 7, no. 4, pp. 1372–1385, 2019. DOI: 10.1039/C8BM01235K. [Online]. Available: https://pubs.rsc.org/en/content/articlelanding/2019/bm/c8bm01235k (visited on 01/06/2020).

[67] W. Y. X. Peh, R. Mogan, X. Y. Thow, S. M. Chua, A. Rusly, N. V. Thakor, and S.-C. Yen, "Novel Neurostimulation of Autonomic Pelvic Nerves Overcomes Bladder-Sphincter Dyssynergia," English, *Frontiers in Neuroscience*, vol. 12, 2018, Publisher: Frontiers, ISSN: 1662-453X. DOI: 10.3389/fnins.2018.00186. [Online]. Available: https://www.frontiersin.org/articles/10.3389/fnins.2018.00186/full (visited on 06/12/2020).

[68] B. De La Franier, A. Jankowski, and M. Thompson, "Functionalizable self-assembled trichlorosilyl-based monolayer for application in biosensor technology," en, *Applied Surface Science*, vol. 414, pp. 435–441, Aug. 2017, ISSN: 0169-4332. DOI: 10.1016/j.apsusc.2017.04.111. [Online]. Available: http://www.sciencedirect.com/science/article/pii/S0169433217311285 (visited on 03/20/2020).

# Chapter 6

# Conclusion

## 6.1 Summary

Selectivity has been a long-standing issue for neuroprosthetics and electroceuticals. They key tradeoff between selectivity and the invasiveness of implanted interfaces, as well as its consequences in terms of the foreign body response has led to side-effects when delivering therapies such as vagus nerve stimulation. These side-effects have reduced patients' quality of life and potentially may lead to deleterious effects, providing a strong incentive to find solutions to this complex problem.

Today the least invasive and least selective cuff-type electrodes are the most widely used for stimulation therapies, and this is likely to remain true for some time owing to the challenge of mitigating inflammation and nerve damage from devices penetrating inside sensitive nervous tissue. Previous work has shown that it is possible to improve the selectivity of well-tolerated electrode implants, and it has been the strategy used in this work.

HFAC block, as a relatively new and promising neuromodulation tool, provided a unique opportunity when combined with conventional stimulation, especially considering the structure and configuration of cuff electrodes which are well adapted to using this technique. As conventional stimulation is excitatory and HFAC block inhibitory, combining stimulation with filtering of

unwanted neural activity enables better control of the resulting action potentials propagating towards end organs, with potential applications for vagus nerve stimulation, functional electrical stimulation of motor nerves, pudendal nerve stimulation for bladder control amongst others, all of which would benefit from the increased functional selectivity afforded by this technique.

To conclude on the main hypothesis of this work it must first be reiterated: that selective stimulation can be carried out by leveraging differences in action potential conduction speeds between small and large fibers, using combined conventional stimulation and block to filter out action potentials propagating in the larger fibers. **According to the data collected during this work, it is not feasible to do this in a practical sense.** What practical means here is that during a typical experiment, **block carryover will be observed after using HFAC for a period of time**, at which point the amount of charge injected into the nerve tissue will presumably reach a threshold beyond which this process is observed. This means the same will likely occur in clinical settings, and must be accounted for when translating any use of HFAC from an experimental setting to a clinical setting. **Block carryover prevents action potential filtering by differences in propagation speed, but in the same stroke enables a similar kind of filtering by using differences in recovery speed from block between small and large fibers.** The data collected during this work and previous literature [1] suggest that myelinated fibers can be affected by block carryover while unmyelinated fibers remain unaffected, providing an opportunity to selectively stimulate unmyelinated fibers. This has many potential applications in neuromodulation where selective activation of these fibers would reduce or eliminate secondary effects associated with therapies requiring this kind of stimulation.

## 6.2 Original Contributions

Throughout the duration of this project, a number of original contributions can be detailed relative to objectives:

- Design, implementation, testing and use in experiments of several stimulator designs,

culminating in a multi-channel, block capable stimulator able to single-handedly carry out combined stimulation and block trials for investigation of selective stimulation. The stimulator has approximately ±15 V of voltage compliance and can deliver up to 10 mA of current in either direction concurrently on all four stimulation channels with arbitrary waveforms and reliable timing due to not using processor control. This makes the stimulator responsive to commands sent at any time from a controlling PC. The stimulator power domain is electrically isolated and communicates to other devices through digital isolators, enabling it to talk directly to recording devices without creating current return paths for stimulation pulses through external devices. Hardware has been designed and implemented for additional features such as automatic self-calibration and real-time monitoring of electrode polarisation for active charge balancing. The stimulator is actively being used by two research groups in two different departments at Imperial College and will contribute to additional partnerships and collaborations with a research group in Italy as well as enabling further research projects within the NGNI research group. During months of experiments, this stimulator has provided consistent performance and demonstrated its durability for use in wet lab environments.

- Adaptation, implementation and testing of an acute *ex-vivo* experimental platforms for small animal neurophysiology at Imperial College based on an experimental setup used at Galvani Bioelectronics. The setup was adapted for use at Imperial within space-constrained laboratory environments, built from scratch and validated for investigation of concurrent HFAC block and stimulation. The potential for optimization of the system was explored with a single container variant providing enhanced monitoring capability for experimental variables and this variant was shown to keep a nerve alive for several hours. The single-container variant used custom 3D printed nerve baths and does not require some of the costlier specialist equipment of the conventional setup such as peristaltic pumps, enabling wider adoption in laboratories. Both the conventional setup and optimized variant are in active use at Imperial College by two research groups and several students, and helped create several ongoing research projects to continue using this system. Potential applications include fundamental neurophysiology, development of novel

stimulation and recording electrode materials, development of new stimulation strategies such as combined stimulation and HFAC block, and potentially others in the future.

- Identification of a suitable experimental approach for investigating selective stimulation using HFAC block by analysis of work in the literature, as well as own work both *in-silico* and *in-vivo*. Demonstrating the limitations of existing computational models of HFAC block with respect to the secondary onset response, block carryover, and quantitative differences in HFAC block frequency and amplitude thresholds by comparing results otained using multiple experimental paradigms. Showing that leveraging action potential propagation speed differences for selectivity using timed HFAC block is unlikely to work due to carryover. Investigating several properties of carryover that have not yet been reported, such as the effect of total accumulated charge and the locality of the effect on the nerve. Showing that carryover provides an opportunity to selectively stimulate unmyelinated fibers, but that modelling is required to predict the duration of carryover events after each use of HFAC for the technique to be feasible. The collected data provides groundwork for additional research on this process we currently know very little about, and that has direct impact on the use of HFAC chronically.

## 6.3 Future Directions

The contributions of this work pertain to different fields and each aspect can be pursued further.

The stimulator described in chapter 3 can be improved. Higher voltage compliance would enable the use of more resistive electrodes while ensuring that that output waveform is not distorted, for example. In this case, hardware exists on the platform that has not yet been utilized by the stimulator, and therefore embedded software development that makes use of the onboard electrode voltage monitor[1] could be the focus of several projects down the line. In its current state, the stimulator is driven by Matlab scripts, and could benefit from a versatile GUI[2] not only to make it more user friendly, but also to unlock its potential as a powerful

[1]This was the focus of a project led by Charalampos Mastrokostas.
[2]This was the focus of a project led by Deland Liu.

arbitrary current waveform generator. The stimulator only operates as a multi-channel device when stimlation and block are delivered in a monopolar manner, however making each channel electrically isolated from the others, while doable, would require substantial changes to the hardware. The potential for using HFAC block in therapy paves the way for adaptation of the current source design into an ASIC as part of a new generation of medical devices capable of both excitatory and inhibitory neuromodulation.

In terms of the experimental setup at Imperial, an ongoing project focuses on improving the usability of the platform by providing modular 3D-printed stands and rods that are more suitable than those available in chemical labs: a key feature would be the ability to precisely adjust the position of stimulation and recording electrodes on the nerve, while retaining excellent stability. The electrodes and nerve tissue are quite fragile, and as they are connected to several other devices a pulled cable can quite easily result in a failed experiment. Work is ongoing to refine the single-container variant of the setup as the hypothesis here is that it will afford better control over experimental variables such as temperature and oxygenation than the conventional setup.

An exciting prospect is to continue investigating the block carryover process and HFAC block-related phenomena in general as one of the primary conclusions of this work is the difference between computation model predictions and experimental observations. This motivates work to understand which parts of the nerve that are not currently modelled could contribute to observed effects such as the secondary onset response and carryover. As of this writing despite there being several reports on this process it is not well understood. What can these observations be tied to at the nerve level, or perhaps at the individual cell level? It is possible that carryover is the result of ion accumulation processes: it has been reported potassium accumulation in the interstitial space between the axonal membrane and myelin can change nerve excitability [2]–[4], and potential limitations in the way membranes are modelled with respect to high frequency signals have also been identified [5] that could help create better models that capture more experimental observations.

## 6.4 Final Thoughts, Lessons Learned

This has been a long road; some of the most important lessons learned include an appreciation for the multi-disciplinary nature of the work and the fundamental differences between computational modelling predictions and the realities of experimental investigation. Experiments are hard in biology - there are so many interconnected systems that it is very difficult to isolate any one of them and obtain useable data, as invariably the most relevant observations can only be obtained when looking at the whole system (living organism) at several time scales (minutes, hours, days, months, sometimes years) in all its glorious and frustrating complexity. For an electronic engineer accustomed to robust and reliable models that confer total knowledge of how a circuit works, even taking into account manufacturing variability, the unknown elements of biology were fearsome... but not insurmountable. By systematically identifying the most important parameters, consulting with experts and reading as much as possible about the studied system, robust experiments can be designed that yield repeatable results.

The experiment itself (and subsequent data analysis) is only part of the work. The importance of understanding the tools at our disposal and how the studied system behaves cannot be understated. Having complete knowledge and control over the tool is part of why a custom stimulator was designed. Another reason was that commercial hardware was not well-adapted to carrying out the envisioned experiments. The same thought process is what drove the search for a controlled experimental environment which could keep a nerve alive and in tightly controlled conditions, especially considering the limitations of *in-vivo* experimentation. Even now additional effort could be spent to improve this setup to better represent the *in-vivo* environment for the nerve and extend the time during which it can be observed.

Another lesson is on the merit (*a posteriori*) of looking at data early on rather than only once the experiments have been completed. There is a balancing act between focusing on the collection of data, as experiments take a lot of time, and taking the time to analyse what has been collected - had this been done before the end of experiments, the last of these would have focused more on how to leverage carryover block for selective stimulation, and perhaps provided more and higher quality data. The key is to plan experiments such that, instead of

searching, often unsuccessfully, for an ideal set of parameters that demonstrates the hypothesis, to systematically explore the parameter set in a way that collects useful data that can be integrated into reports regardless of the experiment outcome. In this way more opportunities for analysis are created, and whatever findings there are can be reported with confidence owing to the repeatability of results. One mustn't rush in thinking a single experiment can yield a concrete answer - slower but steadier investigation is often more successful.

# References


[1] J. J. Waataja, K. S. Tweden, and C. N. Honda, "Effects of high-frequency alternating current on axonal conduction through the vagus nerve," en, *Journal of Neural Engineering*, vol. 8, no. 5, p. 056 013, 2011, ISSN: 1741-2552. DOI: 10.1088/1741-2560/8/5/056013. [Online]. Available: http://stacks.iop.org/1741-2552/8/i=5/a=056013.

[2] W. J. Adelman and Y. Palti, "The Role of Periaxonal and Perineuronal Spaces in Modifying Ionic Flow Across Neural Membranes**This article was prepared at Bethesda, Maryland, with sponsorship of the National Institutes of Health. Reproduction for the purpose of the United Sates Government is permitted.," en, in *Current Topics in Membranes and Transport*, F. Bronner and A. Kleinzeller, Eds., vol. 3, Academic Press, Jan. 1972, pp. 199–235. DOI: 10.1016/S0070-2161(08)61059-X. [Online]. Available: http://www.sciencedirect.com/science/article/pii/S007021610861059X (visited on 03/13/2020).

[3] G. David, J. N. Barrett, and E. F. Barrett, "Activation of internodal potassium conductance in rat myelinated axons.," *The Journal of Physiology*, vol. 472, pp. 177–202, Dec. 1993, ISSN: 0022-3751. [Online]. Available: http://www.ncbi.nlm.nih.gov/pmc/articles/PMC1160482/ (visited on 02/03/2017).

[4] J. Röper and J. R. Schwarz, "Heterogeneous distribution of fast and slow potassium channels in myelinated rat nerve fibres.," *The Journal of Physiology*, vol. 416, pp. 93–

110, Sep. 1989, ISSN: 0022-3751. [Online]. Available: http://www.ncbi.nlm.nih.gov/pmc/articles/PMC1189205/ (visited on 10/06/2016).

[5] C. Bédard and A. Destexhe, "A Modified Cable Formalism for Modeling Neuronal Membranes at High Frequencies," *Biophysical Journal*, vol. 94, no. 4, pp. 1133–1143, Feb. 2008, ISSN: 0006-3495. DOI: 10.1529/biophysj.107.113571. [Online]. Available: http://www.sciencedirect.com/science/article/pii/S0006349508706325 (visited on 02/13/2017).

# Chapter 7

# Appendix

## 7.1 Custom multichannel stimulator top level layout

The custom stimulator plugs directly into the Freescale Freedom®K64F development board and its PCB board has the same length and width. Figures 7.1 and 7.2 show the layout of the board from within Altium Designer™.

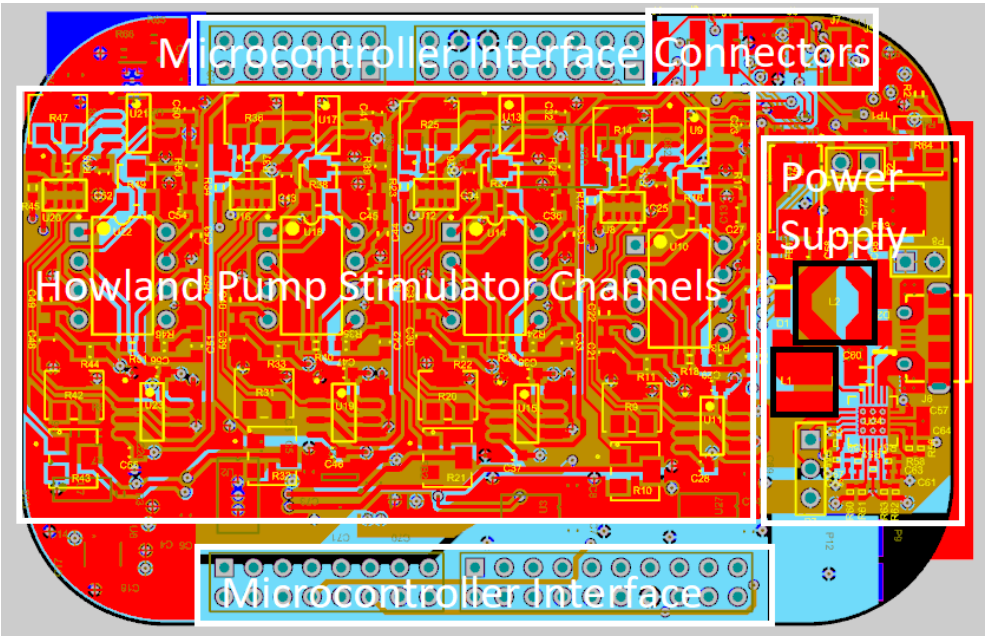


Figure 7.1: Annotated top view of the multichannel stimulator layout.

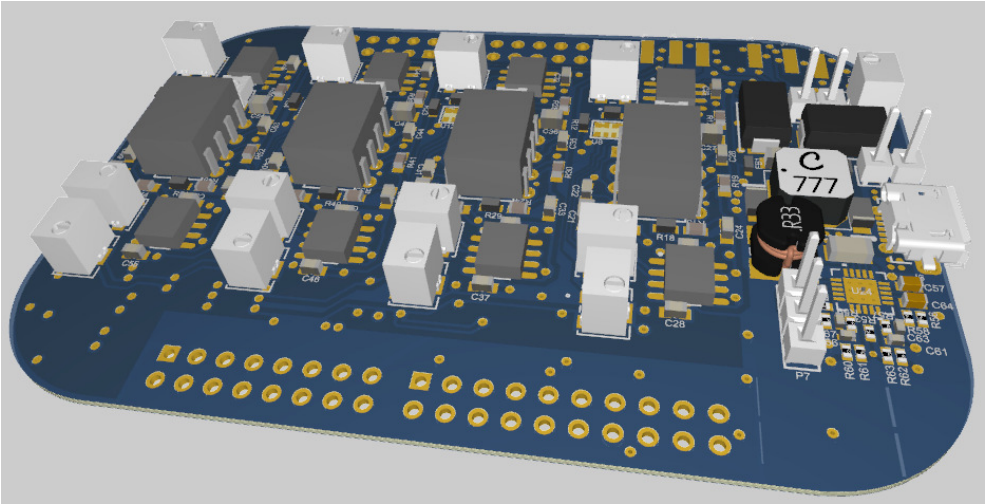

Figure 7.2: 3D view of the stimulator PCB, without the connection headers to the development board for clarity. Some components are not to scale.

## 7.2 Custom conductive elastomer electrode

Cuff electrodes benefit from having wide contacts and being able to inject as much charge as possible into the nerve without causing damage. This makes the use of conductive elastomers attractive due to effectively displacing metals away from sensitive nerve tissue, despite the increase in the resistivity of the electrode compared to a metal variant. The impedance of conductive elastomer at the elastomer-electrolyte interface appears primarily resistive [0]. Conductive elastomer cuffs used for the work described in this thesis were assembled by Estelle Cuttaz.

Figure 7.3: Elastomer electrode used in *ex-vivo* block and stimulation experiments at imperial college. The conductive elastomer is black and encaed in flexible silicone, with a slastic tube to shape the material into a cylinder for use as a cuff electrode. Courtesy of Estelle Cuttaz, Rylie Green research group, Imperial College.

## 7.3 Experimental Protocols

### 7.3.1 Modified Krebs-Henseleit Buffer Preparation

See below page for an SOP used to prepare mKHB buffer. A variant on this SOP is to first prepare a 10X stock solution containing all salts except for glucose and sodium bicarbonate, and adding calcium chloride last to prevent its precipitation. The stock solution can be stored in a refrigerator for a month before it must be replaced. To prepare 1X stock dilute 8 times, add missing sodium bicarbonate and glucose, then add deionized water to reach 10X dilution, resulting in 1X solution.

**Standard Operating Procedure**

**Title: Modified Krebs-Henseleit Buffer Preparation**

**Reference: KHBP1**

**Revision: 1.1**

**Last Modified: 17 June 2019 (Adrien Rapeaux; adrien.rapeaux13@imperial.ac.uk)**

Changelog (compared to 1.0): Added instruction to gas solution using carbogen prior to storage.

Scope: For use in small laboratory animal ex-vivo electrophysiology experiments to maintain nerve tissue viability outside the body.

Target Composition:

| Chemical | Concentration (mM) for 1L | Weight (g) for 1L | Weight (g) for 2L | Weight (g) for 3L | Weight (g) for 4L |
|---|---|---|---|---|---|
| NaCl | 113.0 | 6.603 | 13.206 | 19.809 | 26.412 |
| KCl | 4.8 | 0.357 | 0.714 | 1.071 | 1.428 |
| $CaCl_2$ ($2H_2O$) | 2.5 | 0.367 | 0.734 | 1.101 | 1.468 |
| $KH_2PO_4$ | 1.2 | 0.163 | 0.326 | 0.489 | 0.652 |
| $MgSO_4$ | 1.2 | 0.144 | 0.288 | 0.432 | 0.576 |
| $NaHCO_3$ | 25.0 | 2.1 | 4.2 | 6.3 | 8.4 |
| (+)Dextrose | 5.55 | 0.99 | 1.98 | 2.97 | 3.96 |

1. Weigh salts using precision scale and weighing boats and combine in single container.
2. Place salts in 1-4L bottle (as appropriate with projected use over week) labelled: Modified Krebs Henseleit Buffer, [date of creation], [initials of operator and contact details].
3. Add deionized water to bottle until total volume is 1-4L as appropriate. Can use graduated flask or measuring tube/cup as required.
4. Close bottle securely then shake vigorously to dissolve the salts. The solution will be turbid.
5. Gas solution using carbogen for at least 30 minutes. Check that solution pH is 7.4. Solution should be clear (salts dissolved).
6. Store the bottle in a fridge (4 degrees Celsius) until used to prevent growth of micro-organisms.

Precautions:

Wear Lab Coat, Safety Goggles, Nitrile Rubber gloves.

Avoid producing dust. Wait until dust settles before changing salt during weighing.

Calcium chloride is an eye irritant. Refer to $CaCl_2$ MSDS/ COSHH form.

Dispose in drain (all salts non-toxic and at small concentrations).

### 7.3.2 Rat sciatic nerve dissection protocol

Unfortunately there are no picutres available to describe this protocol owing to regulations on the use of photographic equipment within animal science facilities. The following is a text description for the dissection of rat sciatic nerve as used at Imperial College for the experiments described in chapters 4 and 5.

Requirements:

- 100 mL of iced oxygenated mKHB buffer (see chapter 4 and subsection 7.3.1).
- Blunt standard and fine surgical scissors, standard forceps or tweezers for gross dissection. Very fine or microdissection scissors (preferably angled) and fine forceps for fine dissection.
- sylgard or silicone-coated petri dish
- insect pins to fasten the nerve tissue inside the petri dish
- two sample tubes, at least 5 cm deep, filled with iced oxygenated mKHB buffer.
- microscope or independently fastened strong lens for microdissection

1. The rat is first placed in an anaesthesia chamber to be deeply anaesthetized using 5% isoflurane. After the animal no longer responds to standard noxious stimuli such as toe and forepaw pinch, place prone on a suitable workbench and carry out cervical dislocation to cull. This method substantially improves the quality of dissected tissue compared to carbon dioxide methods owing to the sensitivity of nerves to oxygenation.
2. Immediately place the rat on the dissection workbench and use dissection scissors to sever the calcaneal tendon on the right leg. Use fine scissors to cut through the skin upwards towards the midline or spine, exposing muscle on the entire leg all the way to the spine. The cut should be roughly along the back of the leg following the axis of the tendon.
3. Carefully cut away the muscle plane near the knee joint to expose the sciatic nerve, using fine dissection scissors. The nerve may be anchored to the superficial muscles by fascia

and therefore cutting should not aim to traverse the muscle entirely unless the operator is confident the sciatic will not be cut.

4. Once the sciatic nerve has been found, moisturize the surgical cavity using iced buffer. Repeat this once at least every 5 minutes of dissection; do not allow the tissue to dry.

5. Carefully cut muscle towards the spine that is laying over the sciatic nerve until a characteristic bend (cleft) is found; this will be the approximate location of the upper cut (do not cut yet)

6. Hold the severed end of the calcaneal tendon on the muscle side using tweezers and locate the two sciatic nerve branches which reach the inner side of the ankle. Cut alongside until the gastrocnemius muscle is split, at which point there should a contiguous section of sciatic nerve at least 5 cm in length visible to the eye.

7. Dissect the nerve away from the leg by first cutting at the ankle, removing fascia and musle along the way where possible. Maintaining a minimum of tension on the nerve, cut as near to the spine as possible. The final piece of nerve tissue should measure approximately 5 cm in length.

8. Immediately place the nerve in one of the sample tubes, close and place on ice. Repeat procedure for the left leg. Target a maximum of 10 minutes per leg for dissection.

9. Once ready for microdissection empty one sample tube into the petri dish and pin the nerve onto the silicone, keeping a minimum of tension and avoiding kinks or twists in the tissue. With microdissection tools carefully remove any remaining fascia, muscle tissue and blood vessels from the nerve. Remove any nerve branch not used in the experiment and trim ends to the trunk to avoid any interference with nerve cuff sealing around the nerve.

10. Place nerve in heated, oxygenated mKHB bath, ready to start stimulation and recording. Save other nerve on ice or prepare following the same cleaning procedure depending on experiment requirements.